C. C. Barrett
Code 734

NASA TECHNICAL MEMORANDUM

NASA TM X-1343

NASA TM X-1343

POSTFLIGHT EVALUATION OF ATLAS-CENTAUR AC-8

(LAUNCHED APRIL 7, 1966)

by Staff of the Lewis Research Center

Lewis Research Center
Cleveland, Ohio

NATIONAL AERONAUTICS AND SPACE ADMINISTRATION • WASHINGTON, D. C. • APRIL 1967

NASA TM X-1343

POSTFLIGHT EVALUATION OF ATLAS-CENTAUR AC-8

(LAUNCHED APRIL 7, 1966)

By Staff of the Lewis Research Center

Lewis Research Center
Cleveland, Ohio

NATIONAL AERONAUTICS AND SPACE ADMINISTRATION

For sale by the Clearinghouse for Federal Scientific and Technical Information
Springfield, Virginia 22151 – CFSTI price $3.00

CONTENTS

I. SUMMARY

The AC-8 Atlas-Centaur vehicle, carrying a 1730-pound-mass model of the Surveyor payload, was successfully launched from ETR Complex 36B on April 7, 1966 at 2000:02.090 EST in an attempted two-burn mission. Flight profile through boost phase, Centaur first burn, orbit injection, and the 25-minute orbital coast was normal. However, the second main engine burn required to transfer the spacecraft from the parking orbit into a lunar intercept trajectory was not accomplished because of a deficiency of hydrogen peroxide to operate the boost pumps. Early depletion of the peroxide appears to have resulted from a leak in the system during the extended coast period.

The launch-on-time capability of the Atlas-Centaur vehicle was demonstrated as AC-8 lifted off only 2 seconds after the launch window opened. It was launched on an azimuth of 115^{o} east of true north and was programed to a flight azimuth of 103^{o} east of true north at T + 2 seconds. The Atlas sustainer cutoff occurred 8 seconds early, but extended Centaur engine firing provided adequate compensation. Velocity errors were well within nominal values, and the Centaur closed-loop inertial guidance system injected the AC-8 upper stage into a near-perfect 90-nautical-mile Earth orbit. Structural loading on the vehicle, protection against aerodynamic heating, and separation of jettisonable nose fairing and insulation panels, with the exception of one minor panel hinge motion anomaly, were all nominal for the flight. Winds aloft during the launch operations were seasonably high and resulted in several delayed launch attempts.

A very significant achievement of the flight was the positive control of tank pressure and residual propellants throughout the entire 25-minute, low g coast period. A nonpropulsive hydrogen tank venting system together with energy dissipation devices and variable propellant settling thrust levels to suppress liquid disturbances and control propellant location were adequately and successfully demonstrated. Propellants were retained in a settled condition and would have supported a second engine burn, with satisfactory propellant boost pump operation. Overboard discharge of hydrogen boiloff gas was also accomplished without disturbing the vehicle attitude.

II. INTRODUCTION

The AC-8 Atlas Centaur vehicle was the seventh in a series of development flights in support of the Surveyor lunar program. The primary mission for the Centaur is to launch the Surveyor spacecraft into a lunar intercept trajectory by a direct-ascent single-burn mission or by transfer from a near-Earth parking orbit by restart of the main engines after a given low-gravity coast interval. This mission flexibility would afford maximum launch opportunity at any time of the year. Development of the single-burn mission capability was completed successfully with the AC-6 flight. The AC-8 launch vehicle, however, was the first of two development flights scheduled to demonstrate the two-burn mission capability by attempting restart of the main engines after a 25-minute orbital coast.

Execution of a two-burn mission with a cryogenic system presented unique problems of propellant management under low-gravity conditions. To explore the mechanics of this problem and to develop required design information, an experiment in coast-phase propellant management was conducted on the AC-4 vehicle launched December 11, 1964. The configuration for the AC-4 flight was based on the results of theoretical studies and scale-model tests. Results of this Centaur experiment were very significant and revealed the following:

(1) Large liquid disturbances were generated in the residual propellants at main engine cutoff (MECO)(All symbols are defined in the appendix)

(2) Suppression and dissipation of MECO-induced disturbances required more propellant settling thrust than predicted and also a more positive means of energy dissipation

(3) Failure to settle propellants prevented successful venting of boiloff gases to maintain tank ullage pressure

(4) Liquid ingestion in the vent gas and resulting unbalanced vent thrust forces caused loss of vehicle control

As a result of this flight experience, valuable information was obtained to configure the AC-8 vehicle. The results also pointed out that the model scaling parameters do not account for vehicle induced disturbances in the liquid residuals; and therefore do not predict accurately the propellant behavior in a full-scale configuration. The following design changes were incorporated on the AC-8 vehicle to control propellant behavior and support a restart of the main engines after a low-gravity coast period:

(1) Positive means of energy dissipation. Disturbance of liquid residuals would be reduced and eliminated by addition of a slosh baffle in the tank and energy

dissipators on the LH_2 boost pump volute bleed, the LH_2 duct recirculation line, and the helium pressurization line

(2) Increased propellant settling thrust to suppress amplitude of liquid disturbances by addition of four 50-pound-thrust and four 3-pound-thrust H_2O_2 engines

(3) Uprated attitude control system using four 3.5-pound-thrust and two 6-pound-thrust engines

(4) Redesigned balanced thrust LH_2 vent system

(5) Addition of LH_2 liquid vapor and temperature sensors to define propellant behavior better during coast

In addition, increased performance was provided by use of the uprated RL10A3-3 engines and an improved guidance system flown for the first time on AC-8. The following test control criteria were used for the AC-8 flight:

Basic Structure:

(1) Demonstrate the structural integrity of the Atlas and Centaur vehicles during all powered phases of flight

(2) Verify the structural and thermal integrity of the Centaur nose fairing and insulation panels

Propulsion:

(1) Demonstrate the restart capabilities of the Centaur main engines system in the flight environment

(2) Demonstrate the capabilities of the H_2O_2 engines system to retain the propellants in the proper attitude for main engines restart

(3) Obtain data on the performance of the RL10A3-3 main engines system

(4) Obtain data on the performance of the H_2O_2 engines system

Guidance:

(1) Demonstrate the system integrity of the updated guidance system

(2) Demonstrate that the guidance system provides proper discrete and steering signals to the Atlas and Centaur flight control systems during closed-loop flight

(3) Demonstrate the parking orbit and the guidance equations and associated trajectory parameters of a two-burn mission

(4) Obtain data on the measuring accuracy of the guidance system

Flight Control:

(1) Demonstrate that the flight control system supplies proper signals for attitude control and dynamic stability of the Centaur vehicle

(2) Demonstrate the capability of the Centaur electromechanical timers for two-burn missions

Separation and Jettison:

(1) Demonstrate the spacecraft separation system

General Vehicle Systems:

(1) Demonstrate the capability of the Centaur to perform the revised retromaneuver
(2) Obtain data on the performance of the following Centaur systems:
    (a) Propellant utilization system
    (b) Propellant level indicating system
    (c) Hydraulic system
    (d) Pneumatic system
    (e) Electrical system
    (f) RF systems: telemetry, Azusa, and C-band beacon
(3) Obtain data on the performance of the instrumented Atlas systems

Launch Capability:

(1) Obtain data on the launch-on-time capability (fixed launch azimuth) of the Atlas Centaur

Environment:

(1) Obtain data on the following flight environments: pressures, temperatures, and vibration levels
(2) Obtain data on the space thermal radiation environment, vehicle acceleration, propellant behavior and heat transfer, and propellant tank ullage temperature and pressure histories during coast phase
(3) Obtain data on the orbital environments, terminal behavior, and general post-mission performance of vehicle systems until loss of all data links
(4) Obtain data on the spacecraft environment during the launch-to-spacecraft separation phase of flight

The AC-8 Atlas-Centaur vehicle was successfully launched from ETR Complex 36B on April 7, 1966 at 2000:02.090 EST.

III. PRELAUNCH HISTORY

SUMMARY

The Atlas-Centaur launch vehicle undergoes a series of preflight tests in the interval between arrival and launch day at ETR. These tests, which include (1) the Flight Control and Propellant Tanking Test, (2) the Flight Acceptance and Composite Test, and (3) the Composite Readiness Test, are to ensure that all airborne and ground-support systems are within specifications to support a successful launch. These tests were satisfactorily completed with only a few anomalies.

ARRIVAL AND ERECTION

The Atlas-Centaur launch vehicle (AC-8) arrival at ETR began with the Atlas (184D) booster on January 22, 1966. The Centaur (6D) stage and the interstage adapter arrived January 24, 1966.

Erection of the Atlas booster, and the interstage adapter was completed at Complex 36B on January 28, and the Centaur stage was erected on January 31.

The Surveyor mass model arrived at ETR on January 24. The encapsulation of the model in preparation for preflight testing was accomplished on March 9, and it was mated to the launch vehicle on March 10. The encapsulated model was demated and decapsulated on March 12 for replacement of the S-band transponder. The encapsulated model was remated to the launch vehicle on March 14, demated on March 18 for final flight preparation, and remated to the launch vehicle on March 23 in preparation for launch.

FLIGHT CONTROL AND PROPELLANT TANKING TEST

The Flight Control and Propellant Tanking Test was conducted on March 17 to verify that the launch vehicle could be tanked with propellants and that all vehicle systems and the spacecraft could function properly under cryogenic and operational radiofrequency environments. Only minor discrepancies occurred during the test; these are listed in table III-I.

FLIGHT ACCEPTANCE COMPOSITE TEST

The Flight Acceptance Composite Test (FACT) was conducted on March 11 to verify that the combined Atlas-Centaur-Spacecraft systems were capable of operation with no detrimental interference when subjected to conditions simulating flight.

Because of several discrepancies encountered during the test (table III-I), several additional system tests were performed on the airborne circuits to verify that the telemetry and ordnance circuits were operational. The results of the test were evaluated as satisfactory.

COMPOSITE READINESS TEST

The Composite Readiness Test (CRT) was performed on March 24 to revalidate and verify the proper operation of the vehicle and GSE electrical systems. The test proceeded according to schedule and the results were satisfactory with only one discrepancy, as noted in table III-I.

LAUNCH

The first attempt to launch AC-8 was made on March 29. The count proceeded normally until T - 90 minutes at which time the built-in 1-hour hold was extended to 2 hours and 58 minutes because the winds aloft were unacceptable. Because of this additional delay, no hold was planned at T - 5 minutes. The winds remained unacceptable at T - 5 minutes, however, and a second hold was initiated. Thirty-seven minutes later, the count was resumed and proceeded normally. The engine start sequence was initiated at T - 8 seconds, but at T - 3 seconds the launch release sequence was interrupted because the Centaur aft umbilical panel failed to eject. The launch attempt was aborted and rescheduled for April 5.

The countdown for the second launch attempt began at T - 375 minutes with no planned holds and proceeded normally until T - 90 minutes. At this time, a hold was initiated because the winds aloft were unacceptable. The attempt was aborted 4 hours later.

The third launch attempt made on April 7 was successful, and the vehicle lifted off from ETR Complex 36B at approximately 2000.02 EST, only 2 seconds after the planned T - 0.

SURFACE WEATHER

The atmospheric conditions on launch day were favorable. Surface winds were 7 knots from 0^{o}, visibility was 15 miles (unrestricted), and the temperature was 64^{o} F. Cloud cover was at 20 000 feet and scattered.

WINDS ALOFT

The predicted loads from winds aloft were severe throughout the AC-8 launch operation activities. Predicted vehicle loads due to winds aloft are listed chronologically.

March 29 Launch Attempt: During this countdown, the predicted wind loads increased and changed in both shear and peak velocity. The count was held at T - 90 minutes for 3 hours until the wind profile improved, at which time the count was resumed.

April 5 Launch Attempt: During this countdown, the winds aloft again gave predicted loads above allowable. The count was held at T - 90 minutes for 4 hours. The winds gave no indication of subsiding, and the second attempt was cancelled.

April 7 Launch: The soundings taken early in the morning indicated predicted loads above allowable (caused by a peak velocity of 174 knots and maximum shear of 20 knots per thousand feet). Monitoring of the wind profile during the day, however, indicated improvement of the situation and, at the time of launch, loads were within allowable limits.

AC-8 PRELAUNCH HISTORY - 1966

Arrival of Atlas 184D	January 22
Arrival of interstage adapter	January 24
Arrival of Centaur 6D	January 24
Arrival of payload	January 24
Arrival of nose fairing	January 24
Erection of Atlas 184D	January 28
Erection of interstage adapter	January 28
Arrival of insulation panels	January 31
Erection of Centaur 6D	January 31
Erection of insulation panels	March 4
Mating of encapsulated payload	March 10
Flight Acceptance Composite Test	March 11

Flight Control and Propellant Tanking Test	March 17
Demating of encapsulated payload	March 18
Mating of encapsulated payload	March 23
Composite Readiness Test	March 24
Attempted launch	March 29
Attempted launch	April 5
Launch	April 7

TABLE III-I. - TEST OPERATIONS DISCREPANCIES

Test	Anomaly	Cause
Flight Control and Propellant Tanking Test	Several Atlas LO_2 level probes were reading erratically.	Calibration shift in probe control units.
	Atlas LO_2 temperature at fill and drain valve was out of tolerance.	LO_2 supply was depleted except for 900 gallons.
Flight Acceptance Composite Test	The Centaur umbilical P401 failed to eject.	Mechanical interface problem with nonflight hardware.
	Interruption of release ladder by loss of telemetry signal.	Wiring design error.
	Failure of ordnance (squib simulator box) circuit to respond.	Either error in test harness wiring or incorrect setting on squib simulator box.
Composite Readiness Test	One retrorocket circuit, one insulation panel detonator circuit, and one Atlas-Centaur separation detonator (squib simulator) did not activate.	Critical current range (fuse, relay) response in squib simulator box.

IV. MECHANICAL GROUND-SUPPORT EQUIPMENT

SUMMARY

All mechanical ground-support equipment functioned satisfactorily during the preflight testing and the launch countdown. All specifications were met except for minor deviations that had no apparent detrimental effect on vehicle performance.

PROPELLANT LOADING SYSTEMS

No problems were observed in the performance of the propellant loading systems. Since there were no holds after start of tanking, the usage of LO_2 and LHe were minimal.

PRESSURIZATION SYSTEMS

All pressurization systems performed within required limits. Gas supply pressures were easily maintained above minimum allowable values, as noted in table IV-I.

ENVIRONMENTAL CONTROL SYSTEM

Except for minor deviations, the environmental control system provided the required gas conditioning supply temperatures and flow rates to the vehicle. Flow rates were determined from recorded duct pressures, which had previously been correlated with flow rates by using the permanent flowmeters in the system. Table IV-II is a comparison of specified and actual values.

UMBILICAL BOOM SYSTEM

Centaur Aft Umbilical Panel

Failure of the Centaur aft umbilical panel (figs. IV-1 and IV-2) to eject resulted

in the launch abort on March 29, 1966. Field testing performed at ETR on March 30, 1966, however, could not duplicate the failure. Additionally, a series of tests was conducted at the Point Loma boom test site to determine the cause of failure, but results of these tests were inconclusive. Possible problem areas were investigated, and the following changes were made to increase confidence in the system:

(a) By a minor procedural change, pressure in the 3000-psig helium bottle charge line was relieved prior to panel ejection.

(b) The seal between the airborne half of the panel and the chute on the interstage adapter was positioned below the surface of the chute, and a thin plate was installed over the top of the seal to provide a continuous smooth surface.

(c) The pneumatic pressure that is applied to the panel for primary ejection was lowered from 1200 psig to approximately 750 psig.

(d) All critical dimensions were checked and determined to be within tolerance. No dry film lubrication was applied to any portion of the ground or airborne panel.

After incorporation of these modifications, three successful ejections were accomplished on April 1, 1966.

Boom System Operation

The movement of booms and lanyard cylinders were within specified travel times except for the T - 0 cylinder, which was slightly fast. Table IV-III provides a comparison of specified and actual values.

LAUNCHER

Launcher holddown cylinder pressure blew down from a nominal 5750 to 2480 psig in 0.18 second; specification was 0.45 second maximum. Blowdown time from 2480 to 350 psig was 0.45 second; specification was 0.50 second maximum.

PROPELLANT USAGE

Propellant usage was determined from readings taken at 1630 and 2100 EST. Gas usage was not determined since most gas storage vessels were being charged after 1630 EST. A summary of propellant usage is given in the following table:

Propellant	Available, gal		Consumed, gal
	At 1630 EST	At 2100 EST	
LN_2, Complex 36A	14 000	12 500	1 500
LN_2, Complex 36B	27 700	25 500	2 200
LO_2	39 250	11 950	27 300
LH_2	25 200	12 500	12 700
LHe	900	840	150
RP-1	13 500	1 050	12 450

TABLE IV-I. - PRESSURIZATION SYSTEMS

System supply	Minimum required pressure, psig	Actual minimum, psig
Primary helium	1500 up to engine start	5200
Emergency helium	3500 up to engine start	5200
Routine GN_2	2300 up to area clear	4300
Environmental GN_2	540 up to T - 0	2300

TABLE IV-II. - ENVIRONMENTAL CONTROL SYSTEM

Location	Temperature, ^{o}F		Flow, lb/min	
	Specified	Actual	Specified	Actual
Payload	70±5	70 to 71.5	75±5	69
Electronic compartment	[a]55±5 [b]65^{+5}_{-0}	[a]52 [b]65 to 69	[a]70±5 [b]100±5	[a]70 [b]99
Interstage adapter	[c]110±5 [d]140±5	[c]114 to 116 [d]136 to 143	[c]130±30 [d]130±5	[c]129 [d]136
Atlas pod	50 max	50.5	32 min	32
Atlas thrust section	[e]180 to 147	170.5 to 174.5	[e]60 to 80	76 to 78

[a]Using air.

[b]Using GN_2.

[c]Prior to tanking.

[d]After tanking start.

[e]Over the ranges specified, minimum required temperature is inversely proportional to flow rate.

TABLE IV-III. - UMBILICAL BOOM SYSTEM

Component	Travel time, sec	
	Specified	Actual
T - 4 lanyard cylinder upper boom	0.80 to 0.96	0.91
T - 4 lanyard cylinder lower boom	1.20 to 1.60	1.59
T - 0 lanyard cylinder lower boom	0.80 to 0.96	0.76
Lower boom		
T - 0 to 13.0°	1.10 to 1.70	1.40
T - 0 to 35.0°	2.30 to 3.20	2.60
T - 0 to 55.0°	3.30 to 4.40	3.93
Upper boom		
T - 0 to 3.0°	0.40 to 1.50	0.54
T - 0 to 21.0°	1.60 to 3.00	1.91
T - 0 to 50.0°	3.40 to 4.70	4.58

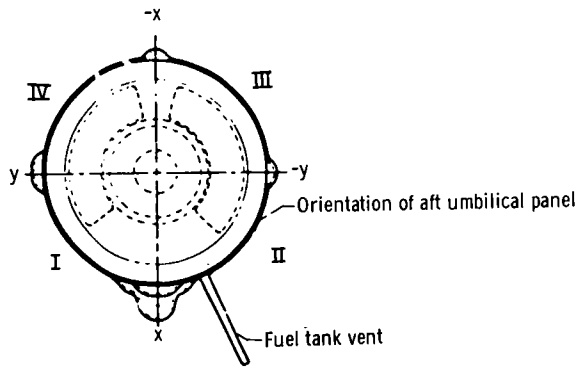

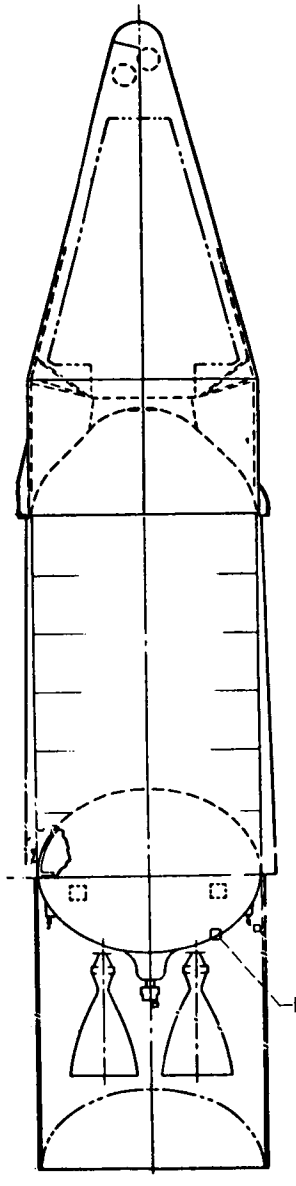

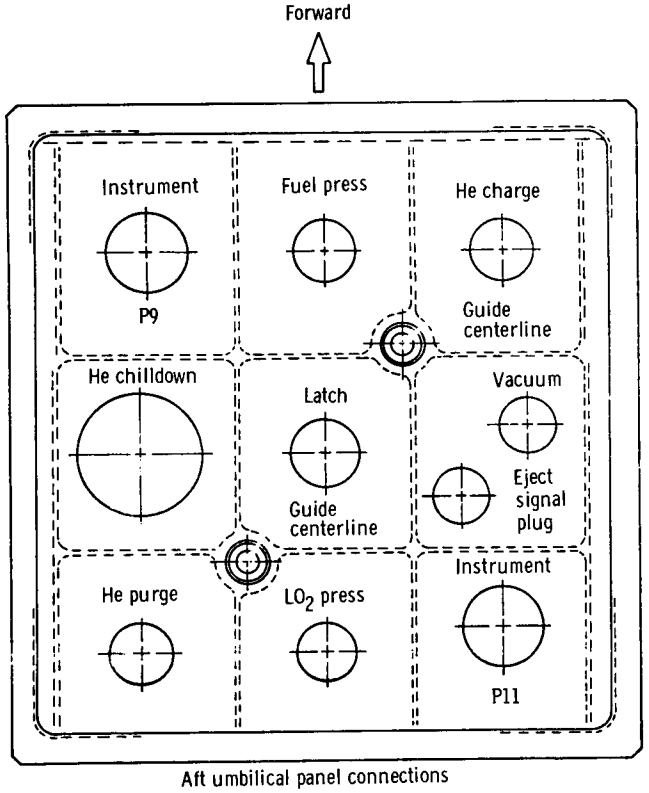

Aft umbilical panel connections

Figure IV-1. - Centaur aft umbilical panel.

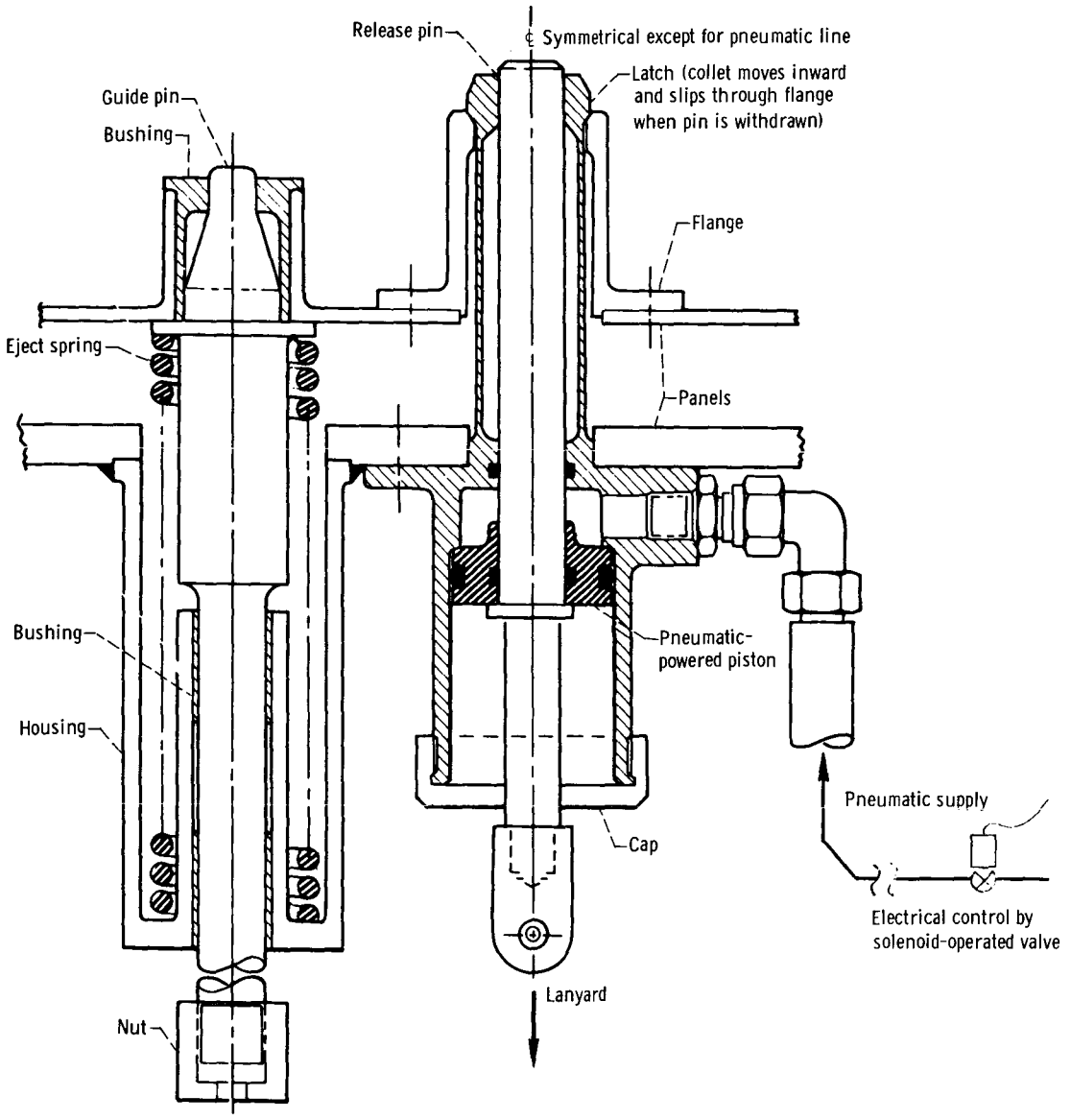

Figure IV-2. - Aft pneumatic umbilical panel and ejection mechanism.

V. TRAJECTORY

SUMMARY

The AC-8 mission was designed to exercise a simulated lunar transfer employing an indirect mode of ascent. As such, the AC-8 vehicle was targeted to pass through a specified point in space at a specified time consistent with fixed launch azimuth, coast time, and orbital energy constraints. Injection into a lunar transfer trajectory was not achieved because the Centaur second burn was not successfully completed. Consequently, consideration was given only to the portion of the flight from lift-off to insertion into the parking orbit. The most significant deviations from the predicted profile were the early occurrence of SECO and lower-than-nominal Centaur engine thrust, both of which were compensated for by a longer-than-planned Centaur engine burn time. There were sufficient excess propellants available to provide for both the added burn time and the additional velocity required to achieve the mission energy if the second burn had been normal.

VEHICLE DESCRIPTION AND FLIGHT PROFILE

The general arrangements of the Atlas, Centaur and mass model spacecraft are shown in figures V-1 to V-3. The launch vehicle is a two-stage configuration consisting of an Atlas first stage and a Centaur second stage. Both stages are 10 feet in diameter and are connected by an interstage adapter.

The Atlas stage, including the interstage adapter, is 75 feet long and is powered by a standard MA-5 propulsion system consisting of two booster engines of 165 000 pounds thrust each, a single sustainer engine of 57 000 pounds thrust, and two vernier engines of 1000 pounds thrust each.

The Centaur stage, including the nose fairing that shrouds the mass model spacecraft, is 48 feet long. Centaur is a high-specific-impulse space vehicle powered by two RL10A hydrogen-oxygen engines of 15 000 pounds thrust each. The RL10 was the first hydrogen-fueled engine to be flown successfully in space.

A schematic diagram of the planned flight profile is shown in figure V-4. The Atlas-Centaur vehicle rises vertically from lift-off until 15 seconds of flight time has elapsed. During this interval, the Atlas-stage Flight Control System rolls the vehicle

from the launcher-alined azimuth to the desired flight azimuth. The vehicle then executes a preprogramed pitch maneuver in the downrange direction. Termination of the booster-phase flight is initiated by a staging discrete (BECO) issued by Centaur guidance when an acceleration level of 5.7 g's is sensed. The booster package is jettisoned 3.1 seconds after the staging discrete is issued.

Centaur guidance steering signals are admitted to the Atlas-stage autopilot 8 seconds after BECO, and the system operates in a closed-loop mode throughout the remainder of the flight. During the sustainer-phase, the insulation panels and nose fairing are jettisoned. The sustainer phase is terminated by a discrete (SECO) from a pressure sensor in the sustainer engine fuel manifold in response to propellant depletion and causes the sustainer and vernier engines to be shut down. Two seconds later, the Atlas and Centaur stages are separated.

Prior to SECO, the Atlas programer initiates the Centaur-stage prestart sequence. The boost pumps are started and brought up to speed. Propellants are flowed through the Centaur fuel and oxidizer systems, chilling down the hardware to preclude cavitation at Centaur MES-1.

The signal for starting the RL10 engines is issued by the Centaur programer. Guidance steering commands are nulled at SECO and readmitted at MES + 4 seconds after the engine start transient has passed. Centaur MECO 1 is commanded by the guidance system when the required velocity for insertion into a 90-nautical-mile circular orbit has been achieved.

Subsequent to injection into the parking orbit, two 50-pound-thrust rocket motors provide initial propellant settling. This phase is programed for a nominal duration of 100 seconds, after which a set of two 3-pound rockets provides a continuous propellant retention thrust throughout the parking orbit coast until the start of prestart events for the second Centaur burn.

The second burn is preceded by operation of two 50-pound rockets to ensure positive propellant settling prior to MES 2, BPS, and engine-chilldown phase. The Centaur engine cutoff (MECO 2) is commanded by the guidance system when the required target orbit conditions are achieved.

Subsequent to termination of second Centaur-powered phase, the programer provides timed discretes for separating the spacecraft from Centaur, for reorienting the Centaur stage, and for the retromaneuver sequence.

A comparison of predicted and actual AC-8 flight event times is presented in table V-I.

TRAJECTORY EVALUATION

The predicted trajectory and performance of AC-8 were based on the mission,

weights, and performance parameters contained in reference 1. The atmospheric model used was that contained in references 2 and 3 together with the April wind profile of reference 4. The postflight trajectory data were based on the best estimate of trajectory (ETR) (from Best Estimate of Trajectory, RCA/AFETR). A postflight weight summary for Atlas and Centaur is presented in table V-II. Wind and atmospheric data were obtained from Rawinsonde measurements.

RAWINSONDE ATMOSPHERE DATA

Atmospheric conditions were determined at the launch site at 1930 EST, approximately 30 minutes before lift-off. Profiles of measured pressures and temperatures as a function of altitude are compared with the predicted values in figures V-5(a) and (b), respectively. Only slight variations were evident between the measured and preflight data. Launch wind magnitude and direction as a function of altitude are compared with the predicted April wind profile obtained from reference 4 in figures V-5(c) and (d).

Comparisons of the preflight dynamic pressure and Mach number profiles with the profiles derived from references 5 and 6 are presented in figures V-6(a) and (b), respectively. Both preflight dynamic pressure and Mach number were very close to predicted profiles except from T + 60 to T + 90 seconds where the actual data were somewhat lower than predicted.

TRAJECTORY DATA

The AC-8 trajectory was targeted such that it would pass through a specified point in space at a specified time consistent with the fixed azimuth, parking orbit coast time, and orbital constraints.

Adequate telemetry and tracking coverage of second Centaur engine start from ground station at Pretoria, South Africa dictated a launch azimuth of 103 degrees and a parking orbit coast time of 25 minutes. Centaur second burn was to be terminated upon attainment of an orbital energy of -0.85 kilometer squared per seconds squared, which would have resulted in the injection of the mass model into a highly elliptical Earth orbit characteristic of a 63-hour lunar transfer ellipse.

Since the AC-8 vehicle did not successfully complete its second burn, position and velocity are shown for only the phase of powered flight through insertion into the 90-nautical-mile parking orbit. Figure V-7 presents comparisons of actual and predicted vehicle position as a function of flight time and as viewed in the vertical and horizontal planes. The AC-8 vehicle followed the predicted path very closely during the Atlas phase of the flight and was slightly depressed during the Centaur phase caused primarily by the

velocity loss due to an early SECO (see table V-I) and a lower-than-nominal Centaur engine thrust. This combination resulted in a longer-than-planned Centaur burn time. The effect of the early SECO can also be seen in figure V-8, which compares predicted and actual flight histories of inertial velocity. Profiles of axial load factor as a function of flight time are presented in figure V-9.

The successful injection of AC-8 into a parking orbit yielded the following comparison of predicted and measured orbital parameters:

Parameter	Predicted	Measured	
		ETR	Goddard
Eccentricity	0.000745	0.00238	0.001952
Inclination, deg	30.8392	30.824	30.8416
Semimajor axis, n. mi.	3531.52	3541.2	3537.64
Perigee height, n. mi.	84.95	90.5	86.68
Apogee height, n. mi.	90.21	107.4	100.49
Period, min	87.73	88.095	88.06

Attainment of injection into the simulated lunar transfer orbit was not possible because of the failure of the Centaur engines to complete the second burn. The parameters of the final orbit of the Centaur and the mass model are as follows:

Eccentricity	0.0085192
Inclination, deg	30.7496
Semimajor axis, n. mi.	3564.0
Perigee height, n. mi.	92.3
Period, min	89.25

The Centaur tank reentered the atmosphere on April 17, 1966.

Assuming that the Centaur engine performance during the second burn would have been similar to that of the first burn, there would have been sufficient excess propellants on board to compensate for the early SECO and low Centaur engine thrust and to provide the additional velocity required to achieve the desired orbital energy of -0.85 kilometers squared per seconds squared.

TABLE V-1. - FLIGHT EVENTS SUMMARY

Event	Time, sec			Event	Time, sec		
	Programer	Nominal	Actual		Programer	Nominal	Actual
Lock LH_2 vent valve		T - 7	T - 7.7	Initiate Centaur propellant settling mode	MECO 1	T + 573.4	T + 575.5
Programer start, 2-in. rise		T + 0	T + 0	End Centaur propellant settling mode	MECO 1 + 100	T + 673.4	T + 675.5
Initiate roll program		T + 2	T + 2.0	Start Centaur propellant retention mode	MECO 1 + 100	T + 673.4	T + 675.5
Initiate pitch program		T + 15	T + 15.1	End Centaur propellant retention mode	MECO 1 + 1454	T + 2027.4	T + 2029.5
Unlock LH_2 vent valve		T + 69	T + 68.5	Start Centaur propellant settling mode	MECO 1 + 1454	T + 2027.4	T + 2029.5
Booster engine cutoff	BECO	T + 142.7	T + 142.2	Start boost pumps	MECO 1 + 1472	T + 2045.4	T + 2047.6
Jettison booster package	BECO + 3.1	T + 145.8	T + 145.3	Prestart	MECO 1 + 1490	T + 2063.4	T + 2065.5
Jettison insulation panels	BECO + 34	T + 176.7	T + 176.8	Start main engines (MES 2)	MECO 1 + 1500	T + 2073.4	T + 2075.5
Unlatch nose fairings	BECO + 60.5	T + 203.2	T + 202.1	Second main engine cutoff	MECO 2	T + 2180.7	T + 2094.5
Fire thruster bottles	BECO + 61	T + 203.7	T + 202.8	Centaur MECO 2 backup (MBU)	MES 2 + 116	T + 2189.4	T + 2191.5
Start Centaur boost pumps	BECO + 62	T + 204.7	T + 204.5	Preseparation arming signal, extend landing gear signal	MBU + 18	T + 2207.4	T + 2210.1
Sustainer engine cutoffs, vernier engine cutoff, start Centaur programer	SECO	T + 237.2	T + 229.5	Unlock omnidirectional antennas signal	MBU + 28.5	T + 2217.9	T + 2220.3
				High-power transmitter on signal	MBU + 49	T + 2238.4	T + 2241.2
Start hydraulic recirculating pump	SECO + 0.5	T + 237.7	T + 230.1	Electrical disconnect	MBU + 54.5	T + 2243.9	T + 2246.4
Separate first and second stage	SECO + 1.9	T + 239.1	T + 231.7	Spacecraft separate	MBU + 60	T + 2249.4	T + 2251.6
Prestart	SECO + 3.5	T + 240.7	T + 233.0	Begin Centaur orientation maneuver	MBU + 65	T + 2254.4	T + 2256.6
Start Centaur main engines	SECO + 11.5	T + 248.7	T + 241.0	Start Centaur lateral thrust	MBU + 105	T + 2294.4	T + 2296.7
Main engine cutoff	MECO 1	T + 573.4	T + 575.5	End Centaur lateral thrust	MBU + 125	T + 2314.4	T + 2316.6

TABLE V-II. - POSTFLIGHT WEIGHT SUMMARY

	Weight, lb
Centaur stage	
Basic hardware:	
Body group	994
Propulsion group	1 234
Guidance group	336
Control group	150
Pressurization group	195
Electrical group	255
Separation equipment	78
Flight instrumentation	539
Miscellaneous equipment	333
Spacecraft	1 730
Total	5 844
Jettisonable hardware:	
Nose fairing	2 033
Insulation panels	1 212
Ablated Ice	50
Total	3 295
Centaur residuals (at MECO 1):	
LH_2 residual	1 467
LO_2 residual	6 278
Gaseous H_2	69
Gaseous O_2	144
H_2O_2	202
Helium	8
Ice	12
Total	8 180
Centaur expendables (to MECO 1):	
Main impulse H_2	3 700
Main impulse O_2	18 991
Gas boiloff on ground H_2	20
Gas boiloff on ground O_2	17
Inflight chill H_2	24
Inflight chill O_2	33
Booster phase vent H_2	37
Booster phase vent O_2	36
Sustainer phase vent H_2	33
Sustainer phase vent O_2	24
Engine shutdown loss H_2	6
Engine shutdown loss O_2	19
H_2O_2	33
Helium	1
Total	22 974
Total tanked weight	40 293
Minus ground vent	37
Total Centaur weight at lift-off	40 256

	Weight, lb
Atlas stage	
Booster jettison weight:	
Booster dry weight	6 186
Booster residuals	1 123
Unburned lubrication oil	31
Total	7 340
Sustainer jettison weight:	
Sustainer dry weight	5 600
Sustainer residuals	2 826
Interstage adapter	1 050
Unburned lubrication oil	19
Total	9 495
Atlas flight expendables:	
Main impulse RP-1	76 561
Main impulse O_2	170 266
Helium-panel purge	6
O_2 vent loss	15
Lubrication oil	169
Total	247 017
Atlas ground expendables:	
Fuel	513
Oxidizer	1 734
Lubrication oil	3
Exterior ice	50
LN_2 in helium shrouds	140
Preignition GO_2 loss	450
Total	2 890
Total tanked weight	266 742
Minus ground run	2 890
Total Atlas weight at lift-off	263 852
Total Atlas-Centaur lift-off weight	304 108

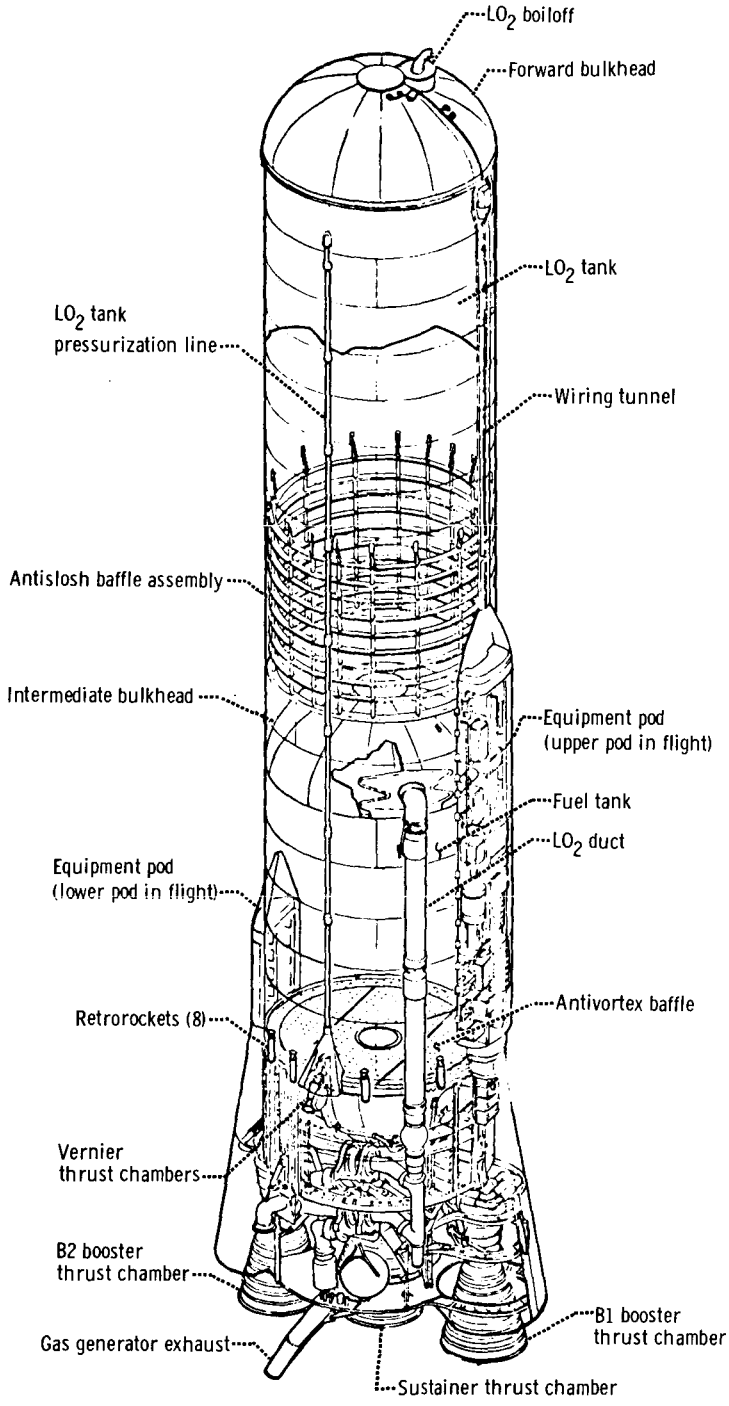

Figure V-1. - General arrangement of Atlas launch vehicle.

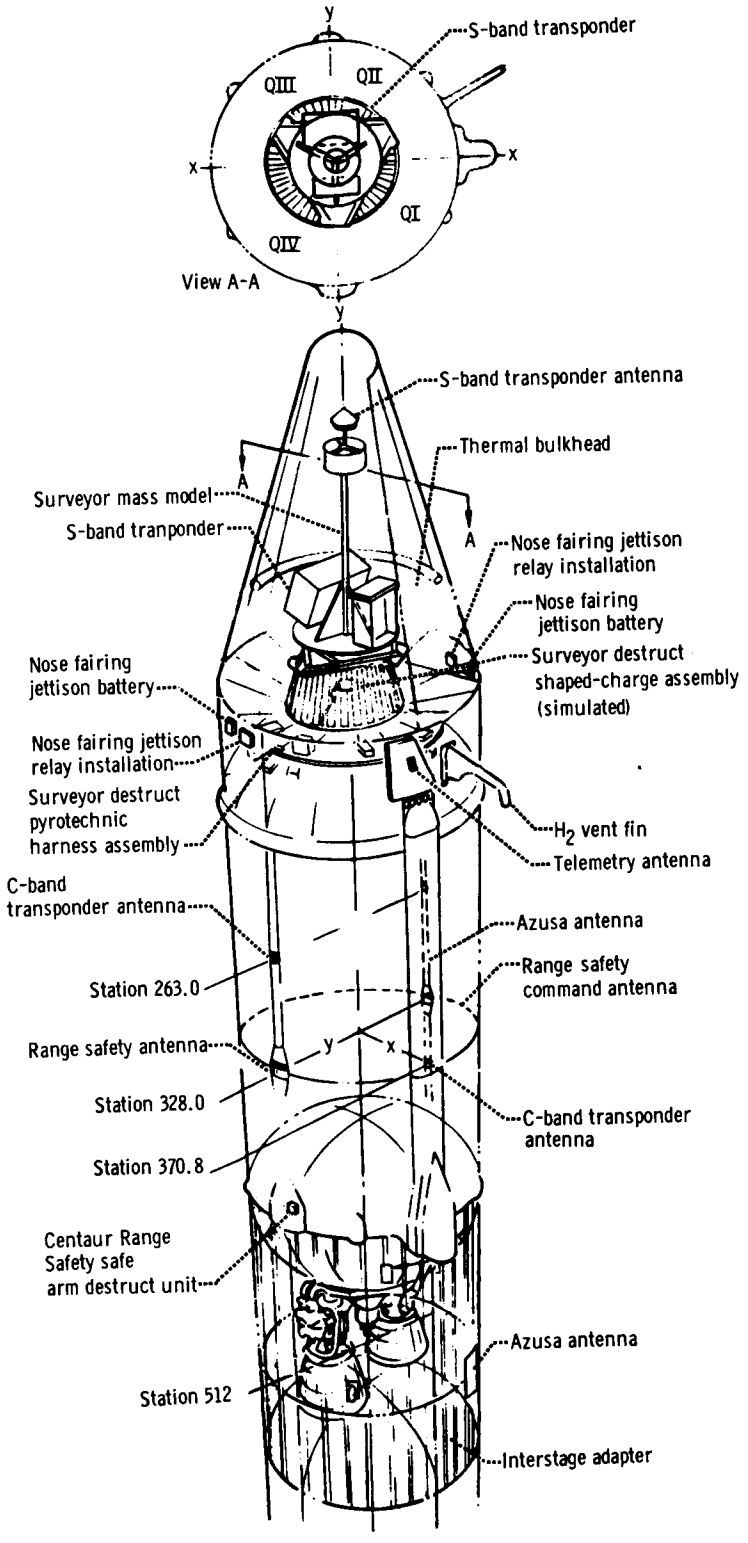

Figure V-2. - General arrangement of Centaur.

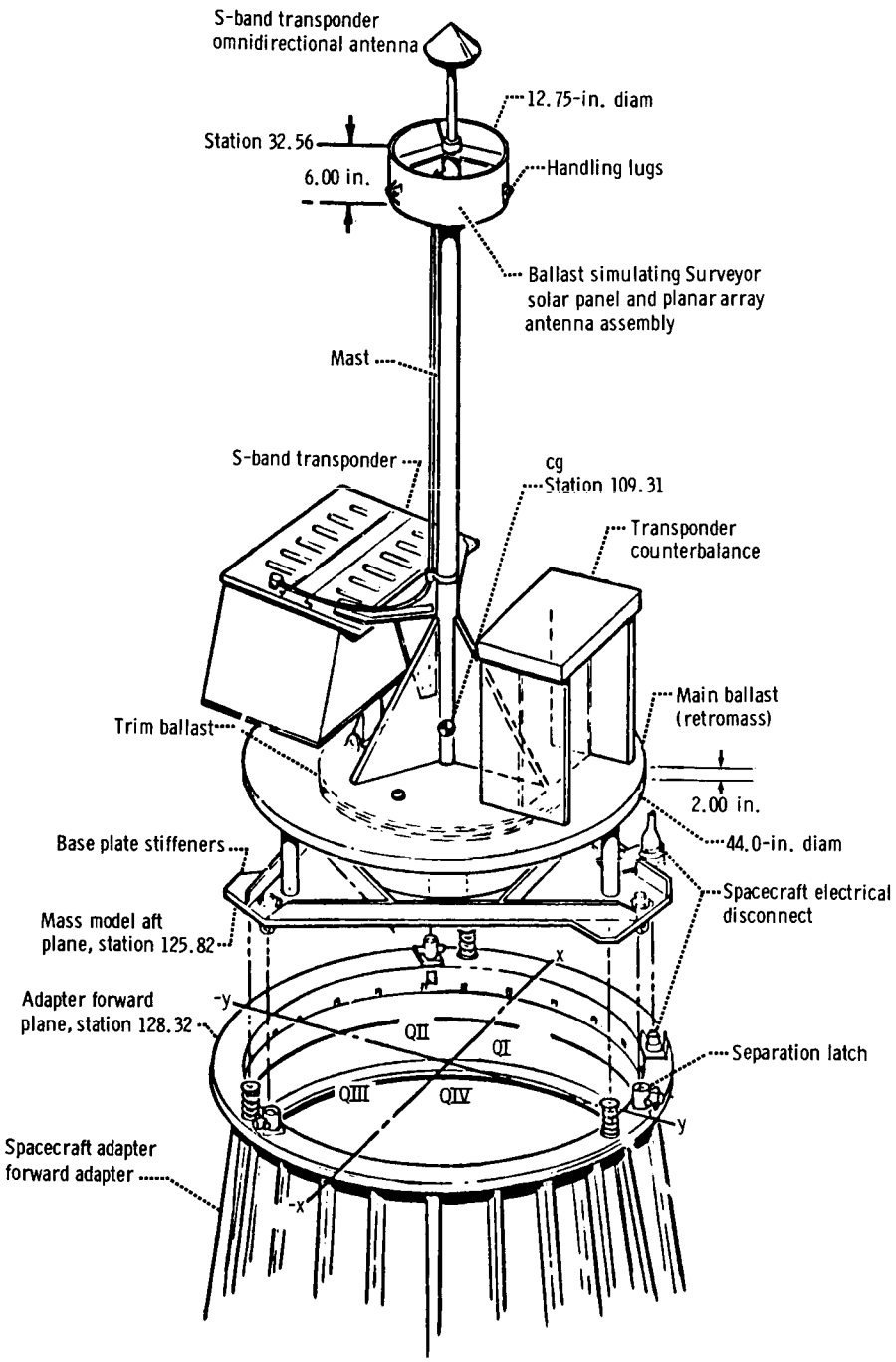

Figure V-3. - Mass model of AC-8.

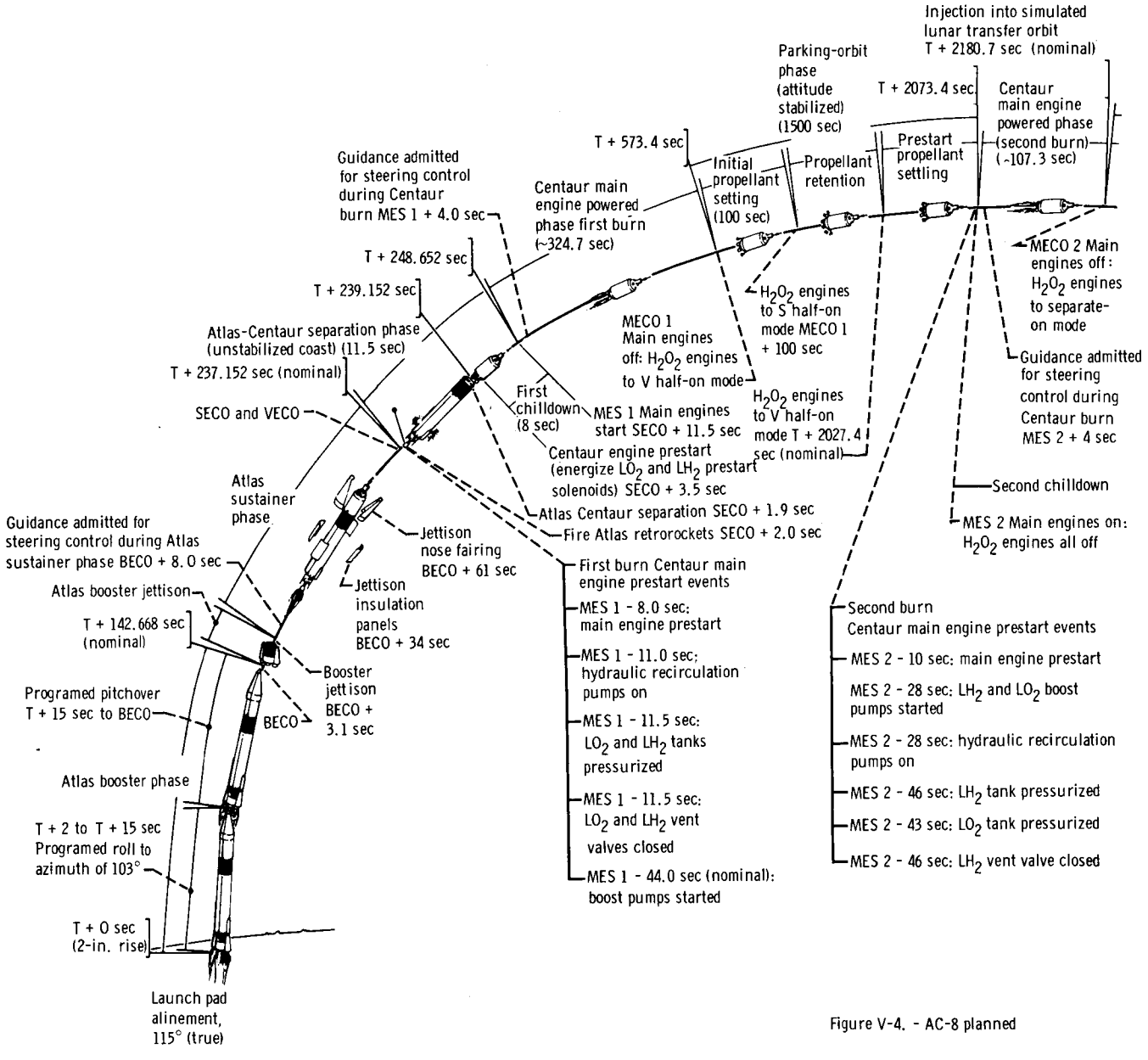

Figure V-4. - AC-8 planned

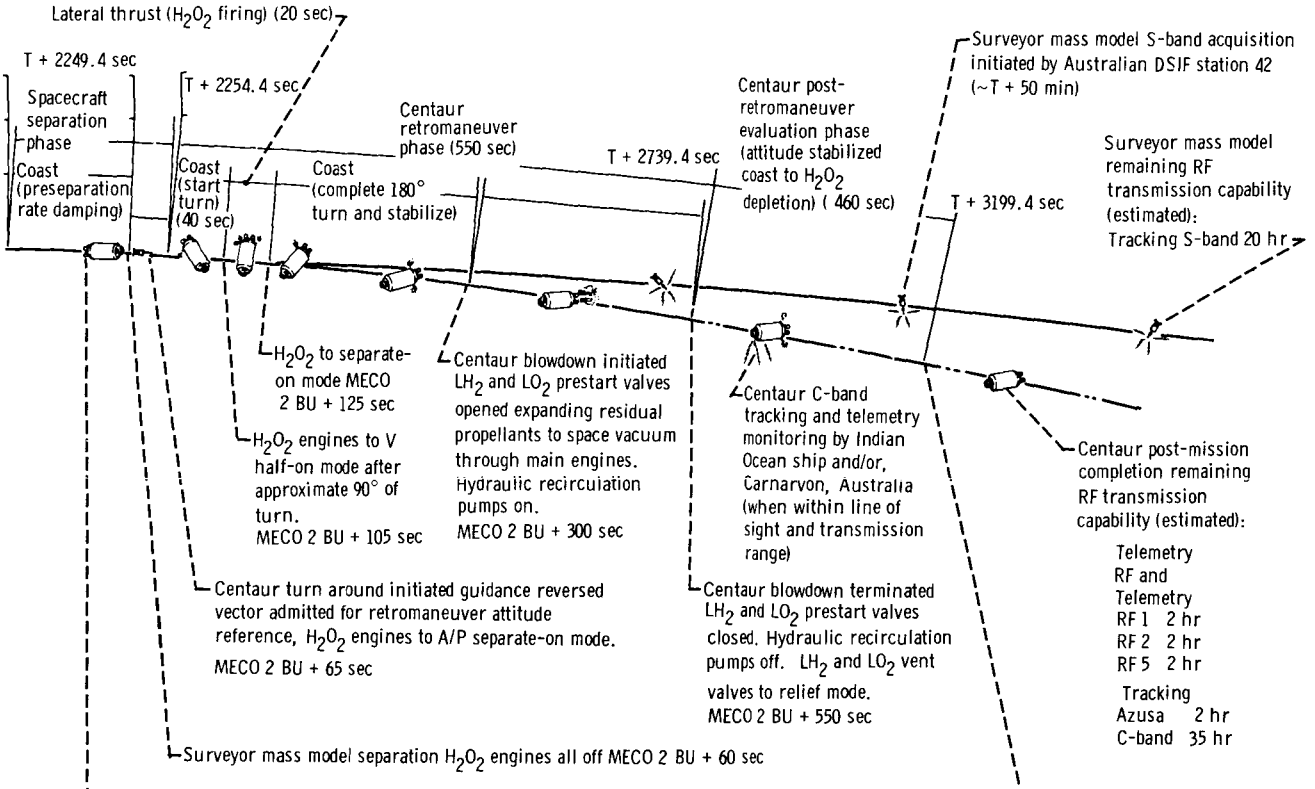

(1) Simulated functions - supporting research and development for operation Surveyor mission (Centaur programer signals only)
MECO 2 BU + 18: Surveyor preseparation arming
MECO 2 BU + 18: extend Surveyor landing legs
MECO 2 BU + 28.5: extend Surveyor omnidirectional antennas

(2) Active functions - supporting Surveyor mass model separation
MECO 2 BU + 49.0: switch S-band transponder transmitter to high power
MECO 2 BU + 54.5: separate electrical disconnect
MECO 2 BU + 54.5: switch Centaur telemetry to spacecraft separation channels

flight sequence compendium.

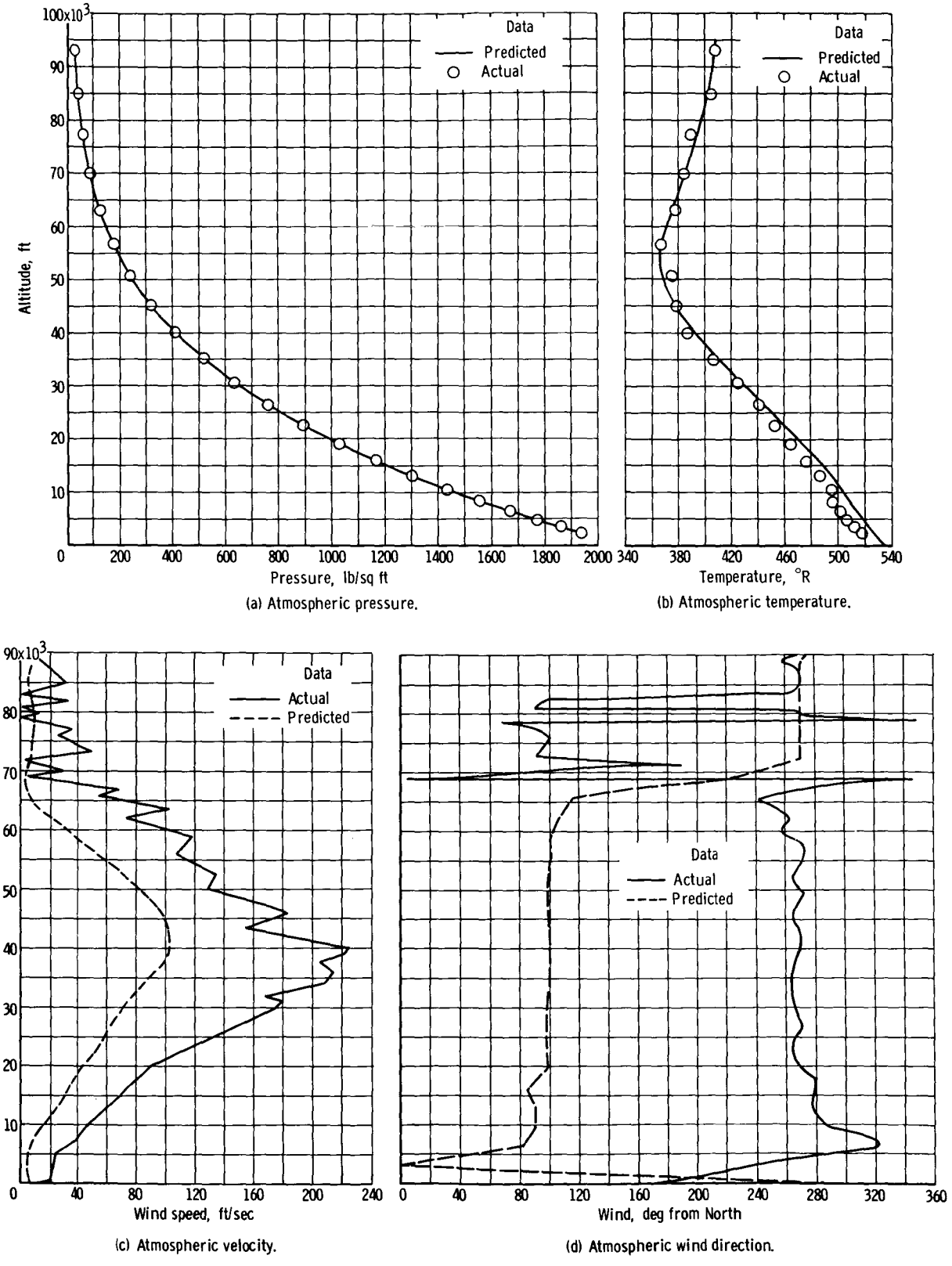

Figure V-5. - Launch conditions.

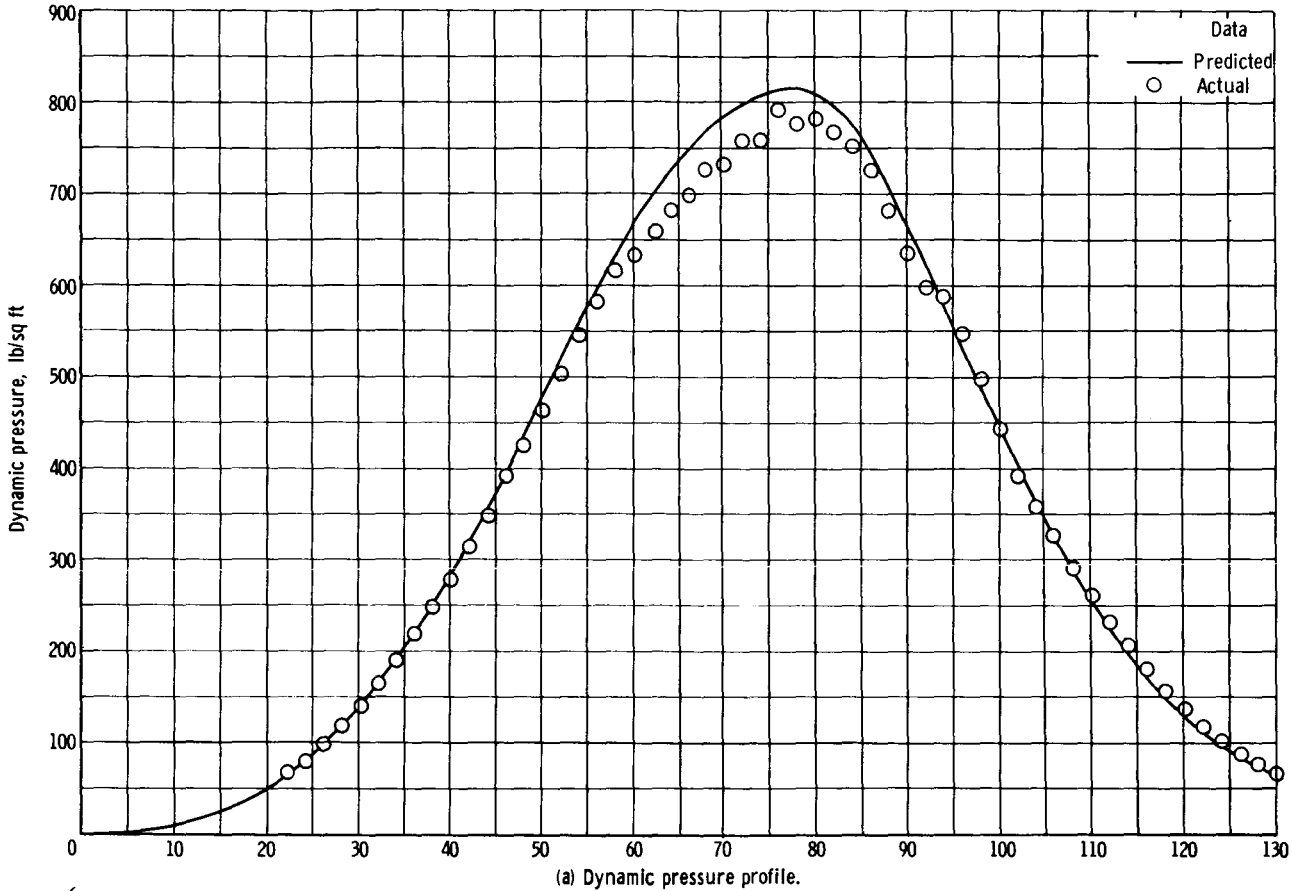

(a) Dynamic pressure profile.

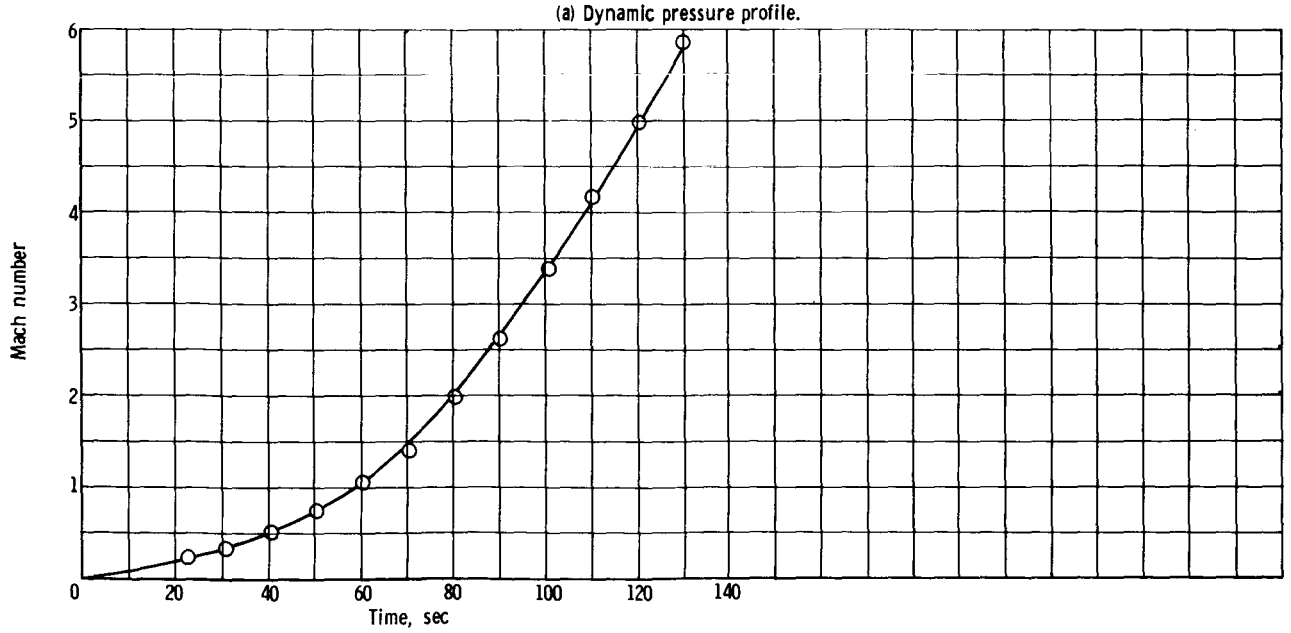

(b) Mach number profile.

Figure V-6. - Aerodynamic parameters of AC-8.

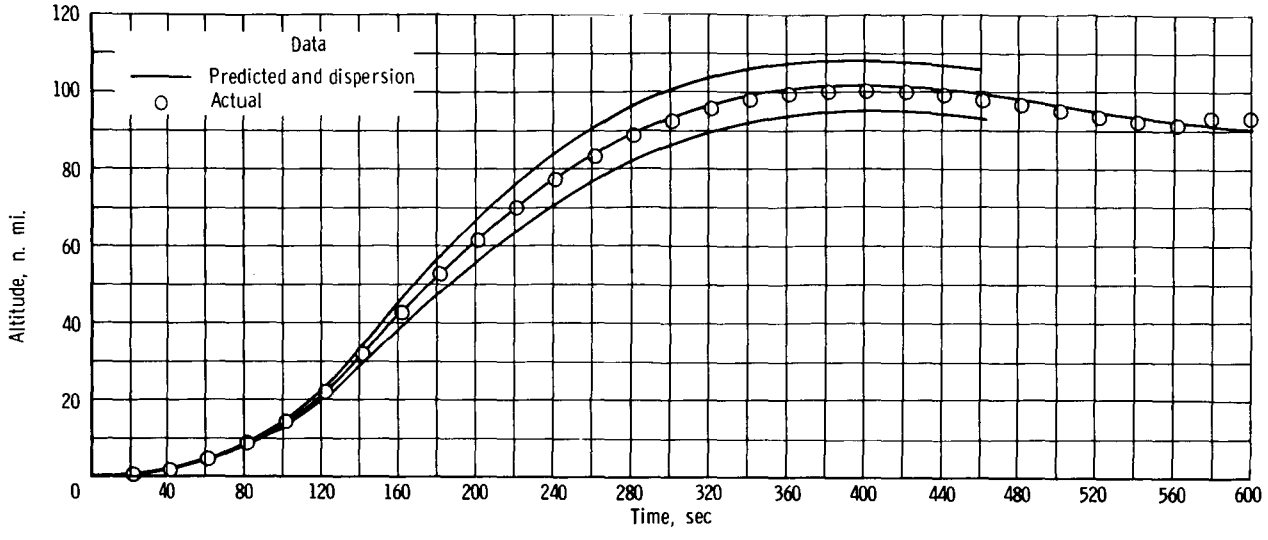

(a) Altitude against flight time.

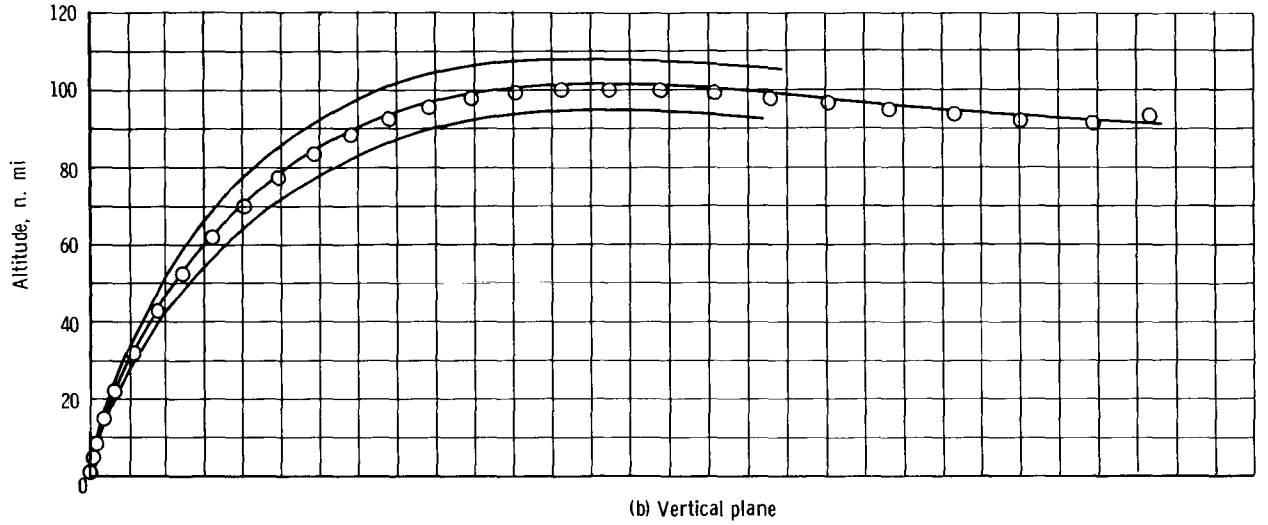

(b) Vertical plane

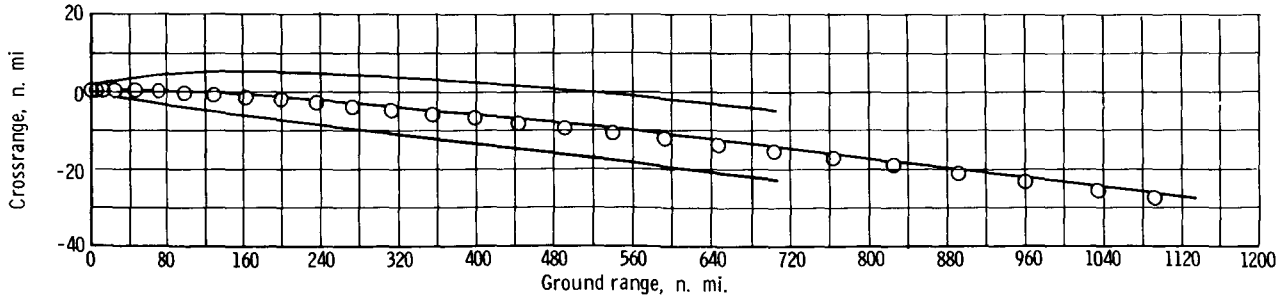

(c) Horizontal plane.

Figure V-7. - Trajectory position comparison of AC-8.

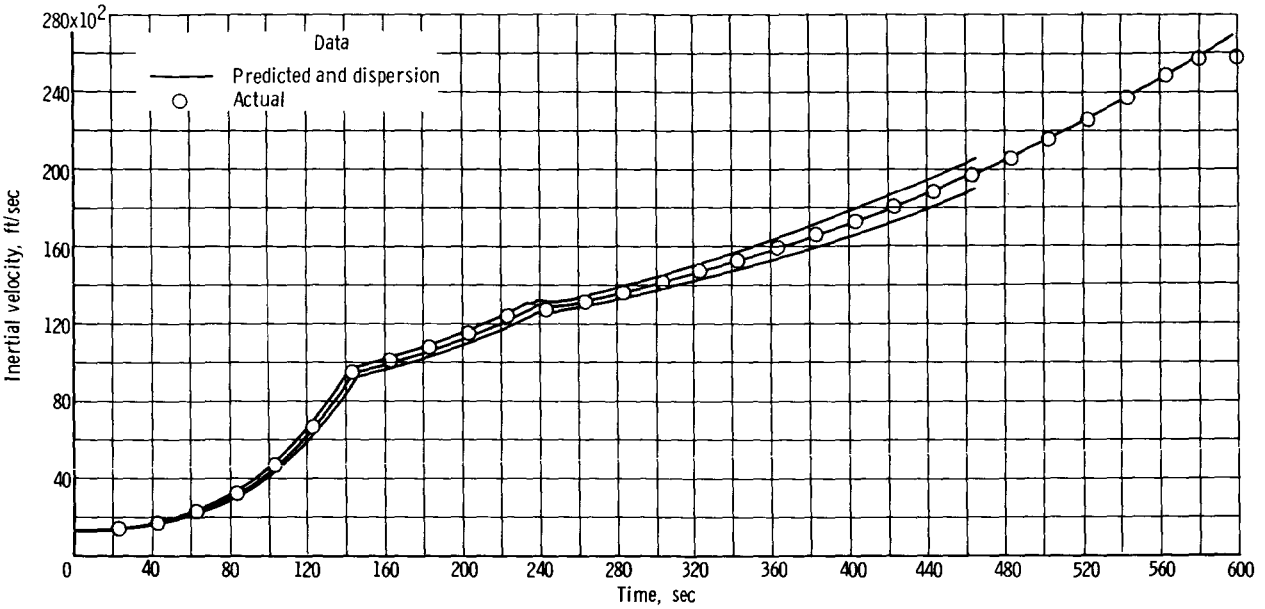

Figure V-8. - Comparison of inertial velocity of AC-8.

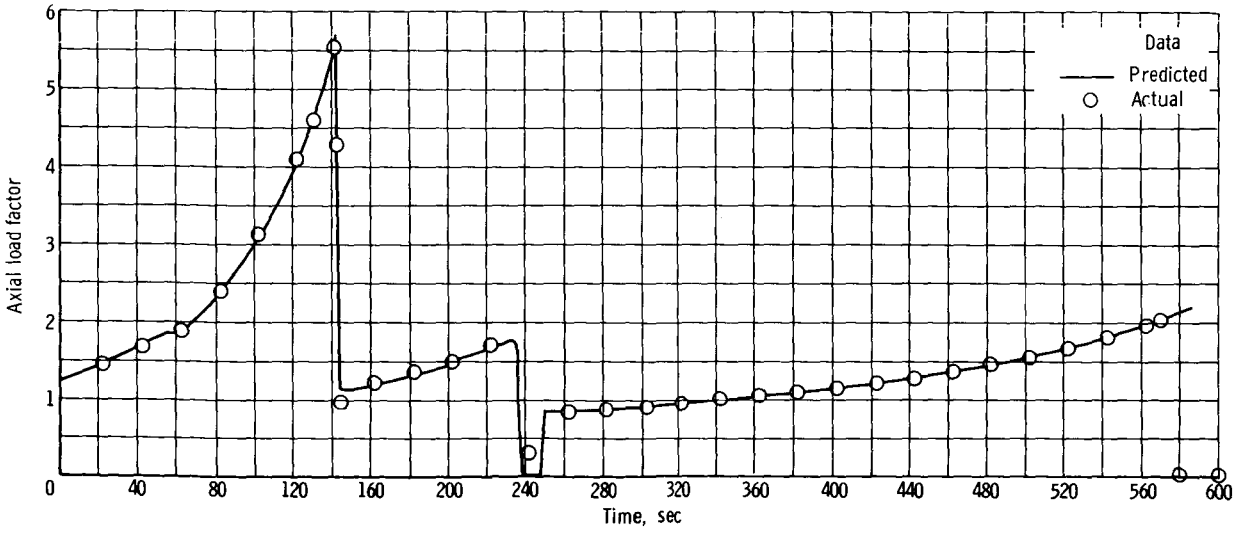

Figure V-9. - Comparison of axial load factors of AC-8.

VI. PROPULSION

SUMMARY

The Atlas and Centaur propulsion systems operated normally through Centaur MECO 1. Second engine burn, following a coast period of approximately 25 minutes, was not obtained as planned. Depletion of the H_2O_2 supply to the turbine drives prevented normal operation of both the LH_2 and the LO_2 boost pumps. A subsequent starvation of propellants to the main engines prevented sustained combustion of either engine. The cause of the H_2O_2 depletion has been attributed to leakage that developed in the S1 and S4 ullage settling engines during the coast phase.

ATLAS PROPULSION

Sustainer engine cutoff (SECO) occurred 8 seconds earlier than predicted because of fuel depletion. This early shutdown was caused by an abnormality in the propellant utilization system (see section VII PROPELLANT SYSTEMS). The early shutdown was compensated for by the performance margin of the vehicle. Steady-state operating conditions are presented with their predicted or acceptance tests values in table VI-I. Performance in terms of thrust, specific impulse, and mixture ratio is compared with predicted values in table VI-II.

CENTAUR PROPULSION

System Description

The AC-8 flight was the first to use prototype RL10A3-3 engines. The primary differences between this engine and those used on previous vehicles were an increase in nozzle expansion ratio (from 40:1 to 57:1), an improved propellant injector, improved turbopumps, and a full admission turbine. The engine was designed to provide higher specific impulse (increased from 433 to 444 (lb force)(sec)/lb mass) and to operate at lower pump net positive suction head (NPSH) levels. The increase in nozzle area ratio was achieved by a reduction in throat area and an increase in nozzle exit area. Chamber pressure was increased from 300 to 400 psia in order to retain the 15 000-pound thrust level per engine.

Disturbances to the fuel mass are introduced by the fuel boost pump volute bleed return flow during pump coastdown following MECO. To minimize these disturbances on

AC-8, the return flow rate was reduced from approximately 340 to 65 gallons per minute and an energy dissipator was installed at the point of entry to the tank. The power level of the fuel boost pump was reduced to prevent overspeeding of the pump during the dead-head period of operation prior to engine start. This power reduction was permissible because the main engine LH_2 pump NPSH requirement had been reduced from 8 to 4 psi, and the flow rate through the boost pump impeller was reduced approximately 275 gallons per minute.

Main Engine Performance

The first-burn engine start transient appeared normal. Thrust chamber pressure rise for the flight and for the engine acceptance tests are presented in figures VI-1 and VI-2, respectively. No significant chamber pressure overshoot, such as that experienced on AC-6, was observed. Turbopump speed reflected neither an overshoot nor a significant lead over chamber pressure during the start transient, as was experienced on AC-6. LH_2 and LO_2 pump inlet conditions for the engine start transient are presented in figures VI-3 and VI-4, respectively. No excursion beyond the steady-state operating limits occurred.

Turbopump housing temperatures during the booster phase of flight exhibited the same characteristics as were noted on AC-6. Fuel pump housing temperature (fig. VI-5) rose steadily to 168° R prior to prestart. LO_2 pump housing temperature (fig. VI-6) decreased slightly to 400° R during the same time period. Higher temperatures were observed on AC-6 and AC-8 than on AC-3 and AC-4. After the flight of AC-6, the temperature difference was attributed to a high thrust-section air-conditioning flow rate. Although the flow rate was reduced for AC-8, no apparent effect on the temperatures was noted. It is now believed that the throttling back of ground LHe flow rates during the AC-6 and AC-8 countdowns was responsible for these higher temperatures. No flight problems are anticipated because the inflight prestart sequence provides an adequate degree of turbopump chilldown prior to engine start.

The start total impulse to 95 percent of rated thrust was calculated to be 2400 and 2010 pound-seconds for the C1 and C2 engines, respectively. These values are within engine specifications.

Steady-state operation of the main engines appeared normal. Table VI-III compared some engine steady-state values with their nominal values. Steady-state performance in terms of thrust, specific impulse, and mixture ratio is presented in table VI-IV.

Chamber pressure decay for both engines began 0.06 second after the first MECO signal. This time delay is similar to those experienced on past flights.

Engine system temperature excursions during the coast phase between MECO 1 and MES 2 are presented in table VI-5. The fuel and LO_2 pump housing temperatures were warmer than any observed on past flights. The AC-8 pump housing temperatures are

compared with those of AC-4 in figure VI-7. The warmer temperatures on AC-8 have been attributed to impingement of the 50-pound H_2O_2 engine exhaust gases on the housing. Thrust chamber jacket temperature, however, was within the band of past flight experience. This was the first flight to utilize temperature patches on the engine bell.

Chamber pressure for the second-burn portion of the flight is presented in figure VI-8(a). Plots of turbopump speed, fuel pump inlet pressure, LO_2 pump inlet pressure, fuel pump discharge pressure, and LO_2 pump discharge pressure are presented in figures VI-9(b) to (f).

Although data from the C1 engine at second burn are similar to those observed during engine tests without ignition, a transient peak in fuel turbine inlet temperature indicated momentary combustion. Failure of LO_2 pump discharge pressure to rise indicated that no LO_2 was pumped to the combustion chamber even though pump speed reached a peak value of 12 600 rpm. Combustion was terminated in the C1 engine by MES + 2.0 seconds. The C2 engine chamber pressure, turbopump speed, and LH_2 discharge pressure began to rise; however, decaying started when the LO_2 side failed to pump. At MES + 1.9 seconds, LO_2 pump discharge pressure started rising, which caused engine chamber pressure, turbopump speed, and LH_2 discharge pressure to rise to their steady-state operating levels. At MES + 2.9 seconds, chamber pressure, pump inlet pressure, and pump discharge pressures began a slow decay. Pump speed began to rise as a result of increased turbine differential pressure. At MES + 18.5 seconds, cavitation of the engine fuel pump (evidenced by a spike in fuel pump inlet pressure) caused the engine to shut down. Following engine shutdown, fuel turbine inlet temperature went off scale high and remained there through programed MECO 2. Because there is not other known energy source adequate to cause such a temperature increase, it is assumed that the engine operated in a low idle mode during this time interval.

Failure of the engines to accelerate and to operate normally during second burn is attributed to a combination of insufficient turbopump cooldown and improper propellant inlet conditions. Both were caused by a depletion of the H_2O_2 supply to the boost pumps.

CENTAUR BOOST PUMPS

First Burn

Boost pump start (BPS) was initiated at T + 204.5 seconds. First indications of gas generator and turbine inlet pressure occurred approximately 1 second after BPS for both the oxidizer and the fuel units. Steady-state values, based on in-flight peroxide bottle pressures, were within 2 psi of predicted values (table VI-VI). Fuel unit gas generator and turbine inlet pressure oscillations of 100 psi peak-to-peak were evident from BPS 1

+ 60 seconds to BPS 1 + 180 seconds. These oscillations have been observed on past flights and ground testing and have no apparent effect on boost pump performance.

The early occurrence of Atlas SECO resulted in a boost pump deadhead time that was 7 seconds shorter than the nominal, but both units accelerated to adequate performance in the time allowed. Steady-state boost pump turbine speeds, shown in figure VI-9, were 2400 and 2300 rpm higher than expected for fuel and oxidizer units, respectively. These high turbine speeds correlate with the pump headrises (fig. VI-10) that were 0.5 and 6.5 psid higher than expected for fuel and oxidizer units, respectively. They also correlate with main engine oxidizer pump inlet pressures, which were approximately 5 psi high. None of these parameters, however, correlate with the boost pump gas generator and turbine inlet pressures.

Neither fuel nor oxidizer pump headrise dipped below the steady-state headrise during the engine start transient, which indicates a normal transient engine propellant flow demand. Oxidizer boost pump inlet pressure (fig. VI-11(a)) reflected the effects of the tank burp and increased from 33.5 psia at BPS to 44.4 psia at SECO. This increase resulted in a boost pump NPSP of 11.2 psi at SECO. The minimum LO_2 ullage pressure during the interval from SECO to MES was 39.7 psia, while the saturation pressure at the LO_2 boost pump inlet remained at 32.8 psia during the same time period. Thus, a pressure margin of +6.9 psi was provided to suppress gas bubble information.

Fuel boost pump inlet pressure (fig. VI-11(b)) increased from 21.4 psia at SECO to a maximum of 21.7 psia because of the fuel tank burp. Fuel and oxidizer boost pump turbine bearing, fuel boost pump peroxide control valve, and fuel boost pump Varobox temperatures are shown in figures VI-12(a) and (b) for the entire flight. No anomalies were evident.

Oxidizer and fuel boost pump inlet temperature measurements indicated liquid conditions from lift-off to MES 2, as shown in figures VI-12(c) and (d).

Second Burn

The second BPS signal was received at T + 2047.6 seconds. First indications of pressure were noted 1 second after BPS for the fuel and oxidizer gas generators and the fuel turbine inlet. The oxidizer turbine inlet pressure transducer failed and did not indicate any increase in pressure (fig. VI-13). Oxidizer gas generator inlet pressure became erratic immediately after BPS, and oscillations appeared in the fuel unit gas generator and turbine inlet pressures at BPS + 5 seconds. At BPS + 8 seconds, all three began to decay rapidly and reached approximately 10 psia at BPS + 28 seconds (MES 2). It appeared that the decay was caused by a reduction in peroxide flow, as opposed to a supply valve closure.

Fuel and oxidizer boost pump turbine speed and headrise appeared normal until BPS + 10 seconds and then decayed rapidly as a direct result of the decrease in turbine inlet pressure (fig. VI-15 and VI-16).

HYDROGEN PEROXIDE ENGINE SYSTEMS

System Description

The H_2O_2 engine system on AC-8 was utilized for (1) propellant settling and retention and attitude control of the vehicle during an extended coast in an Earth parking orbit, (2) attitude control after MECO 2, and (3) vehicle reorientation and retromaneuver after spacecraft separation. The engine configuration system, as shown in figures VI-16 to VI-18, was revised for this mission to include four 50-pound and four 3-pound vernier engines and two 3.5-pound and two 6.0-pound attitude control clusters.

Logic for the peroxide control system, as correlated with the two-burn mission profile requirements, is shown in figure VI-19. The required periods of 100-pound thrust for propellant settling or execution of the retromaneuver were obtained by firing the 50-pound verniers in a "half-on" mode. In this mode, the V2 and V4 engines were prime, but the system logic could switch the firing sequence if required for pitch or yaw control. The P attitude control engines also provided pitch control, and the A engines controlled yaw and roll. Both systems had a common threshold of 0.2 degree per second.

The 6-pound thrust level for the propellant retention during the extended coast phase was accomplished by a switch from the 50-pound engine half-on mode to the 3-pound engine half-on mode at MECO 1 + 100 seconds. System logic was similar to the 50-pound engine half-on mode; the S2 and S4 engines were prime, and the system threshold for attitude control was 0.2 degree per second. The 50-pound engines at this time, however, were in a "separate-on" mode and provided only backup attitude control in pitch or yaw with a threshold set at 0.3 degree per second. The P engines were deactivated during the coast period, and the A engines were used for roll control only.

Peroxide requirements to support the two-burn mission dictated that the peroxide bottle be filled to its maximum capacity of 234.5 pounds. Predicted consumption for the complete mission profile through the retromaneuver gave only a slight margin. Therefore, the leakage of peroxide during the coast phase preempted completion of the flight.

System Performance

Attitude control system performance through the boost-flight phase and midway into the coast phase was normal. Vernier engines provided scheduled thrust for propellant settling and sustained retention, and the attitude control engines adequately corrected any disturbances that may have caused vehicle rates in excess of the established 0.2-degree-per-second threshold. Midway through the coast period, however, at about T + 1360 seconds, there was indication of incipient system deterioration. Abnormal engine firing sequences and sudden cooling of the engine chamber and supply lines developed as a result of peroxide leakage through the engine assembly. This leakage culminated in a shortage of peroxide to operate the boost pumps and a premature termination of the second main engine burn. Discussion of these flight results has been divided, therefore, into four phases: (1) powered-flight phase (2) MECO 1 to T + 1360 seconds (3) T + 1360 seconds to peroxide depletion, and (4) failure analysis.

Powered-flight phase. - Performance of the peroxide system through this flight interval was satisfactory. H_2O_2 bottle and line temperatures, as shown in figures VI-20 and VI-21, were all normal. Termination of ground airconditioning at lift-off caused the line temperatures to drop off sharply, but they began to increase again at about T + 100 seconds as a result of aerodynamic heating. Supply line temperatures rose rapidly at first boot pump start (T + 205 sec) because of warm H_2O_2 flowing from the storage bottle. A similar increase was noted in the P1 and P2 engine supply line temperatures at MECO (T + 575 sec) when the H_2O_2 engines were fired. The increase in temperature of the LO_2 boost pump supply line at MECO was attributed to exhaust impingement from the 50-pound vernier engines, which were fired in the half-on mode for 100 seconds after MECO.

First main engine cutoff to T + 1360 seconds. - The first phase of the peroxide engine control sequence for the coast-phase propellant management, as shown in figure VI-17, was initiated at MECO. The four 50-pound engines were commanded on in the half-on mode, and the V2 and V4 engines fired to provide 100 pounds of thrust for 100 seconds. The 3.5- and 6.0-pound attitude control engines were commanded to a separate-on mode during this time, and both systems would have provided attitude control had the vehicle rates exceed a threshold of 0.2 degree per second.

Response of the system to the engine firing commands was confirmed by the respective engine chamber temperatures shown in figures VI-22 and VI-23 and the vehicle rate and acceleration data shown in figure VI-24. Chamber temperature on the V2 and V4 engines rose sharply to about 800° F during this time and then decreased rapidly at

MECO + 100 seconds when the engines shut down. Chamber temperature on the V1 engine, however, increased less rapidly, since it fired only intermittently. The V3 engine did not fire and did not indicate a temperature change.

Vehicle rate data during this time (fig. VI-24) indicated a relatively constant disturbing torque acting on the vehicle in pitch, yaw, and roll. This was attributed in part to a misalinement of the engine thrust axis. The primary cause, however, was the impingement forces of exhaust gases from the 50-pound engines against main engine nozzles and other components in the propulsion area. Although these disturbance torques were expected, they were larger than predicted, particularly in roll. As a result, a duty cycle of about 58 percent (19 percent was predicted) was required of the A1 and A3 engines to correct the roll error. The pitch error was corrected by periodic firing of P2 and V1, while V4 was cut off momentarily. Short pulses from A4, combined with A3, V1, and V2, corrected the small yaw error.

At MECO + 100 seconds (T + 675 sec), the V2 and V4 engines were programed off and S2 and S4 were programed on as the engine logic switched from the 50-pound half-on mode to the 3-pound half-on mode for the extended propellant-retention phase of the coast period, which required 6 pounds of thrust. The rise in chamber temperatures of S1, S2, and S4 at T + 675 seconds (figs. VI-22 and VI-23) verified that the 3-pound vernier engines fired as commanded. The slower rise of the S1 engine chamber temperature was due to its intermittent firing. S3 was not commanded on and did not show a temperature increase. The disturbance torques in roll, yaw, and pitch, caused by impingement forces of exhaust gases, were still encountered but to a lesser extent because of the reduced thrust level from 100 to 6 pounds. Corrections for these disturbances were made by intermittent firing of the A1, A3, and S1 engines.

T + 1360 Seconds to hydrogen peroxide depletion. - The coast-phase mission continued normally until about T + 1360 seconds, with the possible exception of an unexplained rise of the S4 chamber starting at about T + 1200 seconds. At T + 1360 seconds unexpected and abnormal changes in engine chamber temperatures and vehicle acceleration indicated the incipience of system malfunction. The S4 chamber temperature dropped sharply (fig. VI-23) even though the engine was firing, as shown by the engine commands and vehicle axial acceleration data in figure VI-24. Concurrently, the V4 engine, located adjacent to the S4 engine, indicated a sudden decrease in engine chamber temperature (fig. V-22). Twenty seconds later, the S1 chamber temperature started to decay, though more slowly than S4, and it failed to respond to any firing commands after T + 1443 seconds. The chamber temperature then continued to drop throughout the remainder of the coast phase.

The S4 engine was commanded off at T + 1486 seconds after it had fired almost continuously during the coast period. A few seconds later, it failed to respond to repeated firing commands, and it remained off throughout the remainder of the flight. Because the S1 and S4 engines were inoperative, there were periods of zero axial thrust on the vehicle. Attitude control was maintained throughout the remainder of the coast by periodic firing of the V1 and V4 vernier engines and other attitude control engines. Correlation of the vehicle rate, acceleration, and engine control firing commands during this coast phase period is shown in figure VI-25.

Beginning the MES 2 sequence at MES 2 - 46 seconds (T + 2030 sec), the engine control logic switched from the 3.0-pound half-on mode to the 50-pound half-on mode (fig. VI-19). V2 and V4 engines fired, as verified by the increase in axial acceleration, the rise in chamber temperature, and the related disturbing torques caused by impingement forces. Approximately 25 seconds later (T + 2055 sec), all peroxide engines failed to provide thrust, which caused a loss of vehicle acceleration and attitude control. The boost pump turbine drive also lost power, which indicated a depletion of H_2O_2.

Consumption of H_2O_2 up to this time, based on the commanded firing sequence, is summarized in table VI-VII. The engine "on times" were based on the summation of all firing commands. With nominal flow rates, it was estimated that a total of 182.32 pounds of H_2O_2 were consumed. The addition of 8 pounds of unusable residuals to this amount consumed still fails to account for 44.2 pounds of the 234.5-pound total that was tanked at lift-off.

Failure Analysis

The loss of peroxide, which culminated in failure to complete the second burn, was related to the observed degradation in control system performance starting at T + 1360 seconds. Correlation of other temperature measurements in the engine compartment in quadrant IV (figs. VI-26 and VI-27) and the LO_2 boost pump H_2O_2 supply line (fig. VI-20) also indicated significant changes in temperature at this time.

In general, the warmer temperatures above 0° F began to cool, and the colder subzero temperatures began to warm up. The attitude control bottle strut temperature, which had decreased about 5° F since MECO, started to cool more rapidly at T + 1500 seconds and dropped about 30° F in the next 500 seconds. Concurrently, the aft bulkhead insulation temperature, which had been decreasing, started to increase from -140° F to about -60° F. These temperature trends converging toward a range of 0° F to -30° F were attributed to the H_2O_2 leakage.

Hydrogen peroxide, like any other liquid when expanded into a vacuum, will freeze rapidly because of evaporative cooling. The freezing temperature of H_2O_2 at 1 atmosphere is 11° F. It has a tendancy, however, to supercool by as much as 40° F below its true freezing point. Leakage of H_2O_2 would then tend to drive the surrounding temperatures to around 0° F or slightly below. The possibility of a cryogenic leak is not likely, since such a leak would have tended to depress all surrounding temperatures and this did not happen.

Reconstruction of the flight performance of the peroxide control system (assuming a leak in the components) lends itself to the following explanation: the initial drop in chamber temperature of the S4 engine at T + 1360 seconds was the result of H_2O_2 leakage from the engine. Figure VI-28 shows a sectional drawing of the engine and the thrust chamber where the temperature was measured by a thermocouple clamped to the exterior surface. It is believed that H_2O_2 leaked from around the orifice holder assembly downstream of the flow control solenoid valve and, therefore, could only leak when the engine was commanded on. Since the engine was commanded on continuously during the time the chamber temperature was dropping, H_2O_2 was decomposing in the catalyst bed and the engine was producing thrust, as evidenced by the vehicle acceleration. However, H_2O_2, leaking from around the orifice holder assembly into the vacuum of space, cooled the external surface of the thrust chamber, which caused the sudden reduction in temperature. It is possible that the H_2O_2 froze and built up around the engine B-nut area while the engine was firing.

Later at T + 1486 seconds, S4 was commanded off, but a few seconds later, it failed to fire when commanded on again. During the time the engine was off, the catalyst bed cooled to the point where it would no longer decompose H_2O_2 when flow was resumed. The S4 engine thereafter was commanded on almost continuously. Under this mode of operation, it is likely that the leakage kept the catalyst bed cold and inactive. Also, because of reduced back pressure, the flow through a flooded catalyst bed increases by a factor of about 1.7 times that of a bed-supporting decomposition. Therefore, the external leakage, coupled with the increased flow rate through the inactive catalyst bed, accounts for the early depletion of the peroxide supply.

Leakage through the S1 engine appears to have resulted in the same manner. The failure mode of the engine was different because of its intermittant firing commands. Under this type of operation, evaporative cooling of the H_2O_2 leakage between firings froze the residual H_2O_2 in the heat barrier tube and thereby prevented further flow through the engine. The leakage was less than that experienced on the S4 engine, and the cooling of the thrust chamber appeared more like a normal engine shutdown in space. Temperatures around the S1 engine also did not show any unusual depression as was noted in the S4 engine area.

Leakage of the two S engines is attributed to differential thermal expansion in the overall engine assembly. A large aluminum B-nut, holds the thrust chamber to the heat barrier tube, as shown in figure VI-28. This maintains a metal-to-metal seal between the thrust chamber and the orifice holder and between the orifice holder and the bottom part of the heat barrier tube and the heat barrier. A large variation in temperature can take place in these components, depending on whether the engines are firing in a pulse or in a continuous mode. In addition, the yield strength of the aluminum B-nut is reduced at elevated temperatures.

Two modes of failure were therefore possible: the B-nut could have yielded at high temperatures or the sealing force could have been relaxed because of the potential high loads that were caused by differential thermal expansion. In either case, the seal around the orifice holder could open up and allow leakage. Once the leakage started, thermal changes in the different parts would be aggravated by the evaporative cooling of the H_2O_2 and could conceivably result in greater leakage.

In addition to the preceding theory of engine failure, it is also possible that a leak existed in the H_2O_2 feed system. A combination of leakage from the engines and the feed system would more readily account for the total amount of propellant lost.

TABLE VI-I. - ATLAS STEADY-STATE ENGINE OPERATING CONDITIONS

[Engine serial numbers: booster, 115171; sustainer, 225171; verniers, 335368 and 335341.]

Parameter	Time from lift-off, sec	Nominal value	Test value[a]	Flight value
Booster				
B1 pump speed, rpm	---	6302	A	6360
B2 pump speed, rpm	---	6348	A	6400
B1 LO_2 pump inlet pressure, psia	115	67.0	P	69.8
B2 LO_2 pump inlet pressure, psia	115	67.0	P	74.2
B1 fuel pump inlet pressure, psia	115	55.5	P	54.3
B2 fuel pump inlet pressure, psia	115	55.5	P	53.8
Booster gas generator chamber pressure, psia	100	518.1	A	527.4
B1 thrust chamber pressure, psia	100	573.5	A	580.1
B2 thrust chamber pressure, psia	100	576.9	A	581
Sustainer				
Pump speed, rpm	---	10 083	A	10 150
LO_2 pump inlet pressure, psia	195	55.1	P	45.3
Fuel pump inlet pressure, psia	195	47.0	P	45.7
LO_2 pump inlet temperature, ^{o}F	195	176.5	P	179.3
Fuel pump discharge pressure, psia	200	-----	-	982.7
Gas generator discharge pressure, psia	200	749.6	A	------
Thrust chamber pressure, psia	200	705.2	A	700
Vernier				
V1 thrust chamber pressure, psia	200	359	A	376
V2 thrust chamber pressure, psia	200	352	A	371

[a]A, acceptance data; P, predicted value.

TABLE VI-II. - ATLAS ENGINE PERFORMANCE (DEPRO PROGRAM)[a]

	Flight value	Predicted value
Thrust at lift-off, lb		
Boosters	326 400	325 009
Sustainer	55 834	57 738
Verniers, axial	1 489	
Total	383 723	382 747
Thrust at BECO, lb		
Boosters	374 758	375 544
Sustainer	80 252	81 637
Verniers, axial	1 716	
Total	456 726	457 181
Thrust at SECO, lb		
Sustainers	79 315	79 350
Verniers, axial	1 718	1 716
Total	81 033	81 066
Specific impulse at lift-off, sec		
Boosters	252.0	252.0
Sustainers and verniers	209.5	212.0
Total	244.5	245.0
Specific impulse at BECO, sec		
Boosters	288.1	287.8
Sustainers and verniers	305.7	298.3
Total	291.0	290.5
Specific impulse at SECO, sec		
Total	305.8	303.8
Oxidizer-fuel mixture ratio at lift-off		
Boosters	2.225	2.230
Sustainer and verniers	2.065	2.20
Oxidizer-fuel mixture ratio at BECO		
Boosters	2.335	2.348
Sustainer and verniers	2.560	2.28
Oxidizer-fuel mixture ratio at SECO		
Sustainer and verniers	2.521	2.539

[a]See ref. 5 for explanation of this technique.

TABLE VI-III. - CENTAUR MAIN ENGINE STEADY-STATE

OPERATING CONDITIONS FOR AC-8

Parameter	Nominal	MES + 90 sec	
		C1	C2
LH_2 pump total inlet pressure, psia	30.8	32.5	32.0
LH_2 pump inlet temperature, ^{o}R	38.3	38.3	38.9
LO_2 pump total inlet pressure, psia	59.8	69.2	68.2
LO_2 pump inlet temperature, ^{o}R	176.6	176.2	176.8
LO_2 pump speed, rpm	11 780	11 730	12 130
LO_2 pump discharge pressure, psia	582	598	592
LH_2 pump discharge pressure, psia	967	966	985
LO_2 injector Δ pressure, psid	54.6	57.6	53.4
LH_2 venturi upstream pressure, psia	703.0	719.3	714.0
LH_2 turbine inlet temperature, ^{o}R	353.7	375.9	379.8
Chamber pressure, psia	399.1	388.0	391.3

TABLE VI-IV. - CENTAUR ENGINE PERFORMANCE FOR AC-8

Parameter	Acceptance run	Time from MES 1, sec								
		10	50	90	100	150	200	250	300	330
C1 engine (SN 1905)										
Chamber pressure, psia		387	388	388	388.5	389	389	389	389	389
Thrust, lb force:	15 105									
PWA regression method[a]		15 078	15 077	15 077	15 415	14 870	14 979	14 984	15 012	15 013
PWA C* method[a]		14 548	14 601	14 595	14 800	14 511	14 617	14 615	14 584	14 608
Specific impulse, (lb force)(sec)/lb mass:	442.3									
PWA regression method		441.8	441.8	441.8	436.3	444.9	443.4	443.3	442.9	442.8
PWA C* method		441.3	441.2	441.2	439.7	441.9	441.3	441.3	441.5	441.4
Oxidizer-fuel mixture ratio:	5.163									
PWA regression method		5.119	5.114	5.114	5.737	4.661	4.895	4.910	4.960	4.968
PWA C* method		5.019	5.060	5.044	5.499	4.751	5.003	4.998	4.920	4.980
C2 engine (SN 1906)										
Chamber pressure, psia		385.3	391.3	391.3	391.3	391.3	391.3	391.3	391.3	391.3
Thrust, lb force:	15 126									
PWA regression method		15 121	15 113	15 113	14 450	14 893	15 009	15 008	15 036	15 057
PWA C* method		14 802	15 808	15 078	15 262	14 957	15 058	15 040	15 037	15 058
Specific impulse, (lb force)(sec)/lb mass:	443.2									
PWA regression method		442.3	442.4	442.4	436.8	445.7	444.1	444.1	443.7	443.4
PWA C* method		442.5	441.4	441.4	437.4	443.9	441.9	442.4	442.4	441.9
Oxidizer-fuel mixture ratio:	5.178									
PWA regression method		5.161	5.140	5.141	5.764	4.662	4.918	4.913	4.970	5.009
PWA C* method		5.185	5.342	5.334	5.887	4.936	5.270	5.212	5.203	5.272

[a]See appendix C of ref. 6 for explanation of techniques.

TABLE VI-V. - COAST-PHASE TEMPERATURE SUMMARY FOR CENTAUR PROPULSION AC-8

Parameter	Engine	Time, sec						
		MECO 1	MECO 1 + 100	MECO 1 + 200	MECO 1 + 1000	MES 2 - 75	Second prestart	MES 2
LO_2 pump housing[a]	C1	212.1 °R	375.2 °R	364.7 °R	385.7 °R	421.2 °R	427.7 °R	404.7 °R
	C2	209.7	353.2	347.7	362.7	362.7	406.2	379.7
LH_2 pump housing[a]	C1	41.3	117.2	144.5	208.4	256.7	263.2	79.0
	C2	41.3	102.8	128.9	189.2	234.7	239.7	41.8
Thrust chamber jacket	C1	148.2	211.5	210.3	218.3	228.9	229.4	228.5
	C2	140.3	224.7	223.0	223.0	219.6	229.0	230.6
Engine bell station 489	C1	140.4	217.2	224.1	298.2	-----	-----	333.4
	C2	147.2	258.7	253.8	298.5	-----	-----	313.6
Engine bell station 504	C1	122.9	323.1	323.1	333.2	-----	-----	368.6
	C2	156.7	313.6	248.8	343.8	-----	-----	379.4
Engine bell station 518	C1	185.4	229.2	248.8	320.6	-----	-----	336.8
	C2	118.2	224.6	249.2	309.0	-----	-----	334.2

[a]Primary rise in housing temperature occurred during 100-second interval following MECO 1 as result of H_2O_2 impingement.

TABLE VI-VI. - CENTAUR OXIDIZER AND FUEL

BOOST PUMP TURBINE AND GAS GENERATOR

INLET PRESSURE, FIRST BURN

Pressure, psia	Time from boost pump start, sec			
	10	40	180	370
LH_2 gas generator	97.0	102.0	105.8	105.5
LH_2 turbine inlet	89.2	95.5	98.0	100.0
LO_2 gas generator	109.3	113.1	113.3	113.3
LO_2 turbine inlet	96.6	101.4	102.6	102.6

TABLE VI-VII. - AC-8 HYDROGEN

PEROXIDE CONSUMPTION

[Time, T - 0 to T + 2058 sec.]

Unit	Firing time, sec	Nominal flow rate, lb/sec	Consumption, lb
Boost pumps	379	0.089	33.7
P1	0	0	0
P2	3.7	.0388	.15
A1	99.0	.0225	2.23
A2	1.0	↓	.02
A3	99.7	↓	2.24
A4	2.5	↓	.06
V1	9.6	.333	3.20
V2	122.6	.333	40.80
V3	0	0	0
V4	127.1	.333	42.40
S1	555.0	.0199	11.05
S2	778.0	↓	15.49
S3	210.0	↓	4.18
S4	1337.7	↓	26.80
		Total	182.32

Total H_2O_2 tanked	234.5
Total H_2O_2 consumed	-182.32
Total unusable residual	-8.00
Leaked or unaccountable	44.18

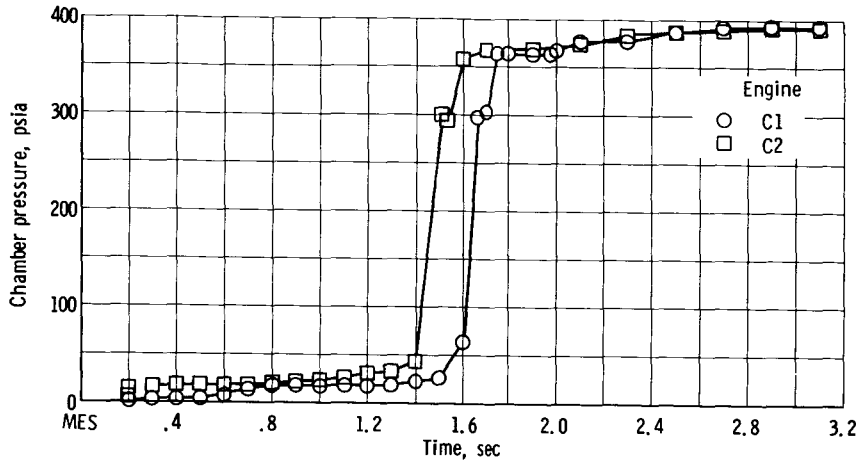

Figure VI-1. - Centaur chamber pressure start transient at first main engine start.

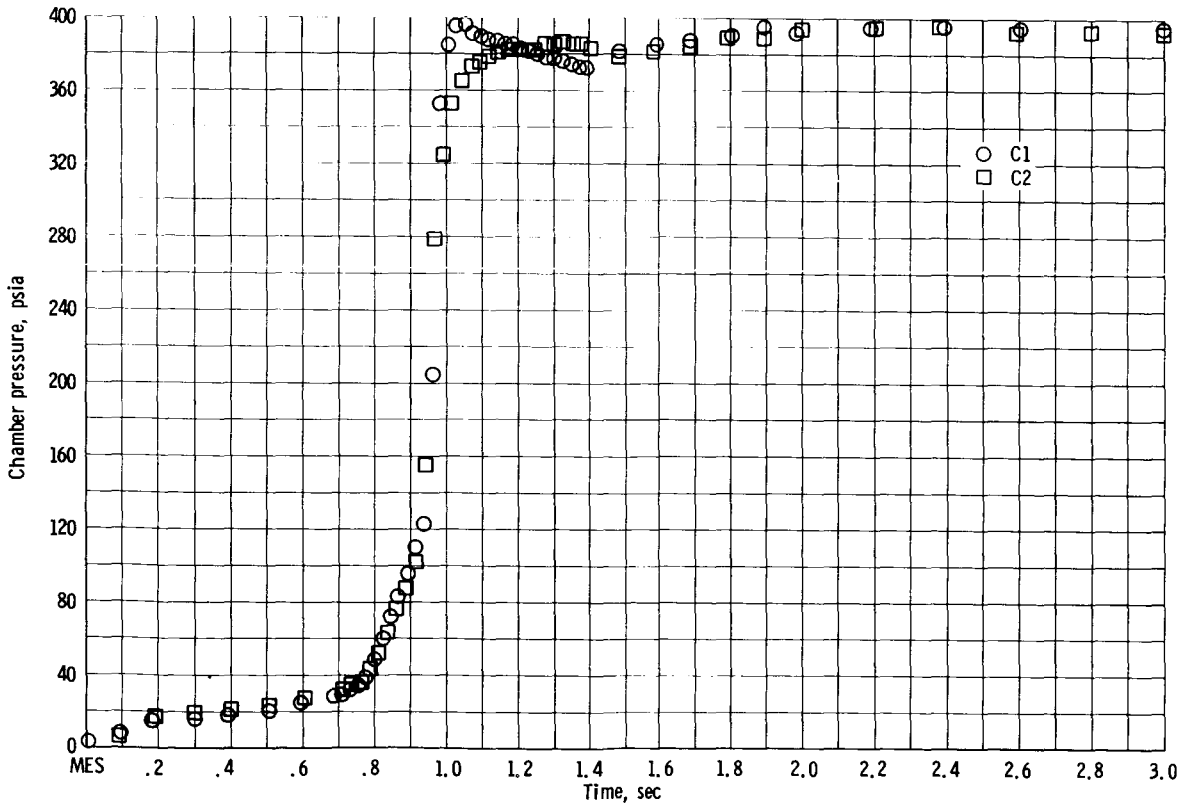

Figure VI-2. - Centaur engine chamber pressure start transient for engine acceptance test.

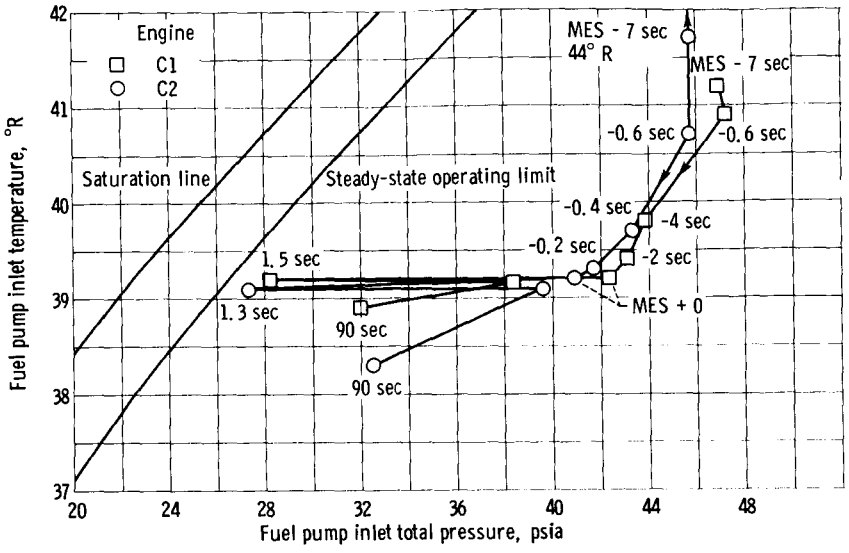

Figure VI-3. - Fuel pump inlet conditions at first engine start.

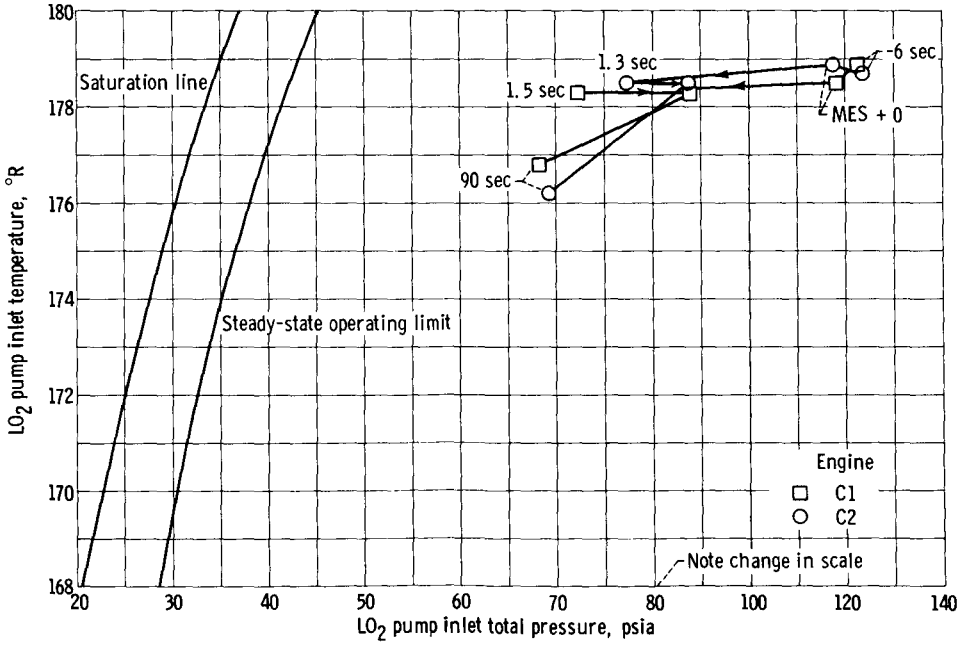

Figure VI-4. - Liquid oxygen pump inlet conditions at engine start.

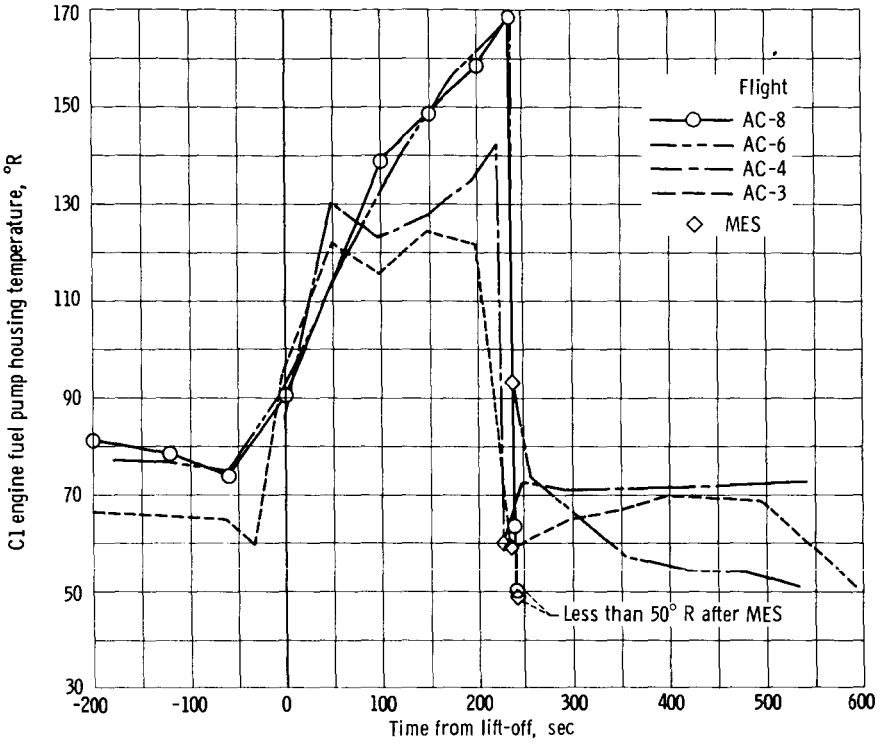

Figure VI-5. - Fuel pump housing temperature.

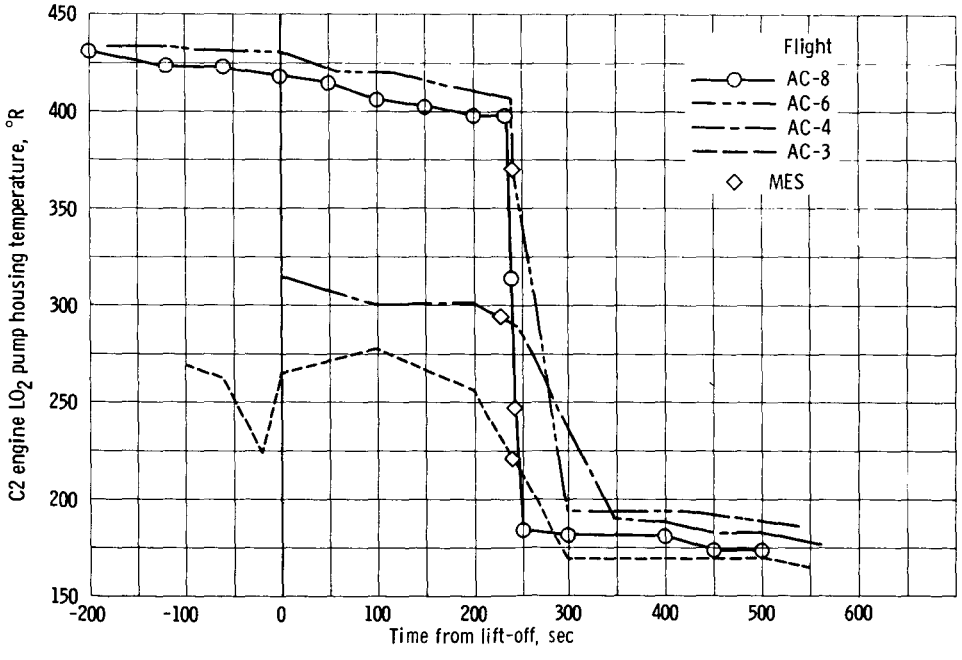

Figure VI-6. - Liquid oxygen pump housing temperature.

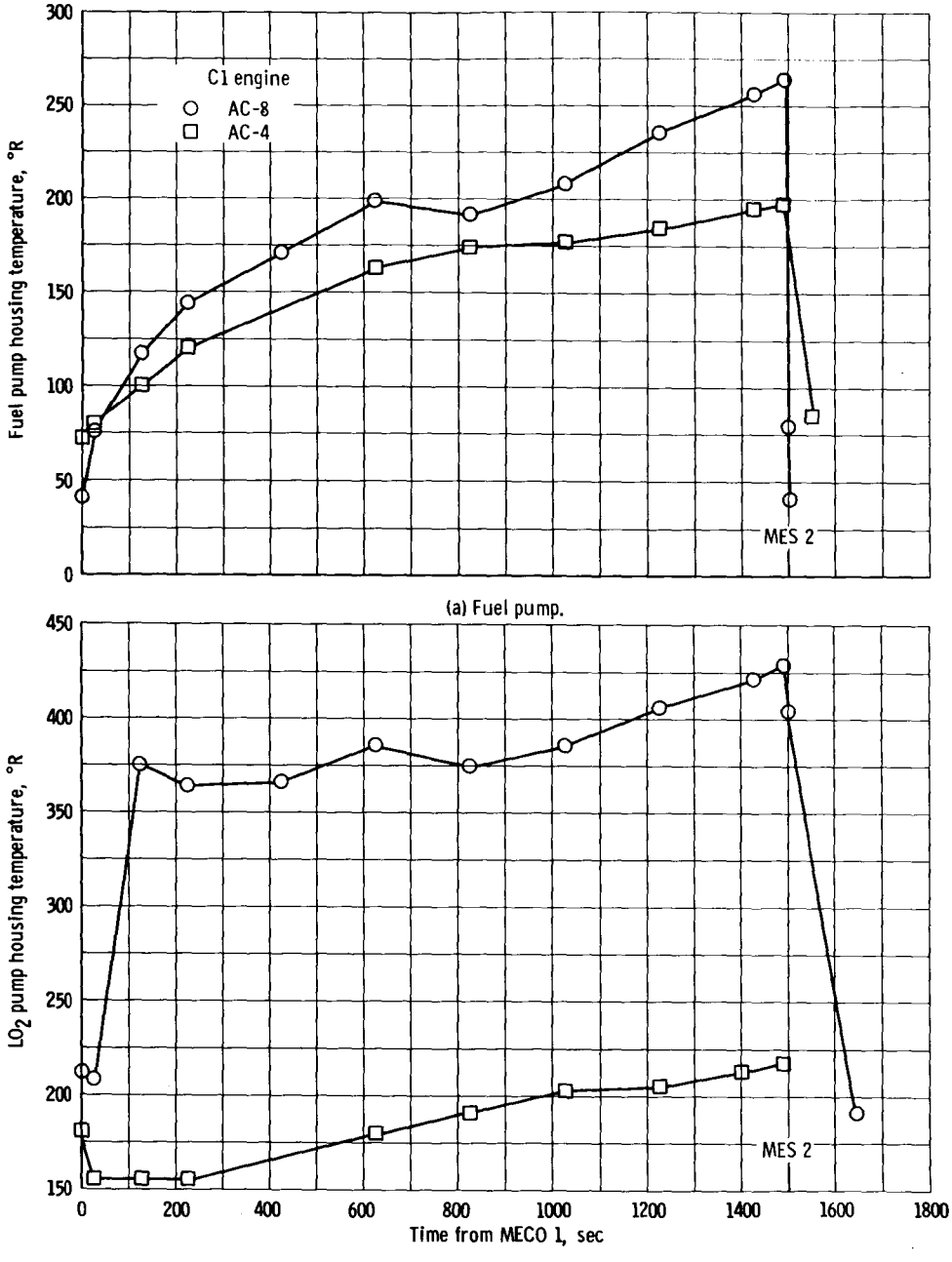

Figure VI-7. - Centaur fuel pump and liquid oxygen pump housing temperature during coast.

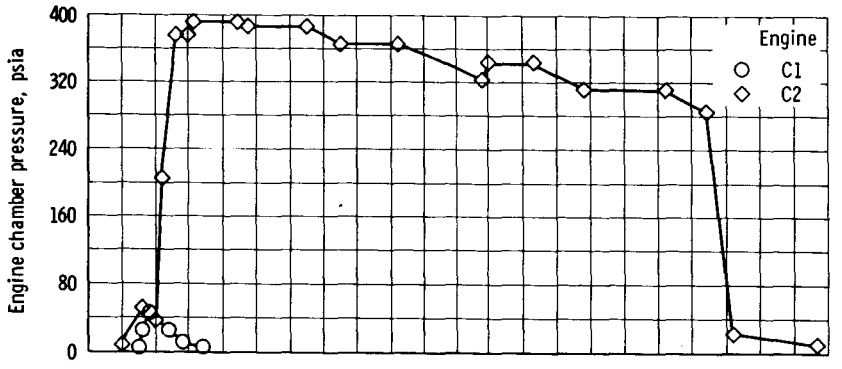

(a) Chamber pressure.

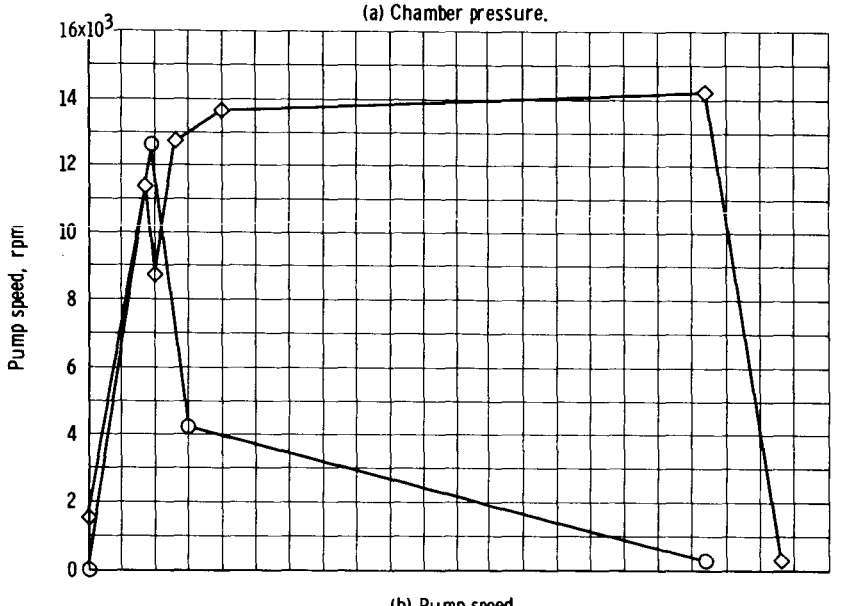

(b) Pump speed.

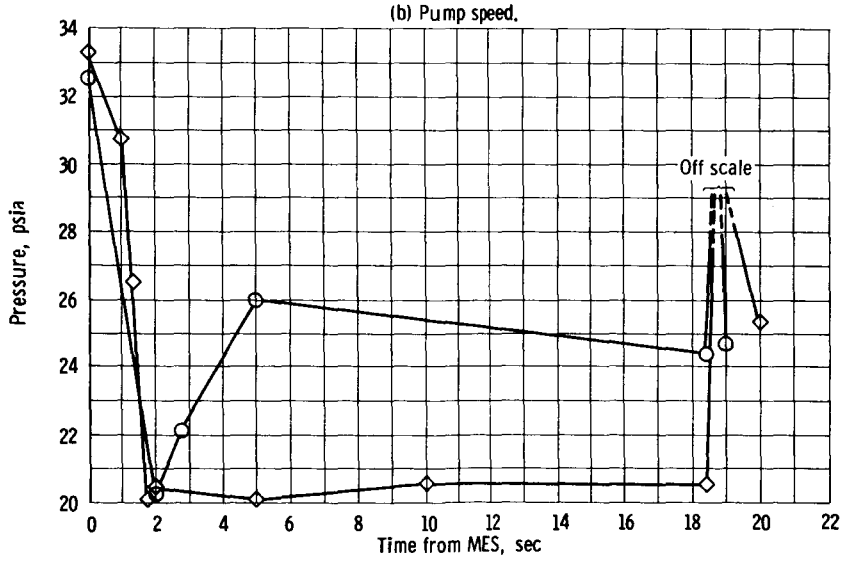

(c) Fuel pump inlet pressure.

Figure VI-8. - Centaur main engine pressures and speeds during second burn.

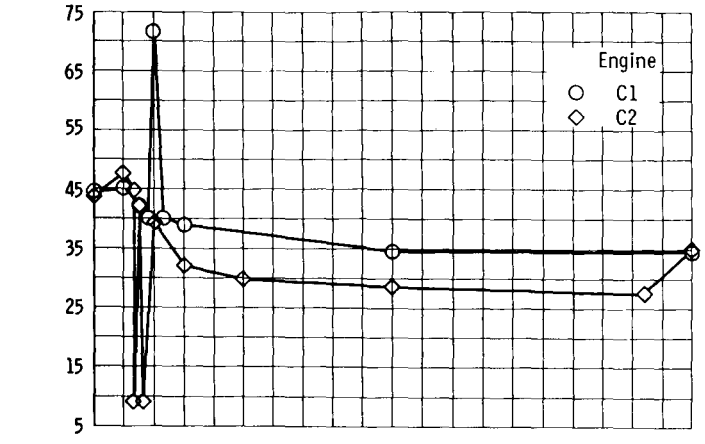

(d) Oxidizer pump inlet pressure.

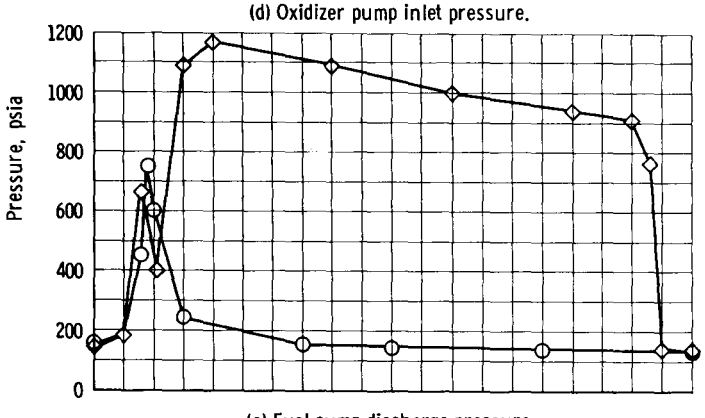

(e) Fuel pump discharge pressure.

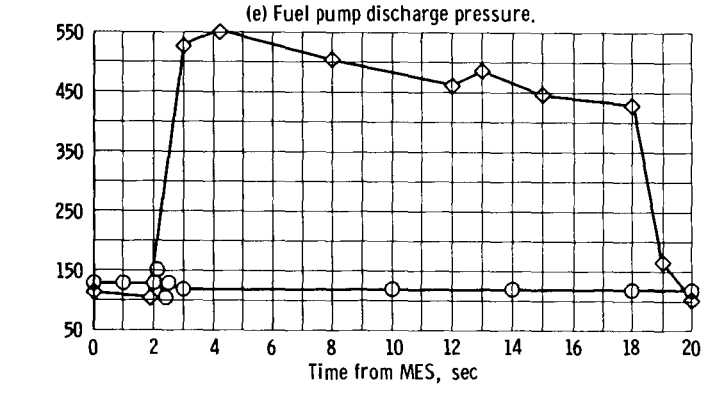

(f) Oxidizer pump discharge pressure.

Figure VI-8. - Concluded.

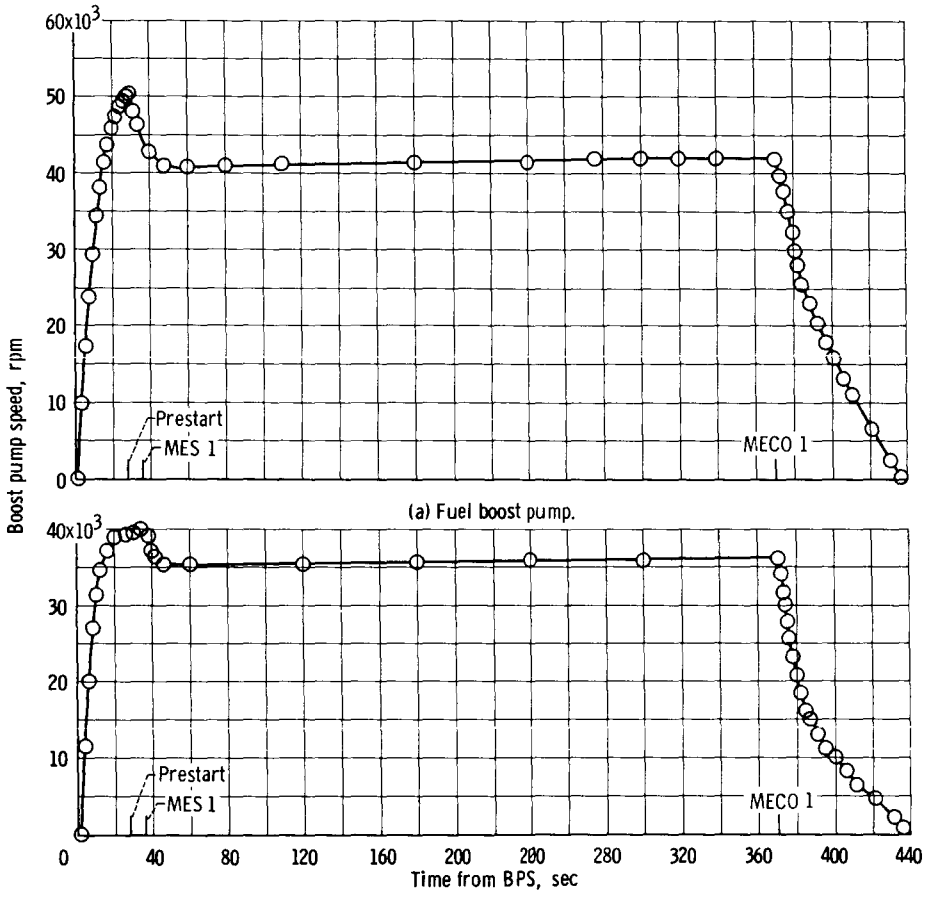

(a) Fuel boost pump.

(b) Liquid oxygen boost pump.

Figure VI-9. - Centaur boost pump speed during first engine burn.

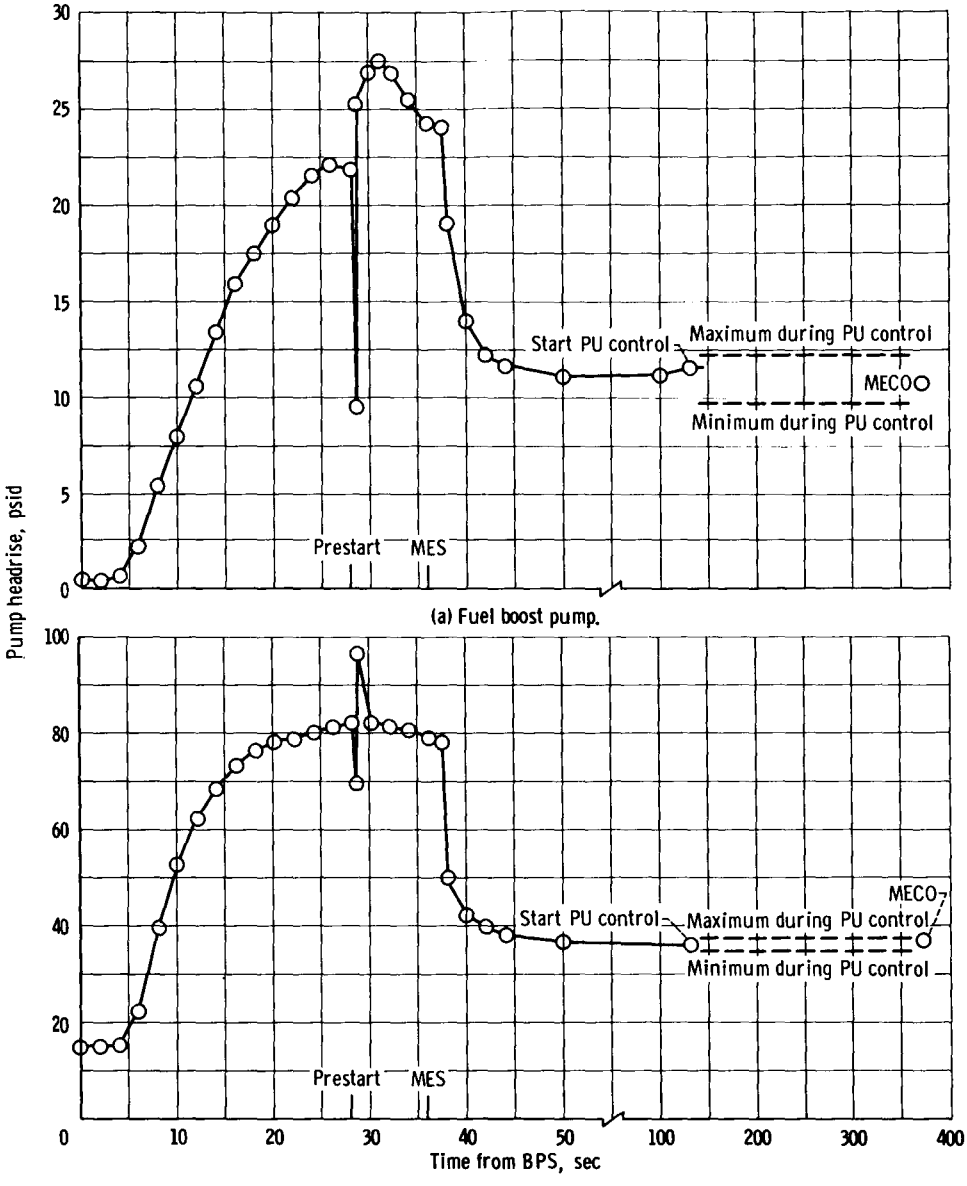

(a) Fuel boost pump.

(b) Oxidizer boost pump.

Figure VI-10. - Centaur boost pump headrise during first burn.

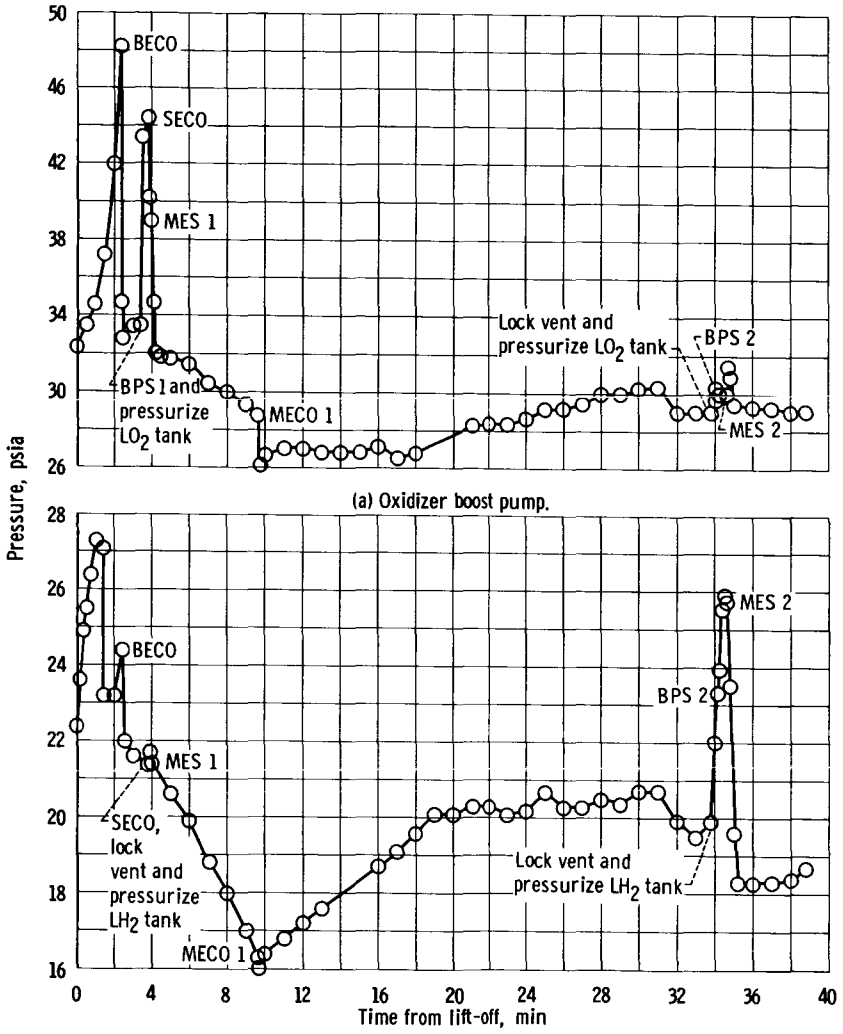

(a) Oxidizer boost pump.

(b) Fuel boost pump.

Figure VI-11. - Centaur boost pump inlet pressure.

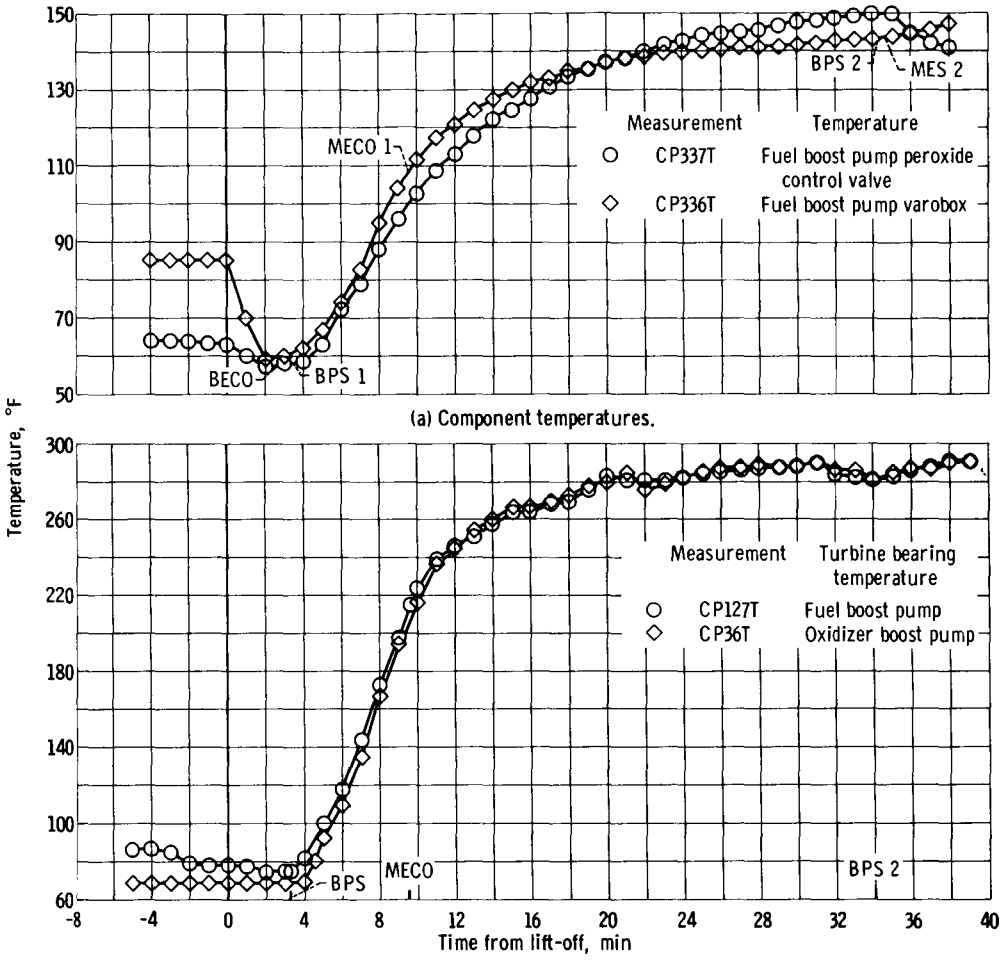

(a) Component temperatures.

(b) Turbine bearing temperatures.

Figure VI-12. - Centaur boost pump temperatures.

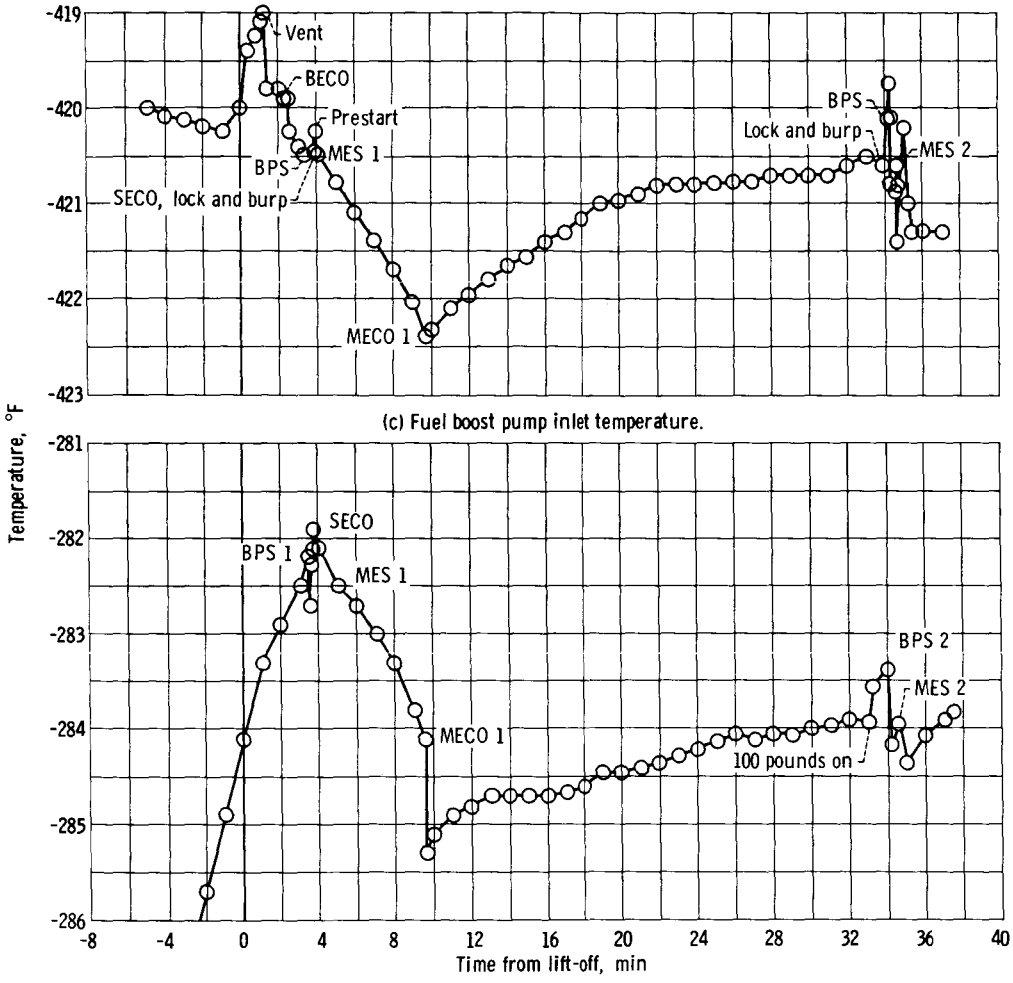

(c) Fuel boost pump inlet temperature.

(d) Oxidizer boost pump inlet temperature.

Figure VI-12. - Concluded.

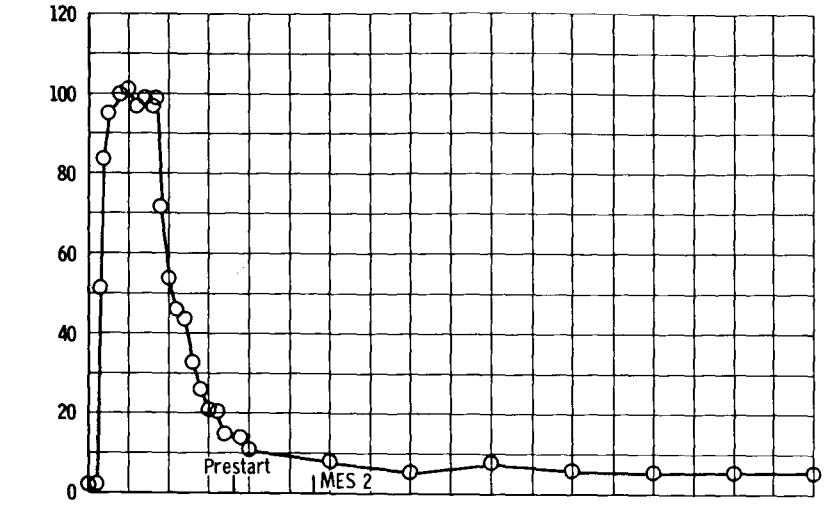

(a) Fuel boost pump gas generator inlet pressure during second burn.

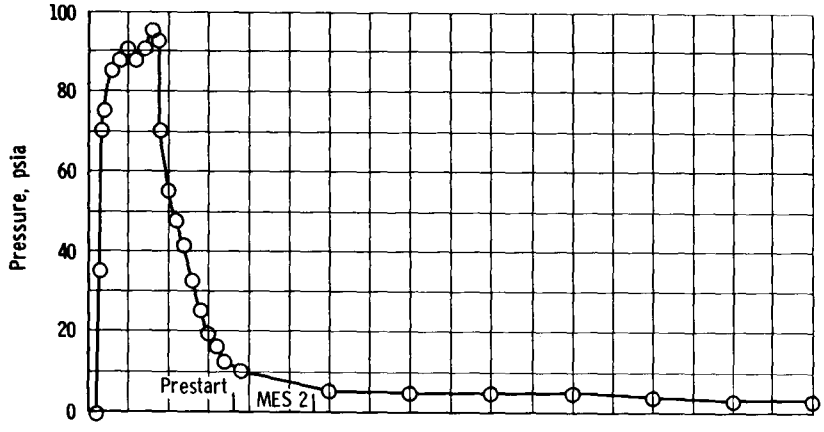

(b) Fuel boost pump turbine inlet pressure during second start.

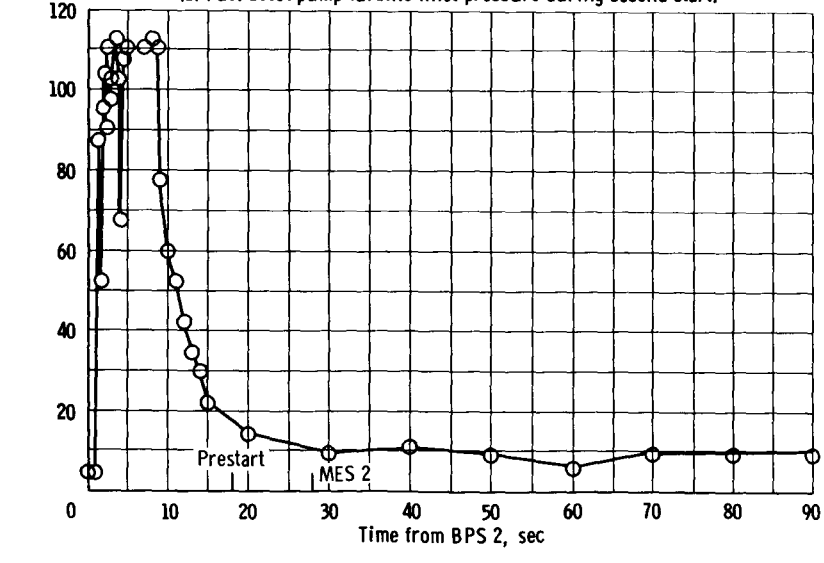

(c) Oxidizer boost pump gas generator inlet pressure during second burn.

Figure VI-13. - Centaur fuel and oxidizer boost pump pressure.

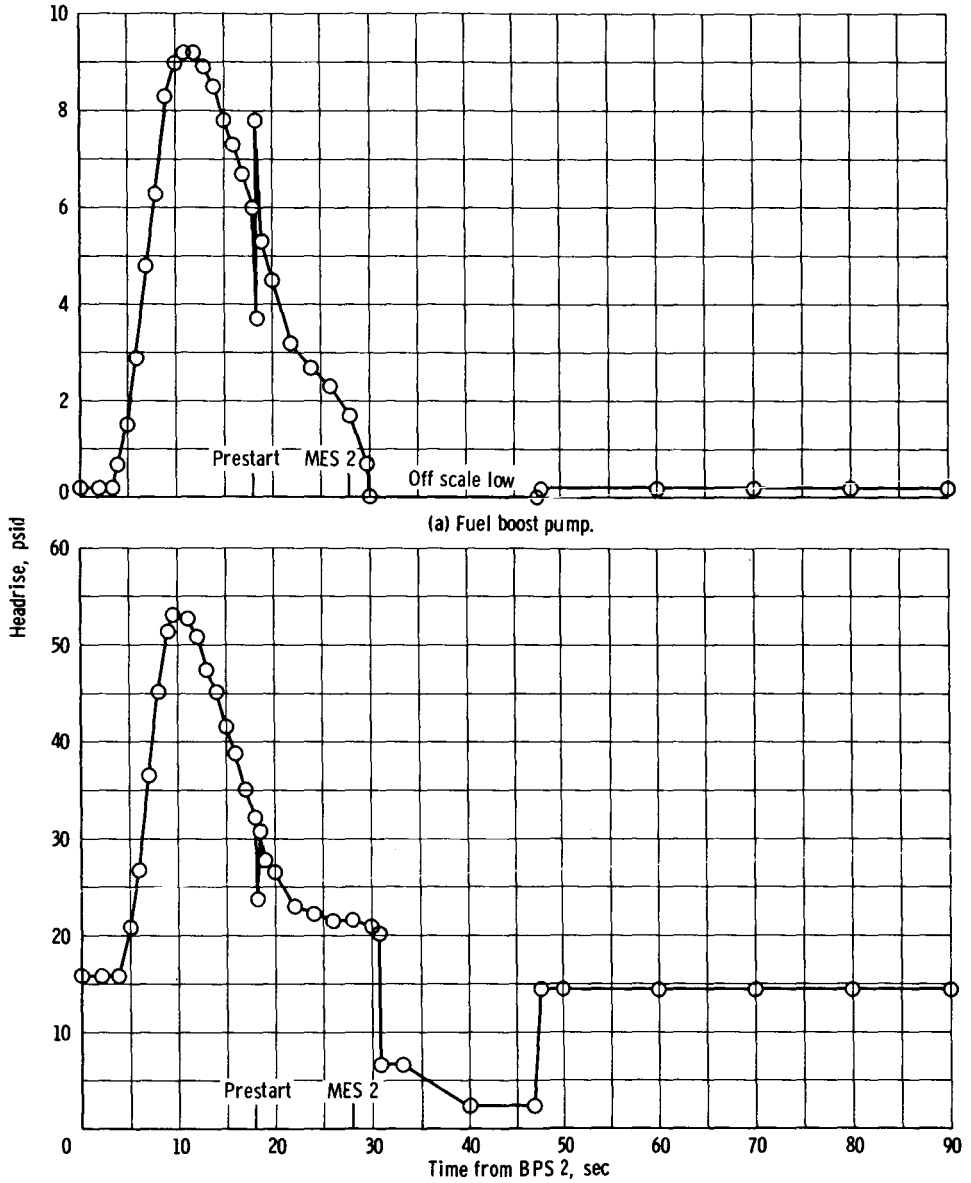

(a) Fuel boost pump.

(b) Oxidizer boost pump. (Absolute values are questionable and shift in zero calibration is suspected.)

Figure VI-14. - Centaur boost pump headrise during second burn.

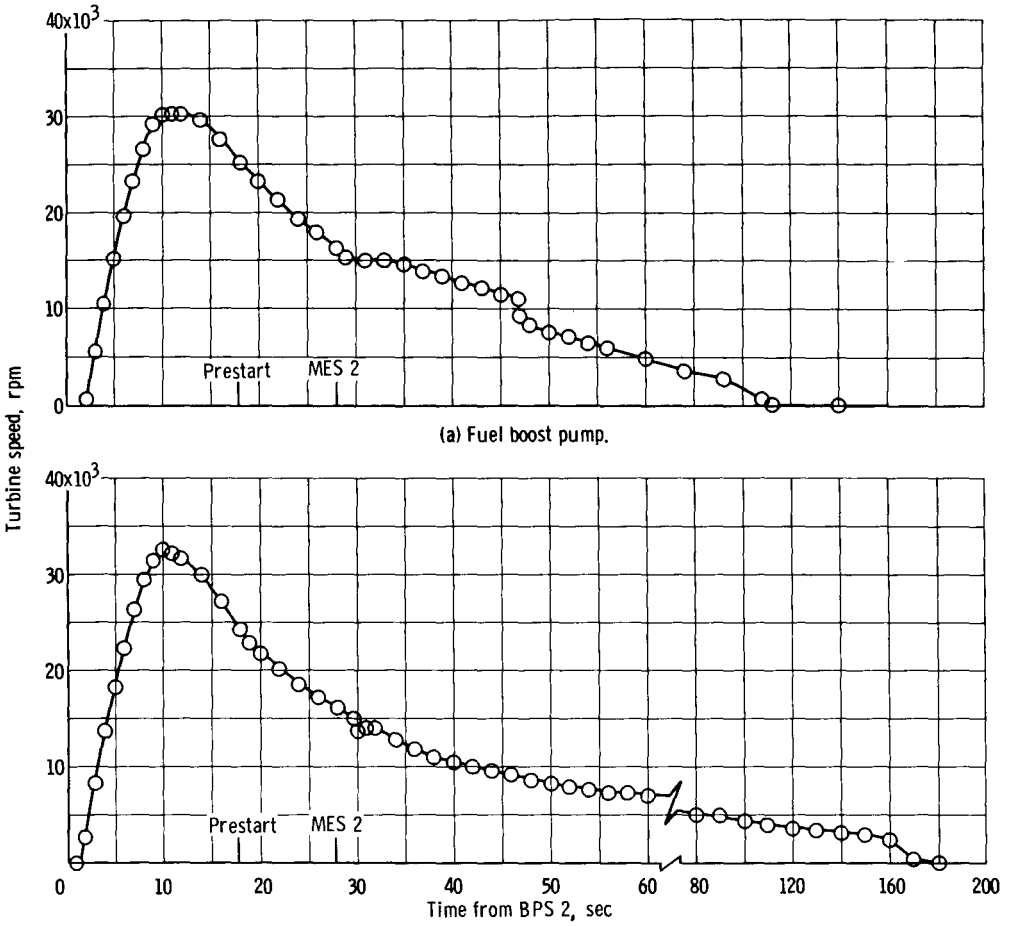

(a) Fuel boost pump.

(b) Oxidizer boost pump.

Figure VI-15. - Centaur boost pump turbine speed during second burn.

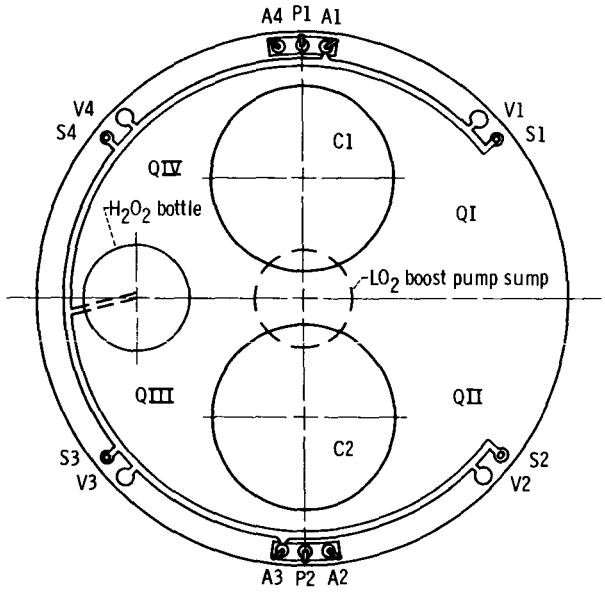

Engine	Thrust, lb	Function
A1, A2, A3, A4	3.5	Attitude control
V1, V2, V3, V4	50.0	Propellant settling, attitude control, retromaneuver
P1, P2	6.0	Attitude control
S1, S2, S3, S4	3.0	Propellant retention, attitude control

Figure VI-16. - Hydrogen peroxide engine arrangement.

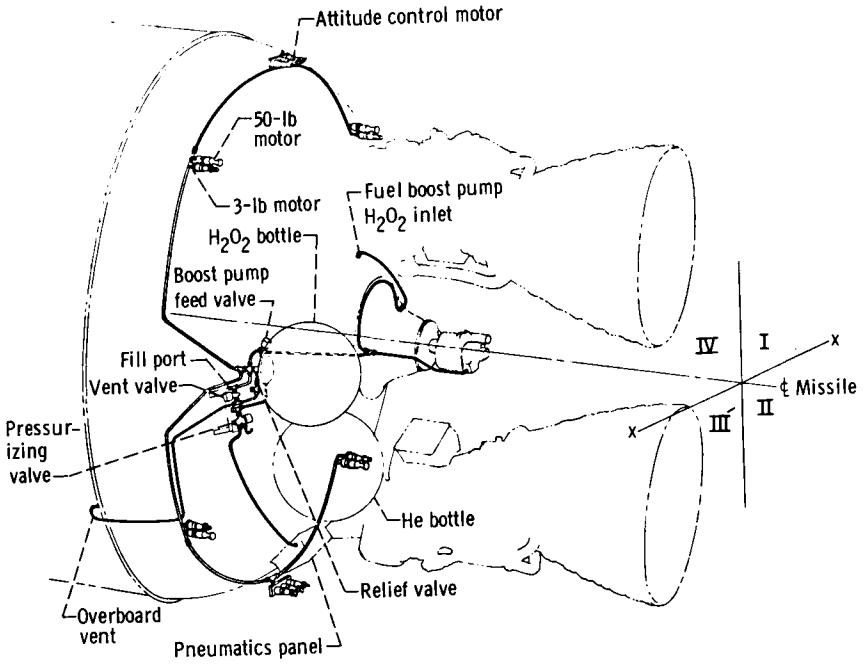

Figure VI-17. - Hydrogen peroxide engine control system for AC-8.

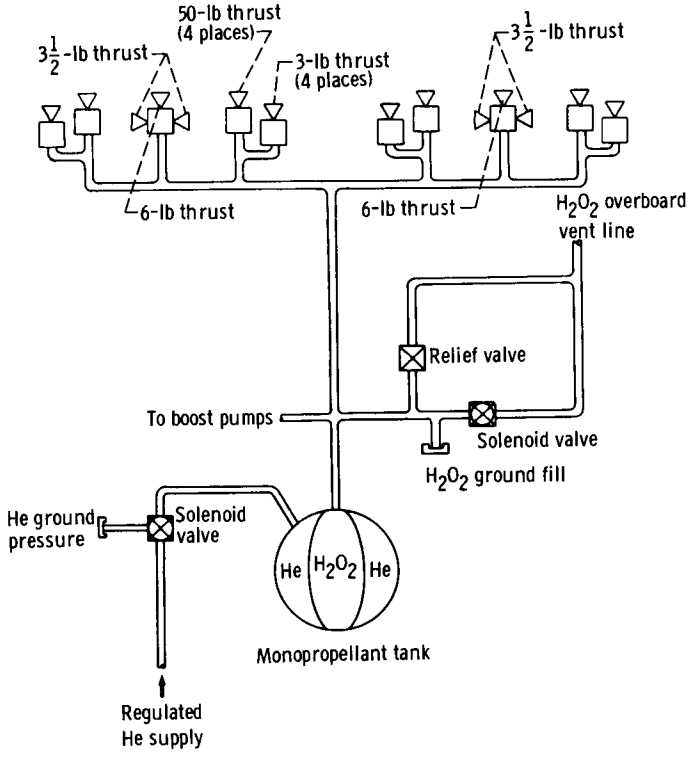

Figure VI-18. - Schematic illustration of reaction engine control system.

Hydrogen peroxide engine control logic		
Item	Half-on mode	
	V engine	S engine
Sequence time	MECO 1 to MECO + 100 sec MES 2 - 46 sec to MES 2 MBU + 105 sec to MBU + 125	MECO 1 + 100 sec to MES 2 - 46 sec
Pitch control	V engine, P engine } >0.2 deg/sec	S engine, primary >0.2 deg/sec V engine, backup >0.3 deg/sec
Yaw control	V engine, A engine } >0.2 deg/sec	S engine, primary >0.2 deg/sec V engine, backup >0.3 deg/sec
Roll control	A engine >0.2 deg/sec	A engine >0.2 deg/sec
Other	S engine off	P engine off

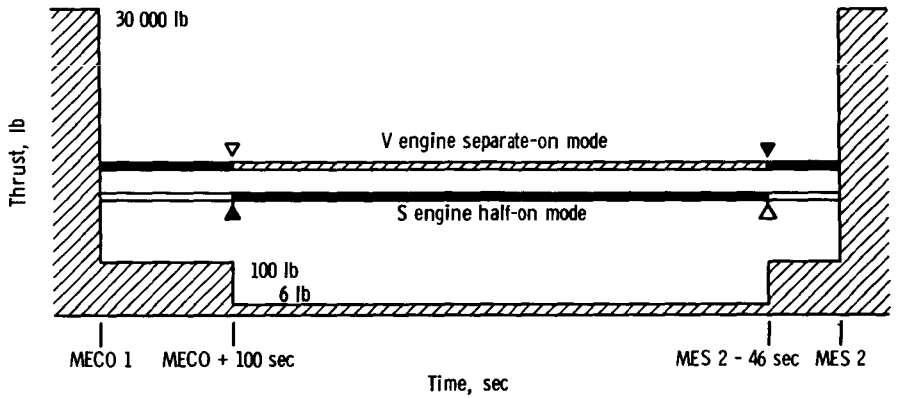

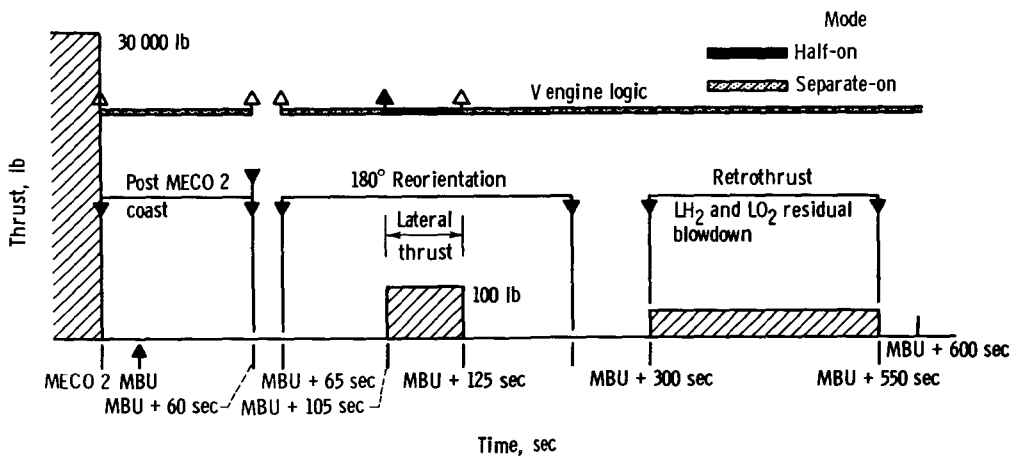

Figure VI-19. - Attitude control engine logic during coast.

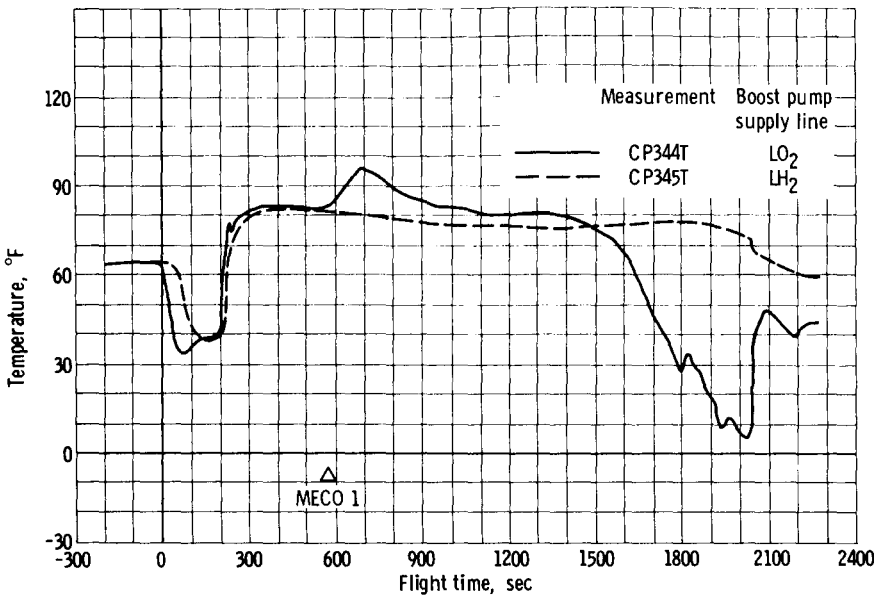

Figure VI-20. - Boost pump hydrogen peroxide supply line temperatures.

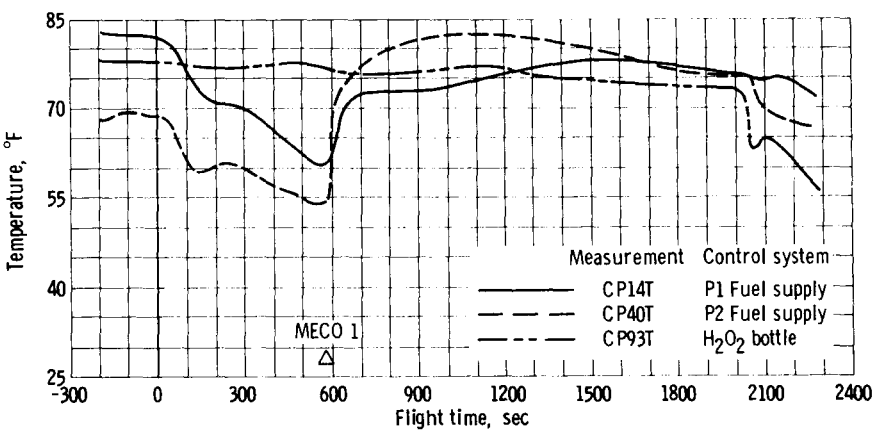

Figure VI-21. - Attitude control system temperatures.

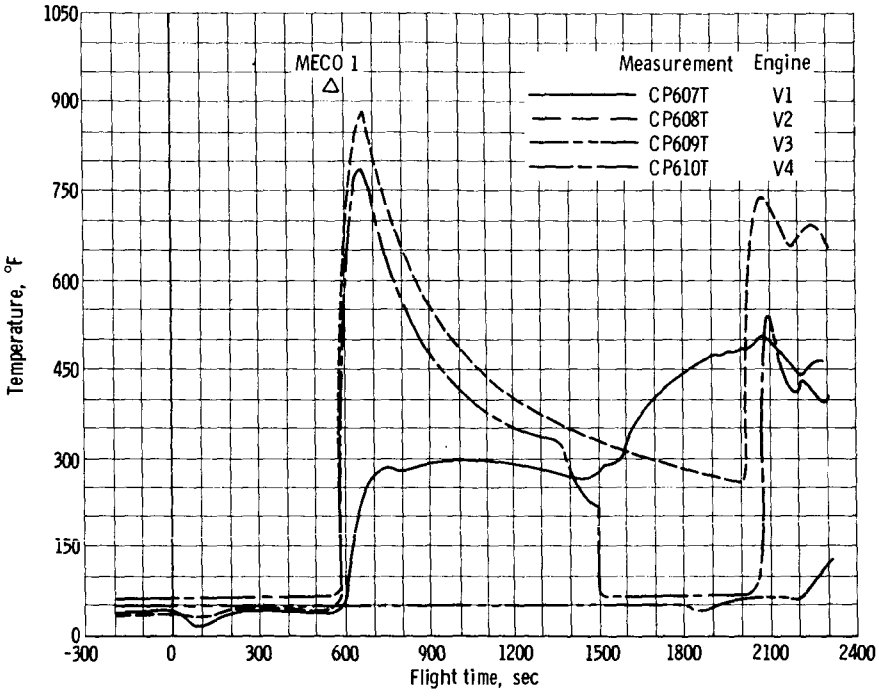

Figure VI-22. - Centaur vernier engine chamber surface temperatures.

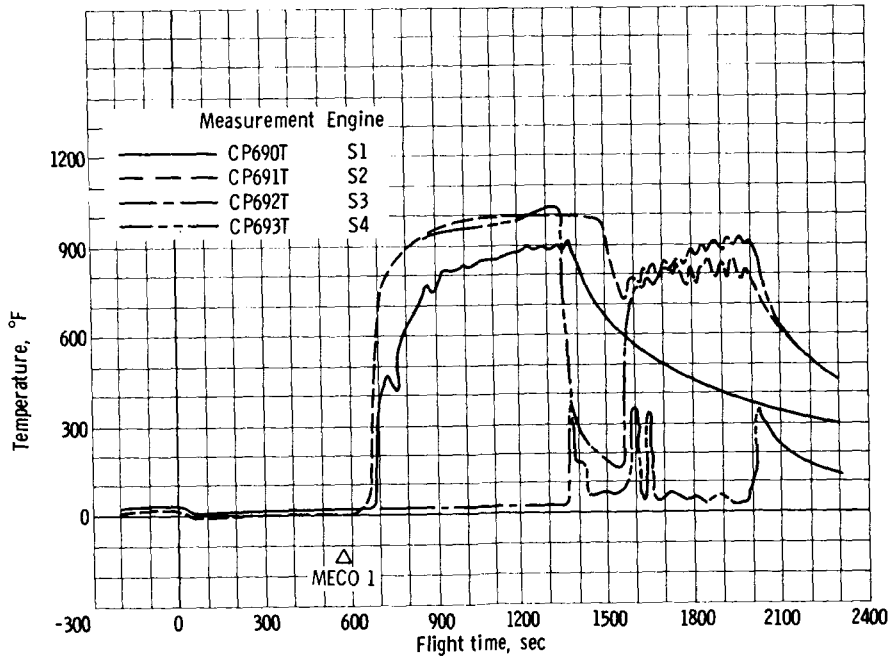

Figure VI-23. - Propellant settling engine chamber surface temperatures.

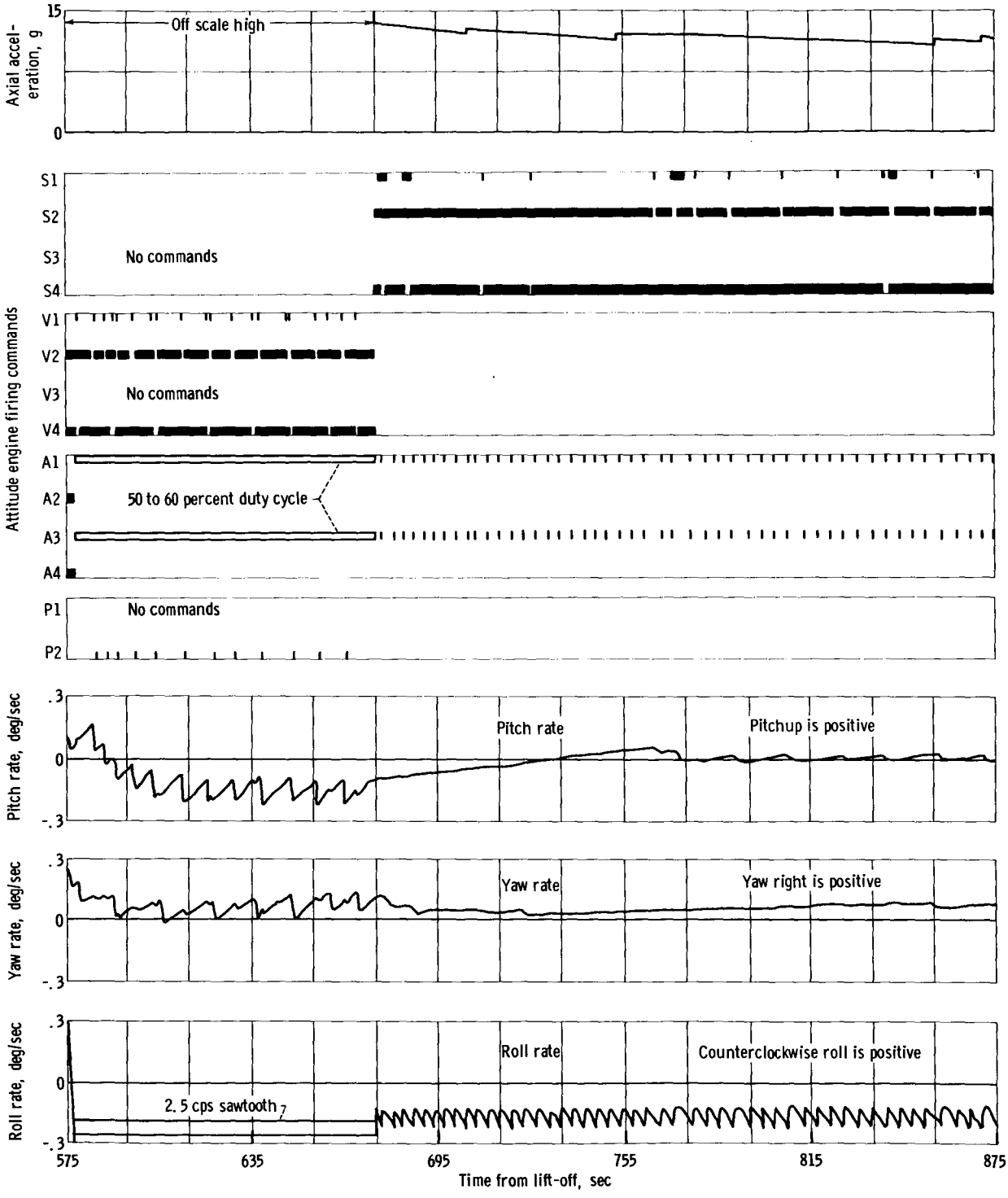

(a) Time, 575 to 875 seconds.

Figure VI-24. - Coast phase attitude control data for AC-8.

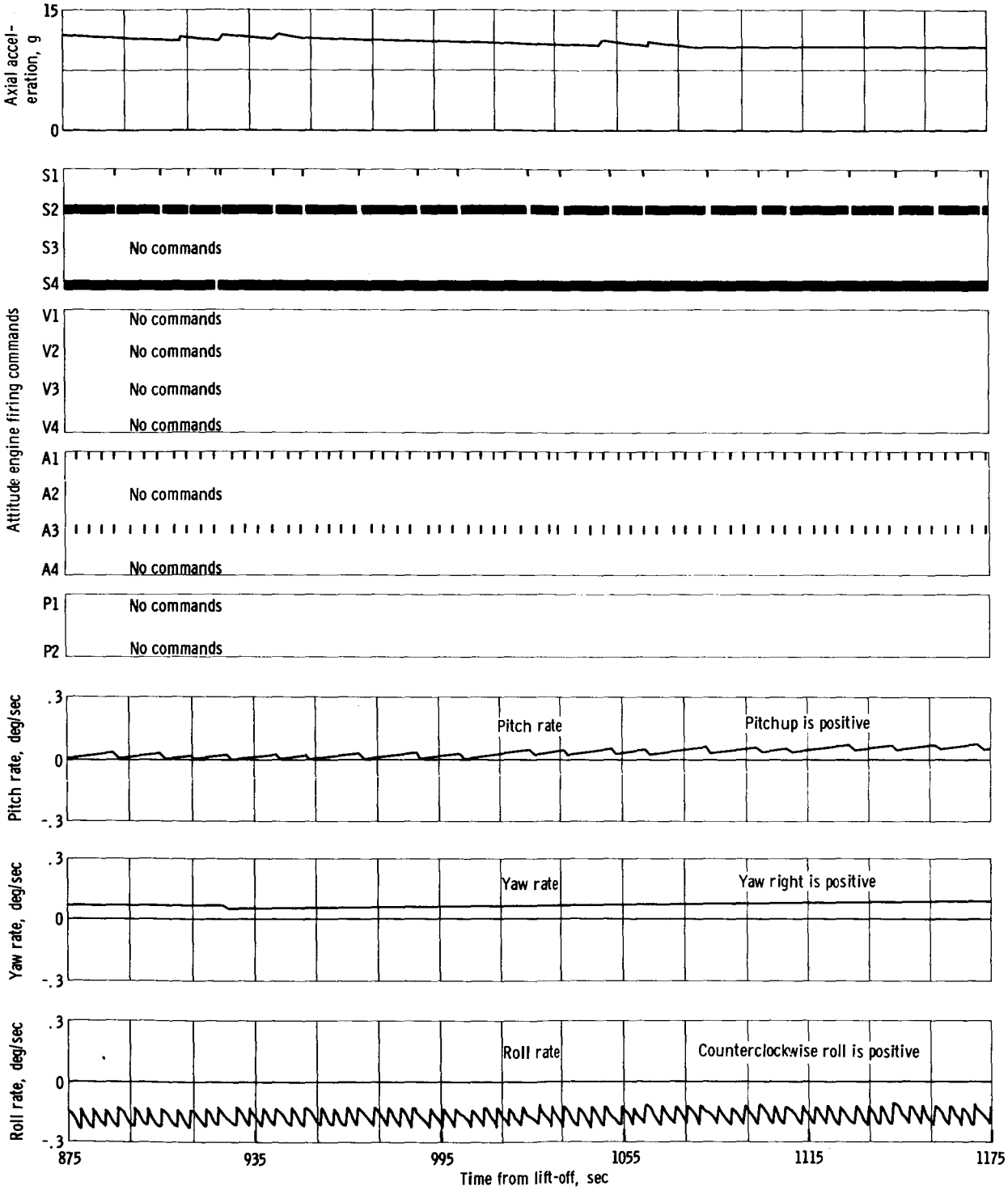

(b) Time, 875 to 1175 seconds.

Figure VI-24. - Continued.

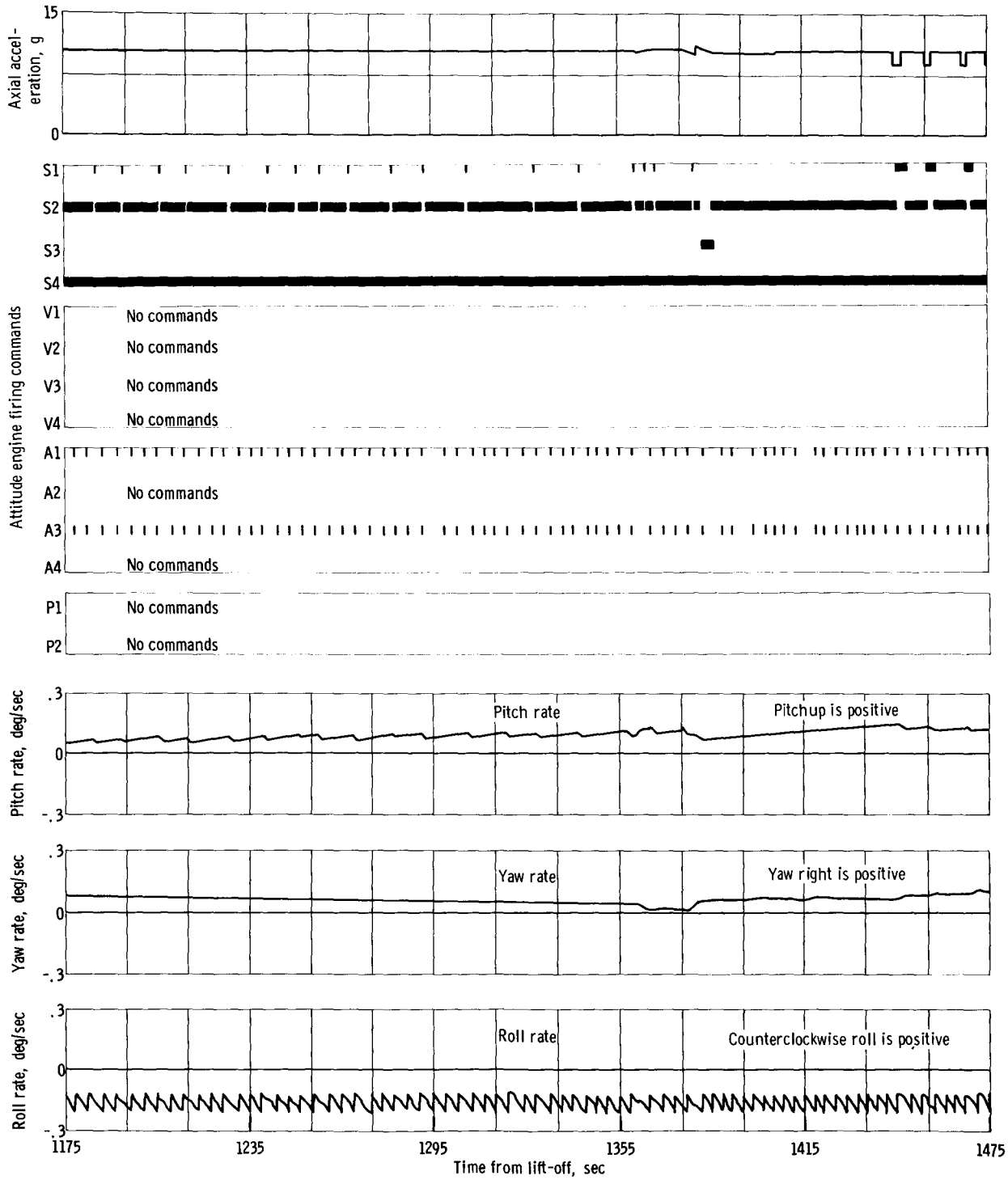

(c) Time, 1175 to 1475 seconds.

Figure VI-24. - Continued.

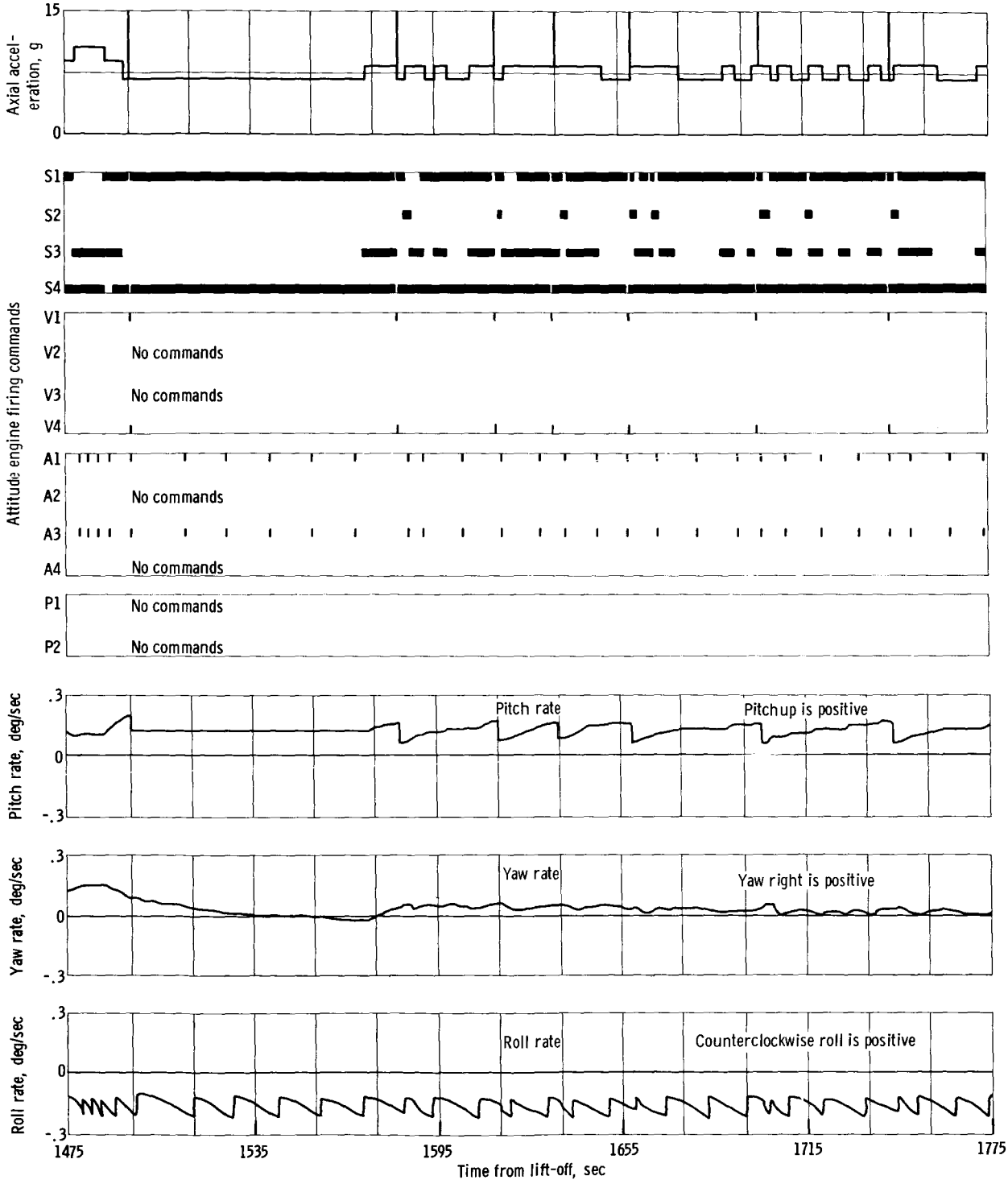

(d) Time, 1475 to 1775 seconds.

Figure VI-24. - Continued.

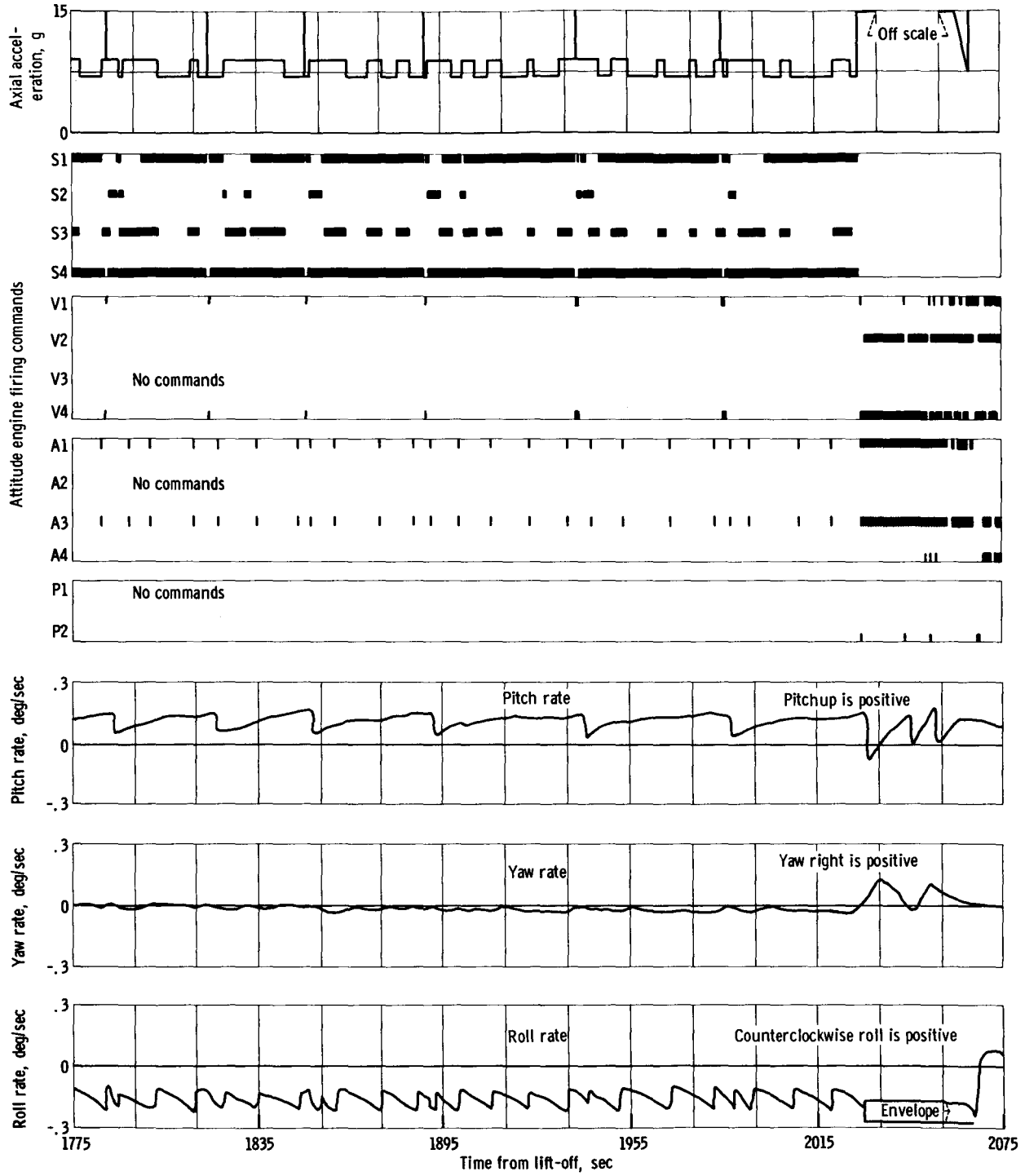

(e) Time, 1775 to 2075 seconds.

Figure VI-24. - Concluded.

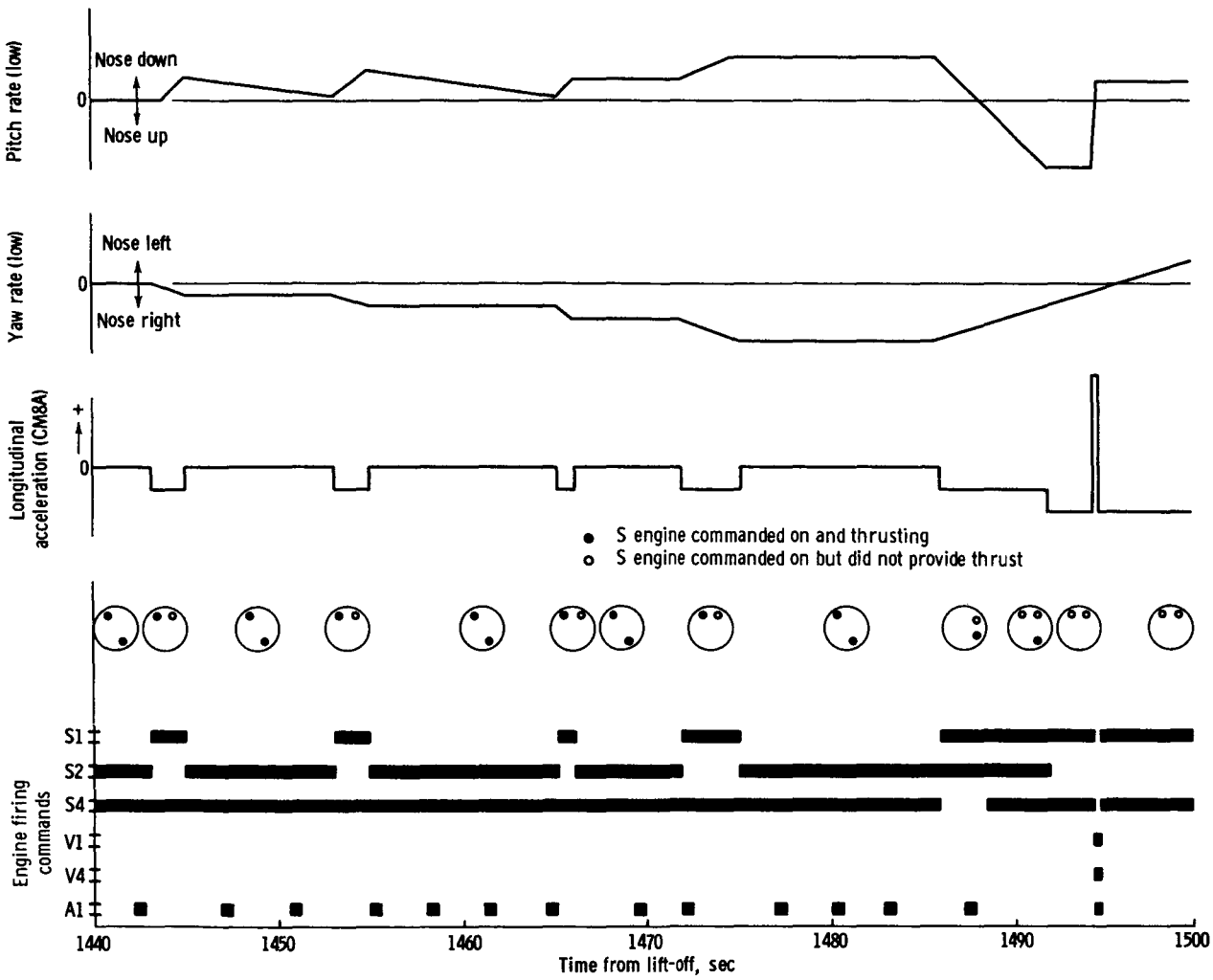

Figure VI-25. - Hydrogen peroxide engine control sequence for AC-8 coast phase.

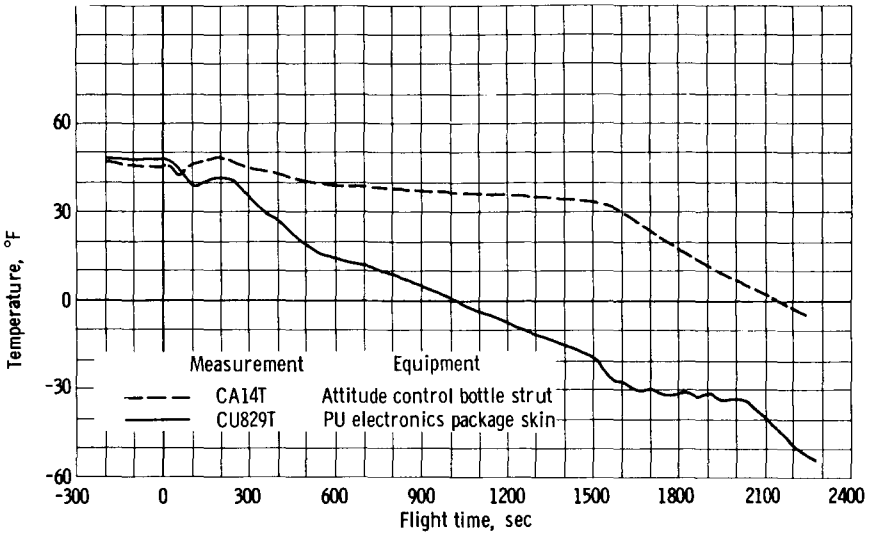

Figure VI-26. - Aft compartment equipment temperatures for quadrant IV.

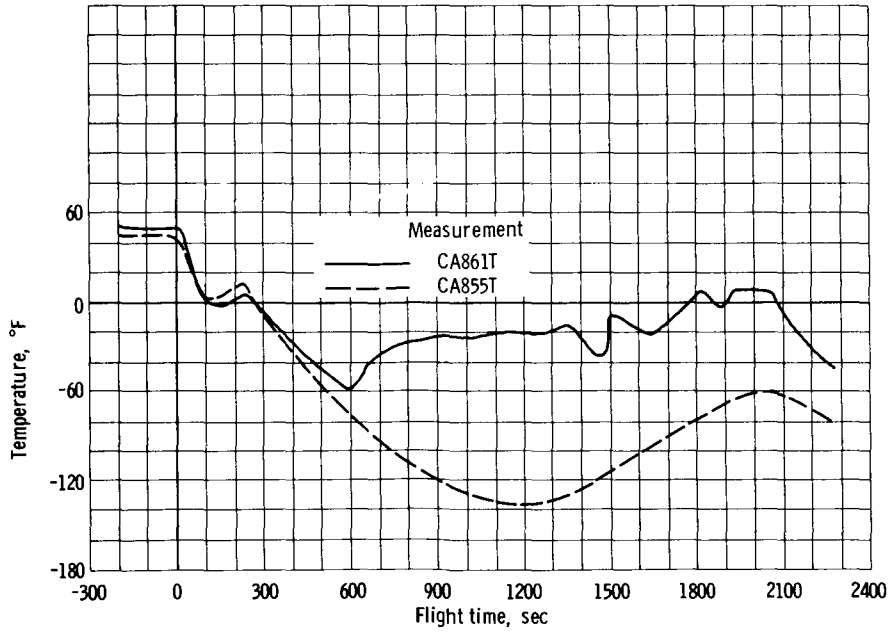

Figure VI-27. - Aft bulkhead insulation temperatures for quadrant IV.

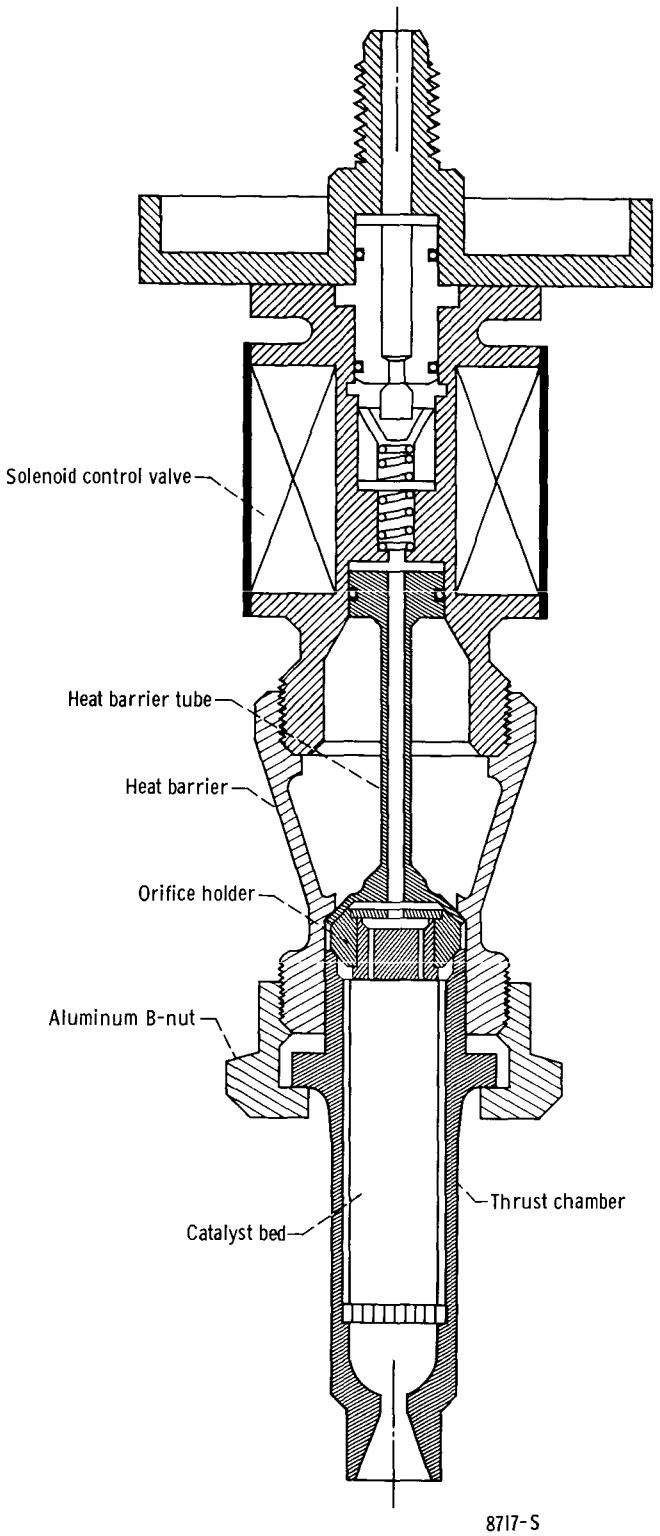

Figure VI-28. Coast phase hydrogen peroxide engine; 3 pounds thrust.

VII. PROPELLANT SYSTEMS

SUMMARY

All propellant systems supported the AC-8 flight satisfactorily. Propellant loading was accomplished on both Atlas and Centaur without incident. The Atlas propellant utilization system did not function properly, and SECO was initiated approximately 8 seconds early by the fuel-depletion sensors. This resulted in an Atlas LO_2 residual of approximatley 1900 pounds. The Centaur propellant utilization system functioned satisfactorily.

Propellant settling and control during the coast phase, which was a major flight objective, was demonstrated successfully. The propellants remained settled throughout the coast with only small propellant disturbances noted at MECO 1. These disturbances were quickly suppressed and damped, indicating satisfactory operation of all energy suppression devices installed.

Stratification of the hydrogen ullage was indicated by numerous ullage temperature sensors installed for the AC-8. These data enable accurate calculations of gaseous residuals and determination of temperature profiles.

ATLAS PROPELLANT UTILIZATION AND FUEL DEPLETION SYSTEM

The Atlas propellant-utilization (PU) system malfunctioned on the AC-8 flight. An early (approximately 8 sec) sustainer engine cutoff (SECO) was initiated by the fuel-depletion sensors. This resulted in a hard shutdown mode rather than the desired LO_2 depletion or soft shutdown sequence. As a result of the early SECO, 1883 pounds of LO_2 residual and 137 pounds of fuel residual remained above the sustainer pump at SECO These residuals were determined by using the fuel-depletion sensor uncovery time and volume at the sensors as well as the LO_2 port uncovery time and volume.

The propellant utilization valve responded correctly to the error demodulator output (EDO) signal given it by the PU system, as shown in figure VII-I and the LO_2 head suppression valve also operated properly in conjunction with the PU valve. There were discrepancies, however, between the propellant head sensing measurements and the EDO. The reason for the PU system malfunction is not known presently.

CENTAUR PROPELLANT UTILIZATION SYSTEM

System Description

The AC-8 flight was the second flight test of the Centaur propellant utilization (PU) system. The system, as shown in figure VII-2, is used during tanking to indicate propellant masses and during flight to optimize propellant consumption. In flight, the mass of propellant remaining in the tanks is sensed by a concentric cylinder capacitance probe and compared in a bridge circuit. If the mass ratio of propellants remaining in the tanks varies from a predetermined ratio (usually 5.0 to 1, oxidizer to fuel), an error signal is sent to the proportional servopositioner which controls the LO_2 flow valve. If the mass ratio is greater than 5.0 to 1, the LO_2 flow is increased to return the ratio to 5.0 to 1. If the ratio is less than 5.0 to 1, the LO_2 flow is decreased. Since the PU probes do not extend the full length of both tanks, PU control is not effected until approximately 90 seconds after main engine start. For this 90 seconds of engine burn, the LO_2 flow control valves are nulled (locked at a nominal mixture ratio of 5.0 to 1).

System Performance

All prelaunch checks of the PU system were within required limits and specifications, as summarized in table VII-I. Since the PU probes do not extend the full length of the tanks, they do not indicate the final amount of tanked propellants.

The system was biased electrically prior to flight to sense 185 pounds of excess LO_2 to compensate for effects such as probe shrinkage, tanking error, tank distortion, density uncertainty, and level lag in the probes. An additional 390 pounds of LO_2 bias were also used to compensate for the predicted 78 pounds of H_2 vented during coast to maintain a ratio of 5.0 to 1 in the tanks at the second main engine start.

The in-flight performance of the system was satisfactory. The LO_2 flow control valves, as shown in figure VII-3, were properly unnulled by the programer at MES 1 + 90.5 seconds and immediately moved to the LO_2-rich stop (mass ratio, 5.58 to 1) by MES 1 + 95.5 seconds. The LO_2 level reached the top of the LO_2 probe at MES 1 + 93.8 seconds, and the LH_2 level reached the top of the LH_2 probe at MES + 104.4 seconds. The levels should reach the probes at approximately the same time, but the late uncovery of the LH_2 probe indicated an amount of tanked LH_2 in excess of the predicted amount. The flow control valves remained on the LO_2-rich stop from MES + 95.5 to MES + 138.3 seconds (Δ time = 42.8 sec). During this time, the system corrected for 226 pounds of excess LO_2. This correction was much less than the 575 pounds of LO_2 bias in the system, and it reflects the excess tanked hydrogen (approx. 62 lb) indicated by the late

probe uncovery. From MES + 138.3 seconds to MECO 1, the valves oscillated about null, but mainly in a fuel-rich condition. This indicated that the engines were tending to burn LO_2 rich but were prevented from doing so by the PU system. The propellant quantities, as indicated by the PU probes, are shown in figure VII-4. Shortly after MECO 1, the LO_2 and LH_2 quantities indicated that propellants were filling the probes. This expected rise of propellants in the probes is caused by the capillary action in a low-acceleration field.

The improper engine operation and subsequent tumbling of the vehicle precluded evaluation of the system performance during the planned second engine burn.

PROPELLANT CONSUMPTION AND RESIDUALS

The propellants consumed by the engines, propellants vented, and propellant residuals were established by using data obtained from the hydrogen vent system and propellant-utilization system. The time that the propellant levels passed the top of the PU probes was used as a reference point for the engine consumption and liquid residual calculations. The gaseous hydrogen residuals were based on the temperature profile in the tank, as shown in figure VII-5. This temperature profile was established from ullage temperature measurements. Gaseous oxygen residuals were calculated assuming saturated O_2 in the tank. The calculations establish the LH_2 level at MECO 1 as station 329, which corresponds to the level indicated by the in-tank liquid-vapor sensors shown in figure VII-6.

The propellant management from lift-off to the first engine cutoff is presented in the following table:

Propellant inventory	Hydrogen, lb	Oxygen, lb
Liquid residual at MECO 1	1467	6 278
Gaseous residual at MECO 1	69	144
Engine consumption	3700	18 991
In-flight chilldown	24	33
Vented during boost	70	60
Engine shutdown loss	6	19
On vehicle at lift-off	5336	25 525

PROPELLANT SETTLING AND CONTROL

Instrumentation and Vehicle Modifications

The AC-8 tank was instrumented extensively with temperature patches on the tank

skin and with liquid-vapor and temperature sensors in the tank, as shown in figures VII-7 and VII-8, to aid in the study of propellant behavior during flight. Data from the AC-4 flight indicated that external energy sources to the propellants at MECO severely disturbed the propellant surface and caused motion of the propellant in the tank, which led to loss of vehicle control. As a result, several internal tank modifications were made to the AC-8 vehicle. These modifications, as shown in figures VII-9 to VII-11, were:

(1) Antiswirl/antislosh baffle at the nominal propellant level at MECO 1

(2) Energy suppression devices on propellant return lines into the tank

(3) Energy dissipator on hydrogen tank helium pressurization line

Also instituted was a schedule of propellant settling and retention thrust, as shown in figure VII-12. This thrust was provided by small H_2O_2 engines mounted on the aft end of the vehicle, as shown in figure VI-30.

Powered Phase of Flight

Propellant behavior during booster, sustainer, and Centaur-powered portions of flight indicated no abnormal behavior. The liquid-vapor sensors, as shown in figure VII-13 in the hydrogen ullage (station 180 and above), responded to tank venting and the surface disturbance caused by pressurizing the tank. The liquid-vapor sensors also responded to the depleting liquid level during engine burn as shown in figures VII-13(a) and (b). The liquid level in the hydrogen tank was established as station 329, as shown in figure VII-6, from tank skin temperature data and liquid-vapor sensor uncovery times. Data from tank skin temperatures were not utilized to determine propellant location and therefore are not presented for the coast phase.

First Main Engine Cutoff and Coast Phase

Propellant disturbances in the Centaur hydrogen tank at MECO 1 were small with only momentary wetting of sensors in the path of the boost pump volute bleed and duct recirculation lines, as shown in figure VII-13(c). This small disturbance was expected and was quickly suppressed and damped, indicating effective operation of the energy suppression devices and settling of the propellant by the 100-pound thrust applied to the vehicle. The liquid-vapor sensors indicated no abnormal propellant movement until approximately T + 1530 seconds. At this time, an alternate wetting and drying occurred of sensors CM25X (station 340, z-axis), CM289X (station 344.9, quadrant II), CM23X (station 316.4, quadrant IV), and CM21X (station 316.4, quadrant IV). These slosh waves, as shown in figure VII-14, had a period of about 2 to $2\frac{1}{2}$ minutes and were probably

started by vernier engines V1 and V4 firing intermittently at T + 1495 seconds. The slosh wave continued throughout the remainder of the coast phase. At boost pump start prior to the second MES, sensors CM15X, CM17X, CM21X, and CM23X indicated momentary wetting. However, propellants were available in the bottom of the tank for engine start. At engine cutoff, all sensors in the tank gave wet indications, which were caused by the improper engine ignition and firing and subsequent propellant sloshing throughout the hydrogen tank.

HYDROGEN ULLAGE TEMPERATURE PROFILE

The Centaur LH_2 tank was instrumented with temperature sensors (fig. VII-8) to map the temperature profile in the tank ullage. These temperature sensors could also have served as liquid-vapor detectors if the propellants had not settled properly during coast phase. As indicated earlier, propellant settling and control were successful in AC-8.

Figure VII-15 shows temperature profiles in the LH_2 tank ullage above station 263. Figure VII-8 shows the location of these sensors. Stratification in the ullage was evident. Sensors CF155T (station 167) and CF157T (station 175), in particular, exhibited strong temperature variations with time in response to the various flight events, such as vent-valve lockup and unlock and GH_2 vent during coast phase.

Sensor CF163T, located at station 263, stayed near the saturation level throughout the controlled flight. This is characteristic of all temperature sensors below that station.

At T - 7.7 seconds, the primary LH_2 vent valve was locked. The ullage temperature at station 167 increased from saturation (approx. 40° R) to 66° R at T + 68.5 seconds, at which time the vent valve was unlocked, and the temperature returned to saturation. This same process was repeated when the vent valve was locked at BECO. The ullage temperature at station 167 increased from essentially saturation at T + 270 seconds to 118° R at MECO 1 (T + 575 sec). Slight cyclical temperature variations of about 10° R magnitude were noted from T + 575 to T + 850 seconds. These were probably generated by gas turbulence set up in the LH_2 tank at MECO and do not indicate any problem in propellant management. The ullage temperature followed a generally increasing trend from MECO 1 to T + 1182 seconds, when the first coast-phase venting was noted. Intermittent GH_2 venting from T + 1182 to T + 2029 seconds caused cyclical variations in ullage temperature.

At T + 2029 seconds, the second burp was initiated in preparation for MES 2. The addition of relatively warm helium caused a sudden sharp rise in the LH_2 ullage temperature.

MES 2 was initiated at T + 2077.8 seconds. The abnormal engine ignition and operation caused the vehicle to tumble, and the temperature sensors indicated an abrupt drop to LH_2 temperatures in response to the propellant slosh.

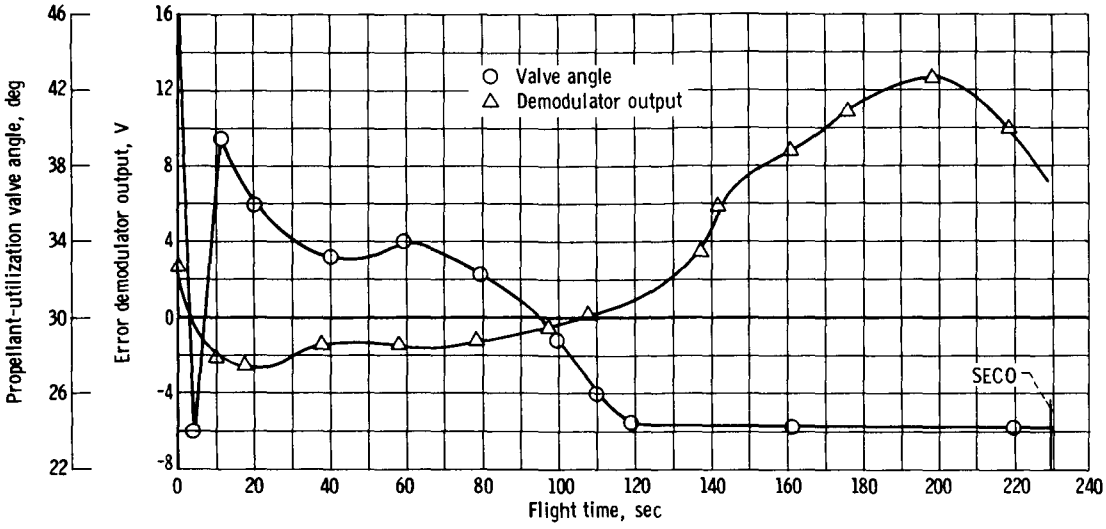

Figure VII-1. - AC-8 Atlas propellant-utilization valve angle and error demodulator output.

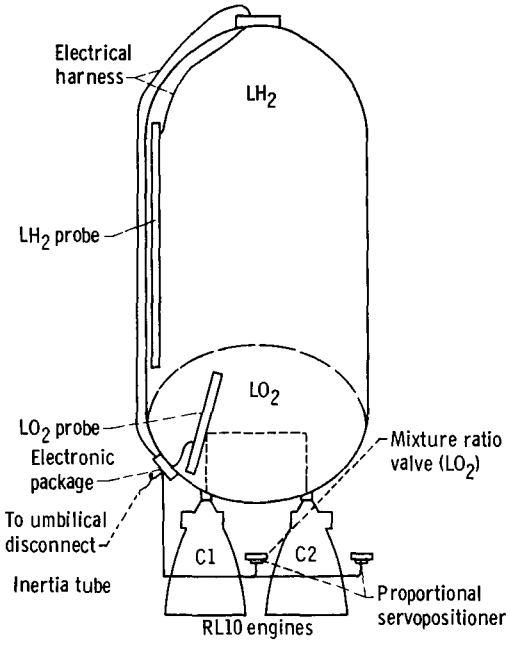

Figure VII-2. - Schematic of Centaur propellant-utilization system.

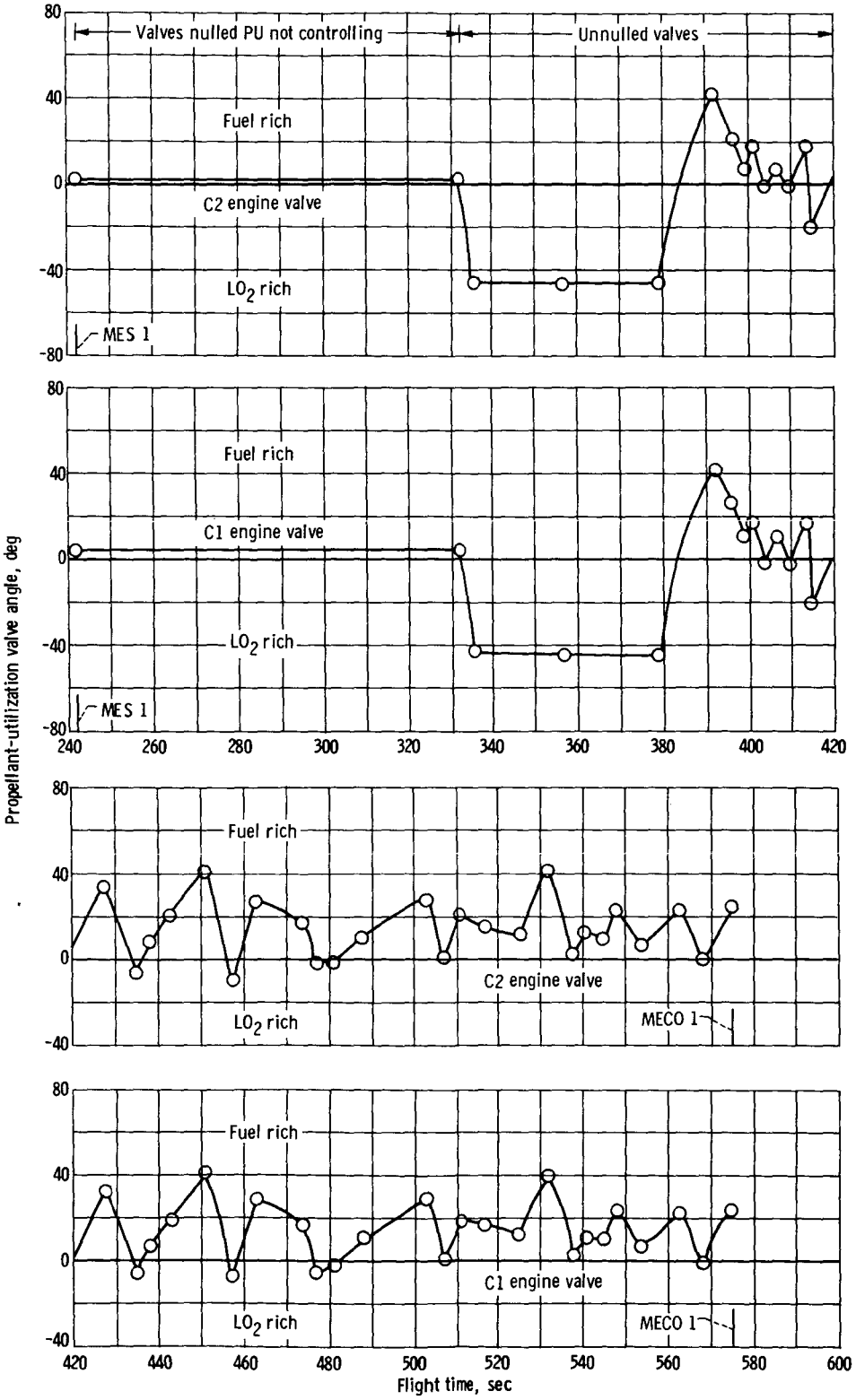

Figure VII-3. - Propellant-utilization valve angle for first engine burn.

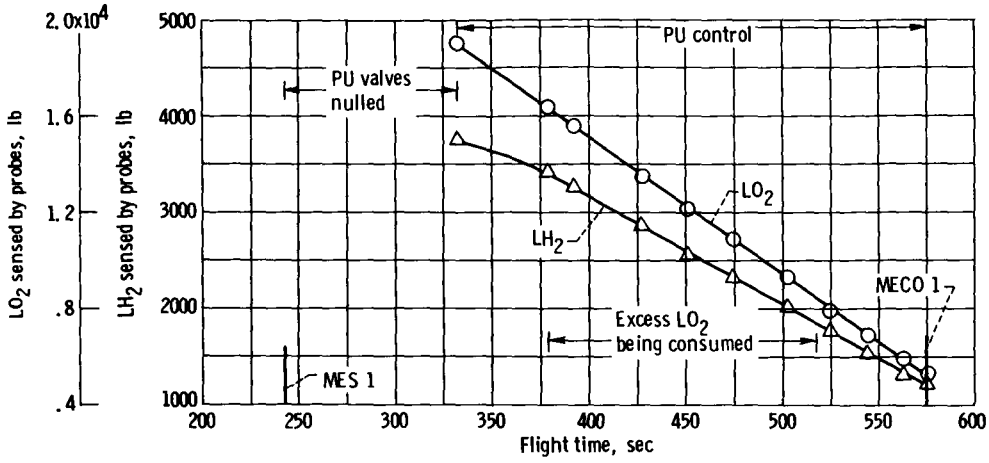

Figure VII-4. - Propellant quantities from propellant-utilization probes as function of time.

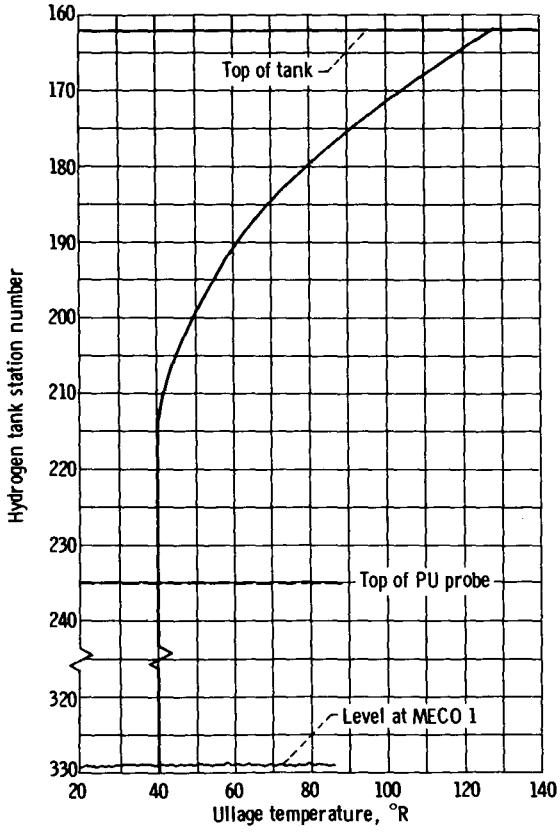

Figure VII-5. - Hydrogen ullage temperature profile at main engine cutoff 1.

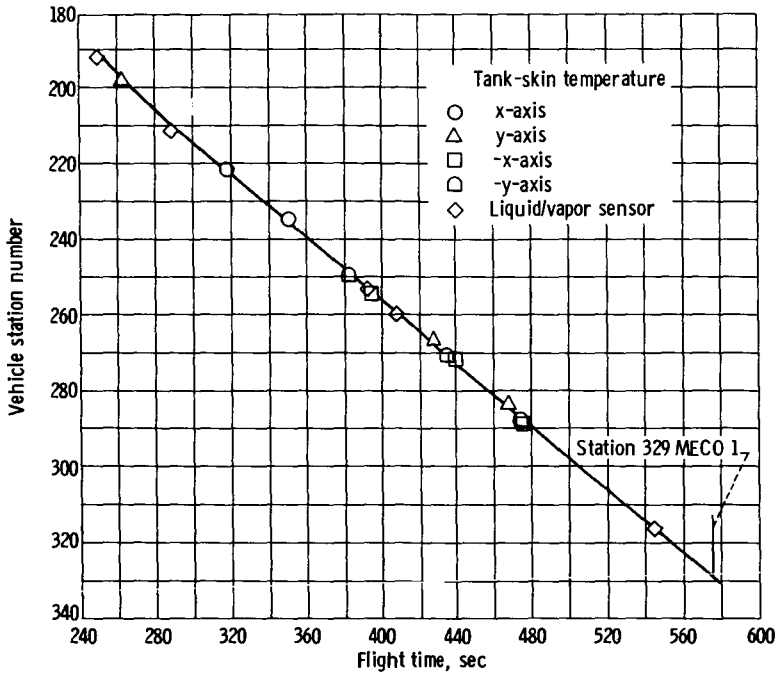

Figure VII-6. - Liquid hydrogen level during first main engine firing.

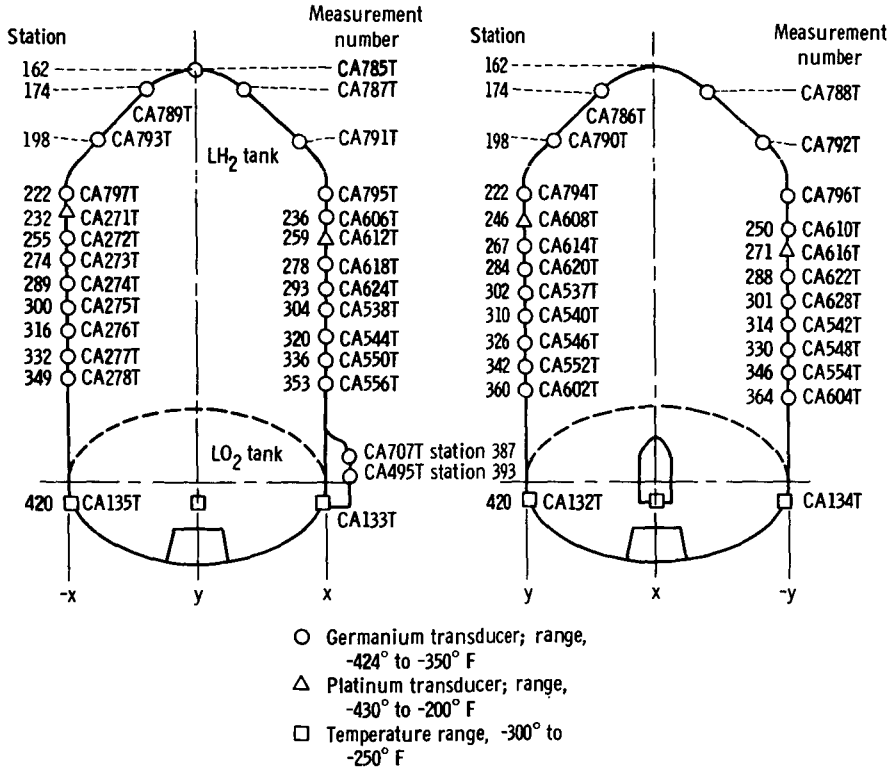

Figure VII-7. - Tank-skin temperature instrumentation for AC-8.

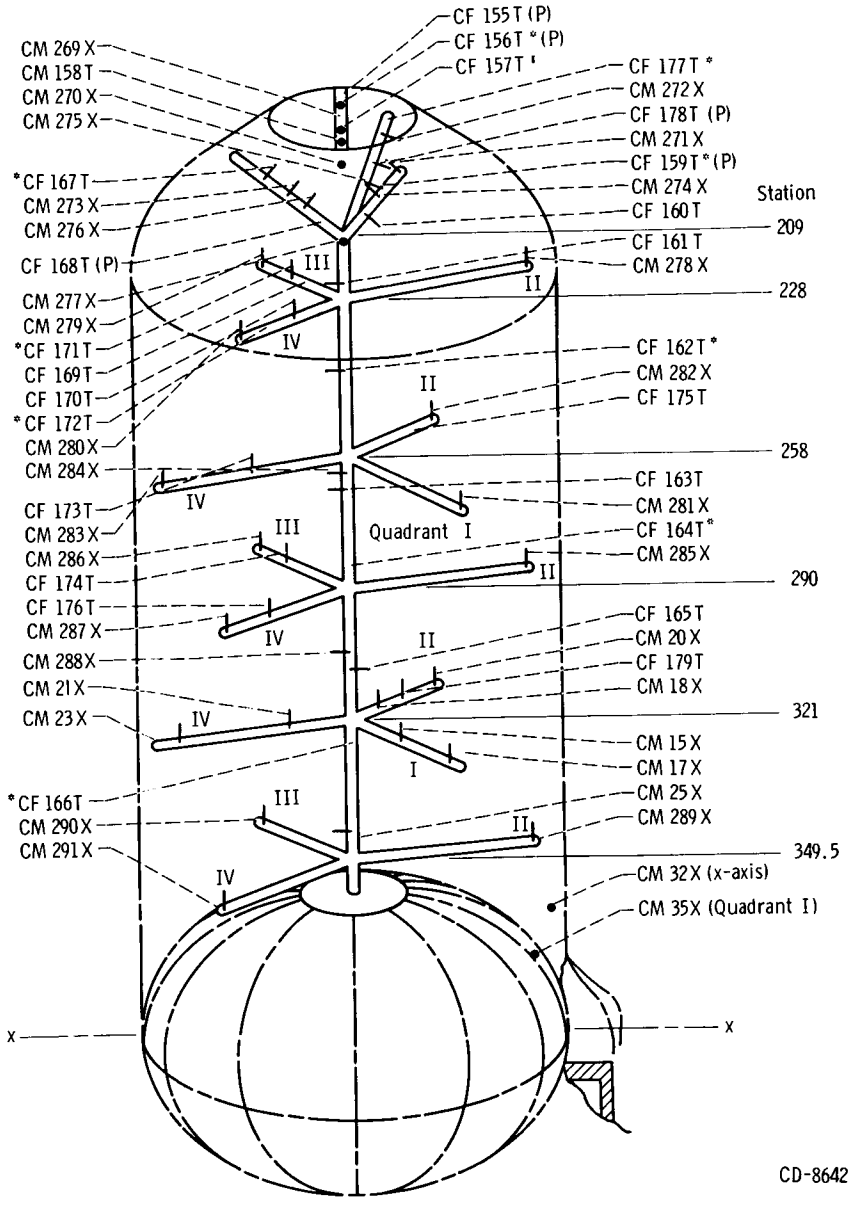

Figure VII-8. - AC-8 liquid-vapor sensors and ullage gas temperature sensors. Platinum transducers are indicated by (P). Asterisks indicate redundant instrumentation.

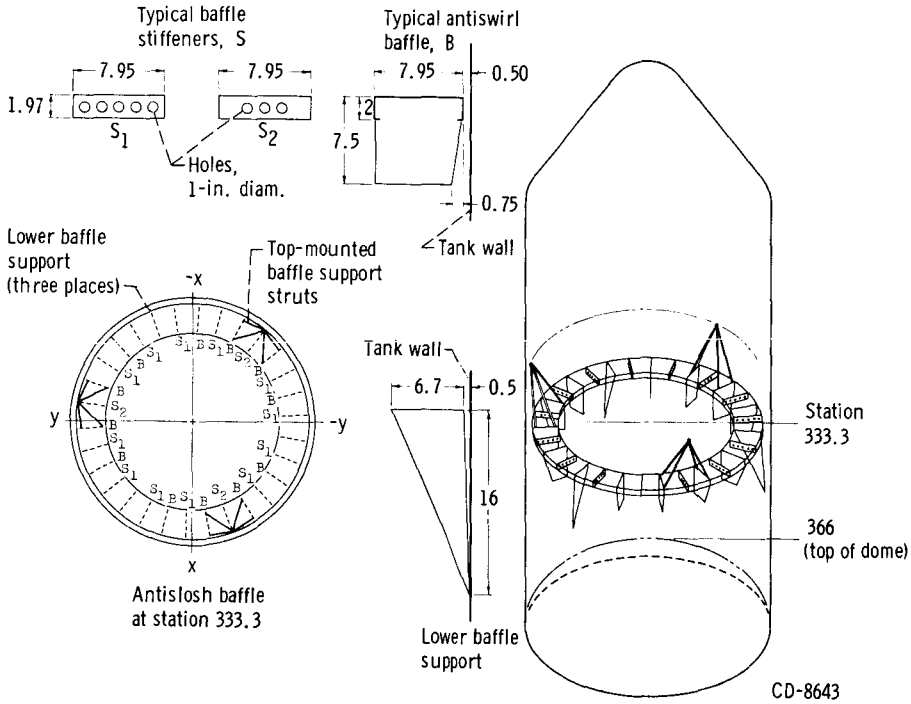

Figure VII-9. - AC-8 liquid-hydrogen-tank ring baffle. (all dimensions are in inches.)

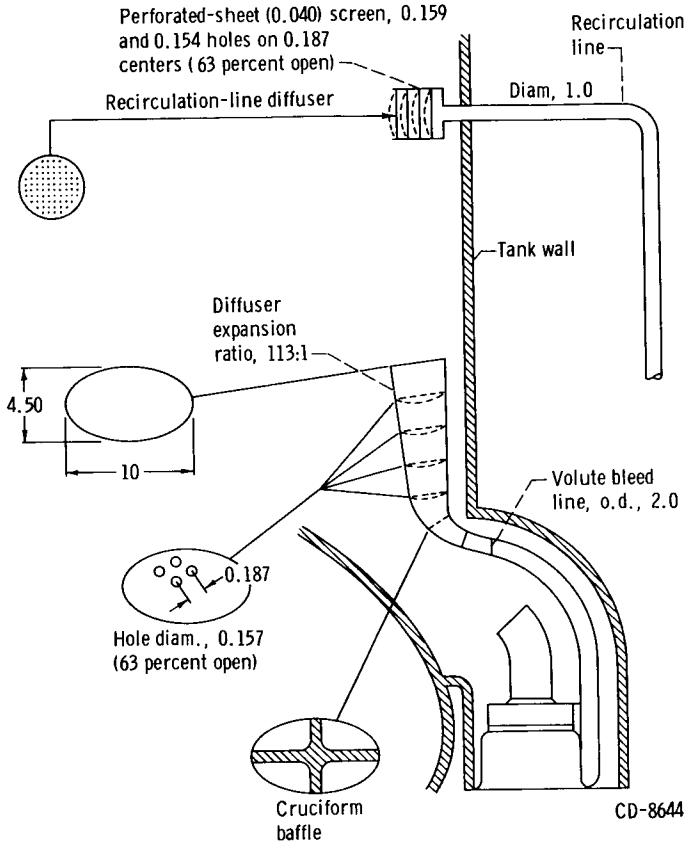

Figure VII-10. - Volute- and recirculation-line energy dissipating diffusers. (All dimensions are in inches.)

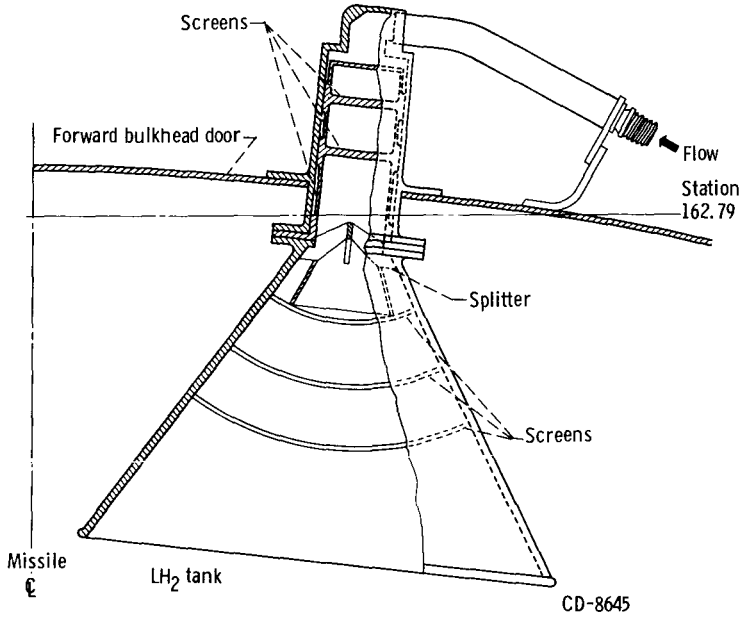

Figure VII-11. - Helium pressurization line energy dissipator for hydrogen tank.

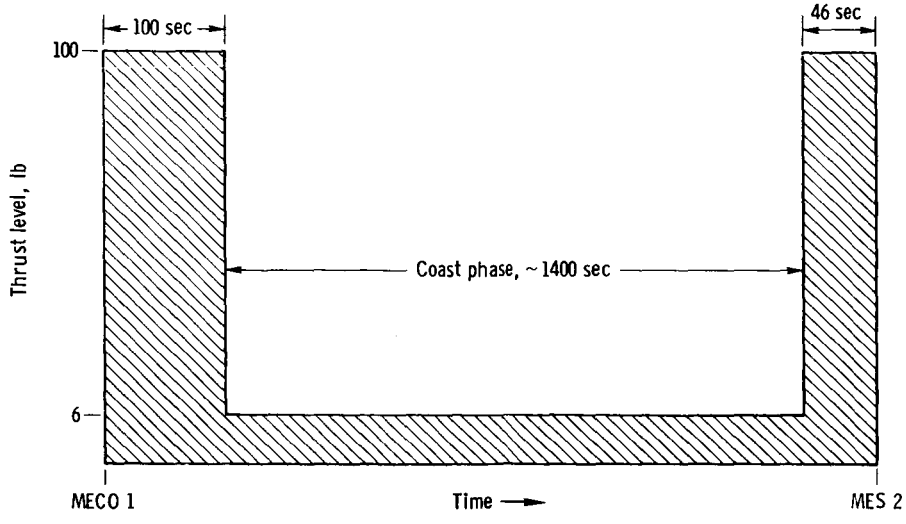

Figure VII-12. - Planned propellant settling and retention thrust schedule for AC-8.

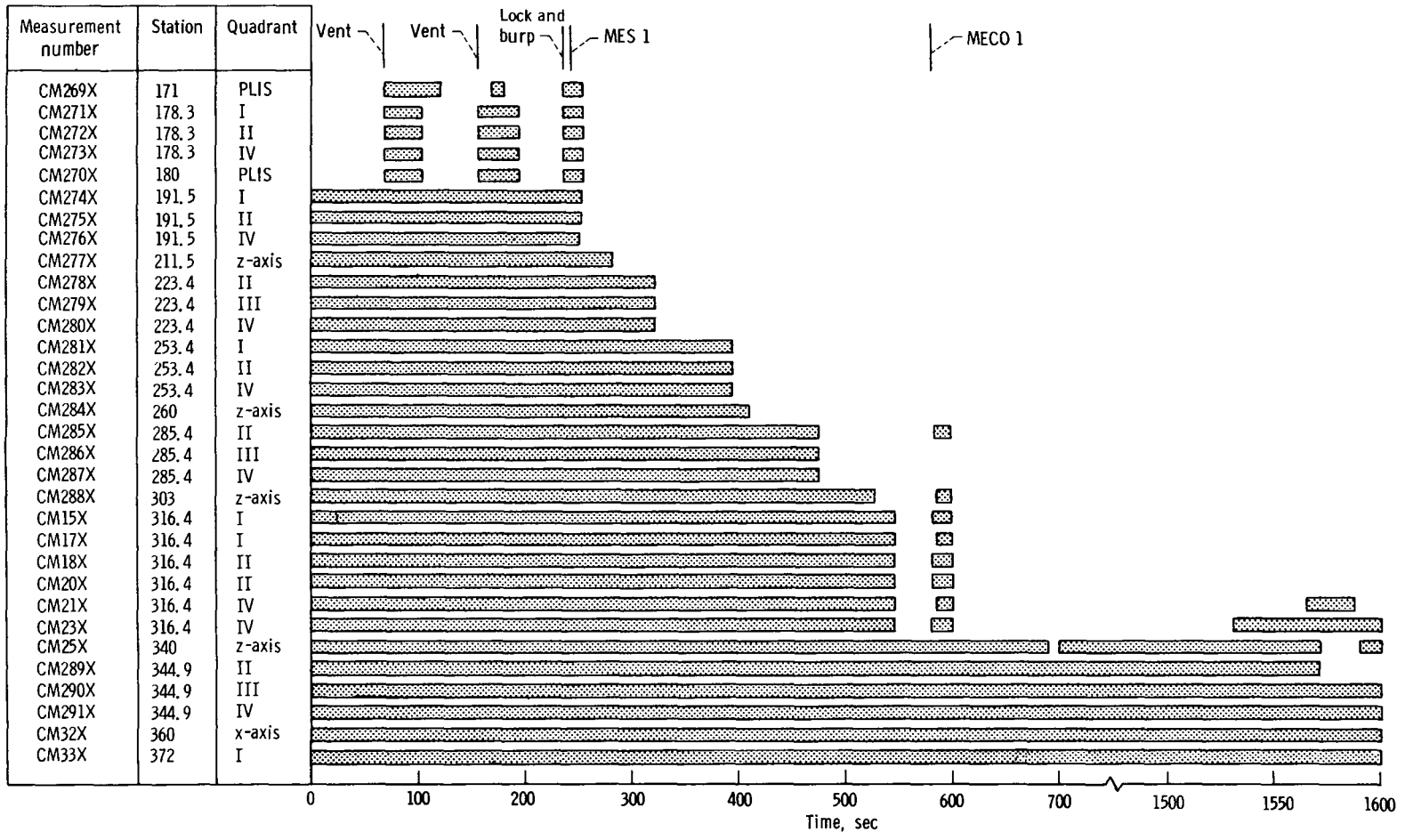

(a) Time, T + 0 to T + 1600 seconds.

Figure VII-13. - AC-8 liquid-vapor sensor behavior.

Measurement number	Station	Quadrant
CM269X	171	PLIS
CM271X	178.3	I
CM272X	178.3	II
CM273X	178.3	IV
CM270X	180	PLIS
CM274X	191.5	I
CM275X	191.5	II
CM276X	191.5	IV
CM277X	211.5	z-axis
CM278X	223.4	II
CM279X	223.4	III
CM280X	223.4	IV
CM281X	253.4	I
CM282X	253.4	II
CM283X	253.4	IV
CM284X	260	z-axis
CM285X	285.4	II
CM286X	285.4	III
CM287X	285.4	IV
CM288X	303	z-axis
CM15X	316.4	I
CM17X	316.4	I
CM18X	316.4	II
CM20X	316.4	II
CM21X	316.4	IV
CM23X	316.4	IV
CM25X	340	z-axis
CM289X	344.9	II
CM290X	344.9	III
CM291X	344.9	IV
CM32X	360	x-axis
CM33X	372	I

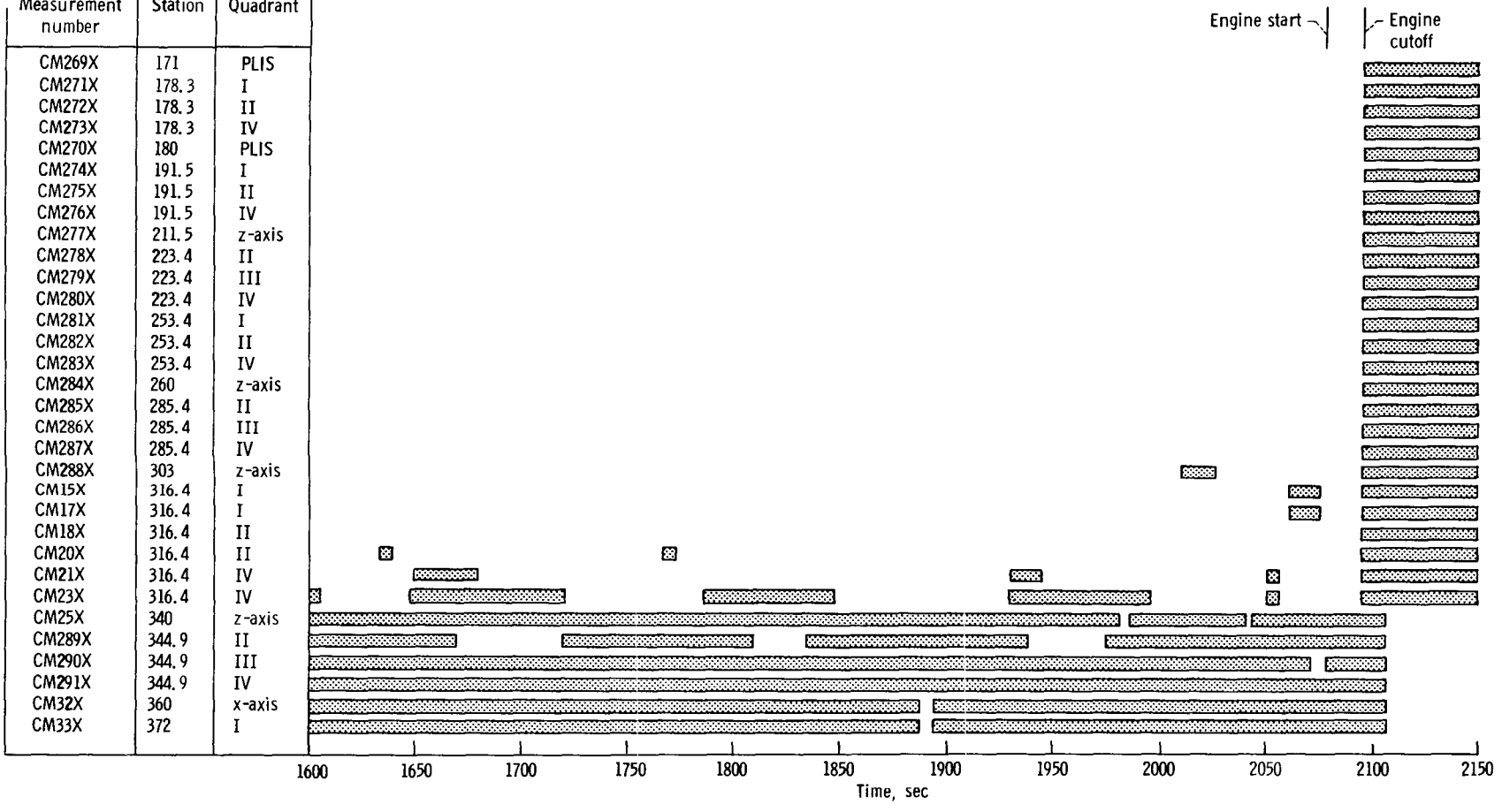

(b) Time, T + 1600 to T + 2150 seconds.

Figure VII-13. - Continued.

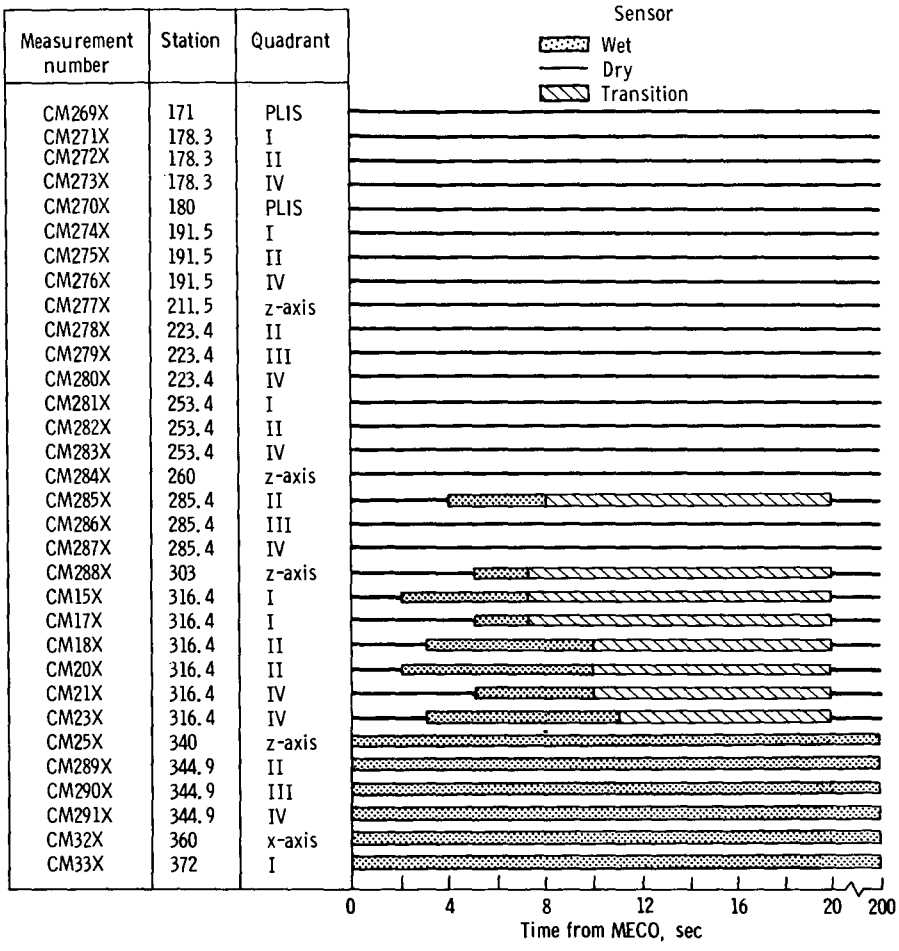

(c) First main engine cutoff.

Figure VII-13. - Concluded.

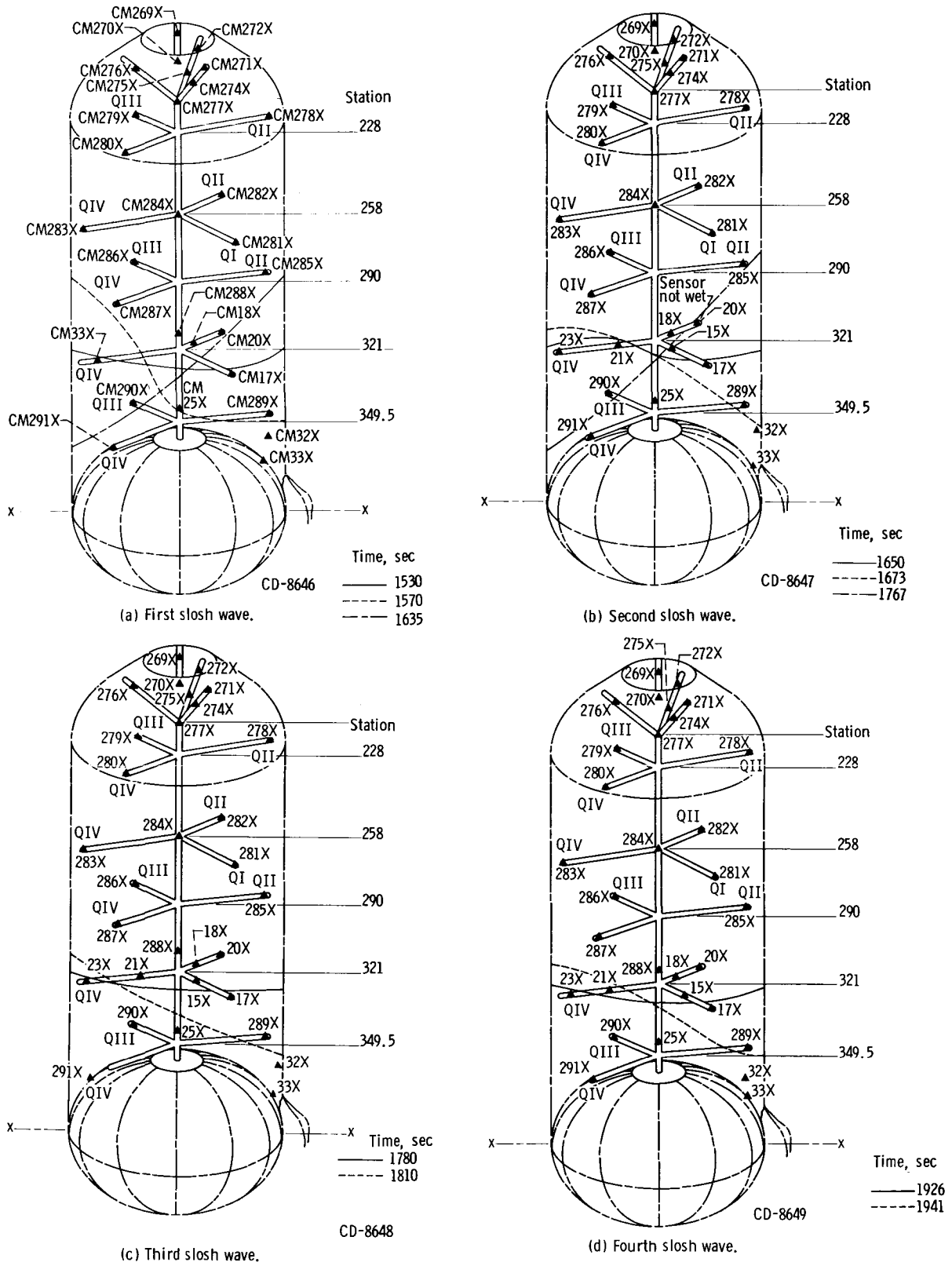

Figure VII-14. - Hydrogen slosh waves during coast.

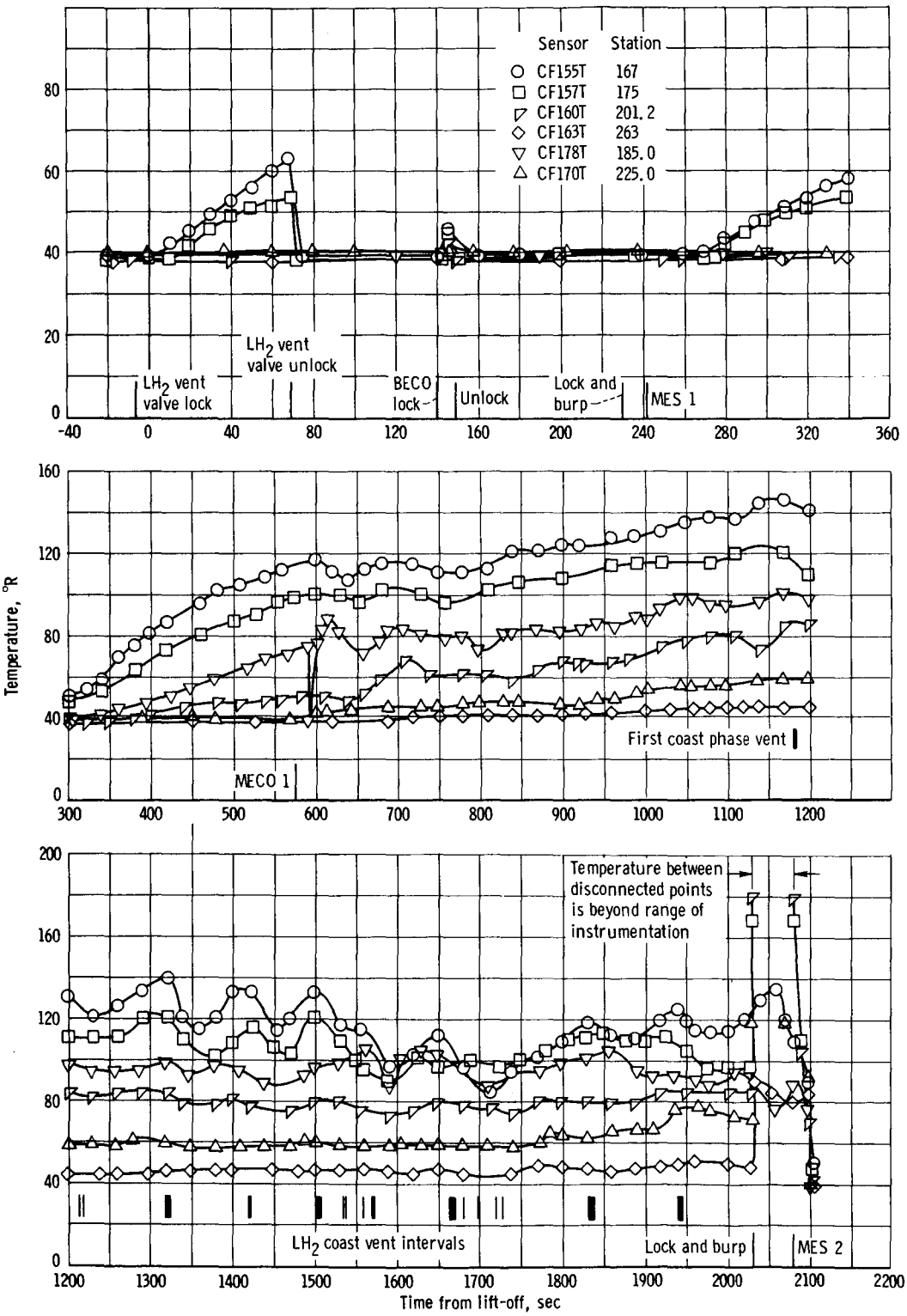

Figure VII-15. - Liquid hydrogen tank ullage temperature profiles.

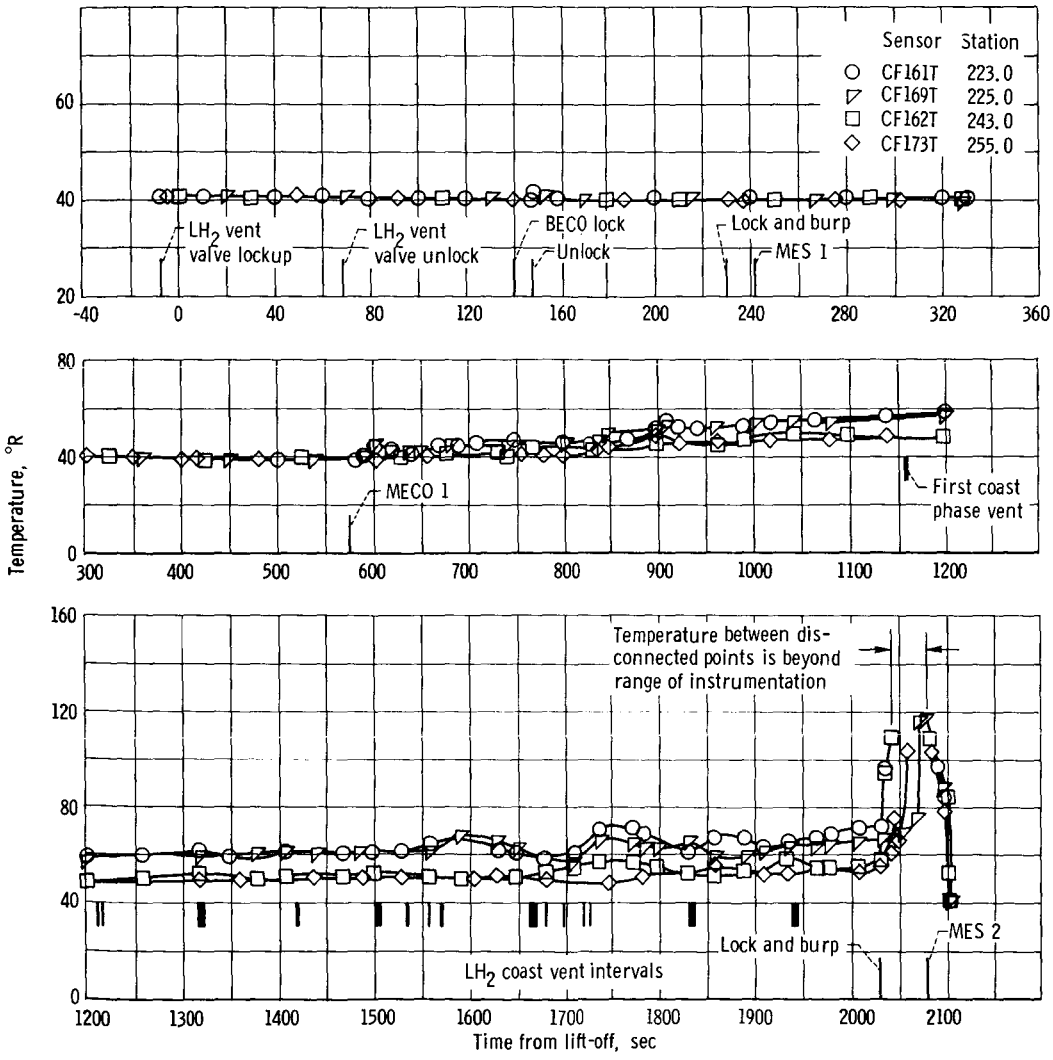

Figure VII-15. - Concluded.

VIII. PNEUMATICS AND HYDRAULICS

SUMMARY

Pneumatic and hydraulic system performance on the Atlas and Centaur was satisfactory and supported fully the AC-8 two-burn mission requirements. Pressure stability and regulation were maintained in both the Atlas and Centaur hydraulic circuits. Pressurization of the propellant tanks was normal throughout powered and coast phase flight, and all vent valves controlled within specified pressure limits. Hydrogen tank pressure rise rates during nonventing periods were 4.05 psi per minute during boost flight and 0.484 psi per minute during coast phase.

Step pressurization (burp) of the Centaur propellant tanks in support of MES for the first and second burn was satisfactory. The LO_2 tank burp during MES 1 was controlled for the first time using a pressure cutoff switch rather than the timed burp that was used on previous flights. At MES 2, with all propellants settled, a timed burp of 18 seconds was employed successfully to step up both LO_2 and LH_2 tank pressures.

Overboard venting of the hydrogen boiloff gas during the orbital coast period was accomplished by using a newly designed balanced thrust vent system. This system performed well, and there was no evidence either of liquid entrainment or of the discharging vent gases creating unbalanced forces on the vehicle.

PROPELLANT TANK PRESSURIZATION

Pressurization of the Centaur propellant tanks was maintained successfully throughout the AC-8 flight. Control of pressure and relief of boiloff gases were accomplished by using a dual vent-valve configuration on the hydrogen tank and a single vent valve on the LO_2 tank. Two of the valves, one on each tank, were solenoid controlled and, on programer command, could be positioned in either a locked (nonventing) or a normal relief mode. Nonventing time for gaseous hydrogen was established from T - 7 to T + 69 seconds and during Atlas booster staging (BECO) to avoid exposure of the vent gases to possible external ignition sources. During these nonventing times, a secondary vent valve, set to relieve at higher pressures, guarded against overpressurization of the hydrogen tank. During the MES sequences, both LO_2 and LH_2 vent valves were locked to allow step pressurization for boost pump start.

Powered-Flight Phase

Hydrogen tank ullage pressures, during prelaunch and initial boost phase of flight, were affected by two significant design changes. The insulation panel helium purge rate during the prelaunch period was reduced from 200 to 90 pounds per hour (thereby reducing the heat input to the hydrogen tank), and the hydrogen vent system was redesigned, as shown in figure VIII-1, to provide nonpropulsive vent capability during the low-gravity coast phase. The net results of these changes were (1) higher LH_2 ullage pressures prior to primary vent-valve lockup at T - 7 seconds because of the increased vent ducting back pressure, and (2) a lower pressure rise rate during the initial primary vent-valve lockup period from T - 7 seconds as a result of the reduced heat input. The hydrogen was tanked to a minimum ullage of only 11 cubic feet.

Tank pressure data during the AC-8 flight are shown in figure VIII-2. As shown, the hydrogen tank ullage pressure was 21.6 psia at the T - 7-second lockup and increased to the relief pressure of the secondary vent valve (26.5 psia) at T + 64.5 seconds. The secondary valve relieved momentarily and, 4 seconds later at T + 68.5 seconds, the primary valve unlocked and tank pressure was relieved. The pressure rise rate during this nonventing period was considered low, 4.05 psi per minute, but was about the same as the 3.73-psi-per-minute rise observed on AC-6. The vent-valve action appeared normal throughout the flight. Relief and reseat pressures were consistent, and there was no evidence of instability or valve leakage.

Step pressurization (burp) of the Centaur propellant tnaks in support of MES 1, as shown in figure VIII-2(b), was very effective. The LH_2 tank burp was 1 second long, and it increased the ullage pressure from 20.2 to 21.5 psia, a Δ pressure of 1.3 psi. The LO_2 ullage pressure during the burp was limited to 40 psi by a limit pressure cutoff switch. With an initial LO_2 ullage pressure of 29.8 psia, an increase of 10.2 psi was attained. It should be noted that the burp command for the LO_2 tank (MES 1 only) was a continuous signal for nominally 44 seconds. Therefore, whenever the ullage pressure decayed, as the burp gas cooled, the limit switch would cycle and the tank pressure would build up again.

The limit pressure switch and the extended burp sequence for the LO_2 tank were incorporated for the first time on AC-8. This change in configuration over earlier time-burp sequences was the result of flight experience on AC-6, wherein the pressurization during MES 1 was marginal. Sizing the burp for the LO_2 tank is governed by the very small ullage (7.5 cu ft) and the maximum tank pressure limits. Pressure was difficult to control with a pure time burp; therefore, the pressure switch system was conceived, and its performance was proven on AC-8.

Ullage temperature data during the powered flight phase, as shown in figures VIII-3(a) and (b), indicated that temperatures were nominal. Some stratification developed in the

hydrogen ullage, and the temperature at the top of the tank reached 118° R at MECO 1. It is also of interest to note that the sudden wetting of the forward bulkhead with LH_2 at MECO did not occur as it had in previous flights, which indicated that the energy suppression devices and increased thrust settling rockets adequately constrained the liquid residual disturbances at MECO.

Coast Phase

Propellant tank pressure and temperature profiles during the coast phase, as shown in figures VIII-2 and VIII-3, indicated a normal behavior. The thermal environment during the coast was reduced markedly by the nighttime launch, and the tank pressure rise rates were less than those predicted for a daytime launch.

The LO_2 tank ullage pressure increased from 27 psia at MECO 1 to a stable value of about 29.8 psia at lockup for MES 2. The LO_2 tank did not vent at any time during the coast phase. Corresponding ullage temperature data were constant at 175° R during the coast, which also indicated a thermally stable LO_2 tank.

The hydrogen tank pressure rise during the initial coast period was relatively slow because of the night environment. Pressures increased from 15.6 psi at MECO 1 (T + 575.5 sec) to 20.5 psia at T + 1182 seconds, when the primary vent-valve opened and began to control tank pressure. This was an average pressure rise rate of 0.484 psi per minute for the nonventing period. The corresponding pressure rise rate prediction for a daytime launch was about 1.0 psi per minute.

The hydrogen tank ullage temperature data (figs. VIII-3(b) and (c)) show appreciable warming in the ullage. Temperatures in the top of the tank increased from about 118° R at MECO 1 to 150° R at T + 1182 seconds, when the primary vent valve relieved for the first time. Thereafter, the venting cycle can be observed from the temperature data, as shown in figure VIII-3(c). Each time the vent valve relieved, hot gas vented off the top of the tank and the temperature dropped. Then, when the valve reseated, the upper layers of gas gradually warmed up again.

The ullage temperature data immediately following MECO 1 were also significant. As shown in figure VIII-3(b), the gas temperature continued to rise for about 25 seconds following MECO and then dropped off and started to vacillate. At MECO + 165 seconds, the temperatures stabilized and began to rise steadily. This phenomena may be explained by slight changes in convective heat transfer from the tank walls to the ullage caused by abrupt changes in vehicle acceleration at MECO and MECO + 100 seconds when the 100-pound ullage rockets cut off. Inertia effects introduced some time lag but, in both instances, there was an adjustment to a new thermal environment. Once the small amount of residual thermal energy stored in the tank walls was released, the tank walls

remained relatively cool. Subsequently, with the thrust level reduced to 6 pounds, as required for propellant retention, the ullage gas temperature increased much less rapidly.

Second Main Engine Start

Prior to the MES 2 sequence, the LO_2 and LH_2 tank pressures were controlled normally at 29.8 and 20.4 psia, respectively. The step pressurization for boost pump start was a sustained burp of 18 seconds in the LO_2 tank and 46 seconds in the LH_2 tank, as shown in figure VIII-2(e). LO_2 tank pressure increased 1.4 psi to 31.2 psia, and LH_2 tank pressure was stepped up 6.4 psi to 26.8 psia. This was adequate to support the engine restart.

Several changes were made in the AC-8 burp configuration as a result of previous flight experience. An energy dissipater was added to the helium discharge line in the hydrogen tank to eliminate the high-velocity gas scrubbing action over the tank walls and across the liquid surface. Results from AC-4 indicated that high-velocity gas injection during burp swept liquid droplets into the ullage. These droplets in turn flashed off, cooled the ullage, and resulted in a depression of the ullage pressure. Inclusion of the energy suppression devices, however, proved successful, and this effect was not encountered on the AC-8 flight.

Actually, the hydrogen tank burp, while satisfactory, was greater than expected and resulted in the secondary vent valve relieving for 12 seconds to maintain tank pressure. This result would have been expected for a normal daytime launch, but it was not normal for the AC-8 conditions. Reason for this disparity may be attributed to events culminating in the premature engine shutdown. Under normal conditions of engine restart, the boost pumps recirculate LH_2 back into the tank in such a manner that the liquid stream turbulates the liquid in the tank and also erupts through the surface to produce a distinct cooling effect within the ullage. These liquid disturbances, while greatly reduced by the addition of energy dissipation devices, are still sufficient to produce a cooling effect in the ullage; this cooling effect in part counteracts the pressure rise during the burp pressurization sequence. On AC-8, however, the cooling effect was not realized fully because the boost pump operation was terminated prematurely by a deficiency of hydrogen peroxide. Consequently, the burp pressurization was more pronounced.

The marked decrease in the ullage pressure after MES 2 is attributed to a depletion of the liquid and also to sloshing of the residuals. Nonsymmetrical engine thrust forced the liquid around in the tank. Thus, a substantial cooling occurred. Premature engine shutdown resulted only 17 seconds later, and the sudden loss of thrust further displaced the liquid residuals. As noted in figure VIII-3(d), the forward bulkhead indicated the presence of LH_2 immediately after MECO. A summary of the tank pressurization data is given in table VIII-I.

HYDROGEN VENTING

Balanced Thrust Hydrogen Vent System

The hydrogen vent system on AC-8 was a redesigned system to provide nonpropulsive venting capability during the low-gravity orbital coast period. This system (fig. VIII-1) was comprised of a 2.5-inch-diameter torus-like ducting located inside the payload adapter with two horizontal ducts extending outward in opposite directions along the y-y axis. Convergent 1.35-inch-diameter nozzles, were installed at the duct exits. The vent valves and inlet ducting were relocated to the forward tank door, such that flow through the valves relieved directly into each side of the torus on the x-x axis. The concept of the torus was to provide equal flow splitting and pressure equalization at the nozzle exits and thereby equal thrust in opposite directions. The nozzle sizing was dictated by requirements to keep the internal-duct Mach number to a minimum, to limit maximum flow rates during the blowdown at T + 69 seconds to 0.7 pound per second, and to maintain tank pressure below 22.0 psia prior to T - 7 seconds.

Performance of the vent system was verified by extensive testing in the Lewis Research Center Space Power Chamber and at the General Dynamics/Convair test site at Point Loma. For maximum steady-state venting conditions, the thrust unbalance force did not exceed 0.15 pound. During non-steady-state venting, with the vent valve cycling, transient fluctuations in the thrust unbalance force were observed. However, these forces were self-cancelling and did not produce any net unbalance force.

Boost-Phase Venting

Performance of the vent system throughout the flight was satisfactory. The added back pressure in the vent system resulted in an ullage pressure of 21.6 psia during the prelaunch count time. This was slightly higher than experienced on previous vehicles, which had less restrictive vent systems. The boiloff rate during this same period was less than 0.3 pound per second. This was less than on previous flights because of a lower heat input caused by the insulation panel helium purge rate, which was decreased from 200 to 90 pounds per hour.

The vent flow rate data during the powered-flight phase are shown in figure VIII-4. Blowdown of tank pressure after vent-valve lockup periods, at T + 68.5 seconds, and after BECO were all accomplished without incident. The maximum vent flow rates, as shown in the figure, peaked out at about 0.748 pound per second. This was slightly in excess of the predicted 0.7 pound per second but did not cause any adverse effects.

A change in the vent-valve mode was observed at about T + 92 seconds. From the

initial blowdown at T + 68.5 seconds to this time, the nozzle inlet pressures remained very steady indicating that the vent valve was not cycling. Beyond this time, however, as a result of rapidly decreasing back pressure at the vent exit, the valve began its characteristic limit cycling at about 2.5 cps. The peak-to-peak vent rate amplitude that resulted from the cyclic motion of the valve indicated values as high as 0.77 pound per second. Gradually, as the boiloff gas was relieved and the tankage restored its thermal equilibrium, the vent rate dropped off and the valve cycled at a progressively lower frequency. Just prior to valve lockup at BECO and MES 1, the valve reseated for about 1 second between cycles. The total hydrogen vented overboard during this period was calculated to be 70 pounds.

Coast-Phase Venting

Hydrogen venting during the orbital coast did not begin until T + 1182 seconds, 607 seconds after MECO 1. During the remaining 847 seconds of the coast phase, the boiloff requirement was low because of the night environment and the tank vented infrequently. There was no evidence at any time of liquid entrainment as the vent gas temperatures were in excess of 100° R. The total hydrogen vented during the coast was calculated to be 5.2 pounds.

Nonpropulsive performance of the vent system was also demonstrated. Comparison of the vent periods with the attitude control system did not indicate any degree of correlation. It appeared that the vent thrust forces were indeed self-canceling and did not impart any torquing motion to the vehicle or, if any unbalanced forces did exist, they did not produce vehicle rates sufficient to exceed the threshold limits of the attitude control system. Pressure measurements across the vent system nozzles also did not indicate any thrust unbalance problem.

ATLAS HYDRAULIC SYSTEM

The performance data received indicated that the Atlas hydraulic system operated normally. Pressure stability and regulation, as shown in figures VIII-5(a) and (b), were maintained in both the booster and sustainer circuits except for some usual transients that occurred at engine start and at BECO. Sustainer and booster system steady-state pump pressure were maintained at 3100 psia.

CENTAUR HYDRAULIC SYSTEM

Evaluation of the data received from the AC-8 flight showed that both C-1 and C-2 hydraulic systems operated properly. Recirculation system operation prior to both engine starts was nominal at values of 120 psia for each engine, as shown in figure VIII-5(c). C-1 main system pressures reached 1155 psia for the first burn and 1110 psia for the second. C-2 pressures reached 1145 psia for the first burn and 1120 psia for the second.

The expected manifold temperature drop from T - 120 seconds, when the recirculation systems were shut down, until main engine start was approximately 10^{o} F, as shown in figure VIII-6. Both manifolds reached maximum temperatures of 172^{o} F at MECO. Temperatures dropped during coast to 90^{o} F on C-1 and 75^{o} F on C-2.

The recirculation systems drove the engines to the commanded null position prior to the first start with the exception of residual separation rate correction deflections. As shown in figure VIII-7 the C-1 engine was off null -0.04^{o} pitch and -0.26^{o} yaw. C-2 engine was off null -0.25^{o} pitch and -0.26^{o} yaw. These positions indicated that a slight separation disturbance caused a pitchup, yaw right, and slight clockwise roll.

Recirculation system operation prior to second start was nominal, and vehicle rates were almost nonexistent. Both engines were commanded hard-over to compensate for the differential impulse created by the C-1 engine thrust decay. In an attempt to compensate for vehicle tumble, the C-2 engine hit the stops five times at an average frequency of 0.3 cps.

TABLE VIII-I. - AC-8 PNEUMATICS SYSTEM DATA SUMMARY

Time, sec	Event	LO_2 tank pressure, psia	LH_2 tank pressure, psia	LH_2 pressure rise rate, psi/min	Helium burp, lb	Helium bottle		Engine control regulator out, psia	H_2O_2 bottle pneumatic pressure, psia
						Pressure, psia	Temperature, ^oR		
T - 7	Lock LH_2 valve	30.3	21.6	-----	----	3246	536	463	324
T + 64.5	Secondary LH_2 valve vent	----	26.5	4.05	----	----	---	---	---
T + 204	Lock LO_2 valve	29.8	----	-----	0.03	3211	533	---	---
	Burp LO_2 tank	40.0	----	-----		----	---	---	---
T + 229	Lock LH_2 valve	----	20.2	-----		----	---	---	---
	Burp LH_2 tank	----	21.5	-----		3026	523	---	---
T + 242	MES 1	39.5	20.8	-----	----	----	---	---	312
T + 575	MECO 1	27.0	15.6	-----	----	2977	521	444	312
T + 675	Thrustoff (100 lb)	28.1	16.5	-----	----	2881	---	---	---
T + 1182	LH_2 coast vent 2	28.9	20.5	.484	----	----	---	---	---
T + 2029	Lock LH_2 and LO_2 valves	29.8	20.4	-----	----	2756	520	444	310
	Burp LO_2 and LH_2 tanks	31.2	26.8	-----	3.8	936	362	---	---
T + 2160		29.8	21.5	-----	----	1153	449	---	---

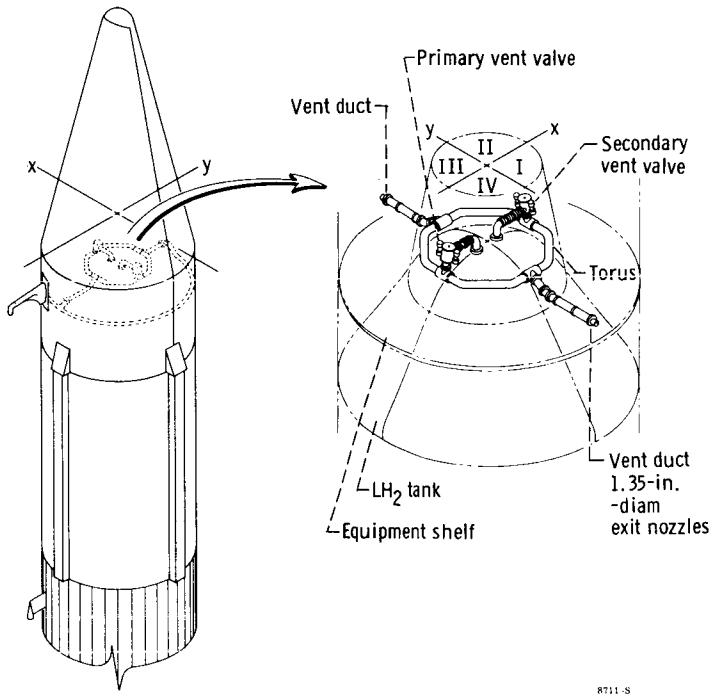

Figure VIII-1. - Balanced thrust hydrogen vent system for AC-8.

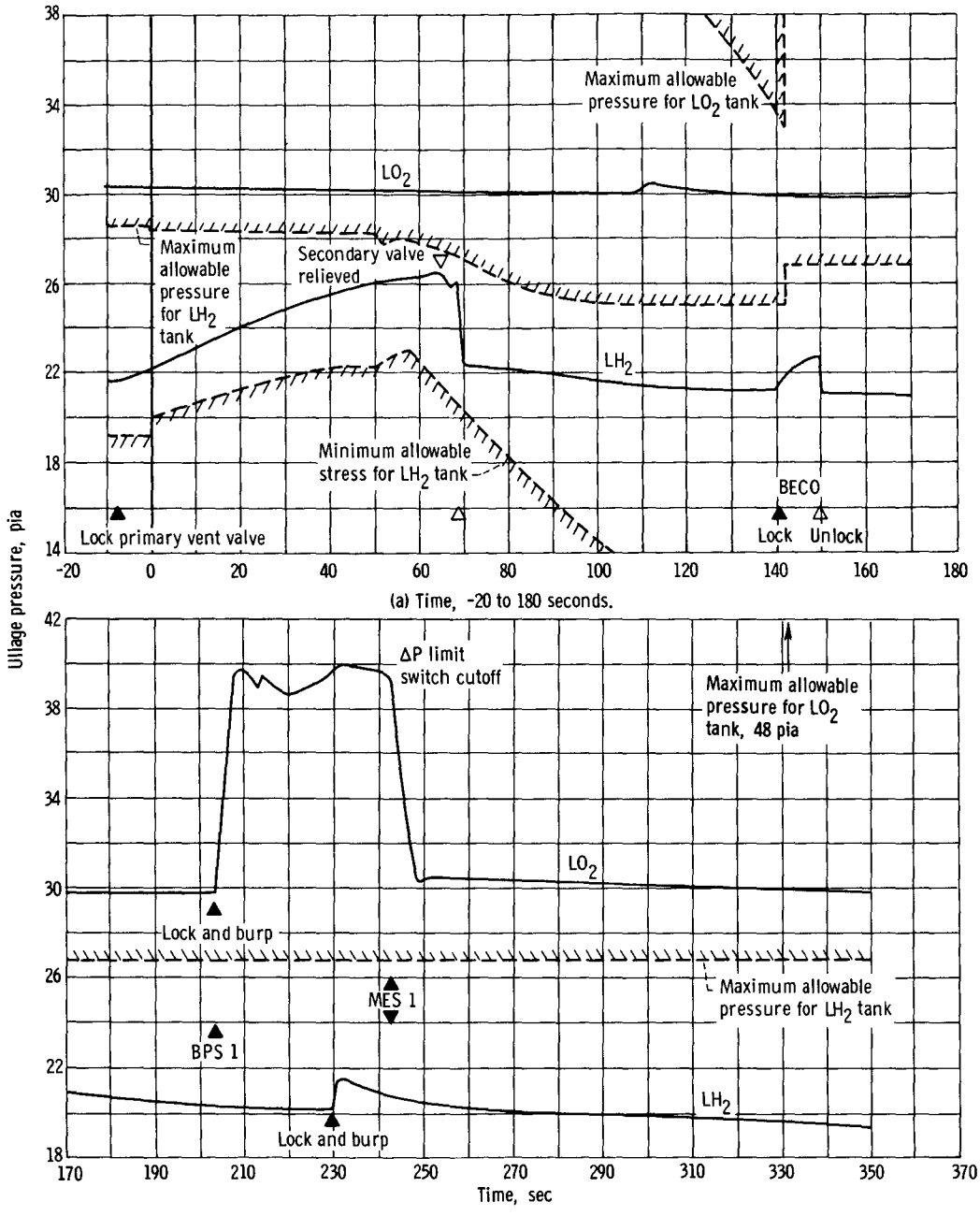

Figure VIII-2. - AC-8 pressure profiles for liquid hydrogen and liquid oxygen tanks.

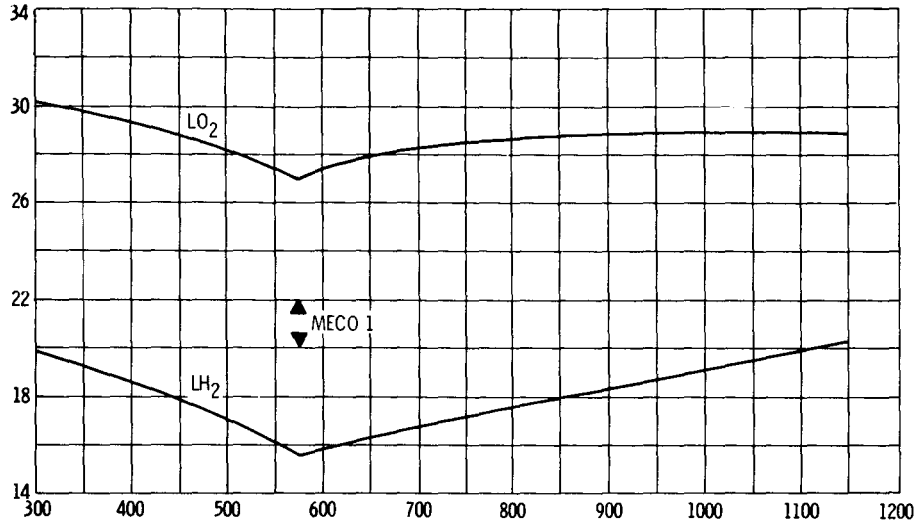

(c) Time, 300 to 1200 seconds.

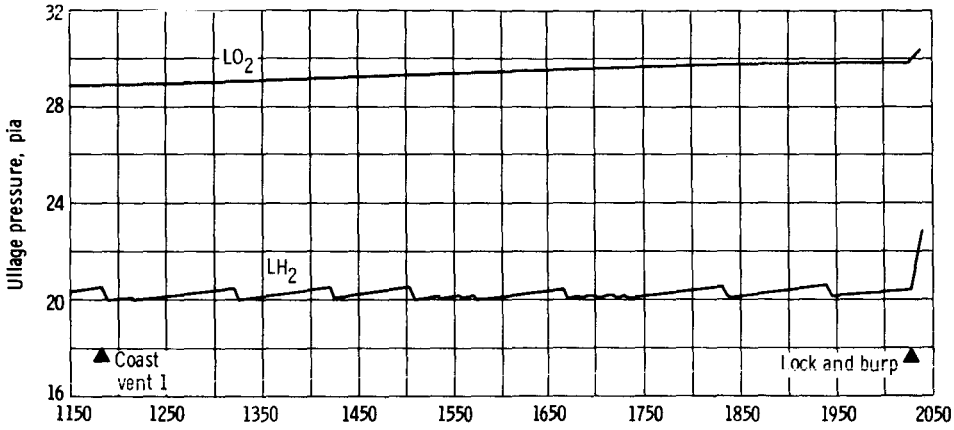

(d) Time, 1150 to 2050 seconds.

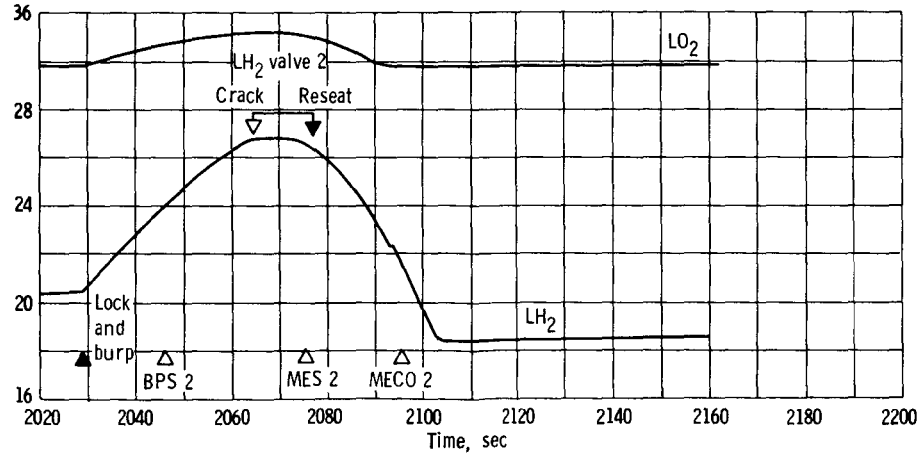

(e) Time, 2020 to 2200 seconds.

Figure VIII-2. - Concluded.

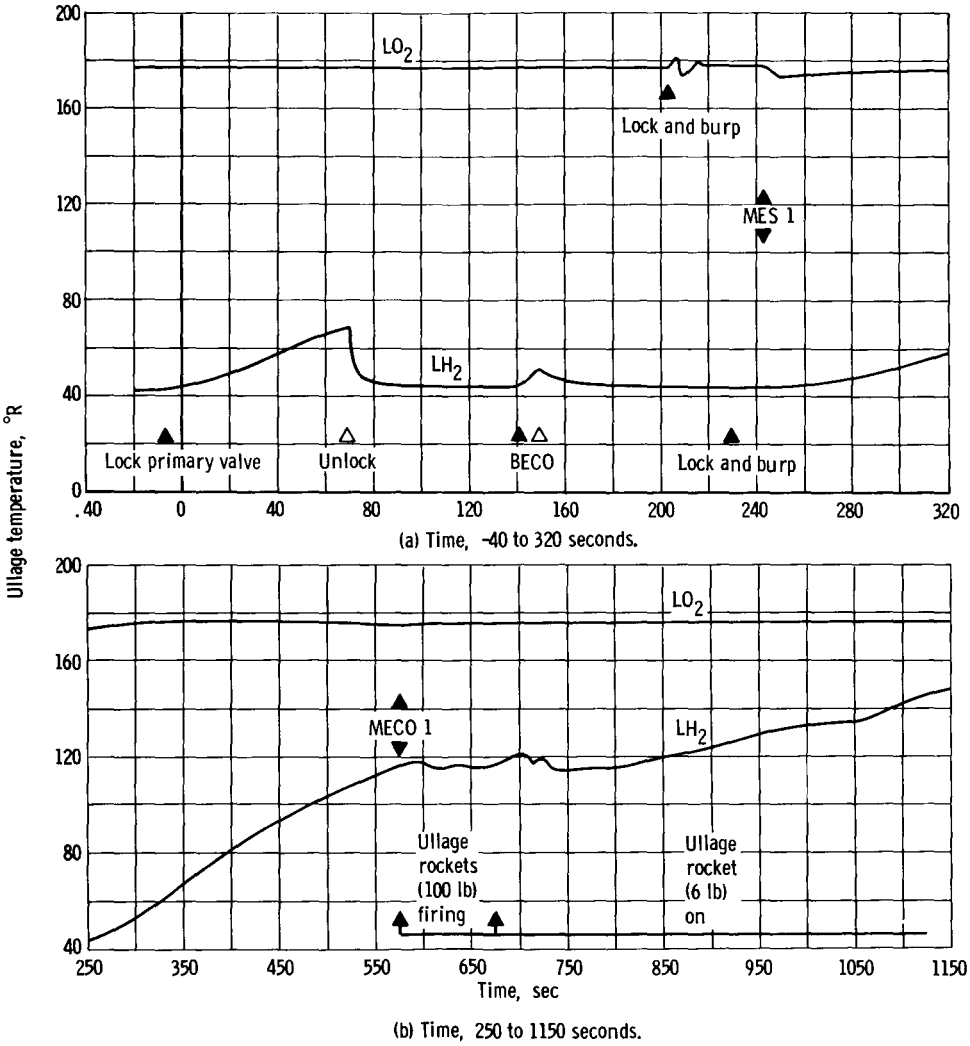

Figure VIII-3. - Liquid hydrogen and liquid oxygen ullage temperatures for AC-8.

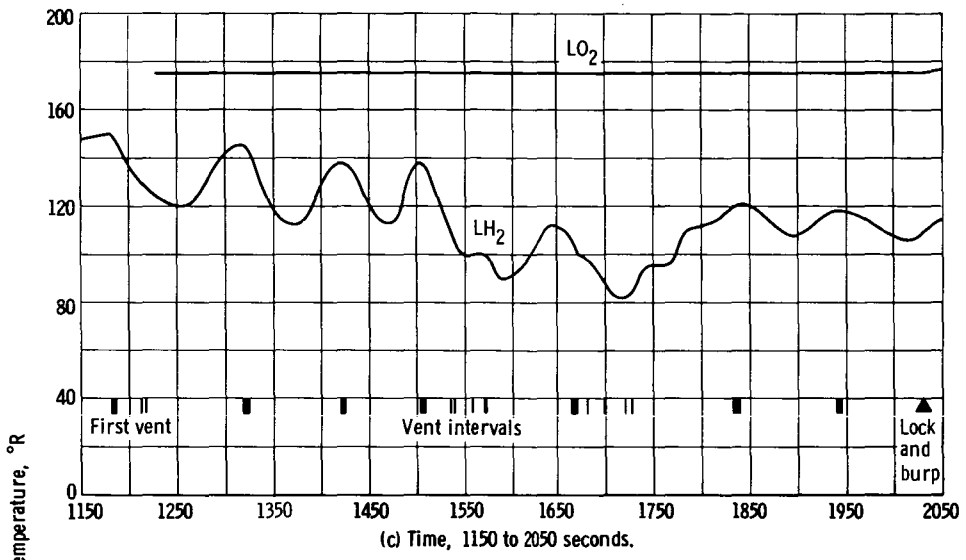

(c) Time, 1150 to 2050 seconds.

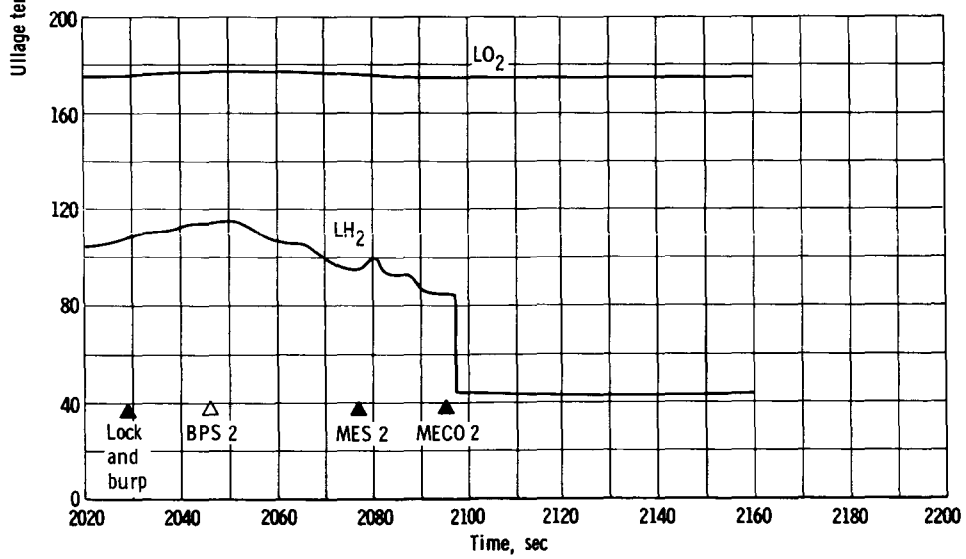

(d) Time, 2020 to 2200 seconds.

Figure VIII-3. - Concluded.

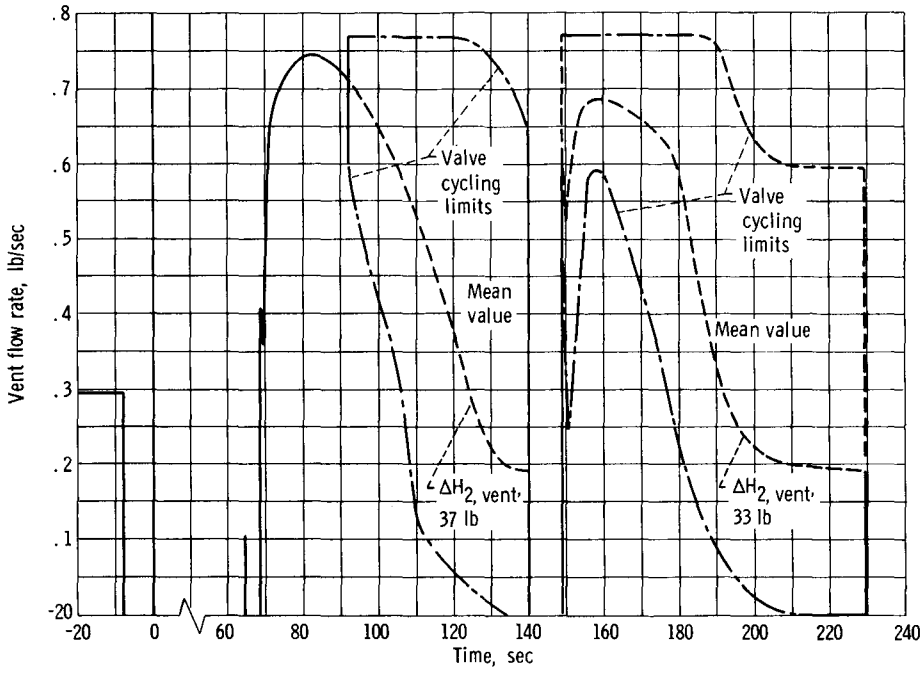

Figure VIII-4. - Hydrogen vent flow rate for AC-8 boost phase.

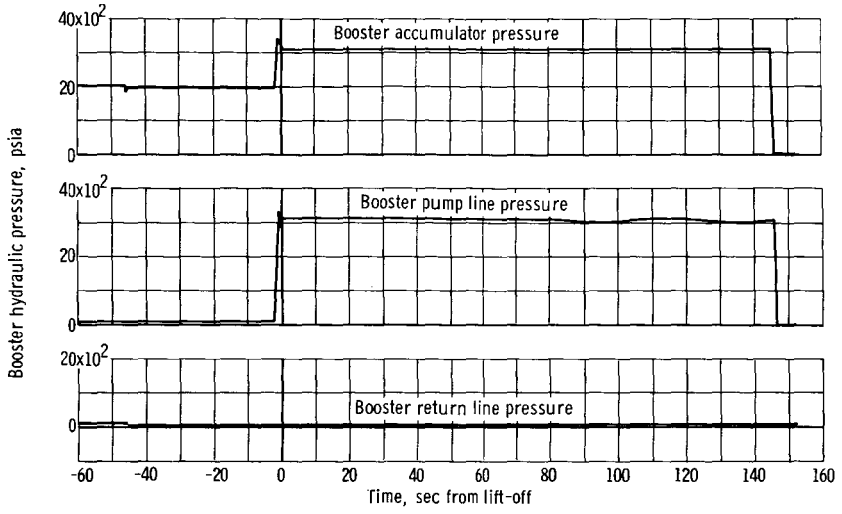

(a) Booster hydraulic pressures.

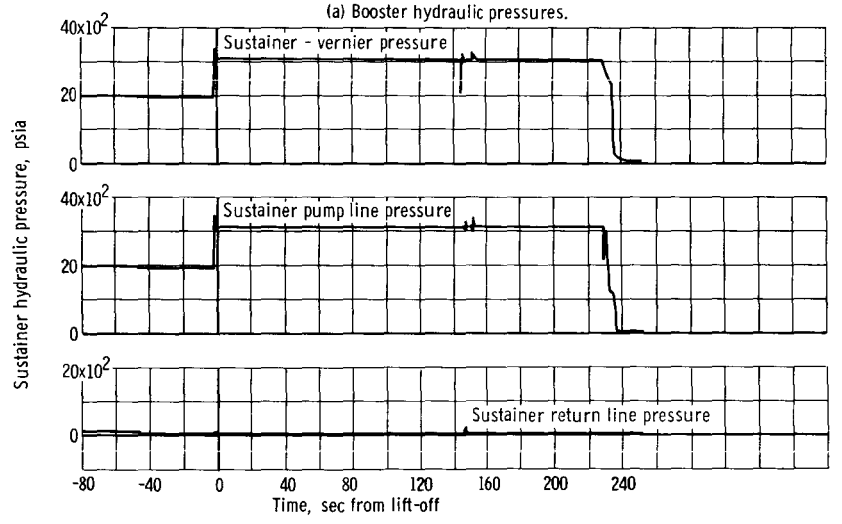

(b) Sustainer hydraulic pressures.

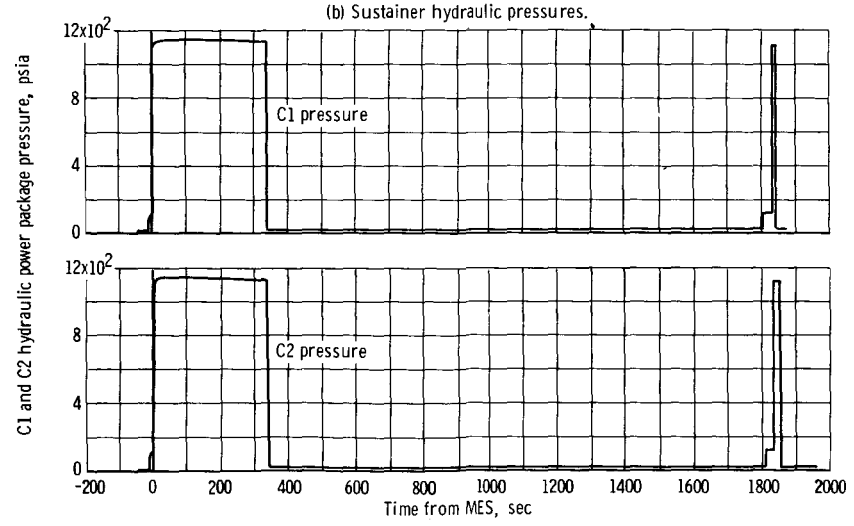

(c) C1 and C2 hydraulic pressures.

Figure VIII-5. - Hydraulic pressures as function of time.

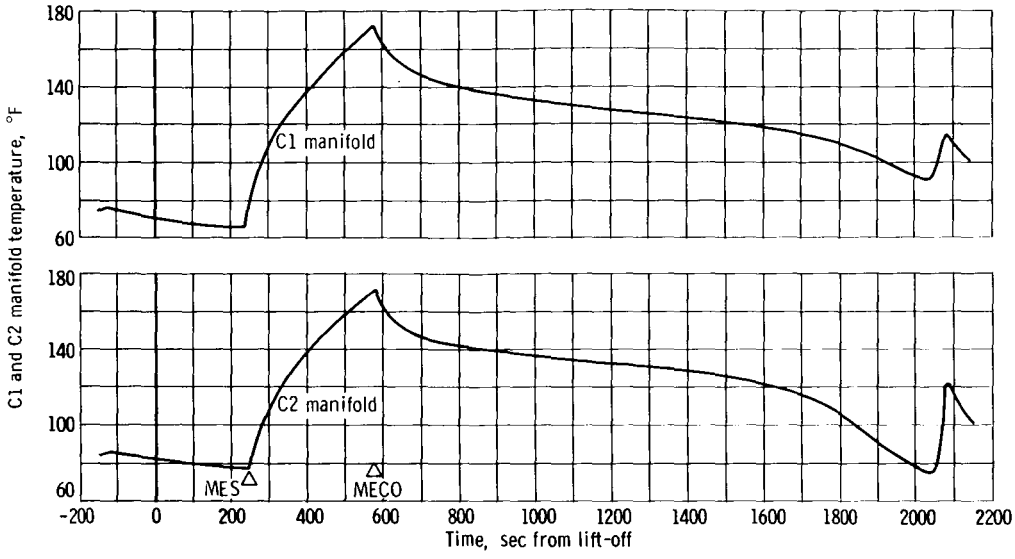

Figure VIII-6. - Hydraulic manifold temperatures as function of time.

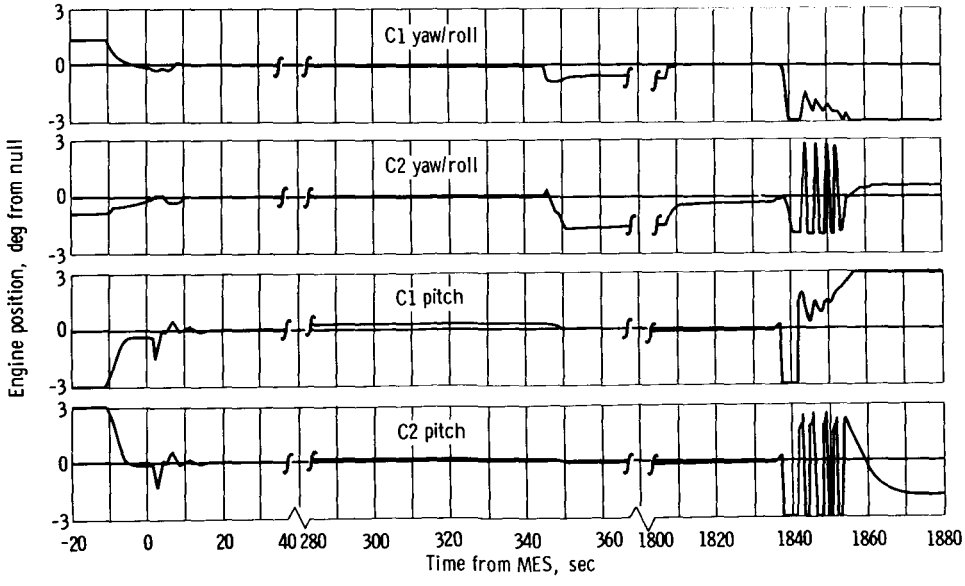

Figure VIII-7. - Engine position as function of time through engine start and cutoff transients.

IX. EXTERNAL TEMPERATURE ENVIRONMENT

SUMMARY

The external temperature environment experienced on the AC-8 vehicle indicated a less than nominal heating trajectory. Limited use of Thermolag provided additional protection for the nose fairing and insulation panels.

NOSE FAIRING

The AC-8 nose fairing was instrumented as shown in figure IX-1 to aid in the study of the internal and external surface temperature profiles. The resulting temperature - time curves are shown in figures IX-2 to 5, and the maximum external temperatures are summarized in table IX-I. In general, the actual temperatures ranged from 50° to 200° F below the predicted temperature.

The temperature profile along the -y-axis of the axis of the fairing is shown in figure IX-3. The internal temperatures were maintained below 85° F, which indicated that the Thermolag operated efficiently in reducing heat conduction through the fairing walls. The external temperature measurements were located in a 4-inch-diameter area that was void of Thermolag, and all temperatures were below the predicted, which indicated a less than nominal heating trajectory.

The nose-cap stagnation point internal and external temperature measurements were invalid. The temperatures at positions 30° and 60° from the z-axis indicate that the maximum stagnation point temperature would have been approximately 600° F. The AC-8 nose-cap thickness was increased from 0.2 to 0.32 inch to reduce internal cap temperatures. This appeared to have been sufficient since the internal cap temperature was a maximum of 85° F, which is much less than the predicted 200° F.

The maximum temperature experienced on the vehicle as a result of aerodynamic heating was 775° F on the leading edge of the hydrogen vent stack, 18 inches outboard of the vehicle.

INSULATION PANELS

The AC-8 insulation panels were instrumented as shown in figure IX-6. The internal panel temperatures (fig. IX-7) varied between -365° and 340° F at lift-off and between -355° and -330° F at panel jettison. The aerodynamic heating of the flat portions of the panels was moderate, as shown in figures IX-7 and IX-8, and maximum temperatures between 170° and 230° F were established. The low temperatures at lift-off (20° to 25° F) were attributed to the night launch.

The external temperature profile along the x-axis of the wiring tunnel and boost pump fairing is shown in figure IX-9. The 310° F maximum recorded on the boost pump fairing was 90° F less than the predicted 400° F.

INTERSTAGE ADAPTER

The AC-8 interstage adapter temperature instrumentation is shown in figure IX-10. The adapter temperatures were uniform and moderate, and the maximum temperatures are summarized in table IX-II. All adapter temperature transducers were located in areas void of Thermolag.

COAST-PHASE SPACE HEATING

A total of 15 calorimeters (5 black, 5 white, and 5 gold), as shown in figure IX-11, were installed on the AC-8 forward equipment shelf to determine the heat input to the Centaur LH_2 tank during flight. Because the AC-8 mission was completed in the shadow of the Earth, only Earth thermal radiation was of significance. The resulting net heat flux to the LH_2 tank was low and represented minimum heating values. The net heat flux into the four areas of the cylindrical portion of the LH_2 tank and their mean values are presented in figure IX-12. The average net heat flux during coast was 8.3 Btu per hour per square foot.

ATLAS LIQUID OXYGEN TANK SKIN TEMPERATURES

Maximum temperatures recorded during the AC-8 flight were slightly higher than for either the previous AC-4 two-burn mission or the AC-6 single-burn mission. The time of maximum temperature was also slightly earlier in flight, but this may be attributed to the uprated booster engines on AC-8. All temperatures, however, are within

acceptable structural limits. A comparison of maximum flight temperatures and times of occurrence for AC-4, AC-6, and AC-8 is given in table IX-III.

INTERNAL COMPARTMENT TEMPERATURES AND GAS CONDITIONING

Tables IX-IV and IX-V show the temperatures throughout the electronics compartment and in portions of the thrust section at lift-off, MES 1, and MES 2. The temperatures at lift-off indicated that the conditioning gas distribution systems maintained satisfactory thermal control in both compartments and that no appreciable amount of cold insulation panel purge helium leaked past the station 208 seal into the electronics compartments. The tabulated data also show that all packages and systems remained at acceptable temperature levels throughout the flight up to MES 2.

TABLE IX-I. - NOSE FAIRING EXTERNAL TEMPERATURE SUMMARY

Measurement	Station	Axis	Thermolag	Maximum temperature, ^{o}F		Maximum time, sec	
				Predicted	Actual	Predicted	Actual
CA402T	19	y	No	230	240	135	120
CA408T	72	y	No	405	225	140	120
CA416T	125	y	No	230	270	145	120
CA422T	185	y	Yes	210	(a)	108	(a)
CA403T	19	-y	No	405	280	135	120
CA409T	72	-y	↓	405	305	140	120
CA417T	125	-y	↓	405	320	145	121
CA423T	185	-y	↓	210	150	130	130
CA80T	Stagnation point	z	↓	790	(a)	145	(a)
CA958T	30^{o} from stagnation point	z at 135^{o}	↓	690	495	145	148
CA959T	60^{o} from stagnation point	z at 135^{o}	↓	450	395	145	148
CA419T	125	-x	↓	230	270	95	130
CA410T	72	x	Yes	230	180	96	150

[a]Data invalid.

TABLE IX-II. - INTERSTAGE ADAPTER SKIN TEMPERATURES

Measurement	Station	Quadrant or axis	Maximum temperature, ^{o}F		Maximum time, sec	
			Predicted	Actual	Predicted	Actual
AA244T	418	IV at 290^{o}	285	175	140	118
AA104T	431	IV at 291^{o}	340	264	↓	118
AA105T	446	↓	↓	246	↓	118
AA106T	461	↓	↓	269	↓	128
AA107T	490	↓	↓	267	↓	124
AA108T	519	↓	↓	254	↓	128
AA109T	533	↓	↓	268	↓	124
AA871T	503	-y	↓	235	↓	137

TABLE IX-III. - ATLAS MAXIMUM SKIN TEMPERATURES AT LO_2 TANK

ADJACENT TO STATION 570 JOINT

Measurement	Station	Quadrant	Temperature, °F			Time, sec		
			AC-4 (second burn)	AC-6 (first burn)	AC-8 (second burn)	AC-4 (second burn)	AC-6 (first burn)	AC-8 (second burn)
AA918T	575	15°	255	245	302	122	115	118
AA919T	575	135°	---	245	248	---	115	125
AA920T	575	225°	280	255	313	132	115	114
AA921T	576	45°	---	240	270	---	115	118
AA922T	576	180°	245	309	334	130	128	127
AA923T	576	315°	280	280	302	132	120	118
AA924T	614	150°	220	220	231	135	115	126
AA925T	614	180°	---	255	245	---	110	113
AA926T	614	210°	205	220	252	122	115	118
AA927T	614	330°	190	200	218	125	120	131

TABLE IX-IV. - ELECTRONICS COMPARTMENT TEMPERATURES

Measurement	Location	Temperature, °F			
		Lift-off	MES 1	MES 2	Allowable
CA1T	Rate gyroscope	46	46	---	0 to 160
CE29T	Inverter	89	122	197	0 to 200
CE81T	Main battery, external	64	60	---	40 to 200
CI1T	Guidance platform	64	70	72	30 to 120
CI3T	Signal conditioner	47	45	---	30 to 130
CI4T	Guidance computer skin	66	75	---	30 to 130
CI23T	Pulse rebalance package skin	57	64	---	30 to 130
CI40T	Computer input-output unit	59	61	---	30 to 130
CI228T	Platform electronics	49	47	---	---------
CS83T	Automatic pilot servoamplifier	36	38	45	0 to 160
CS300T	Sequence timer	55	57	---	-35 to 170
CT15T	Telemetry RF unit 5	51	50	---	0 to 110
CT94T	Telemetry RF unit 1	39	43	---	0 to 110
CT95T	Telemetry RF unit 2	54	54	60	0 to 110
CT98T	Telemetry multicoupler	30	24	---	-30 to 165
CT202T	C-band beacon transponder skin	54	53	---	-80 to 167
CZ1T	Azusa transponder casting	72	76	---	32 to 130

TABLE IX-V. - THRUST SECTION TEMPERATURES

Measurement	Location	Temperature, °F			
		Lift-off	MES 1	MES 2	Allowable
CP14T	P1 fuel supply	80	69	75	140 max
CP40T	P2 fuel supply	70	61	71	140 max
CP93T	H_2O_2 bottle	74	77	64	140 max
CU829T	PU electric package skin	71	75	52	20 to 129

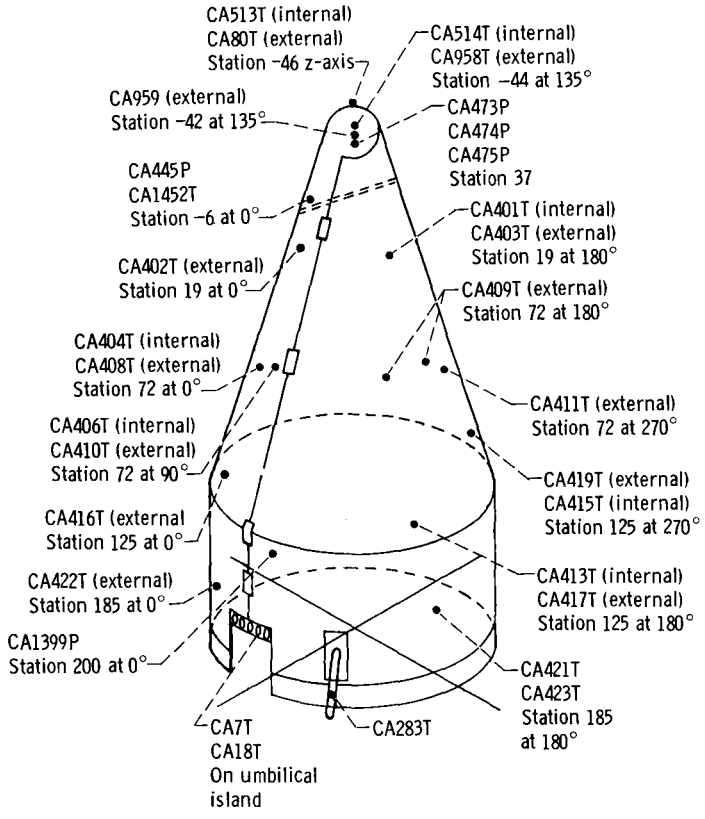

Figure IX-1. - Nose fairing instrumentation.

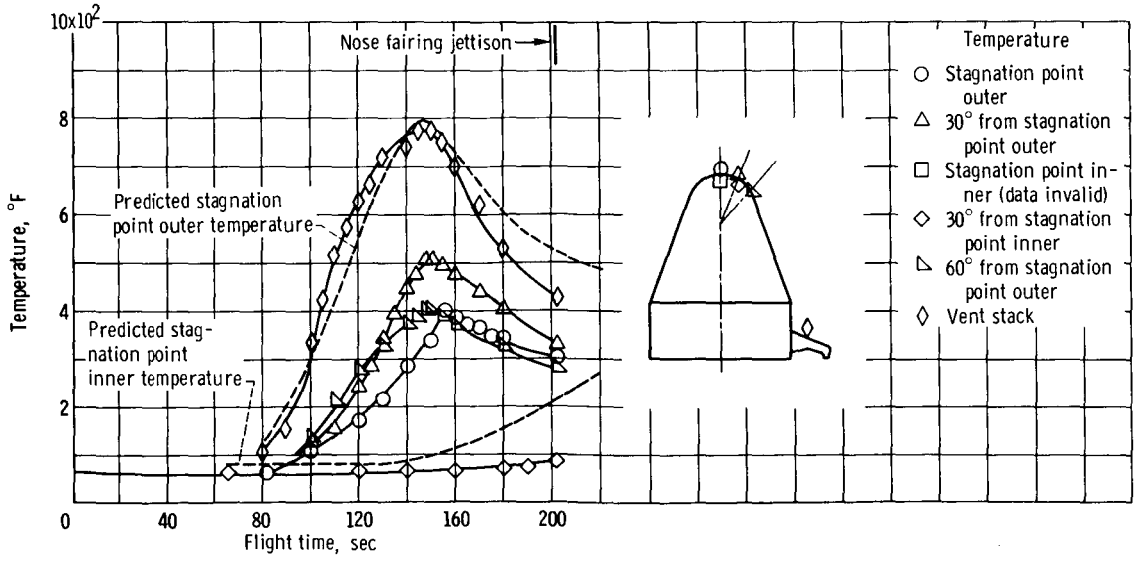

Figure IX-2. - Nose cap and vent stack temperatures.

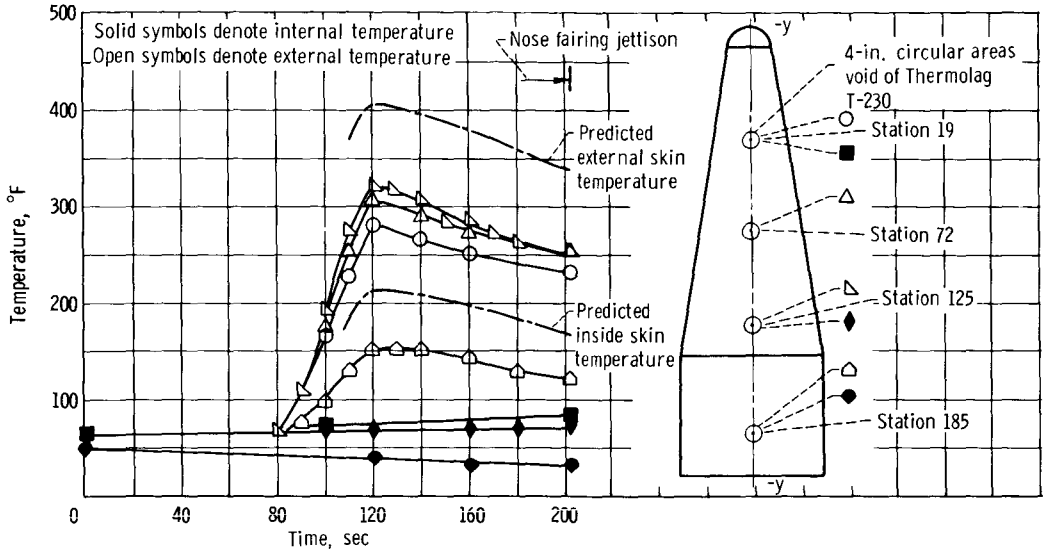

Figure IX-3. - Nose fairing skin temperature at -y-axis.

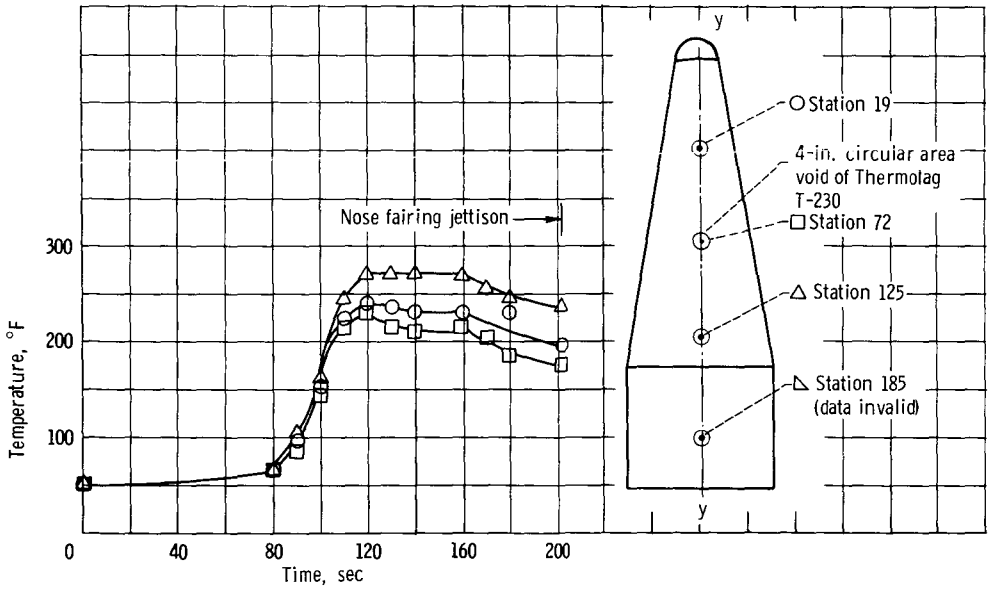

Figure IX-4. - External nose fairing temperatures at y-axis.

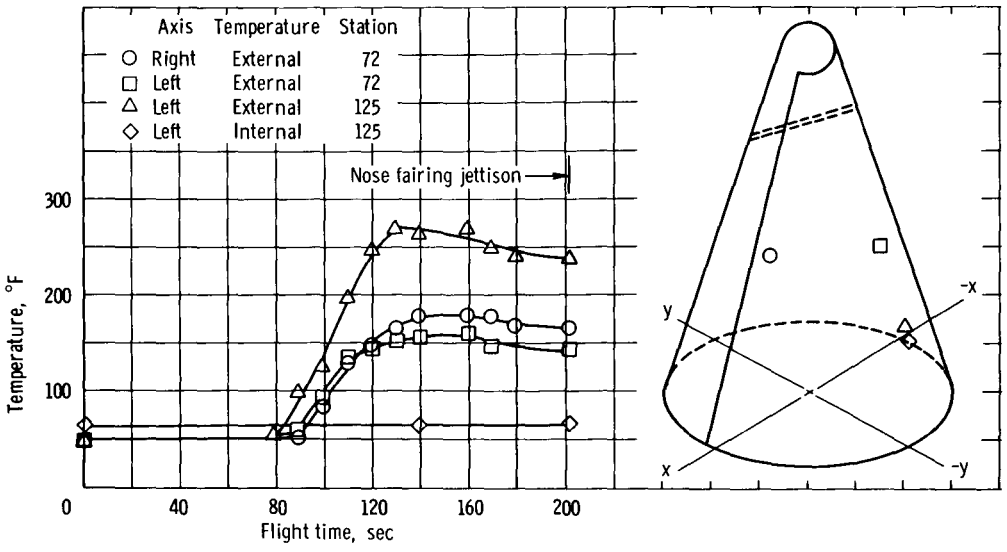

Figure IX-5. - Nose fairing temperatures. (All external temperatures are covered with 0.033-in. coating of Thermolag T-230.

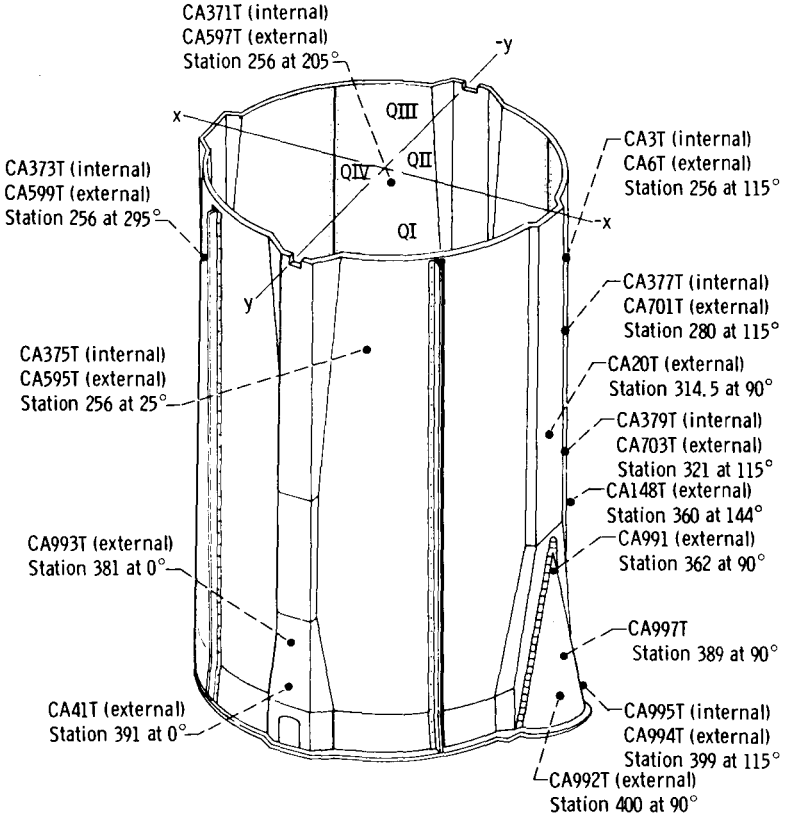

Figure IX-6. - Insulation panel instrumentation.

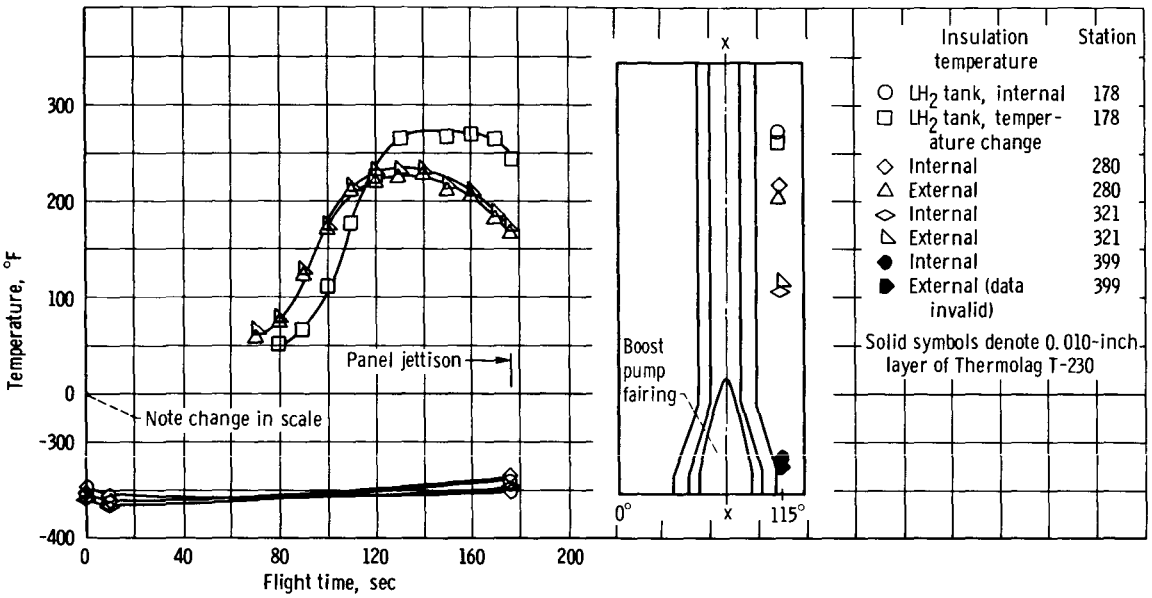

Figure IX-7. - Insulation panel temperature profile.

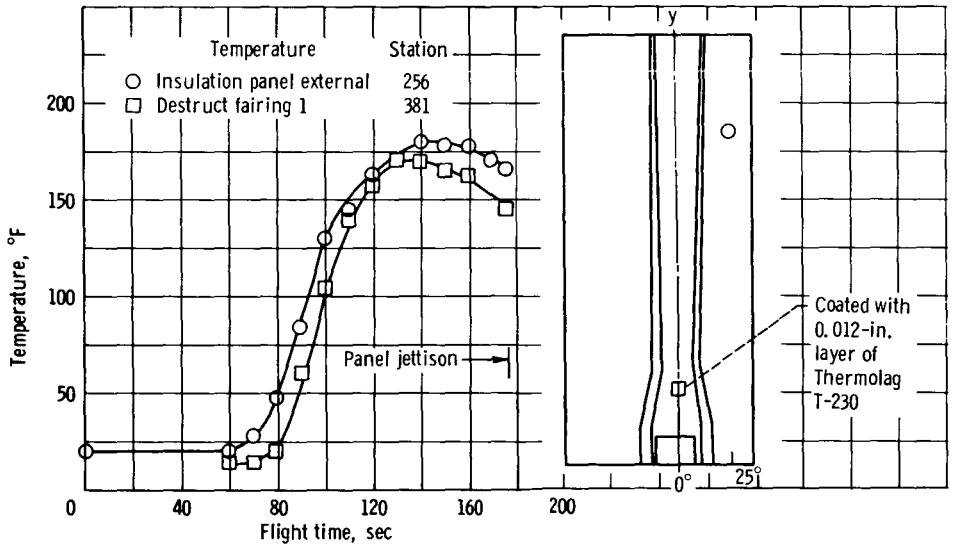

Figure IX-8. - Insulation panel and destruct fairing temperatures.

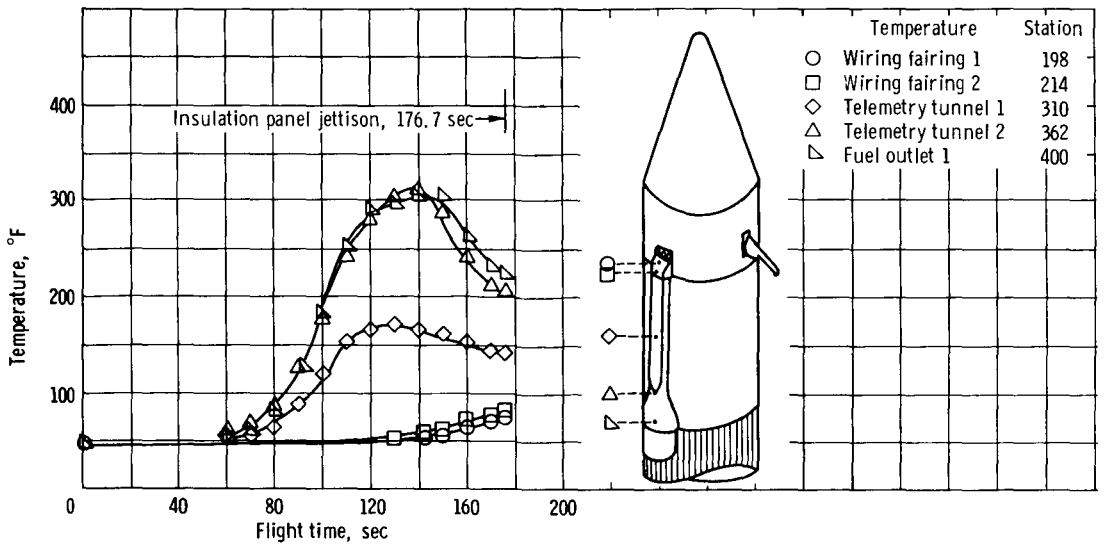

Figure IX-9. - Wiring fairing, telemetry tunnel, and boost pump fairing temperatures at x-axis.

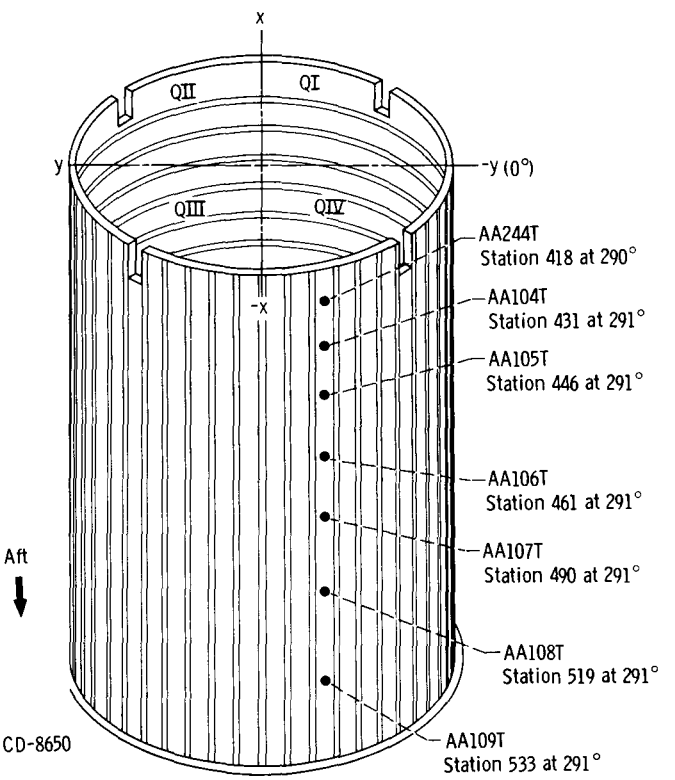

Figure IX-10. - Interstage adapter temperature instrumentation.
(Note that all temperature transducers are in area void of Thermolog.)

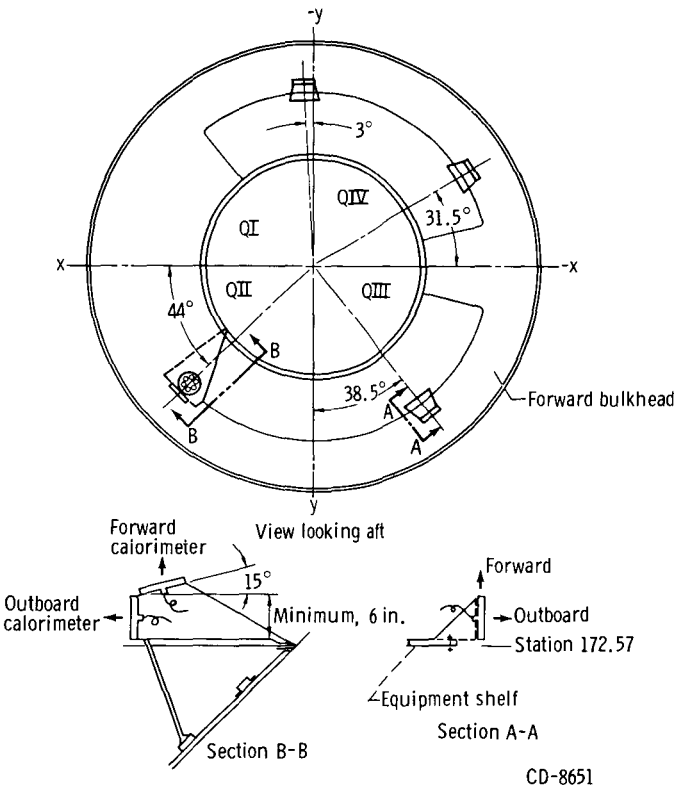

Figure IX-11. - AC-8 calorimeter locations.

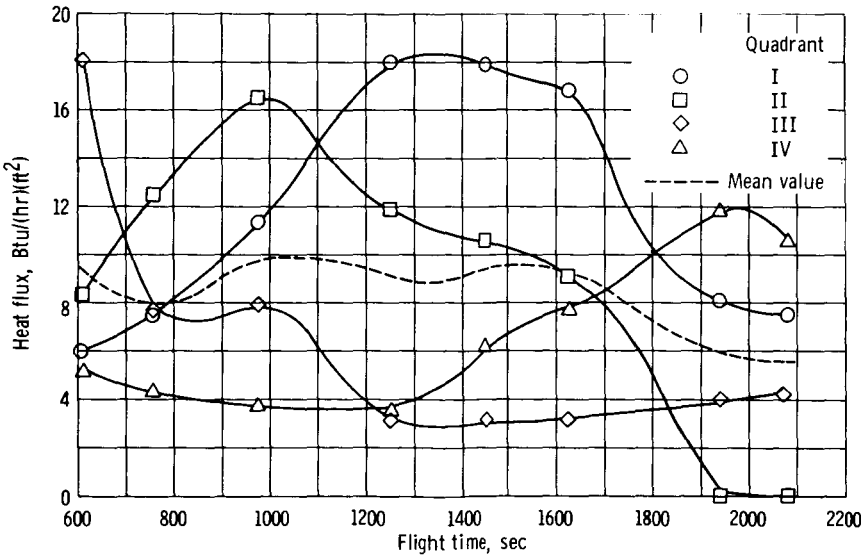

Figure IX-12. - Net heat flux into Centaur hydrogen tank wall.

X. VEHICLE STRUCTURES

SUMMARY

The vehicle structural system performed satisfactorily on the AC-8 flight, and all structural objectives were achieved. The peak longitudinal load factor was 5.66 g's at BECO. Aerodynamic bending loads were within vehicle capability. Atlas booster engine gimbal angles were less than 2.6° throughout flight compared with a 3° maximum angle predicted by the preflight wind sounding analyses.

AC-8 was the first Atlas-Centaur vehicle to be instrumented for launcher transients. First and second peak kick strut loads agreed well with time of holddown pin pull and kick strut lockup, respectively, confirming the analysis of the cause of these maximum loads. The maximum kick strut load of 30 000 pounds was the second peak load and was less than the 34 000-pound load measured on an SLV-3 Atlas 7110. The fuel staging valve housing instrumentation indicated a 0.07-inch repositioning of the poppet toward closing at second peak kick strut load. The fuel manifold strut loads indicated a reduction immediately following engine ignition and an increase to a maximum loading at time of peak kick strut loads.

All flexible linear shaped-charge separation systems performed normally and initiated successful separation of the various structural elements. Vehicle jettison systems appeared to function normally except for an anomaly during insulation panel jettison. The Centaur-Surveyor (mass model) separation system performed normally even though the vehicle was tumbling during separation.

VEHICLE LOADS

Longitudinal and Bending Loads

Vehicle accelerometers indicated that the longitudinal load factor buildup was as expected. A maximum value of 5.66 g's was reached at BECO, which was within the range of $\pm 3\sigma$ g's (5.62 to 5.78 g's).

The vehicle bending moments were less than the maximum predicted values. The maximum values were based on T - 2 hour wind sounding data, which indicated that the Atlas booster engine pitch gimbal angle would be 3°. The maximum Atlas booster engine

pitch gimbal angle recorded during the flight was 2.6°, as shown in figure X-1 at T + 70 seconds.

Atlas Launcher Transients

Investigation of the failure of AC-5 at lift-off indicated a possibility that the fuel duct support structure at the booster fuel staging valve could have failed or that dimensional tolerances plus structural deflections on both sides of the staging valve might have been sufficient to allow the valve poppet to close and shut off the fuel flow to the booster engines. Longitudinal oscillations at lift-off on AC-5 and AC-6, which both used 165 000-pound thrust booster engines, were three times the magnitude of earlier flights, which used 154 000-pound thrust booster engines. Analyses indicated that, during release of the vehicle, the launcher mechanism forces, which are a function of the ratio of thrust to weight, were the primary cause of the longitudinal oscillations and the additional loads imposed on the vehicle. Additionally, the increased load from these oscillations was approaching the limit for the Centaur forward bulkhead. Also, lateral oscillations caused by the launcher were raising the loads that were seen by the spacecraft. As a result, AC-8 was instrumented to monitor the effect of the launcher on the vehicle acceleration and on the booster fuel staging valve and support struts of the Atlas.

Figure X-2(a) shows the launcher and vehicle in holddown position. Details of the release arm and mechanism assembly in the position prior to lift-off and in the position at kick strut lockup are shown in figures X-1(b) and (c), respectively.

Launcher effect for this flight was less than on previous flights since the ratio of thrust to weight at 2-inch rise for AC-8 was only 1.257, as compared with a value of 1.276 for AC-6. This difference resulted in a lower acceleration at lift-off. The longitudinal accelerometer at station 173 (CM101A) had a peak-to-peak maximum value of 0.58 g about a 1.21 g centerline value for AC-8 as compared with a peak-to-peak maximum value of 0.94 g about a 1.25 g centerline for AC-6.

Figure X-3 shows the loads experienced by the launcher kick struts and the longitudinal acceleration of the vehicle. The three peak loads were observed on each kick strut. The second and third peak loads for the B2 strut were higher than those for the B1 strut, and the third peak for the B2 strut occurred about 0.01 second later than the corresponding peak for the B1 strut. The maximum load measured on AC-8 was 30 000 pounds on the B2 strut. The maximum load measured on SLV-3 Atlas 7110 (also using 165 000-lb thrust booster engines) was 34 000 pounds.

The occurrence of the second peak load on the kick struts, as shown in figure X-3, just preceded and is believed to have been the primary cause of the start of the vehicle cyclic longitudinal acceleration. Examination of the data confirmed the original analysis

of the cause of the first and second peak kick strut loads. The start of launcher arm pin pull at approximately 0.225 second agrees well with the start of the first kick strut peak. The time that the kick strut starts to rotate the launcher arm (kick strut lockup) agrees well with the start of the second peak load.

The pressure decay of the launcher holddown cylinder to release the vehicle was within specification, as shown in figure X-4. Vehicle vertical displacement is shown in figure X-5. Time of the first motion of the vehicle and of the holddown arm was between T - 0.27 and T - 0.22 second, based on both the holddown cylinder strain measurements (AL1037S and AL1038S) and the vehicle vertical motion measurement (AM1003H). Holddown pressure in the cylinder was 1400 and 980 psi, respectively, at these times. A theoretical determination of first motion using thrust, weight of vehicle, force due to the auxiliary support stabilizers, force due to lift-off umbilicals and geometry of the system gives a lift-off pressure of approximately 2000 psi in the holddown cylinders. Discrepancies caused by cylinder friction and variations in the auxiliary support stabilizer and umbilical lift-off forces would account for the difference from the theoretical.

The booster fuel staging valve was instrumented with three transducers (AP1085D, AP1086D, AP1087D) arranged around the periphery of the valve housing to indicate motion at the separation plane and, therefore, to indicate valve poppet position. The valve location and separation plane are shown in figure X-6 with the transducers mounted between points A and B. Figure X-7 shows the valve housing motion (hence, poppet motion). During fuel flow at ignition and early thrust buildup, the valve housing motion was in a direction to open the poppet wider, as referenced to the fully tanked condition, by less than 0.01 inch. With thrust buildup complete, the poppet had repositioned to a more closed position by 0.04 inch, as referenced to the fully tanked condition. At start of vehicle rise (T - 0.22 sec) and during the first 0.4 second of vehicle motion, the housing indicated that the poppet continued to move in a closing direction of approximately 0.01 inch further. At first peak kick strut load at T + 0.235 second, the poppet closed additionally and, at second peak kick strut load, a maximum poppet reposition of 0.07 inch from tanked condition toward closing was indicated. At the third peak kick strut load, the poppet was at a slightly less closing position than this maximum. The three transducers showed a variation of position with respect to each other, which indicated a misalinement of the valve and manifold. Values of poppet motion given are an average of the three. AP1087D indicated the least motion and AP1085D the greatest motion, which was 0.1 inch in a closing direction at second peak kick strut load.

Booster fuel manifold support struts, as shown in figure X-8, were instrumented to measure the loads during launch. Figure X-9 shows the strut loads. The analysis of strut loads indicates a tension load in strut P2 for the fully tanked condition, a compressive load in P4, and either a tension or compression load in P6 depending on alinement and vibration loads. Strut P2 experienced a maximum change in load at T - 0.8 second in

a compressive direction of 600 pounds. The overall effect was a 600-pound reduction in the P2 strut tension load. At T + 0.55 second, a peak tension load increase of 150 pounds above the fully tanked load occurred on P2. This increase was approximately 2 percent of the limit design load. The peak was in a wave series originating at kick strut second peak load. Strut P4 has a 300-pound maximum load in a tension direction at T - 0.84 second and also at T - 0. This was a reduction of the compression load existing before launch. At T + 0.55 second, a peak 60-pound compressive load beyond the fully tanked load was indicated on P4, increasing the prelaunch compression load by approximately 2 percent of the limit design load. Again, this peak was in a series originating at second maximum load on the kick strut. The frequency of these waves was approximately 6 cps with a peak-to-peak value of 300 pounds. On strut P6, the load varied from the tanked condition by 400 pounds in compression to 600 pounds in tension.

Centaur Propellant Tank Ullage Pressures

The LH_2 and LO_2 tank ullage pressures were within the predicted range for all periods of the flight (fig. VIII-2). A minimum ΔP of 4.0 psi across the intermediate bulkhead occurred at approximately T + 64 seconds and reached a maximum of 20.0 psid at Centaur MES 1.

Atlas Intermediate Bulkhead Differential Pressure

The Atlas LO_2 tank ullage pressure programing system, incorporated to maintain sufficient bulkhead differential pressure during launch transient with 165K booster engines, was effective. It was designed to reduce Atlas LO_2 tank pressure by approximately 5 psi for the first 20 seconds of flight. A satisfactory differential pressure of 11.5 to 12.7 psi across the intermediate bulkhead was maintained for this period of time. At T + 20 seconds, the return to full flight pressure in the LO_2 tank was initiated by the programer and completed approximately 3 seconds later.

A minimum value of 8.1 psi differential pressure across the bulkhead was experienced at T + 94 seconds. The maximum value of 25.2 psi occurred immediately following BECO at T + 143 seconds. The range of differential pressures encountered on the AC-8 flight was compatible with previous flight experience and approximated those experienced on AC-6.

LO_2 and fuel tank ullage pressure histories were similar to AC-6 with differences of 1 to 2 psi occurring in some portions. Differential pressure and LO_2 and tank ullage pressure histories for this flight are shown in figures X-10 to X-12.

SEPARATION SYSTEMS

Insulation Panel Separation

Sixteen breakwires were attached to the insulation panel hinge arms and the interstage adapter to record panel separation. Eight breakwires, one on each hinge, recorded panel separation after a 35^{o} panel rotation, and eight additional breakwires recorded panel separation after a 1.5-inch displacement of hinge arm from hinge pin. For normal jettison, the 35^{o} breakwires break first, while hinge arms are engaged on hinge pins, and the 1.5-inch breakwires break after the panels have separated from the hinge pins. In addition, one break-corner breakwire was installed on the aft quadrant II portion of the quadrant I-II (wiring tunnel) panel. Inspection of the recovered AC-6 quadrant I-II panel indicated that the aft quadrant II corner had broken during either reentry or panel jettison. The break-corner sensing wire was installed on AC-8 to determine if the panel fails during jettison. Figures X-14 and X-15 illustrate all breakwire and hinge locations.

A review of these breakwire measurements (AA201X to AA217X) revealed that the 1.5-inch breakwire (AA215X) on the quadrant IV hinge arm of the quadrant IV-I panel broke 0.1 second after flexible linear shaped-charge (FLSC) activation followed 0.08 second later by breakage of the 35^{o} breakwire (AA207X) on the same hinge arm (fig. X-4). This early breakage of both the 1.5-inch and 35^{o} breakwires on one hinge arm indicates this hinge disengaged prematurely. The remaining hinge on the quadrant IV-I panel rotated about its hinge pin, carrying the entire panel weight, breaking the 35^{o} and 1.5-inch breakwires, as nominally predicted. The improper hinge disengagement (as indicated by AA215X breakwire) and the resultant asymmetrical panel hinge loads subjected the vehicle to a clockwise torque. The vehicle guidance system immediately corrected for this disturbance. With the exception of the premature disengagement of the quadrant IV hinge of the quadrant IV-I panel, all other hinges rotated as predicted, breaking 35^{o} and 1.5-inch breakwires in proper sequence (see tabulation of breakwire times in fig. X-14). The break-corner breakwire (AA217X) broke subsequent to panel separation, which indicated that the wiring tunnel panel (quadrant I-II) did not witness structural failure in this area during the separation process.

The successful separation of the insulation panel, nose fairing, and staging systems (AC-6 and AC-8) verifies the capability of the FLSC separation systems to sustain cryogenic thermal cycles without critically affecting their functional reliability.

Nose Fairing Separation

Separation of the nose fairing occurred at T + 202.0 seconds. No excessive vibrations were observed on accelerometers at this time. Verification of separation was confirmed by the cessation of all nose fairing instrumentation data at this time. Surveyor

compartment pressure (CY8P) droppped from atmospheric pressure at T + 10 seconds to zero at T + 110 seconds. As expected, no indication of pressure buildup was witnessed at thrustor bottle activation.

The nose fairing hinge strain gage data indicated that the maximum loads occurred at nose fairing jettison, as shown in figure X-16. Just prior to nose fairing jettison, the tension load on the hinge fitting was 3090 pounds. At jettison, the compression force in the hinge fitting reached a maximum value of 3475 pounds. These loads are well within the allowable tension or compression load of 6000 pounds.

A portion of the pitch axis bending moments on the nose fairing was transmitted into the hinge fittings during the launch and Mach 1 - max q periods of flight, but the loads on the hinge fittings were not significant. There was also a slight tension increase in the fittings at BECO and insulation panel jettison.

Atlas-Centaur Separation

The stage separation process was initiated by the linear shaped-charge firing at T + 231.35 seconds, which severed the interstage adapter at station 413. The retrorockets fired approximately 0.1 second later to decelerate the Atlas. Accelerometer data indicated that all eight retrorockets ignited.

The rate and displacement gyros mounted on the Atlas indicated that it rotated approximately 0.18^{o} about its yaw axis at the time it cleared the Centaur. This created a lateral motion of 1.8 inches at the forward end of the interstage adapter.

The more critical motion is the pitch motion, since there is less radial clearance between the interstage adapter and the Centaur mounted hardware in this direction. The rate gyro indicated an apparent rotation of 0.3^{o} at the instant the Atlas cleared the Centaur. The resulting vertical motion at station 413 was 3.0 inches out of a nominal 15 inches allowable.

Spacecraft Separation

Centaur-Surveyor (mass model) separation occurred at T + 2251.6 seconds. Data from extensionmeters CY2D, CY4D, and CY5D, as shown in figure X-17, indicate all three latches actuated within 1 to 2 milliseconds of each other. The three jettison spring assemblies satisfactorily traveled their 1-inch stroke without hangup and yielded approximately identical stroke - time data. The separation was nominal and produced no significant spring-induced tipoff rate in the mass model. Figure X-18 shows a comparison between extensionmeters CY4D on AC-6 and AC-8. The lighter payload and excessive

Centaur residual tumbling rate (approximately 23 deg/sec) on AC-8 considerably shortened the separation time (0.110 sec on AC-8, 0.136 sec on AC-6).

Surveyor separation latches had been preloaded to 2500 + 800 - 0 pounds before launch. Accurate preload of 3000 pounds was measured before launch at only one leg (leg 3) because of loss of strain gages on legs 1 and 2. The latch loads were not monitored during flight.

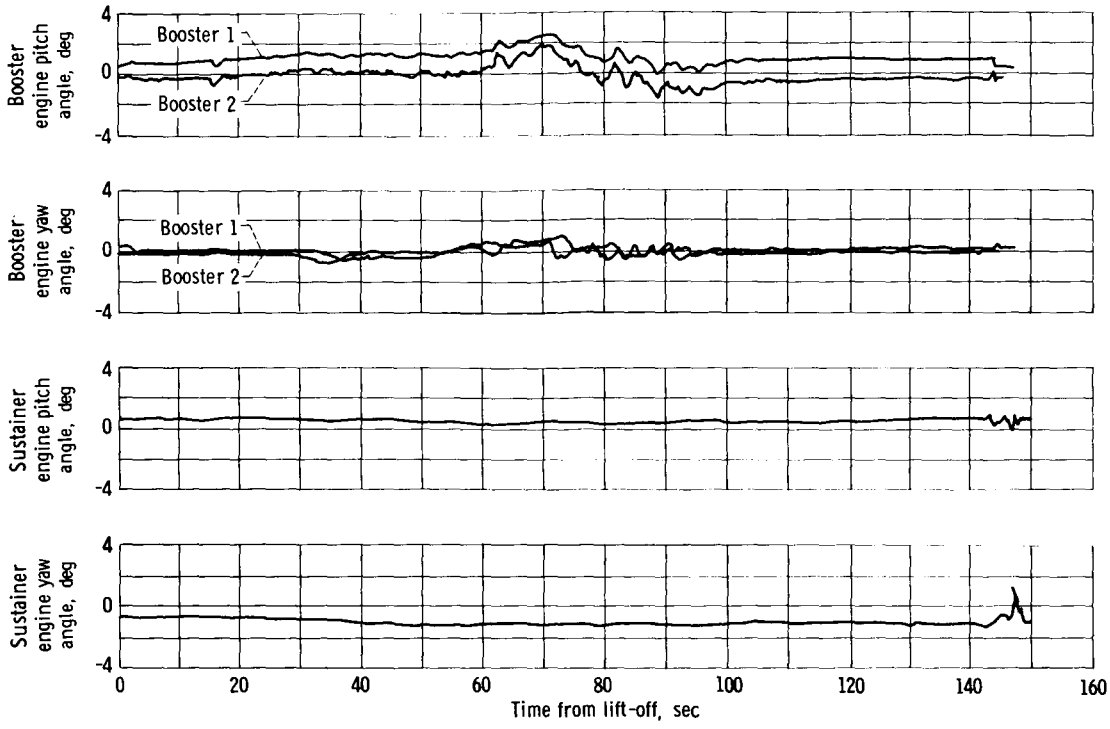

Figure X-1. - Atlas engine deflections during atmospheric ascent.

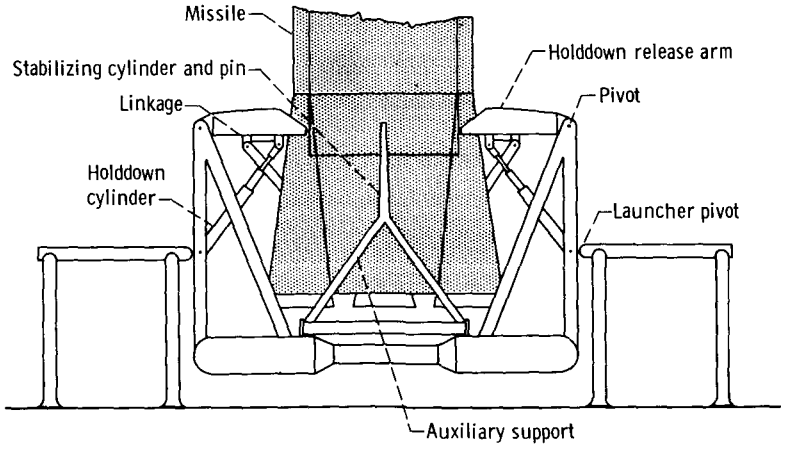

(a) Launcher and vehicle in holddown position. 8714-S

Figure X-2. - Launch assembly.

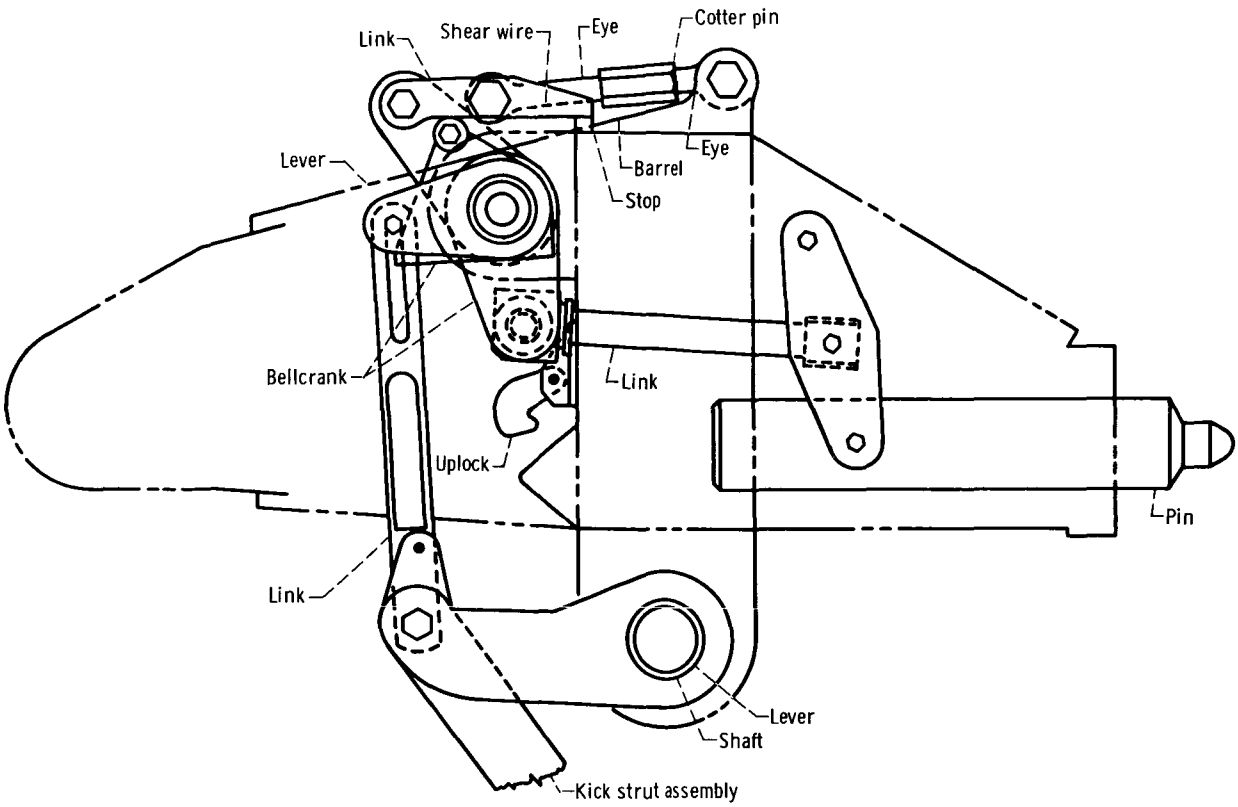

(b) Release arm and mechanism assembly prior to lift-off.

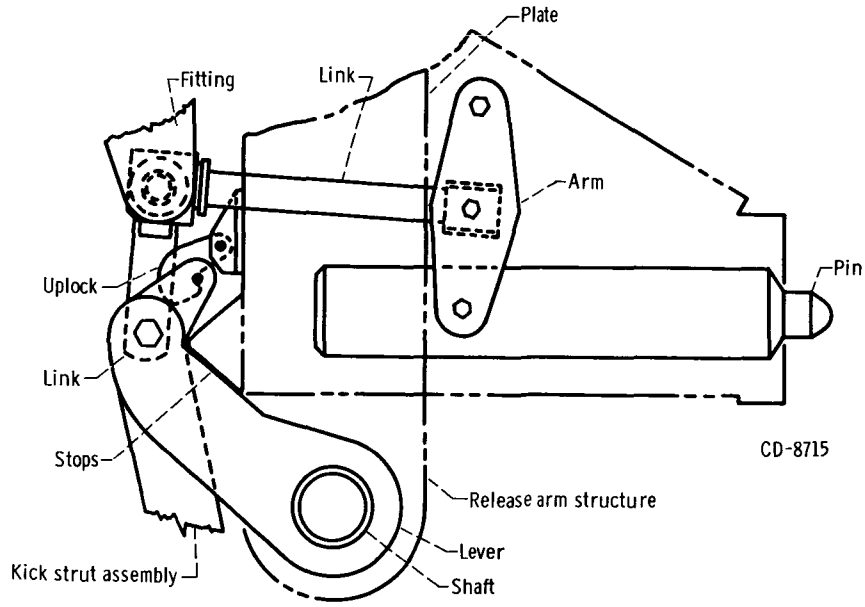

(c) Release arm and mechanism assembly at kick strut lockup.

Figure X-2. - Concluded.

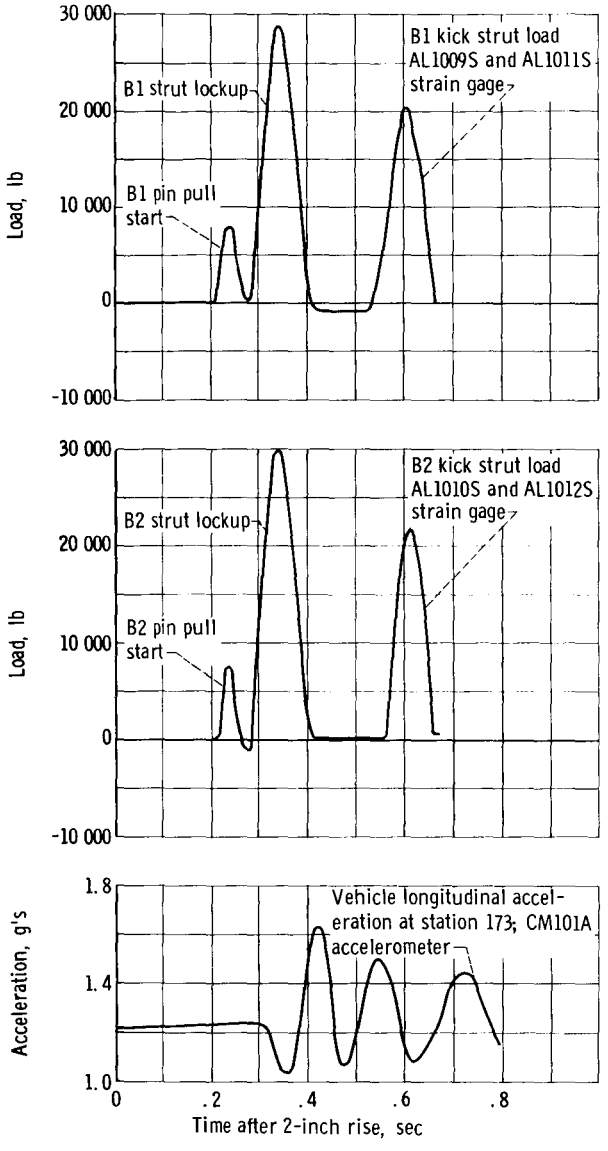

Figure X-3. - Kick strut loads and vehicle longitudinal accelerations.

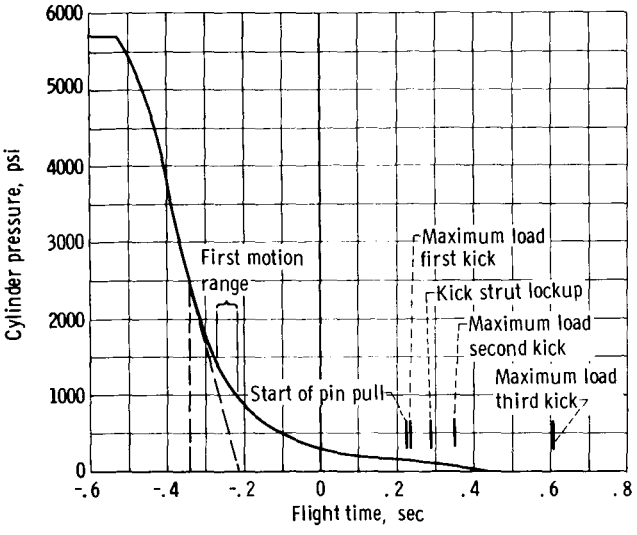

Figure X-4. - Launcher holddown cylinder pressure decay.

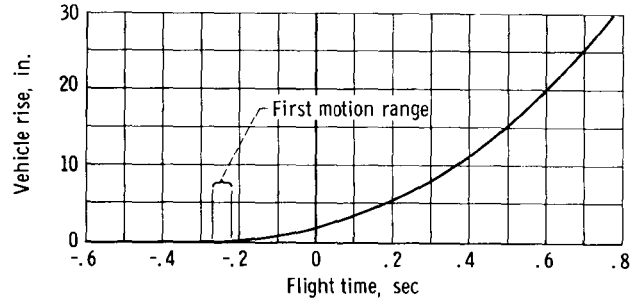

Figure X-5. - Vehicle vertical displacement.

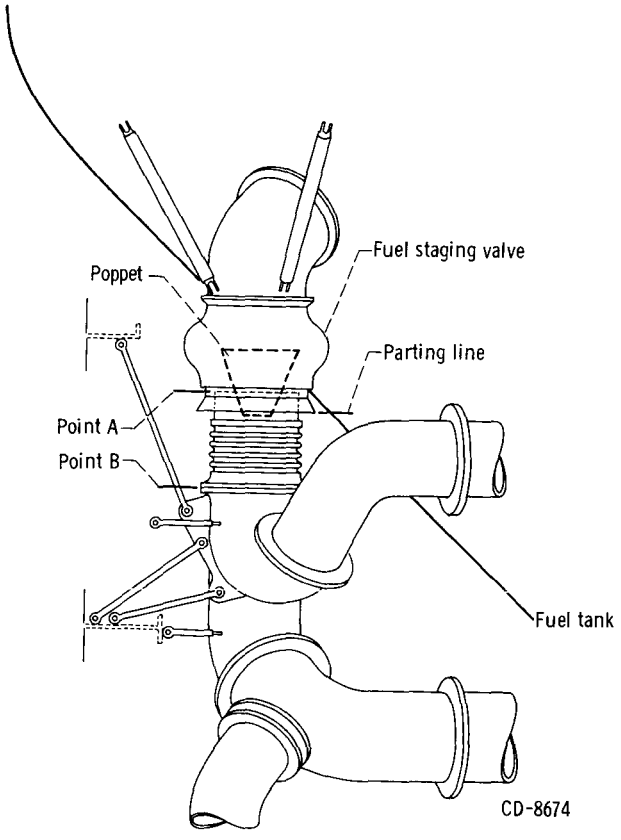

Figure X-6. - Staging valve and motion transducer location.

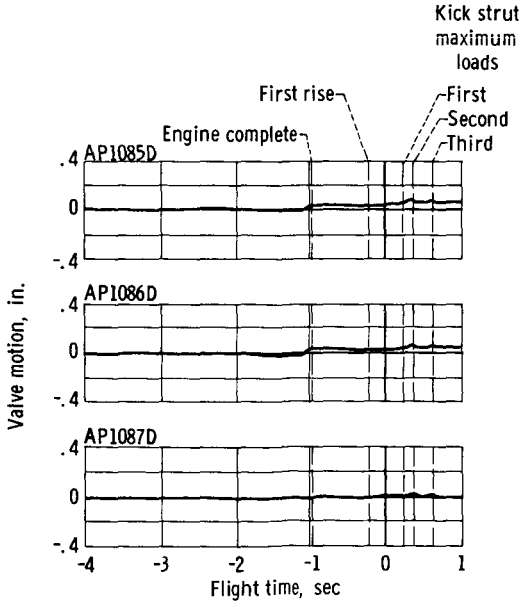

Figure X-7. - Booster fuel staging valve body motion. Positive valve motion denotes housings opening and poppet closing; negative valve motion denotes housings closing and poppet opening.

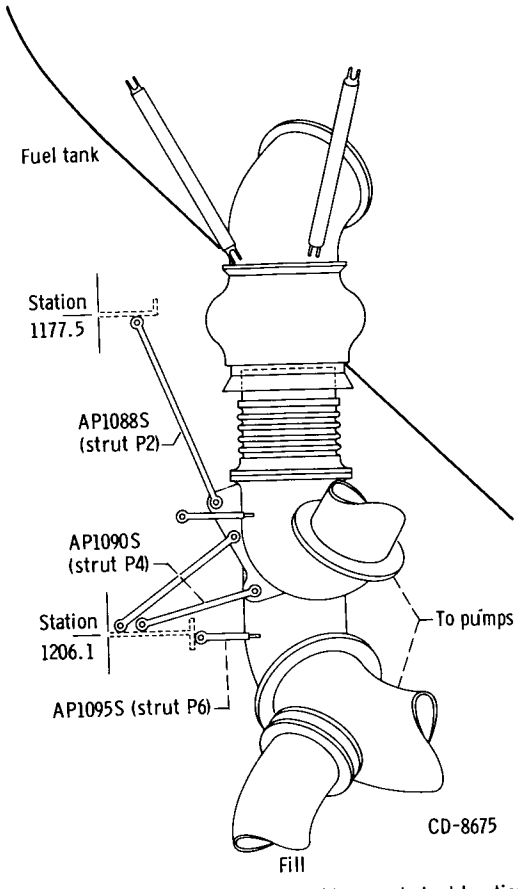

Figure X-8. - Booster fuel manifold support strut locations.

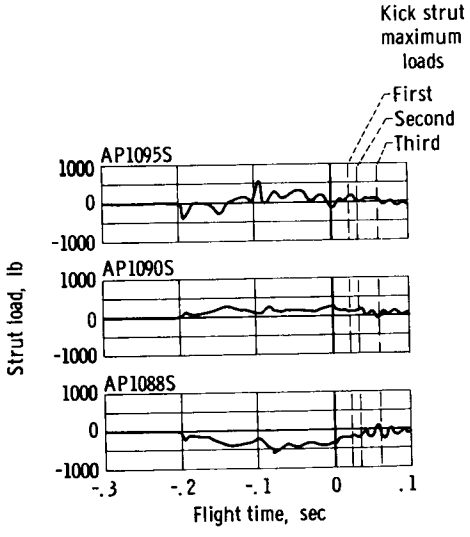

Figure X-9. - Booster fuel manifold support strut loads (referenced from tanked condition). Positive strut load denotes tension load; negative strut load denotes compression load.

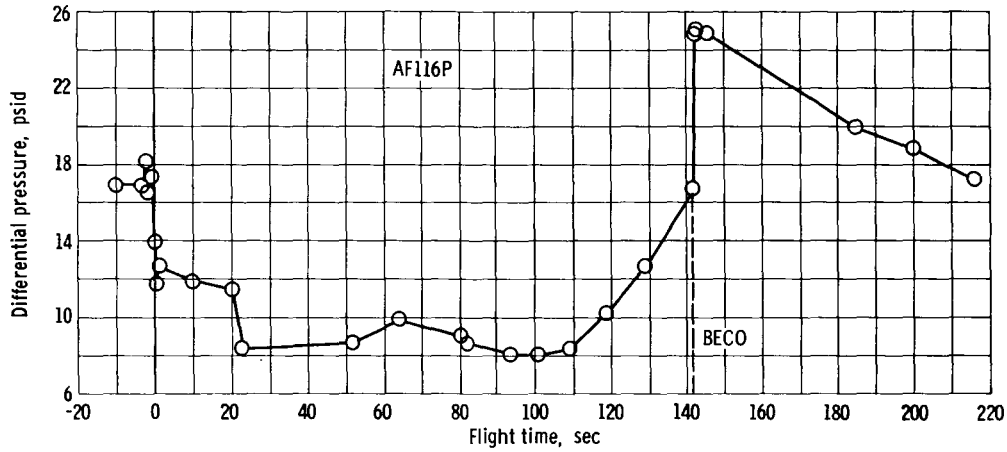

Figure X-10. - Atlas intermediate bulkhead differential pressure for AC-8.

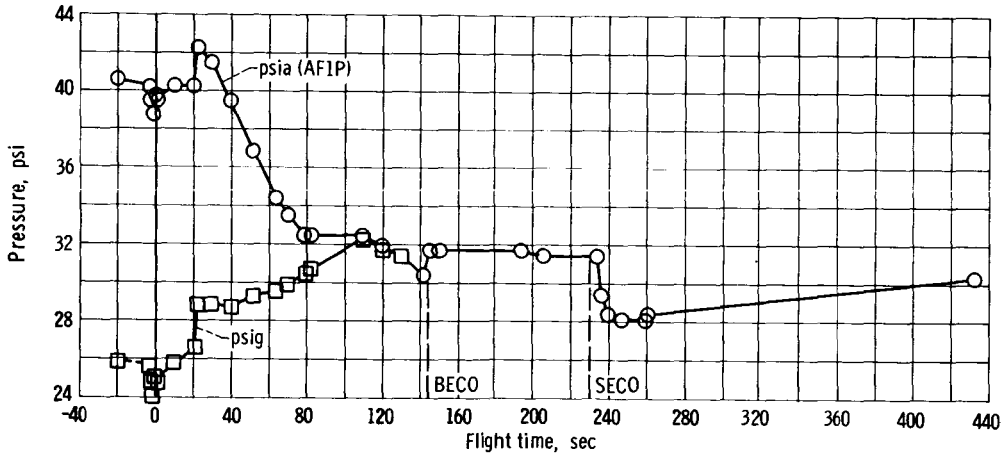

Figure X-11. - Atlas liquid oxygen tank helium ullage pressure for AC-8.

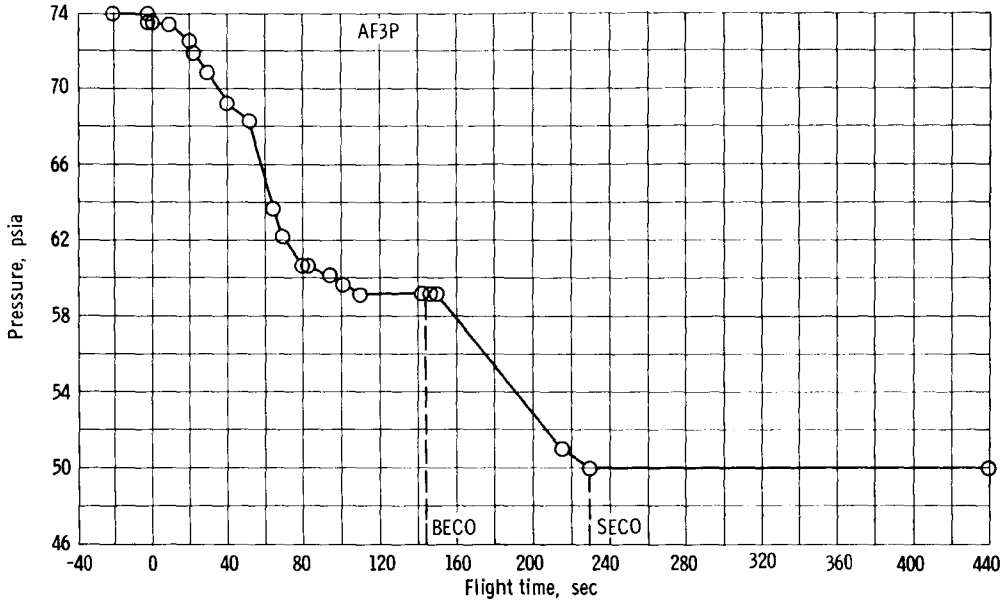

Figure X-12. - Atlas fuel tank helium ullage pressure for AC-8.

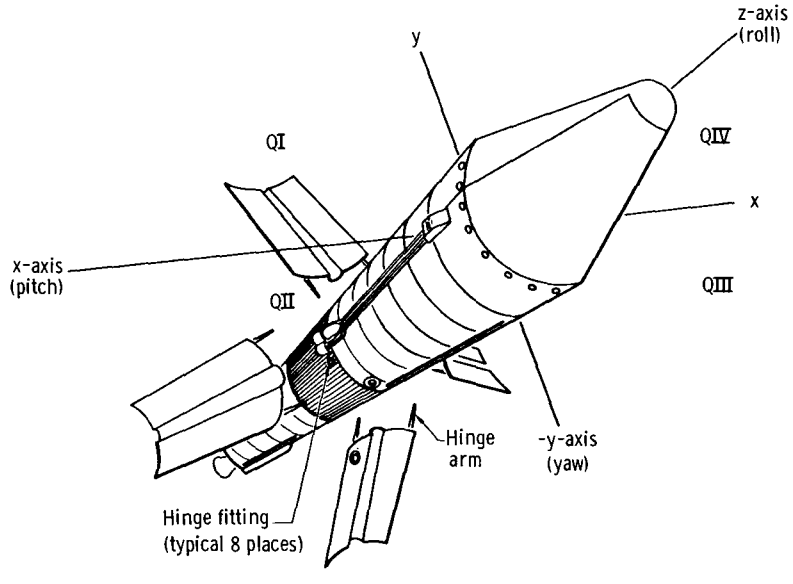

Figure X-13. - Jettisonable insulation system.

Breakwire			Quadrant		Break time, sec
35°	1.5 in.	Break corner	Panel	Hinge arm	
-------	AA215X	-------	IV-I	IV	176.11
AA207X	-------	-------	IV-I	IV	176.19
AA202X	-------	-------	I-II	II	176.36
AA201X	-------	-------	I-II	I	176.42
AA204X	-------	-------	II-III	III	------
AA205X	-------	-------	II-IV	III	176.44
AA203X	-------	-------	II-III	II	176.45
AA208X	-------	-------	IV-I	I	------
AA206X	-------	-------	III-IV	IV	176.47
-------	AA210X	-------	I-II	II	------
-------	AA209X	-------	I-II	I	176.71
-------	AA211X	-------	II-III	II	176.74
-------	AA213X	-------	III-IV	III	176.75
-------	AA212X	-------	II-III	III	176.77
-------	AA214X	-------	III-IV	IV	176.78
-------	AA216X	-------	IV-I	I	176.87
-------	-------	AA217X	I-II	---	176.97

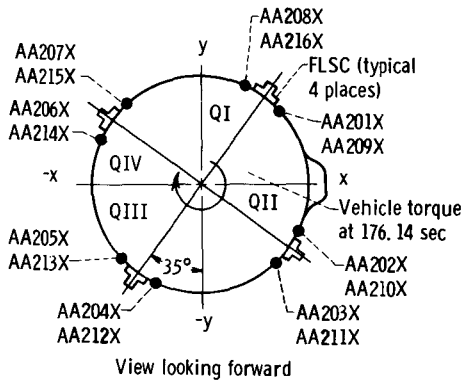

Figure X-14. - Insulation panel hinge breakwire data. Flexible linear shaped-charge activation, 176.01 seconds; rate gyroscope (C572) anomaly, 176.14 seconds.

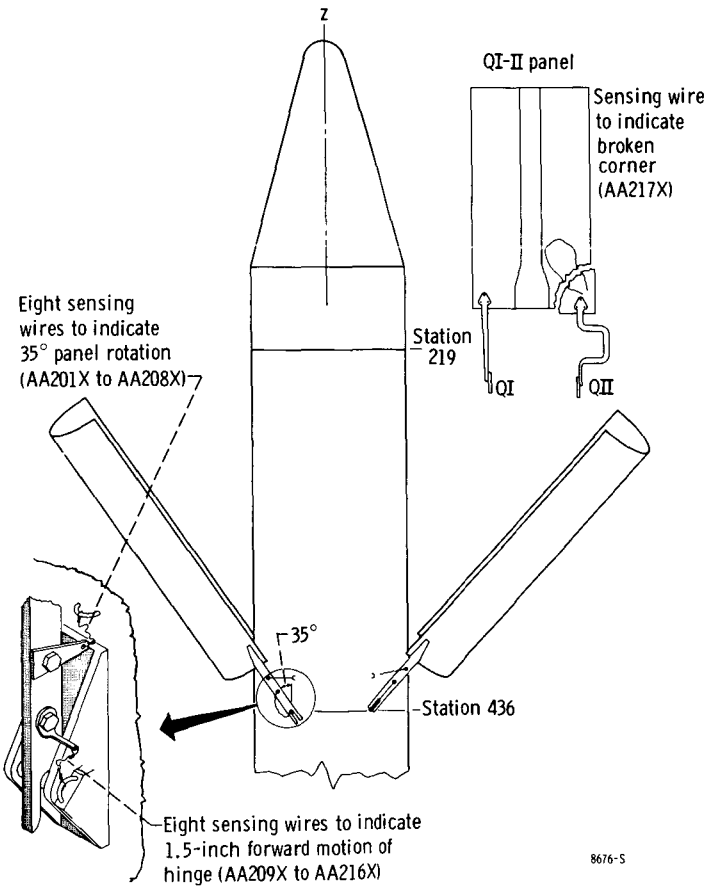

Figure X-15. - Insulation panel breakwire location.

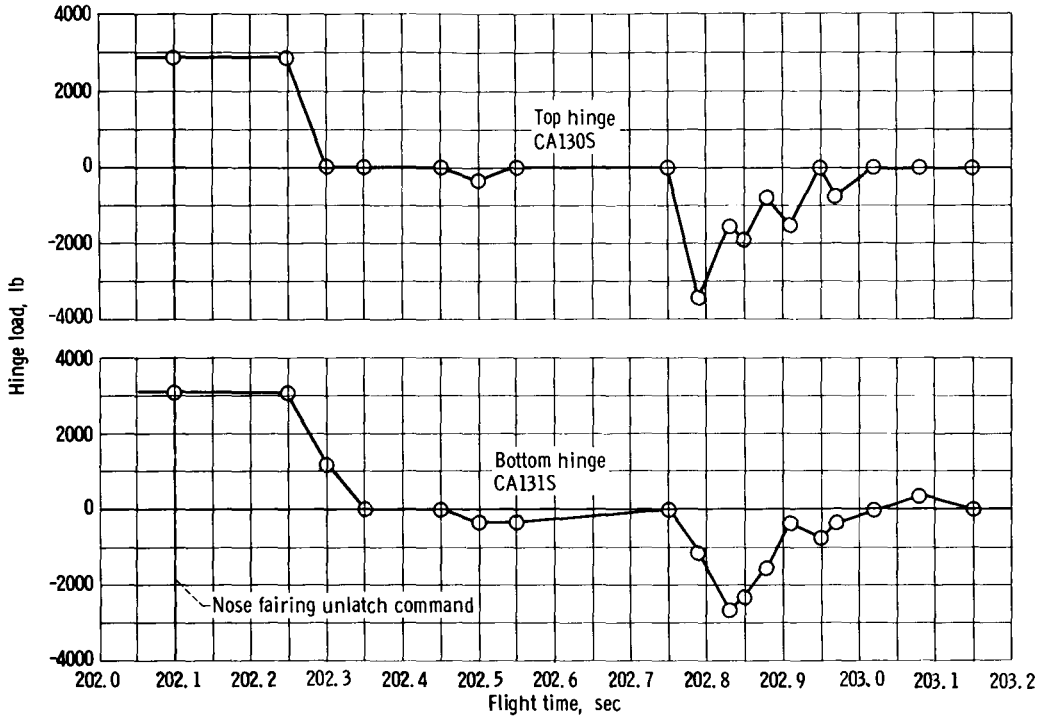

Figure X-16. - Nose fairing hinge fitting longitudinal loads. Positive hinge load is tension load.

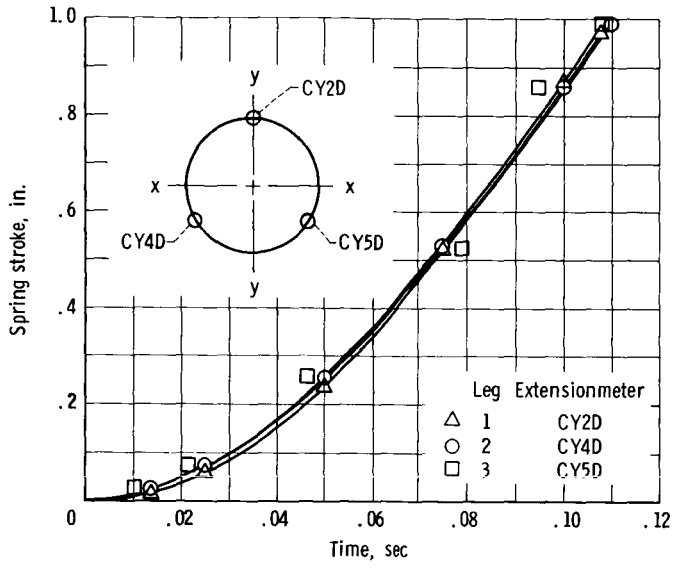

Figure X-17. - Centaur-Surveyor separation spring assembly stroke for AC-8.

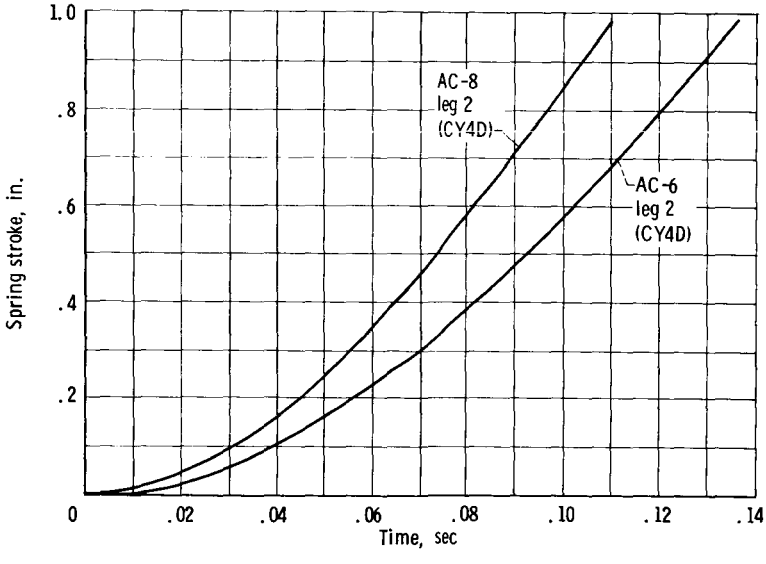

Figure X-18. - Comparison of AC-8 and AC-6 spring stroke spacecraft separation.

XI. FLIGHT DYNAMICS AND CONTROL

SUMMARY

Longitudinal oscillations observed at lift-off were 40 percent less than those seen on AC-5 or AC-6. An unusually high roll rate transient occurred at insulation panel jettison. Analyses of the Atlas-Centaur flight control telemetry data indicated satisfactory control system performance through the powered phase of flight. Data during coast showed that the attitude control system logic was operating properly. The attitude control system maintained the longitudinal axis of the vehicle in the plane of the trajectory and parallel to the local horizontal throughout the 25-minute coast phase. Loss of hydrogen peroxide prior to MES 2 prevented proper engine firing and resulted in tumbling of the Centaur vehicle. Programer discretes, however, were still being generated after the abortive engine shutdown.

ATLAS

Flight dynamics data during the Atlas powered flight were taken primarily from the Centaur rate gyros. The Centaur rate gyros were not activated for control purposes but were monitored for supporting data and correlation with the Atlas rate gyros.

The Centaur roll rate gyro at lift-off indicated one cycle in a counterclockwise roll direction of 1.5 degrees per second at the rigid body roll frequency of 0.8 hertz. Centaur pitch and yaw rate gyros showed transients at a maximum rate of ±0.6 degree per second at the second modal frequency of 6.3 hertz. These oscillations, seen on previous vehicles, decayed by the time the roll program was initiated at T + 2 seconds. Previous Atlas-Centaur vehicles have shown similar oscillations. Integration of the roll rate gyro output from T + 2 to T + 15 seconds verified satisfactory completion of the Atlas roll program, indicating a clockwise roll maneuver of 11.94° at an average rate of 0.92 degrees per second. The desired launch azimuth was 103°, rolling from a pad heading of 115°.

Longitudinal oscillations occurred at approximately the same time as in previous flights (fig. XI-I). The lift-off perturbations, as indicated by z-axis accelerometers, were 0.29 g single amplitude about a 1.21 average g level at a frequency of 6.14 hertz. This amplitude was approximately 40 percent less than that seen on the AC-6 and AC-5

flights, but approximately 60 percent greater than on AC-2, AC-3, and AC-4 flights. The peak disturbance occurred at 0.33 second after 2-inch rise and continued with decreasing amplitude for about 15 seconds.

Approximately 0.7 second after 2-inch rise, large disturbances were indicated on the Centaur roll rate, yaw rate, and pitch rate gyros and on the Atlas roll rate and displacement gyros. The Centaur yaw signals indicated a second mode (6.3 Hz) deflection of 0.024 inch at station 173, while the pitch signal indicated a 0.0548-inch second mode deflection at station 173.

The first and second mode frequencies plotted against time are shown in figure XI-2. The flight frequencies showed approximately the same relation to theoretical values as in previous flights.

Lateral bending mode deflections are shown in figure XI-3, as calculated from Centaur pitch and yaw rate gyros located at station 173. The design allowable modal deflections are only critical from 44 to 80 seconds after lift-off. The first modal deflections in the yaw and pitch planes during the critical time period were less than 10 percent of the design allowable deflection. The second modal deflections were less than 10 percent of allowable for the critical range, but were twice as high at 0.7 second after lift-off than those observed on previous flights.

Figure XI-4 shows a comparison of first mode maximum bending deflections during AC-2, AC-3, AC-4, AC-6, and AC-8. This comparison indicates that the lateral first mode deflection for this flight was higher at BECO than in previous flights.

The pitch rate gyro indicated proper initiation of the pitch program at T + 15 seconds. The following table is a comparison of the programed and actual pitch rates, as indicated by the Centaur pitch rate gyro,

Time, sec	Programed pitch rate, deg/sec	Telemetered pitch rate, deg/sec
0 to 15	0	0
15 to 23	.63	.63
23 to 34	.72	.71
34 to 45	.54	.52
45 to 55	.66	.72
55 to 65	.66	(a)
65 to 75	.66	(a)
75 to 85	.72	(a)
85 to 100	.51	.55
100 to 120	.36	.35
12 to BECO	.24	.23

[a]Vehicle dynamics prevents an accurate estimate of rate.

Low-order rigid body and propellant slosh oscillations were observed throughout booster and sustainer flight. A comparison of analytical and flight telemetered data is shown in figure XI-5. These correlations indicate that present methods of analysis in determining flight frequencies are acceptable.

A roll transient at the insulation panel jettison event (T + 176 sec) occurred and imparted a roll rate of 2 degrees per second peak to peak. This rate was similar to that on AC-6 (for further discussion, see section X VEHICLE STRUCTURES).

Figure XI-6 presents a comparison of the insulation panel jettison transient for AC-3, AC-4, AC-6, and AC-8, as seen from the Centaur roll rate gyro at station 173.

CENTAUR

Centaur MES 1 was commanded by the programer at T + 241 seconds (SECO + 11.5 sec). Rates imparted to the vehicle due to differential thrust buildups (approximately MES 1 + 1.5 sec) were 4.39 degrees per second nose up, 0.31 degree per second nose left, and 1.27 degrees per second clockwise roll. The pitch rate was nearly three times greater than those observed during the AC-4 and AC-6 flights, representing a large differential thrust buildup. Corresponding engine deflections were C1 pitch, -1.68 degrees, C2 pitch, -1.62 degrees, C1 yaw, -0.64 degree, and C2 yaw, 0.32 degree. Low-order rigid body and propellant slosh oscillations were observed throughout booster and sustainer flight. A comparison of analytical limit cycle frequencies and flight telemetered data is shown in figure XI-5. MECO 1 occurred at T + 575.5 seconds. The Centaur propellant settling engines were commanded on at this time for 100 seconds, providing at least 100 pounds of force. This was confirmed by differentiating guidance generated thrust velocities. A roll duty cycle of approximately 50 percent was observed to occur from T + 575.5 to T + 675.5 seconds. This was caused by impingement forces from the V2 and V4 engines acting on the main engines bells and providing a clockwise disturbing torque. The 50-percent duty cycle was approximately four times greater than predicted. The 6-pound propellant retention engines were commanded to the half-on mode of operation at T + 665.5 seconds. The roll duty cycle decreased to 6 percent and persisted until T + 1490 seconds, when the axial accelerometer indicated a drop to nearly zero acceleration for 80 seconds. Differentiation of thrust velocities from guidance confirmed the 6-pound thrust level and the drop to zero acceleration. Figure VI-24 shows the axial acceleration, attitude engine commands, and rate gyro data throughout coast. Venting dynamics and coast phase operation is further explained in section VIII PNEUMATICS AND HYDRAULICS. MES 2 was commanded at T + 2075.5 seconds. Improper engine operation caused the vehicle to cone at a maximum roll rate of 144 degrees per second.

The vibration environment of the AC-8 flight, as monitored by five accelerometers,

was similar to previous flights and was well within design proof test levels.

The maximum vibrations are given in table XI-I. As expected, the largest vibrations occurred at launch and flight events such as nose fairing jettison, start of boost pump. "Time sharing" of telemetry precluded a complete picture of the flight vibration but, from available data, the maximum vibration in the guidance area was 2.28 g's (P-P), the C1 gimbal mount was 2.5 g's (P-P), the LH_2 vent valve was 12.6 g's (P-P), the LO_2 boost pump was 6.25 g's (P-P), and the LH_2 boost pump lateral vibration was 5.06 g's (P-P).

A power spectrum and amplitude spectrum analysis was performed wherever possible in order to gain an insight into how the actual flight vibration compared on all usable accelerometer measurements and qualification levels with both previous flights. The plots of power spectral density (fig. XI-7) and amplitude spectrum (fig. XI-8) herein are for flight times at which maximum vibration occurred (using existing instrumentation).

Examination of the power spectral density (fig. XI-7) for the LH_2 boost pump showed maximum sine peaks within the 100- to 200-hertz band occurring with a level of 0.005 g^2 per hertz, which was significantly lower than the qualification level. There was also some vibration in the 350- to 400-hertz band.

Figure XI-8 presents a comparison of AC-8 and AC-4 vibrations with the qualification level. Both AC-4 and AC-8 levels were below the design test levels and, in most cases, the AC-4 maximum peak (root-mean-square frequency and amplitude or max sinusoidal peak) was higher and at a different frequency than AC-8. The LH_2 vent valve (fig. XI-8(a)) indicated a quasisinusoidal amplitude spectrum with the maximum root-mean-square sine peak of 0.88 g at a frequency of 175 hertz, and a random root-mean-square level of 0.08 g (based on a sine calibration).

TABLE XI-I. - MAXIMUM VIBRATIONS

Location	Station or quadrant	Axis	Measurement	Time, sec	Maximum g's (P-P)	Frequency band of data channel, Hz	Time of occurrence
Guidance platform mount	QII	y	CA89φ	4.8	2.28	0 to 1000	At launch
C1 gimbal mount	Station 453 QI	z	CA31φ	1.0	2.5	0 to 1000	At launch
LH_2 vent valve	Station 160	x	CA136φ	-1.5	12.6	0 to 1000	At launch
LO_2 boost pump	Station 467	x	CP556φ	223.2	6.25	0 to 1000	18 seconds after start of boost pump
LH_2 boost pump	Station 412 QII	y	CP590φ	0	5.06	0 to 600	At launch

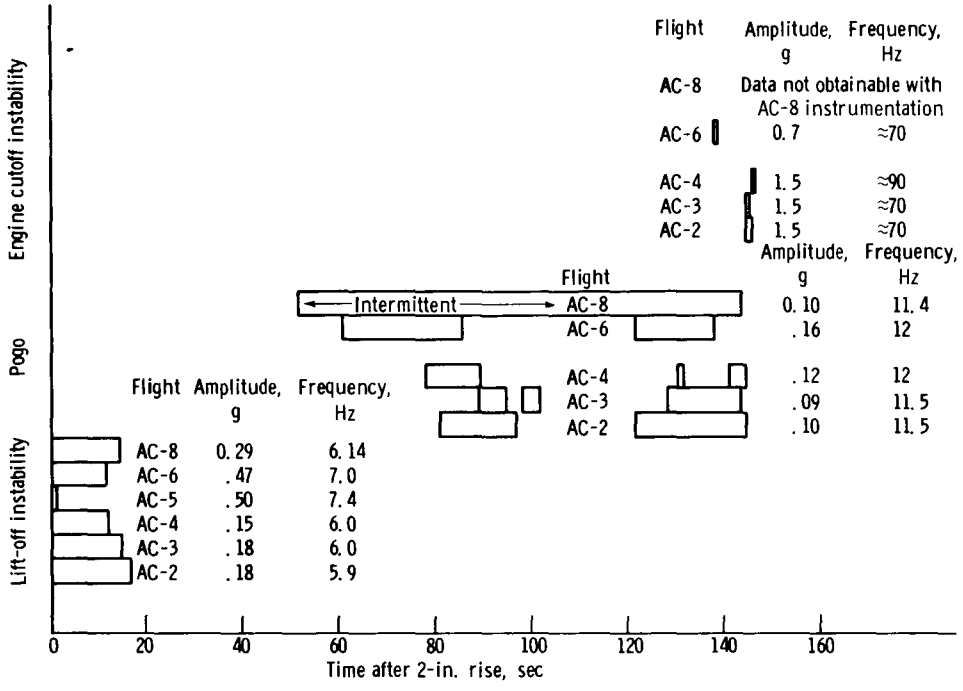

Figure XI-1. - Longitudinal oscillation occurrences, frequencies, and maximum amplitudes for Atlas-Centaur flights. (Amplitudes shown are single amplitudes.)

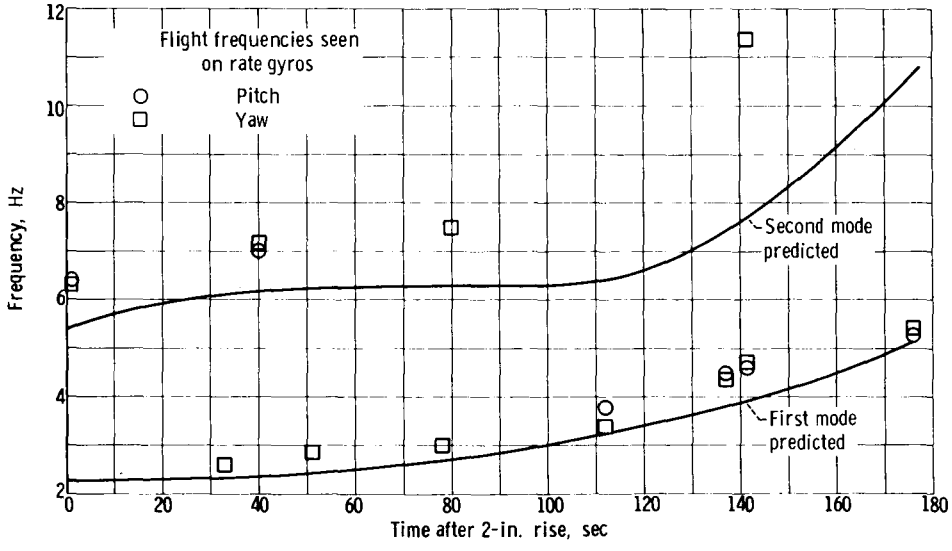

Figure XI-2. - Comparison of flight bending frequencies with theoretical bending frequencies.

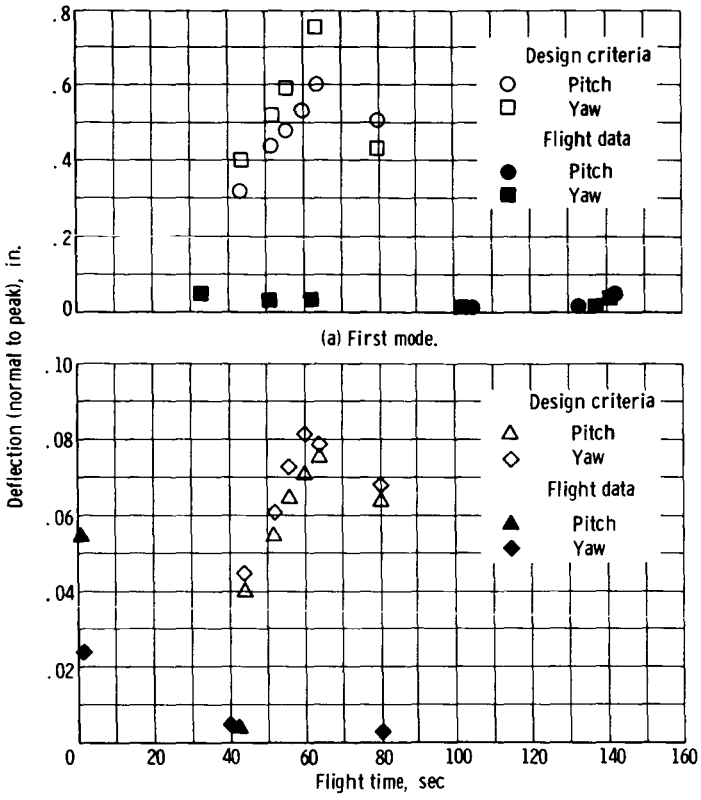

Figure XI-3. - Flight data and design criteria for wind-gust modal amplitudes, pitch, and yaw planes at station 173.

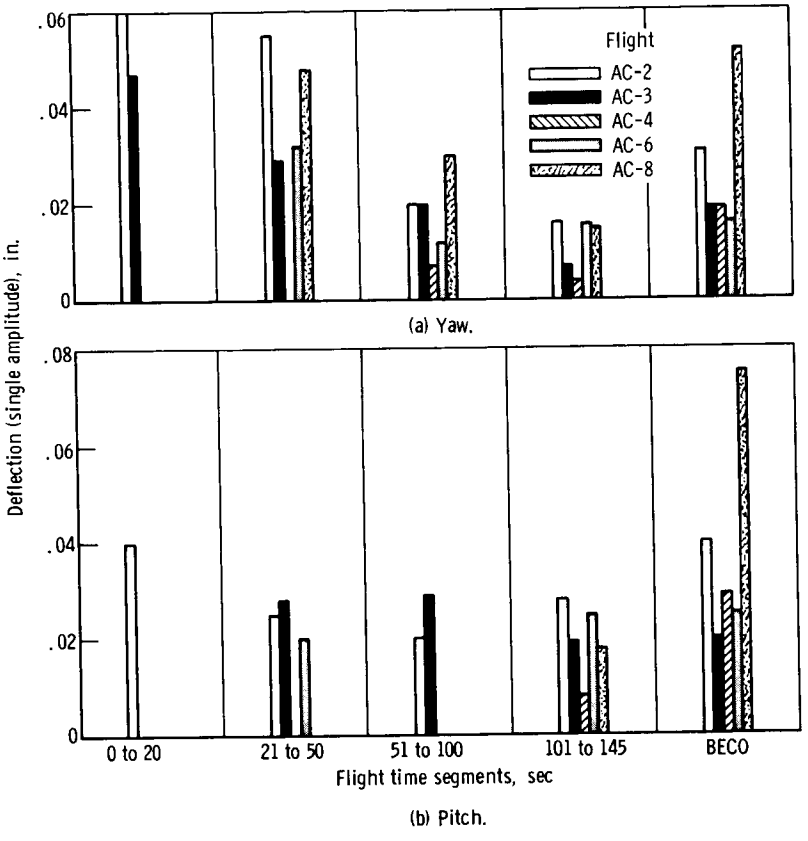

Figure XI-4. - Maximum first modal amplitudes at station 173.

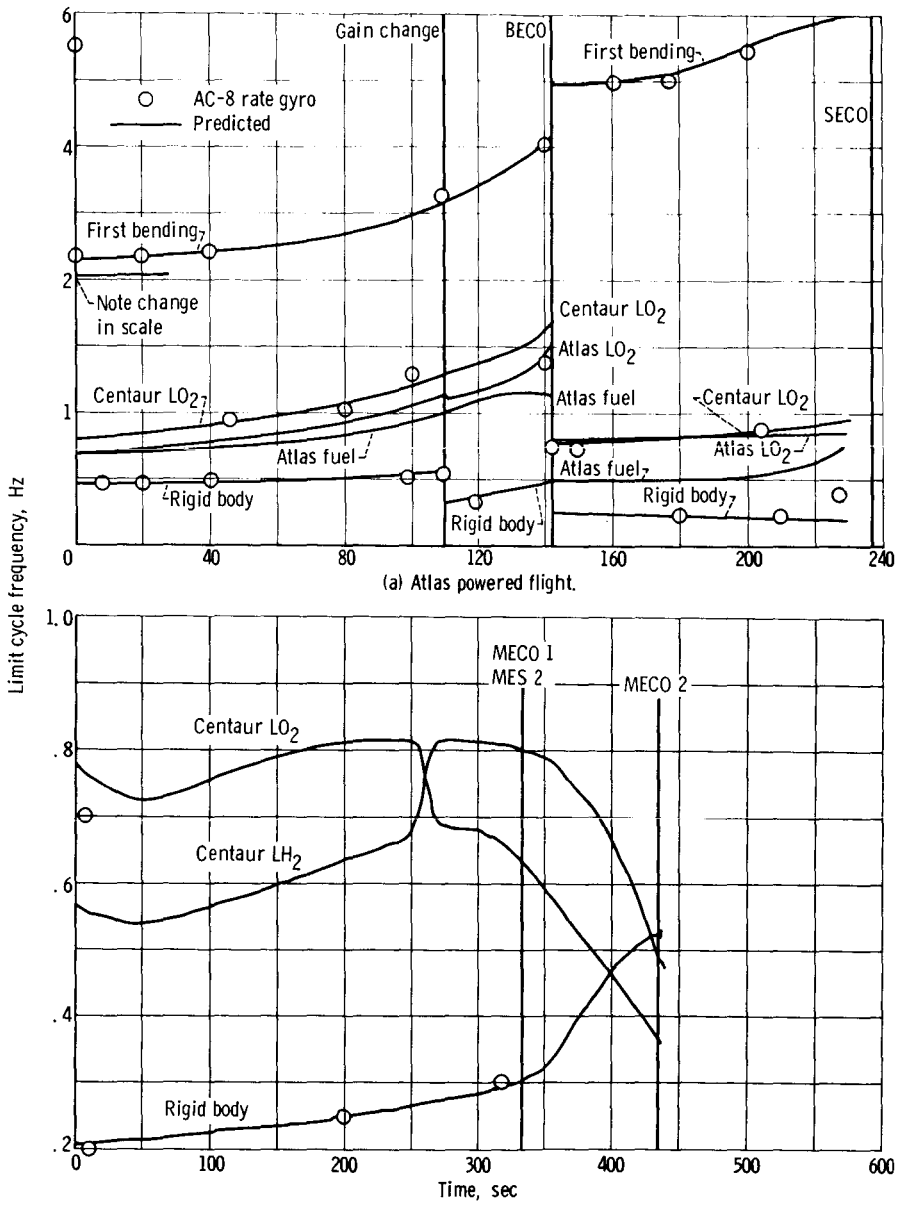

Figure XI-5. - Comparison of limit cycle frequency during Atlas and Centaur powered flights.

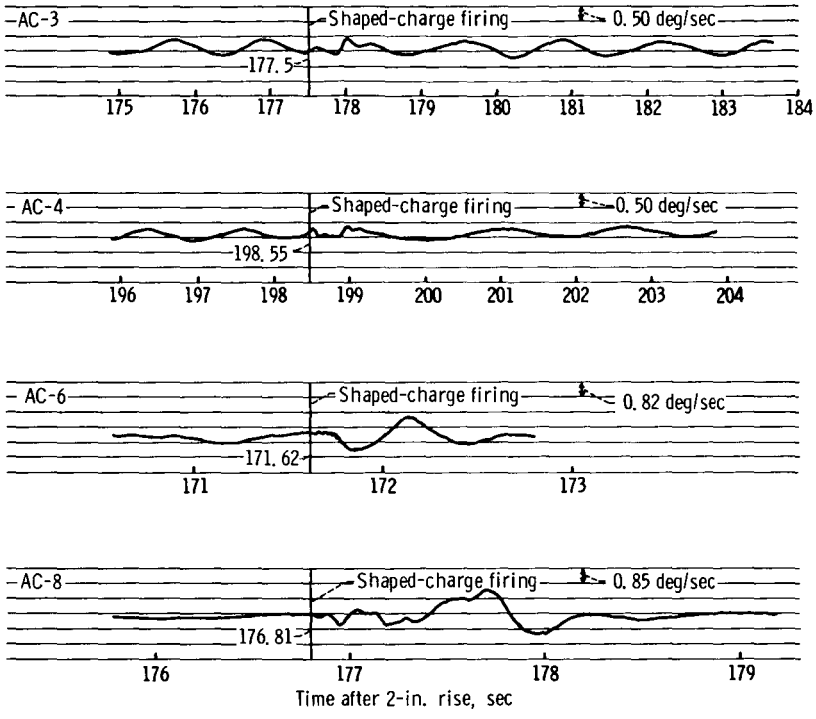

Figure XI-6. - Insulation panel jettison transient on Centaur roll rate gyro at station 173.

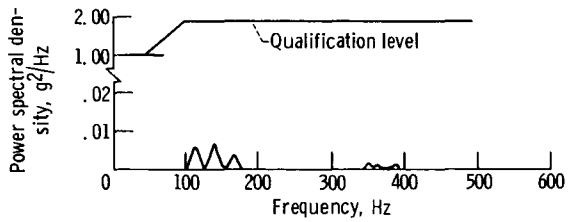

Figure XI-7. - AC-8 vibration level for CP590φ liquid hydrogen boost pump. Time interval, 2 seconds (launch); bandwidth, 20 hertz.

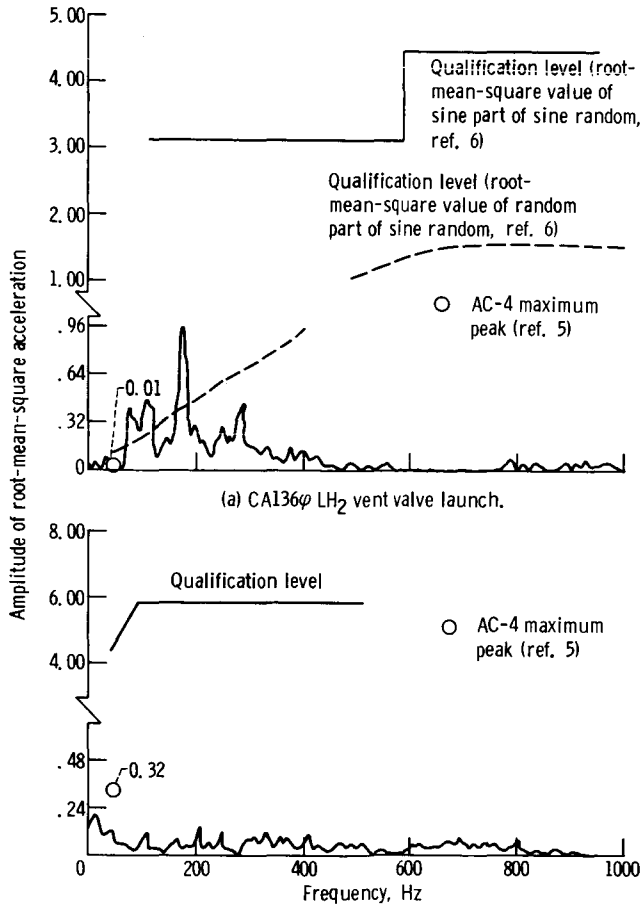

(a) CA136φ LH_2 vent valve launch.

(b) CP556φ LO_2 boost pump launch.

Figure XI-8. - AC-8 amplitude spectrum.

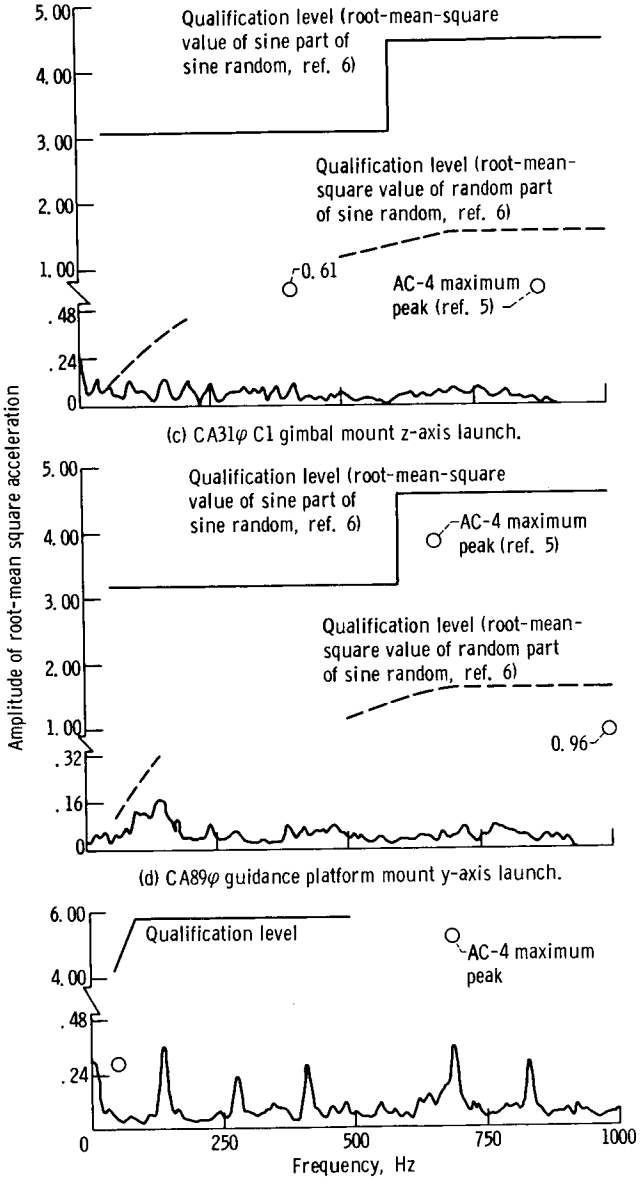

(c) CA31φ C1 gimbal mount z-axis launch.

(d) CA89φ guidance platform mount y-axis launch.

(e) CP556φ LO_2 boost pump. Time, T + 223.2 to T + 223.7 seconds.

Figure XI-8. - Concluded.

XII. GUIDANCE

SUMMARY

The Centaur guidance system (Missile Guidance Set 30) was calibrated on F - 0 day, and the shifts in d parameters were well within the uncertainties of the calibration model. A statistical analysis of the calibration history of the system is presented in table XIII-I. All primary flight objectives were satisfactorily demonstrated with one exception: Guidance data required to determine lunar injection errors were not obtained because of failure to accomplish the second burn. Parking orbit injection errors determined by a comparison between the ETR best estimated trajectory and telemetered guidance data were -0.5, -3.3, and -4.2 feet per second for the U-, V-, and W-accelerometer loops, respectively.

The guidance computer operated flawlessly to the end of telemetry coverage at 2 290 seconds. All expected guidance discretes were issued, and equation branching occurred as expected. The airborne computer generated BECO command at T + 142.3 seconds at an acceleration of 5.661 g's (nominal was 5.7 g's) as calculated from digital data. MECO 1 was generated at T + 575.5 seconds, approximately 1.5 seconds later than nominal. The longer burn, required to compensate for SECO, occurred 7.9 seconds early. Analysis of the energy at MECO 1 indicates an 11-millisecond cutoff extrapolation error because of accelerometer quantitization. This compares favorably with the maximum expected value of ±30 milliseconds. The 11-millisecond extrapolation error corresponds with a 0.7-foot-per-second velocity error.

SYSTEM CONFIGURATION AND TEMPERATURE ENVIRONMENT

A list of the individual guidance package serial numbers and measured skin temperatures is given in the following table. The temperatures prior to launch were comparable to those measured on previous vehicles and were well within the specific limits. The inertial component heaters were operating in their control bands throughout the flight, and no anomalies were apparent on the telemetered temperature control amplifiers output data.

Component	Serial number	Time, sec		
		T - 5	T + 500	T + 2200
		Temperature, ^{o}F		
Platform	G6	66.4	72.6	73.6
Pulse rebalance	F1	59.2	66.4	Not available
Platform electronics	G7	50.0	51.0	↓
Computer				
Memory section	014	66.4	76.0	
Input/output section	014	53.0	64.0	
Signal conditioner	I7	47.1	45.2	
Auxiliary signal conditioner	F1	----	----	----

STEERING LOOPS

During booster phase of flight, the airborne computer did not generate steering signals; therefore, the resolver chain input signals should have been maintained at null. Actually the signal conditioner outputs were 350 millivolts above null because of a bias caused by vehicle harnessing. At T + 149 seconds, the computer entered the sustainer phase and began to generate steering signals, as indicated by a change in the U-, V-, and W-analog steering signals. The Y-resolver chain output indicated a pitchdown steering command. The X-resolver chain output indicated no significant change in yaw steering. At SECO, the Y-resolver chain output indicated a small pitchdown maneuver, and the X-resolver chain outputs remained at null, indicating that the vehicle was steering to the proper vector. After the attempted MES 2, analog signals of the X- and Y-resolver chain outputs indicated that the vehicle was coning.

TORQUING LOOPS

At T - 7 seconds, the guidance system entered the flight mode, as verified by large changes in the analog torquing signals. During booster phase of flight, the analog torquing signals indicated satisfactory performance of all three loops. Immediately after BECO, a large change in U- and W-torquing occurred because of significant decreases in the U- and W-acceleration effects on gyro g sensitive terms. During sustainer phase of flight, the U- and V-loops perform satisfactorily but, at the time of nose fairing jettison, the W-torquing loop indicated a change equivalent to 0.9 degree per hour. This change

would have caused a velocity error of 12 feet per second in the V-accelerometer loop, but non was observed in either digital or analog data. The anomaly appears to be an error in the analog telemetry instrumentation. Similar shifts in W-torquing analog signals also occurred at nose fairing jettison on the AC-4 and AC-6 flights, where the performance otherwise was normal. Torquing loop performance was satisfactory during Centaur burn, during the coast phase, and after the second Centaur ignition.

ACCELEROMETER LOOPS

Oscillograph recordings of the 14.4-kilohertz demodulator output voltages indicate satisfactory performance of the accelerometer loops throughout the flight. A shift in pendulum offset of 1 arc-second occurred in the U-channel at BECO, and it returned to nominal at nose fairing jettison. The pendulum offset was confirmed by the 27-percent, 4/1 limit cycle at BECO. A history of the accelerometer ΔV-outputs is contained in table XIII-II. Most time intervals exhibited 3/2 or 2/2 limit cycle. The guidance system was designed to force a 2/2 or 3/2 limit cycle to minimize torque generation reaction torque (TGRT) effects, and the limit cycle history confirms proper accelerometer loop operation.

SERVOLOOPS

Telemetry signals of the four torque motor inputs and 7.2-kilohertz demodulator outputs indicated that the gimbal control amplifiers performed satisfactorily during flight. At T + 2 seconds, gimbal 1 responded to the start of the roll program. At T + 15 seconds, gimbal 3 reflected the start of the pitch program and, at T + 45 seconds, gimbal 4 was ungaged. Gimbal 4 uncaged at 18.9 degrees of pitch, as calculated from the nominal pitch program for AC-8. Nominal uncage is 20±5 degrees. During boost phase, gimbal 1 oscillated at a frequency of 0.40 hertz, indicating response to rigid body yaw. During sustainer burn, gimbal 2 and 4 oscillated at a frequency of 0.75 hertz, which was indicative of Atlas or Centaur LO_2 sloshing. After BECO, gimbal 3 responded to the pitch down maneuver, while gimbal 1 remained stable indicating no perceptable change in yaw. At Centaur MES, gimbals 1 and 3 responded to a slight yaw and pitch maneuver. These gimbals oscillated at a frequency of 0.20 hertz, which is characteristic of Centaur rigid-body oscillation. During this time, gimbal 2 oscillated at a frequency of 0.50 hertz, which was indicative of LH_2 sloshing. At MECO 1, gimbal 1 responded to a yaw maneuver and, 3 seconds later, gimbal 4 responded to a roll correction.

Twenty-nine seconds prior to MECO 1, gimbal 3 indicated the beginning of a pitch correction, which was completed at MECO + 44 seconds. Both the torque motor input and

7.2-kilohertz demodulator output signals confirmed that the inner block remained stable throughout the coast phase.

ERROR SEPARATION

Analysis of the velocity data during the coast period indicated very small accelerometer bias errors. The errors derived were 22, 22, and -59 micro-g's for the U, V, and W accelerometers, respectively. This compares well with the predicted 1σ in-flight system performance of 42 micro-g's based on the error model, which includes a 34-micro-g calibration uncertainty. Telemetered gimbal motor demodulator outputs indicated an average platform pitch error of approximately 7 arc-seconds (well within the expected tolerance). After removing the free-fall bias errors from the velocity residuals, the following errors were indicated by a least-squares separation: U-accelerometer scale factor, 40 ppm; V-accelerometer misalinement with respect to the U-axis, -35 arc-seconds; V-gyro mass unbalance input axis (MUIA) drift, 0.10 degrees per hour per g. The velocity residuals and indicated errors are plotted in figures XIII-1 to XIII-3.

TABLE XII-I. - CALIBRATION DATA

Units	Parameter	Axes	Launch value	Launch shift (run-to-run)	Root mean square of run-to-run shift	Points	[a]1σ
Accelerometer scale factor, none	D1	U	1.140116	0.000013	0.000019	13	0.000070
	D2	V	1.219888	.000011	.000022	13	.000150
	D3	W	1.213825	-.000012	.000020	13	.000150
Accelerometer non-orthogonality, arc-sec	[b]D4	U to V	458	18	13	10	30
	[b]D5	U to W	-132	22	9	10	50
	[b]D6	V to W	147	6	76	10	100
Accelerometer bias, $\mu g'$ s	D7	U	-1117	6	15	13	100
	D8	V	-1905	9	18	13	161
	D9	W	[c]261	-34	41	13	161
Gyro constant torque, deg/hr	D10	U	0.87	0.03	0.06	13	0.12
	D13	V	-.21	.02	.05	13	.06
	D16	W	.76	.06	.08	13	.12
Gyro mass unbalance input axis, deg/hr/g	D11	U	0.16	-.06	0.11	13	0.30
	D14	V	.02	.15	.08	13	.12
	D17	W	.39	.02	.07	13	.30
Gyro mass unbalance spin axis, deg/hr/g	[b]D12	U	-0.73	-0.05	0.04	6	0.21
	[b]D15	V	-.44	.08	.10	6	.21
	[b]D18	W	-1.59	.05	.10	6	.40

[a]Specification for Vehicleborne Guidance Set.

[b]Cooldown values listed; vehicle calibration technique does not exist.

[c]Adjusted for the observed shift when switching to internal power.

TABLE XII-II. - LIMIT CYCLE HISTORY

Event	Computer time, sec	U-direction					V-direction				W-direction			
		4/2	3/2	2/2	2/3	Other	3/2	2/2	2/3	Other	3/2	2/2	2/3	Other
		Percentage frequencies of limit cycles												
Go inertial	0 to 8		2.39	95.25	2.36		1.81	96.47	1.72		31.72	68.26	0.01	
Lift-off	8 to 10		6.43	87.26	6.31		7.09	85.71	7.14	One 3/3	38.97	60.72	.12	0.18 Percent of 4/2
Increase in acceleration														
1 g	10 to 76		13.89	85.55	.57		3.53	95.86	.61		50.07	49.93		One 3/1
2 g	76 to 108		61.45	38.55			10.58	89.42			59.31	40.69		
3 g	108 to 130	18.40	80.71	.88			17.98	82.02			63.92	36.08		
4.7 g	130 to 150	64.02	24.52			9.29 Percent of 4/1 2.12 Percent of 5/2 .05 Percent of 3/1	26.97	73.03			72.85	27.15		
BECO	150 to 151	15.36	41.06	4.43		27.47 Percent of 4/1 10.49 Percent of 5/2 1.18 Percent of 3/1	29.51	70.49			69.93	30.07		
Sustainer	151 to 236		46.37	53.61		Three 4/2	8.02	91.96	.02		10.44	89.55	.01	
SECO	236 to 237		61.57	38.43			10.62	89.38			9.34	90.66		
Coast	237 to 249		5.66	92.98	1.33		2.06	96.73	1.19	One 1/1 One 2/1	1.86	96.99	1.13	One 2/1 One 2/4 One 1/3
MES	249 to 250		1.68	97.42	.90		1.57	96.97	1.46		1.23	97.65	1.12	
Increase in acceleration														
1 g	250 to 352		29.04	70.94	.02		5.46	94.52			3.85	96.12		
2.1 g	352 to 582		48.14	51.85	.01		9.14	90.85			.97	96.45	2.58	
MECO 1	582 to 583		75.40	24.60			13.94	86.06				92.40	7.60	
Thrust coast														
100 lb	583 to 683		2.31	96.21	1.48		1.45	97.32	1.23	One 2/5	.98	97.91	1.11	
6 lb	683 to 1618		1.62	96.80	1.58	One 4/2	1.34	97.38	1.28		1.00	97.98	1.02	One 2/4
6 lb	1618 to 1728		1.66	96.63	1.71		1.35	97.30	1.35		1.05	97.84	1.11	
6 lb	1728 to 2038		1.63	96.78	1.59		1.34	97.38	1.28		.94	98.10	.96	
100 lb	2038 to 2082		1.43	97.08	1.48		1.29	97.46	1.25		.94	97.97	1.09	
Centaur second burn	2082 to 2100		4.41	87.21	8.37	One 1/3	4.78	88.42	6.80		4.66	87.05	8.29	
Centaur second burn	2100 to 2177		2.20	95.92	1.88		2.07	96.25	1.68		1.48	96.52	2.00	
Coast	2177 to 2254		1.26	97.49	1.25		1.10	97.82	1.08		.84	98.33	.83	

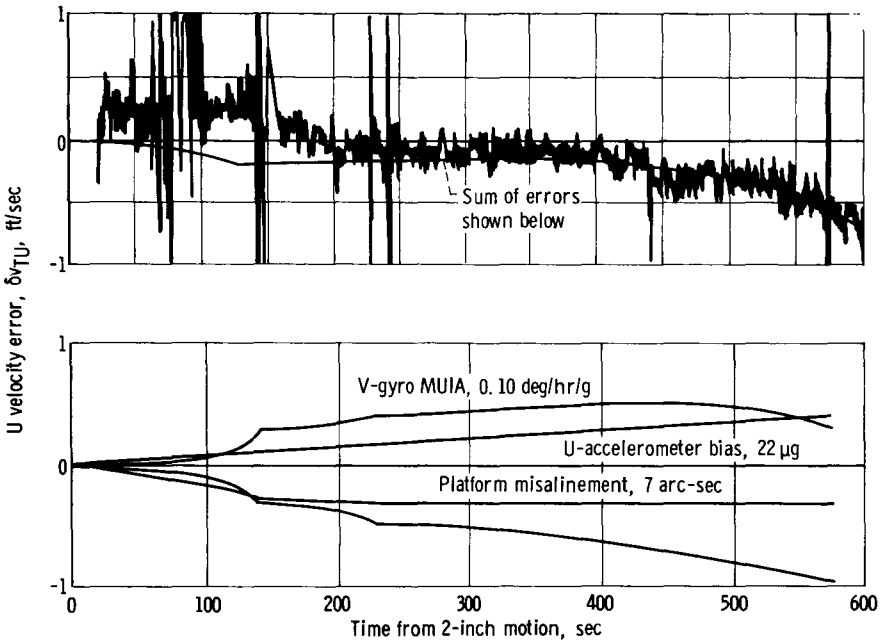

Figure XII-1. - U-error separation.

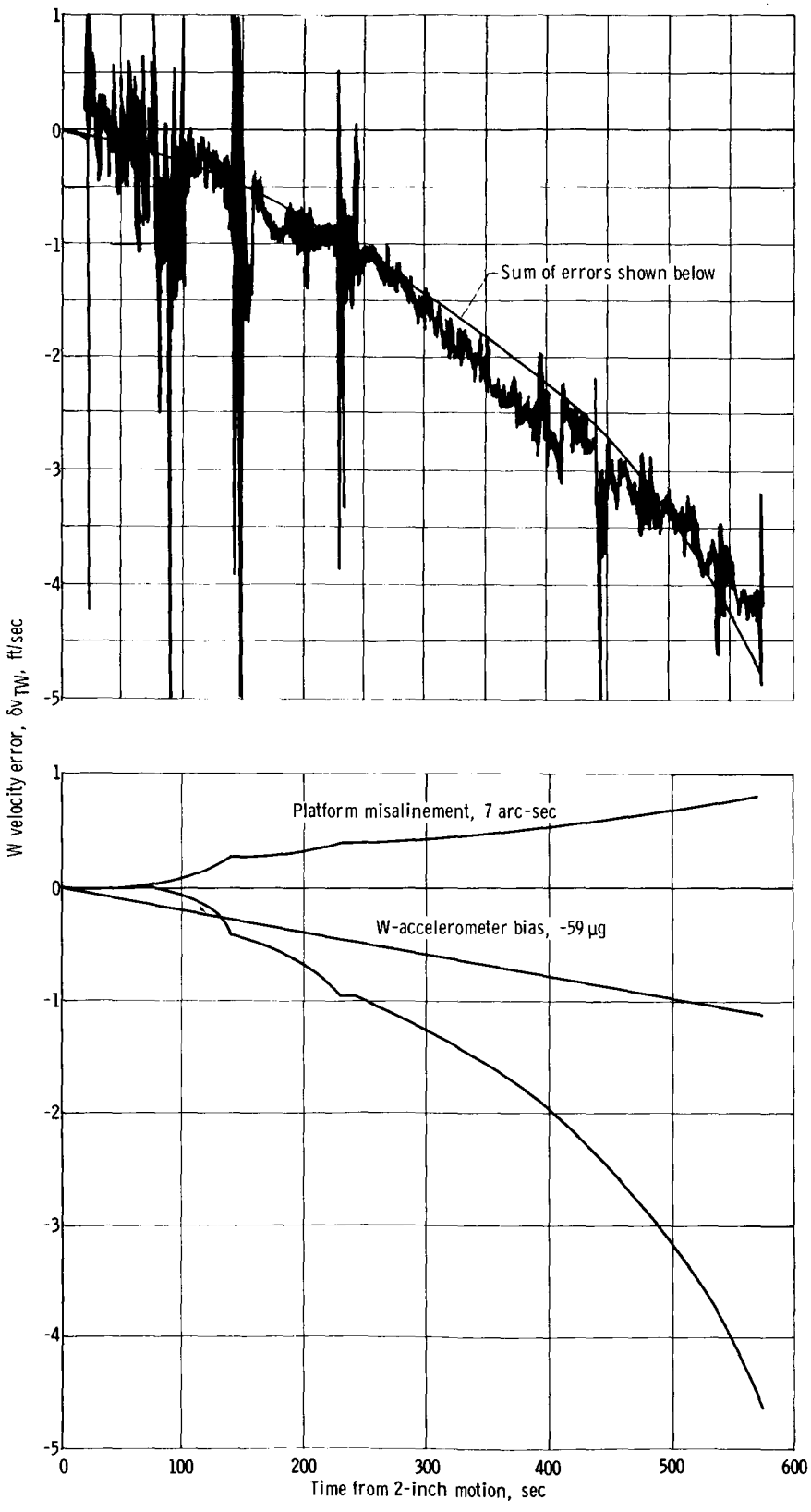

Figure XII-2. - W-error separation.

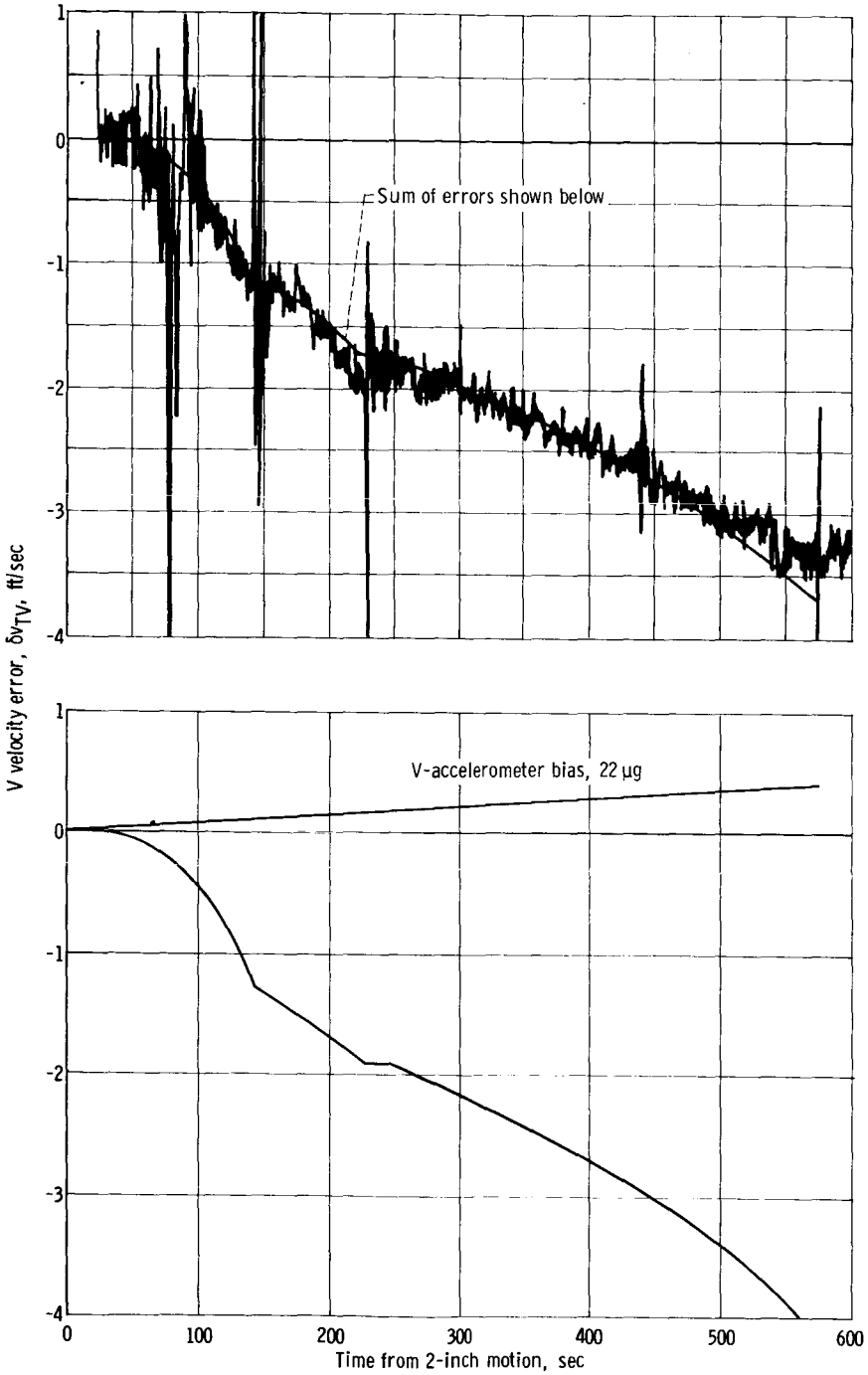

Figure XII-3. - V-error separation.

XIII. ELECTRICAL SYSTEMS

SUMMARY

The Atlas-Centaur electrical system performance was normal throughout the flight, and all voltage and current levels were within specification limits. Electrical power configuration differed from the AC-6 flight in that Centaur telemetry was powered by a separate 100-ampere-hour battery and changeover switch. The high-energy (1 A - 1 W) squibs that were used successfully on the preceding flight were used again to provide greater protection from stray currents and static discharges. Squib simulators were used during ground tests to verify proper performance of the pyrotechnic systems.

All four telemetry systems (three Centaur, one Atlas) functioned properly. No loss of data has been attributed to noise or to malfunction of these systems. Signal strength was excellent, and coverage was continuous until loss of data occurred between the stations at Tananarive, Malasy Republic, and Carnarvon, Australia, because of the MES 2 anomaly and subsequent abnormal trajectory.

The C-band and Azusa Glotrac tracking systems provided excellent data quality and coverage throughout the flight until failure to obtain a proper second engine burn, which resulted in departure from the expected trajectory and loss of tracking at Carnarvon. Spacecraft tracking by S-band radar was accomplished by the JPL Deep Space Network despite the abnormal trajectory.

The Atlas and Centaur-Surveyor Range Safety systems performed satisfactorily throughout powered flight. The command to disable the Range Safety system, transmitted from Antigua at T + 600 to T + 622 seconds, shortly after MECO 1, was received satisfactorily.

Launch logic was essentially the same as for AC-6. The countdown proceeded smoothly and with no apparent anomalies in the electrical system. Problems with the inadvertent separation switch monitor and the second-stage engine control panel, which were noted in the two earlier launch attempts, were corrected by appropriate action. Landline data indicated that all parameters were within expected values at lift-off.

ATLAS-CENTAUR ELECTRICAL SYSTEMS

Atlas

The major Atlas electrical system components included a manually activated main vehicle battery, two telemetry batteries, and a three-phase, 400-cycle rotary inverter. The main battery bus voltage indicated near nominal voltage throughout powered flight. On transfer to internal power, the battery voltage dropped momentarily to 26.4 volts, recovering to 27.6 volts in approximately 200 milliseconds. A steady-state low of 28.3 volts was recorded at lift-off and a high of 28.4 volts was reached at loss of signal.

Centaur

The Centaur vehicle power requirements were adequately supplied by one main missile battery, one telemetry battery, two range safety command batteries, two pyrotechnic batteries, and a 400-cycle static inverter. The use of an additional changeover switch and battery to supply telemetry and Azusa power requirements was the only notable configuration change to the Centaur electrical power system.

The main battery voltage and current were near nominal throughout the flight. Vehicle system dc input indicated a level at lift-off of 27.9 volts. A low of 27.3 volts was recorded during the MES sequence (maximum loading), and a high of 28.3 volts was reached during the coast phase.

The 14-ampere preload of the main battery prior to changeover to internal power preconditioned the battery to accept Centaur load. Preconditioning of the battery minimized the voltage drop at changeover that could be detrimental to the dependent systems. The resulting battery voltage level dropped to approximately 26.6 volts on transfer (specification limit is 26 V minimum). The main missile battery current (measurement CE1C) was 47 amperes at lift-off and reached a high of 69 amperes during the MES sequence. Comparison of the profile for ground test battery load current with the flight-recorded profile showed close correlation between sequential events (fig. XIII-1). Several pulses were noted on the current recording from T + 1490 to T + 1820 seconds. Transient peaks of 250-millisecond duration and approximately 3-ampere magnitude were caused by the operation of the vernier engine solenoid to effect pitch corrections. These pulses were observed at the following times (not shown in fig. XIII-1): T + 1491, T + 1581, T + 1614, T + 1633, T + 1657, T + 1700, T + 1743, T + 1786, and T + 1820 seconds.

The telemetry battery, which supplied power to Azusa and telemetry systems, operated satisfactorily, supplying nominal voltages throughout flight. The transfer to

internal power was accomplished in less than 200 milliseconds by the telemetry change-over switch with a resulting momentary dip in battery voltage to 26.1 volts, recovering to 27.7 volts steady state. The battery voltage was 28.9 volts at lift-off and increased to 29.2 volts to the end of data acquisition, while supplying a sustained load of 21 amperes.

The Centaur static inverter operated normally from launch countdown to the end of acquired data. Some apparent anomalies in the ac voltage, current and frequency data near the end of data acquisition have been attributed to noise and interference resulting from the abnormal vehicle trajectory.

Voltage regulation was within tolerance with voltage readings of 115.6, 116.0, and 115.8 volts at lift-off for phases A, B, and C, respectively. During flight, all three voltages increased slightly because of a decrease in load and a resulting increase in leading power factor. The leading power factor at lift-off was 0.95. Inverter frequency was crystal controlled and remained constant at 400.0 hertz. Inverter skin temperature measured 89° F at lift-off and increased gradually to a maximum of 202° F at T + 2220 seconds, the end of data acquisition. Data obtained from the second pass at Cape Kennedy, at T + 100 to T + 103 minutes, indicated that the inverter had cooled to 135° F. Electrical systems landline and telemetered data are given in table XIII-I. Inverter temperature trend during flight is shown in figure XIII-2.

INSTRUMENTATION

The instrumentation system of the AC-8 vehicle monitored 475 measurements on the Centaur vehicle and 134 measurements on the Atlas. A tabulation of the various subsystem measurements is given in table XIII-II. Of the 609 measurements, 6 yielded no valid data while 41 yielded partial or only qualitative data.

The following measurements yielded no valid data:

(1) Autopilot programer radial vibration (AA4480) was inactive throughout flight. The cause for this failure is unknown.

(2) Nose cap angle of attack calibration (CA475P) exhibited abnormal data shifts throughout the flight. The cause is unknown.

(3) C1 gimbal mount z-axis vibration (CA310) became noisy at Centaur MES and remained so throughout the flight.

(4) LH_2 vent valve vibration (CA1360) exhibited an unstable bias condition at T + 42.8 seconds and beyond. The exact cause for this failure is unknown, but it may have been caused by an electrical intermittency in the accelerometer-to-amplifier cable or connector. This problem has occurred before, and a low-noise RF cable and a new connector are planned for future vehicles.

(5) LO_2 tank skin temperature (CA134T) indicated an abrupt open circuit at the time

of the insulation panel shaped charge firing. The failure is probably the result of shaped charge firing.

(6) Forward bulkhead skin temperature (CA352T) indicated an open circuit prior to launch. Cause of failure is not known.

The following measurements yielded partial or only qualitative data:

(1) C1 LH_2 pump inlet pressure (CP52P) exhibited an intermittent open condition from T + 94 seconds to Centaur MES. There was no loss of data from this measurement since the problem occurred only during the booster phase of flight, and the measurement was active during the Centaur phase of the flight.

(2) Surveyor compartment ambient pressure (CY8P) indicated an intermittently open condition from lift-off to nose fairing jettison. The measurement yielded valid data thereafter. The cause of the problem is not known.

(3) Forward bulkhead skin temperature (CA792T) indicated an electrically open condition at T + 1020 seconds and for the remainder of the flight.

(4) LH_2 tank insulation panel delta temperature (CA6T) displayed erratic temperature fluctuations from launch to insulation panel jettison. The bonding of the thermocouple may have broken down; therefore, the data from this measurement were only qualitative.

(5) Aft bulkhead insulation temperature (CA853T) indicated an open circuit at T + 1205 seconds.

(6) Of the 50 germanium element temperature patches installed on the LH_2 tank skin, 32 exhibited an abrupt warming immediately after insulation panel jettison. Following panel jettison, data were qualitative on 24 of these measurements and totally lost on 8. The measurements are

CA272T	CA537T	CA554T	CA620T
CA273T	CA538T	CA556T	*CA622T
CA274T	CA540T	CA602T	*CA624T
*CA275T	CA542T	CA604T	*CA628T
CA276T	CA544T	*CA606T	CA707T
CA277T	*CA548T	CA610T	CA795T
*CA278T	CA550T	*CA614T	CA796T
CA495T	CA552T	CA618T	CA797T

(Measurements starred indicate data lost after insulation panel jettison.) Reason for the sudden temperature change has not been established. These measurements were redundant to the 32 liquid vapor sensors and 15 ullage temperature sensors, located inside the LH_2 tank, which enabled the liquid-vapor interface and ullage temperatures to be determined.

(7) Platinum temperature patches (CA608T, CA612T, CA616T, and CA271T) on the

tank skin remained at 0 to 2 percent of full scale throughout the flight. Some activity was expected.

(8) The wrong range of the single-axis milli-g longitudinal accelerometer (CM8A) was telemetered. Instead of telemetering the coarse range of the accelerometer (±15 milli-g's), the fine range (±1.5 milli-g's) was telemetered. This was because of an error in harnessing. However, the data received from this range of the accelerometer were very useful.

(9) Longitudinal acceleration of ±15 milli-g's (CM8A), longitudinal acceleration of ±0.5 milli-g (CM10A), and longitudinal acceleration of ±5 milli-g's indicated a shift in bias when compared to other flight data. During the start of the propellant retention coast phase, these measurements read the following milli-g outputs: CM8A, 1.35 milli-g's; CM10A, off scale high; CM38A, 0.7 milli-g. The expected positive g value based on 6 pounds of thrust and calculated vehicle weight of 13 850 pounds is 0.453 milli-g. Based on guidance accelerometer data, this value was calculated to be approximately 0.45 milli-g. The possible cause of this bias shift has not been determined, but an inflight zero-g calibration was obtained during the interval that the H_2O_2 system failed to provide any axial thrust, and the accelerometer data could be corrected and used with confidence.

TELEMETRY SYSTEMS

Atlas

The PAM/FM/FM Atlas telemetry system had been reduced to one telemetry package (RF 1, 229.9 Mc). All operational measurements were transmitted by this telemetry package via two antennas located in the B1 and B2 pods. Performance of the telemetry package was excellent, all commutators were within speed tolerance, and signal strength as recorded by the ground station indicated satisfactory transmitter operation. No measurements were lost because of noise or failures in signal conditioners. Atlas coverage is summarized in figure XIII-3.

Centaur

Three PAM/FM/FM telemetry links (subsystems 1, 2, and 5), which were similiar in configuration to the AC-6 telepaks, were coupled to a single antenna by a multicoupler for Centaur. The antenna was mounted on a ground plane on top of the umbilical island and radiated RF energy through the nose fairing until nose fairing jettison. Operational

measurements were telemetered on subsystem 1; the coast phase experiment measurements and other research and development measurements were assigned to subsystems 2 and 5. All telemetry packages were located on the equipment shelf. Telemetry transmitter frequencies and power were as follows:

Subsystem	Frequency, Mc	Power, W
1	225.7	4
2	235.0	4
5	259.7	4

Analysis of the data indicates that all the subcarrier oscillators were well within frequency tolerance. The commutators were initially within speed specification and did not exhibit significant drift. The telemetry battery current and voltage were within the predicted values. Temperatures were well within tolerance and are summarized in the following table:

Subsystem	Temperature, ^{o}F			
	T - 0 seconds	T + 500 seconds	T + 1300 seconds	T + 2300 seconds
1	39	44	48	48
2	53	59	59	62
5	51	53	57	53

Centaur coverage is summarized in figure XIII-4.

RANGE SAFETY

The Surveyor inadvertent separation switch continuity monitor was intermittent on the April 6, 1966 launch attempt; hence, it was not possible to ascertain whether the Surveyor Range Safety system was in a go condition. Since the Surveyor Range Safety system was not required for AC-8, the continuity monitor was removed from the launch sequence for this flight. The Atlas and Centaur-Surveyor Range Safety Command (RSC) systems performed satisfactorily throughout the flight. The only command to the system was transmitted from Antigua shortly after MECO 1 to disable the range safety system.

All RSC receiver signal strengths were excellent except for a drop in indicated signal strength for Centaur RSC receiver 2, which occurred at T + 566.5 seconds (-89 dBm) and T + 588 seconds (-89.5 dBm). A phase shift through the Centaur ring coupler attenuated

the signal strength; however, the reduced signal was still within the sensitivity limits of the receiver.

Block diagrams of the Atlas and Centaur RSC systems are shown in figures XIII-5 and XIII-6, respectively. Figure XIII-7 depicts the operation of the various ground transmitters in supporting these systems.

ATLAS-CENTAUR TRACKING SYSTEMS

C-Band Radar

The C-band transponder on the Centaur stage provided tracking information for the entire flight. Coverage was excellent except for loss of data at Carnarvon, Australia, due to the MES 2 anomaly and the subsequent abnormal trajectory. C-band coverage is shown in figure XIII-8. Transponder temperature remained well within expected limits throughout the flight.

Preflight testing of the transponder had been expanded to include spectrum analysis and pressurization tests at Cape Kennedy shortly prior to launch. A partial failure of the transponder on AC-6 had been attributed to either or both of these areas.

Glotrac

A Centaur-stage Azusa type C transponder and antenna system, in conjunction with continuous multiple station coverage by Glotrac segment I, enabled flight position and velocity data to be determined with high precision. The Glotrac segment IV baseline system at Pretoria provided precision tracking coverage of the Centaur second burn. An Azusa interstage adapter antenna was used to provide coverage through the early flight phase, since the insulation panels covered the Centaur-mounted antenna at this time. At panel jettison, the dc power to the coaxial circuit was interrupted to switch transponder output to the Centaur-mounted antenna. Glotrac coverage is shown in figure XIII-9.

S-Band Radar

The Surveyor mass model contained an S-band transponder assembly and an omni-directional antenna mounted on top of the forward mast. The transponder operated in a low power mode (100 mW) until approximately 11 seconds prior to spacecraft separation, at which time the Centaur programer initiated a switchover command to high power mode.

The spacecraft was acquired by the Johannesburg deep space instrumentation facility (DSIF) approximately 2128 seconds after lift-off, and two-way lock was obtained. Tracking continued for approximately 23 hours at the following by the Deep Space Networks at the following: Johannesburg, South Africa; Goldstone, California; Madrid, Spain; Tidbinbilla, Australia; and Ascension Island. Tracking information is given in figures XIII-10 and XIII-11.

GROUND SUPPORT EQUIPMENT PRELAUNCH OPERATIONS

The final countdown proceeded according to schedule with no anomalies observed. Landline instrumentation data indicated that all electrical measurements were within required limits. One change had been made in the prelaunch procedures to provide for activation of the Atlas telemetry battery at T - 173 minutes in lieu of T - 290 minutes. This reduced the total period of activation prior to launch and allowed for the possibility of extended holds during the uncertain weather conditions.

Two electrical ground support equipment (GSE) changes were accomplished prior to start of countdown:

(1) The second-stage engine control panel was modified to permit purge control of the Centaur main engines up to the moment of umbilical ejection.

(2) The spacecraft inadvertent separation switch monitor circuit, which displayed an intermittent condition in the aborted launch attempt on April 5, was inaccessible for trouble shooting. This could have caused a delayed or aborted launch since it comprises part of the prestart logic. This indication, however, was not critical for the AC-8 launch, and the circuit was bypassed in the GSE.

The pyrotechnic circuits were checked by squib simulators. These simulators are highly effective in verifying that the voltage and current at each squib will be of sufficient magnitude to fire that squib at the correct time.

Some of the more significant terminal countdown events are shown in table XIII-III, together with expected and the actual times of occurrence for this and for the previous flight.

TABLE XIII-I. - ELECTRICAL PARAMETERS

Measurement	Measurement number	Landline corrected meter reading at T - 0 seconds		Telemetered corrected flight data
		Nominal	Measured	
Centaur				
Main battery, V	CE28V	26.0(min.)	27.9	----------
Main battery, A	CE1C	80(max.)	-------	(a)
Telemetry battery, V	CT144V	26.0(min.)	[b]28.9	29.1(max.), 28.7(min.)
Telemetry battery, A	CT14C	(c)	[d]33.6	22(max.), 18(min.)
Pyrotechnic battery 1, V	CE5014V	[d]34.7(min.)	[d]35.8	(f)
		[b]15.0(min.)	(e)	
Pyrotechnic battery 2, V	CE5042V	[d]34.7(min.)	[d]35.6	(f)
		[b]15.0(min.)	(e)	
RSC battery 1, V	CE1021V	[d]33.2(min.)	33.5	(f)
		[b]30.0(min.)	32.5	
RSC battery 2, V	CE1022V	[d]33.2(min.)	33.7	(f)
		[b]30.0(min.)	32.6	
Inverter phase A, V	CE51V	115±1.2	115.6	115.6 to 116.4
Inverter phase B, V	CE52V	115.0±1.2	116.0	116.0 to 116.8
Inverter phase C, V	CE53V	115.0±1.2	115.8	115.8 to 117.8
Inverter phase A, A	CE2C	(c)	(g)	1.76 to 1.82
Inverter phase B, A	CE3C	(c)	(g)	1.36 to 1.40
Inverter phase C, A	CE4C	(c)	(g)	1.40 to 1.48
Inverter frequency, Hz	CE50Q	400±0.2	400.0	(h)
Inverter skin temperature, °F	CE29T	100(max.)	89	(i)
Atlas				
Main battery, V	AE28V	26.5(min.)	28.3	28.4(max.), 28.3(min.)
Inverter phase A, V	AE51V	115.3±1.7	--------	114.6(max.), 114.0(min.)
Inverter frequency, Hz	AE50Q	402.0+1.5 -0.5	402.1	403.3(max.), 402.1(min.)

[a]See fig. XIII-1.

[b]Full load.

[c]Not given.

[d]Open circuit.

[e]Not monitored.

[f]Data not telemetered; landline measurement only.

[g]Not recorded.

[h]Steady throughout flight.

[i]See fig. XIII-2.

TABLE XIII-II. - AC-8 ATLAS AND CENTAUR MEASUREMENTS

Airborne systems	Measurement type														
	Acceleration	Rotation rate	Current	Deflection	Power	Vibration	Pressure	Frequency	Rate	Strain	Temperature	Voltage	Discrete	Digital	Total
Atlas															
Airframe						1	9				21		21		52
Range safety												3	1		4
Electrical								1				2			3
Pneumatics							7				2				9
Hydraulics							6								6
Guidance															---
Miscellaneous	1														1
Propulsion		3		2			20				2		7		34
Flight control				11					3				7		21
Telemetry											1				1
Propellants							2					1			3
Azusa															---
Spacecraft															---
Total	1	3	-	13	-	1	44	1	3	-	26	6	36	-	134
Centaur															
Airframe						3	2			2	162		1		170
Range safety												2	8		10
Electrical			4					1			3	4			12
Pneumatics							10				23		2		35
Hydraulics							2				6				8
Guidance	3										6	27	4	1	41
Miscellaneous	8			1								1	32		42
Propulsion		4				2	22				46		20		94
Flight control									6		2	4	30		42
Telemetry			1								6	2			9
Propellants				2							1	2			5
Azusa					1						1				2
Spacecraft				3			1				1				5
Total	11	4	5	6	1	5	37	1	6	2	257	42	97	1	475

TABLE XIII-III. - SIGNIFICANT TERMINAL COUNTDOWN EVENTS

Event	Landline measurement	Time of occurrence, sec		
		Expected	Actual	
			AC-6	AC-8
Engine start command	AP1161X	T - 7.83	T - 8.27	T - 9.03
Command to eject upper umbilicals	CN1614X	T - 3.41	T - 3.20	T - 3.20
Umbilicals ejected:				
P401	CN1351X	T - 3.21	T - 3.17	T - 3.15
P402	CN1352X	↓	↓	↓
P403	CN1353X			
P404	CN1354X			
Aft plate ejected	CN1396X	T - 3.14	T - 3.10	T - 3.03
Ignition complete (main stage limiter)	AP1617X	T - 2.17	T - 2.15	T - 2.10
Vehicle release	AP1577X	T - 0.80	T - 0.78	T - 0.83
2-Inch motion	AM1030X	T - 0	T - 0	T - 0
Upper boom solenoid valve	CN1464X	T + 0.00	T + 0.00	T + 0.00
Auxiliary 2-inch motion	CN1474X	T + 0.03	T + 0.04	T + 0.04
Umbilicals ejected (Atlas):				
P1002	AN1061X	T + 0.03	T + 0.04	T + 0.01
P1003	AN1062X	↓	↓	↓
P1005	AN1063X			
P1007	AN1064X			
P4001	AN1065X			
Lower boom solenoid valve	CN1465X	T + 0.25	T + 0.26	T + 0.26
8-Inch motion	AN1827X	T + 0.26	T + 0.27	T + 0.24
Umbilical P1001 ejected (Atlas)	AN1060X	T + 0.29	T + 0.34	T + 0.28
42-Inch motion (umbilical P609 ejected)	AN1066X	T + 0.98	T + 0.85	T + 0.98

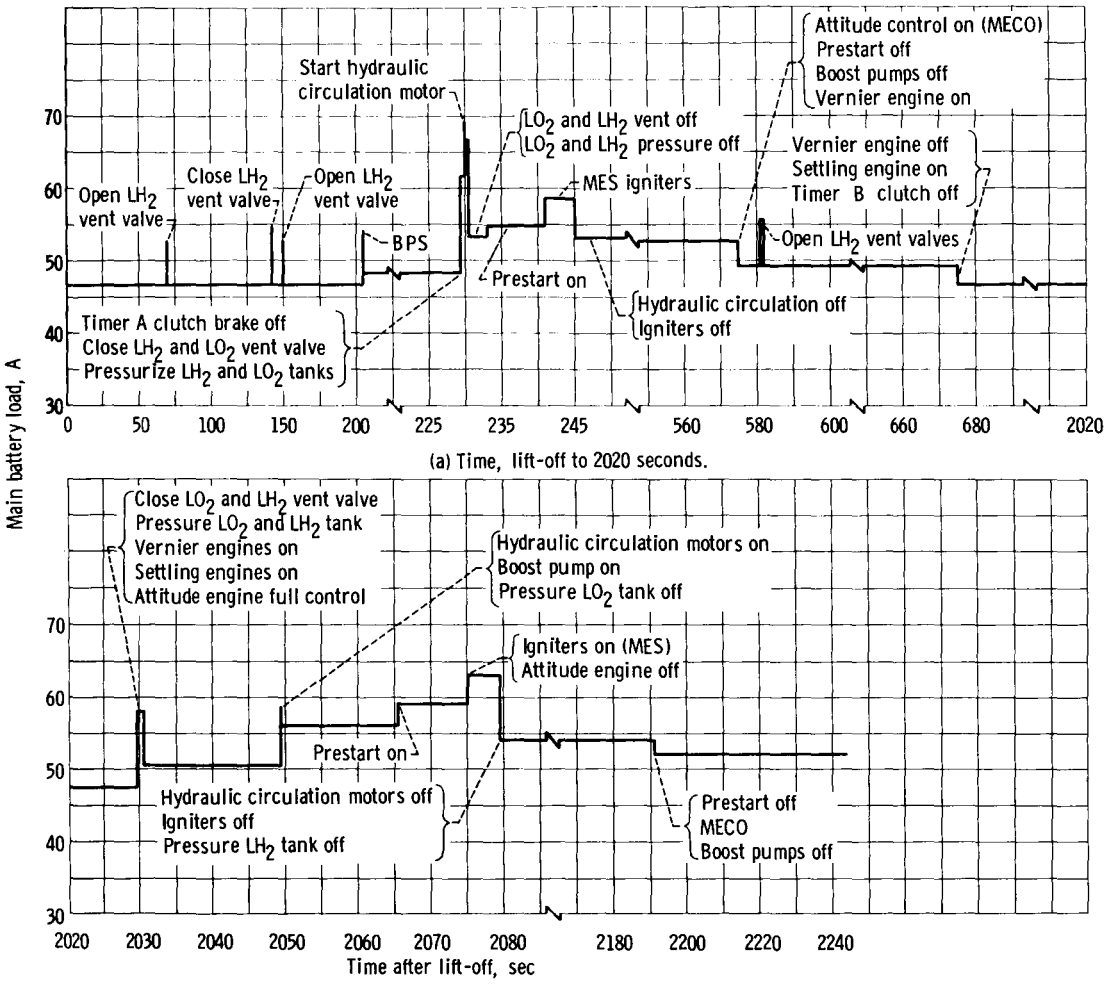

Figure XIII-1. - Centaur AC-8 main vehicle battery load profile.

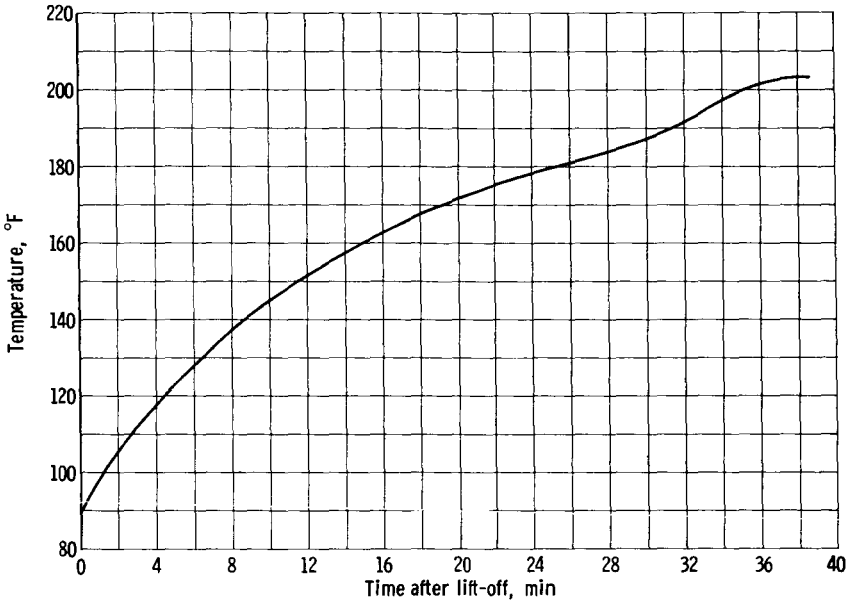

Figure XIII-2. - Centaur static inverter skin temperature.

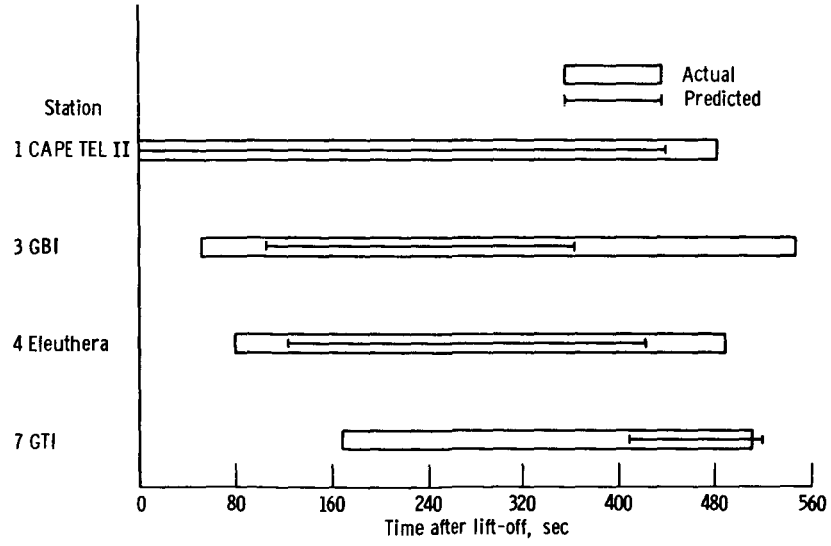

Figure XIII-3. - AC-8 Atlas telemetry coverage.

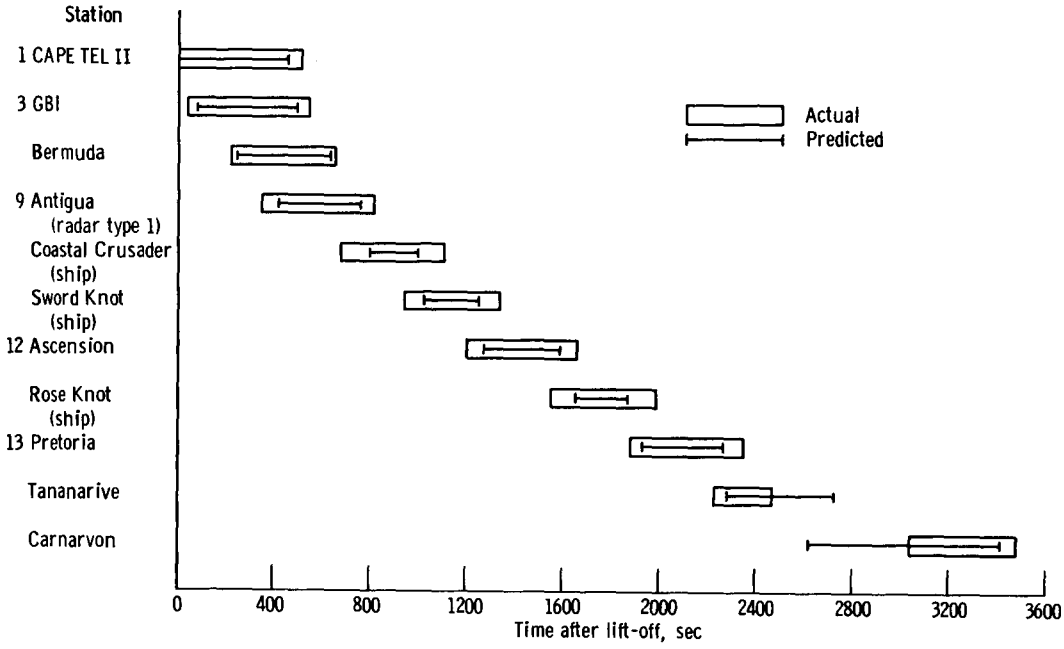

Figure XIII-4. - AC-8 Centaur telemetry coverage.

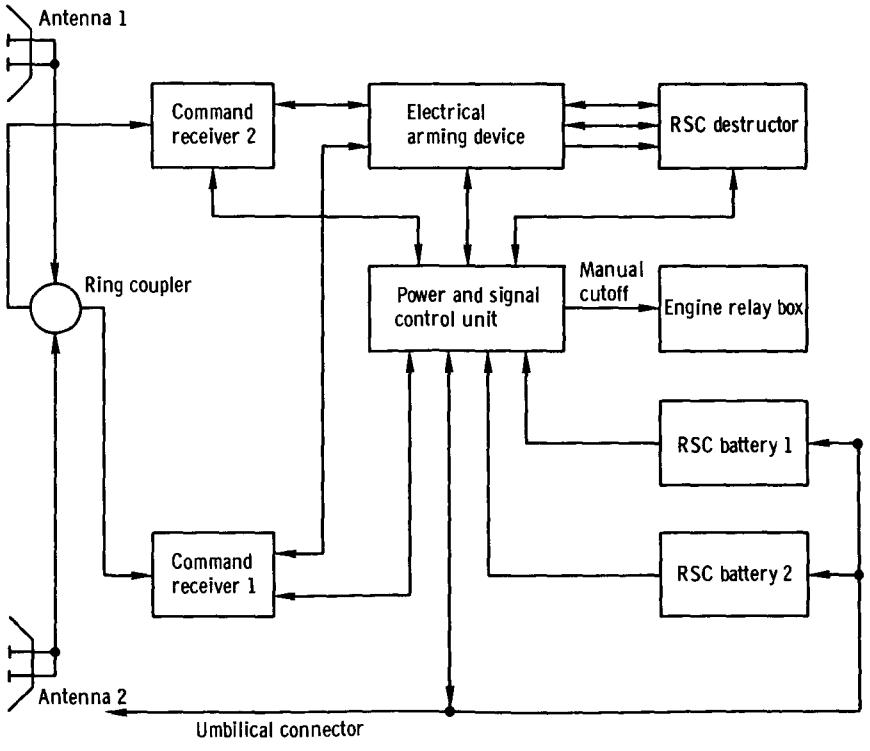

Figure XIII-5. - Block diagram of first-stage Range Safety Command system.

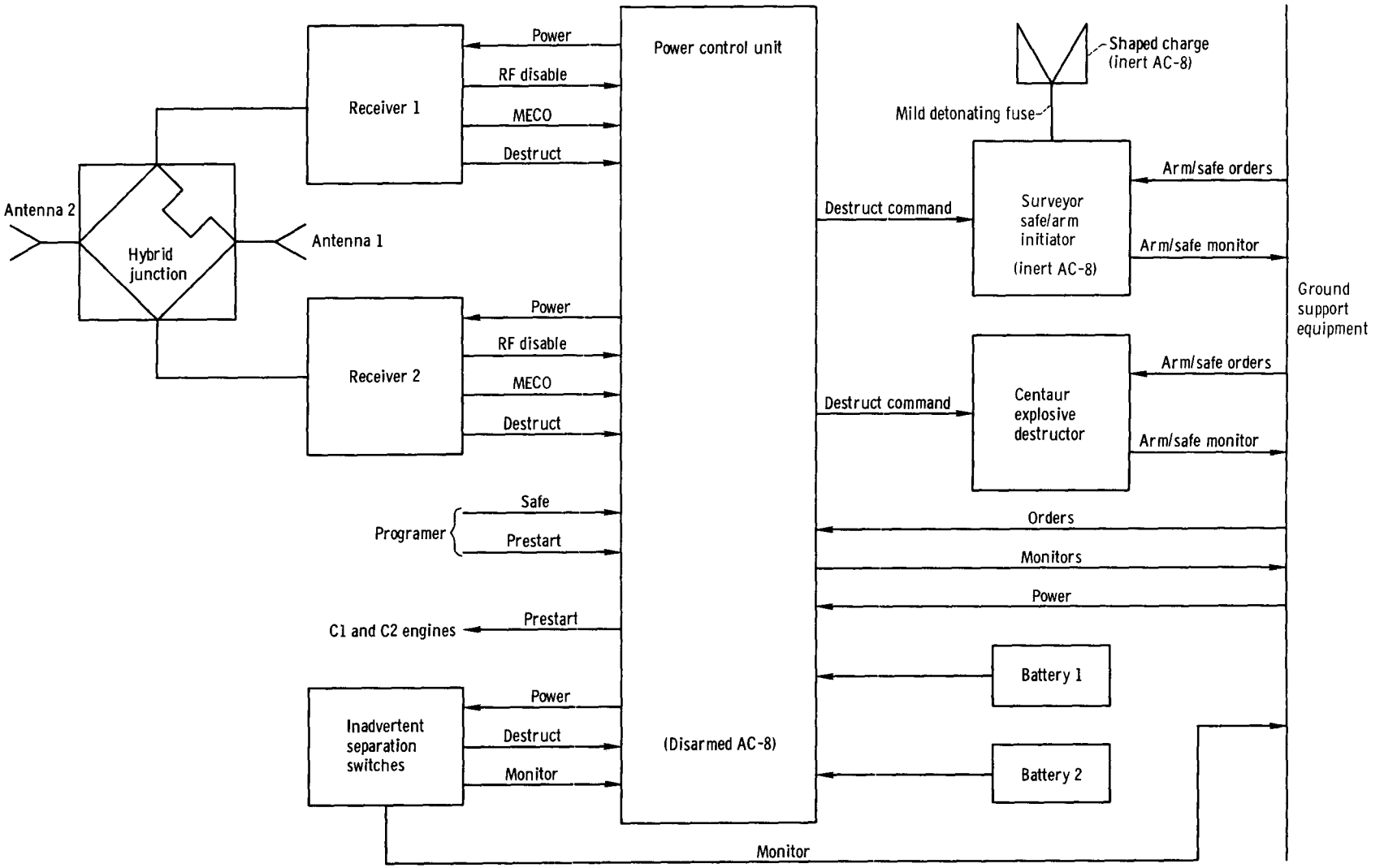

Figure XIII-6. - Block diagram of second-stage Range Safety Command subsystems.

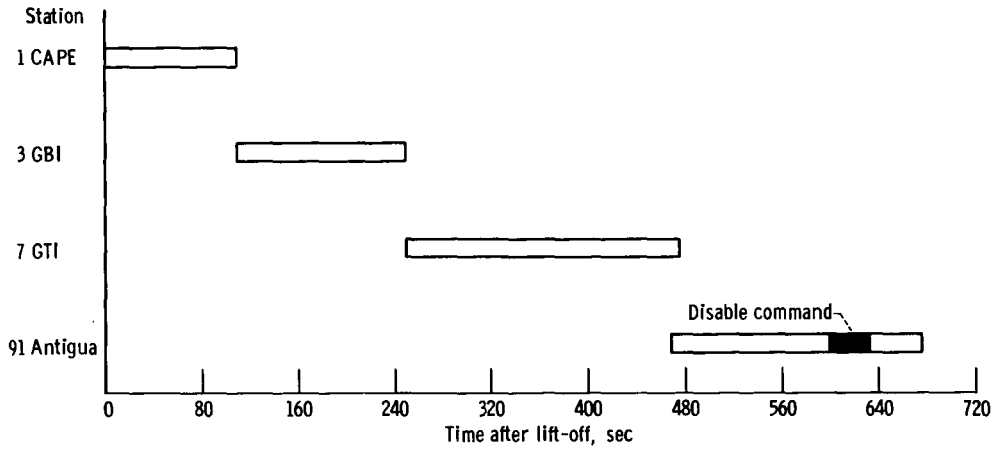

Figure XIII-7. - AC-8 Range Safety Command system transmitter utilization.

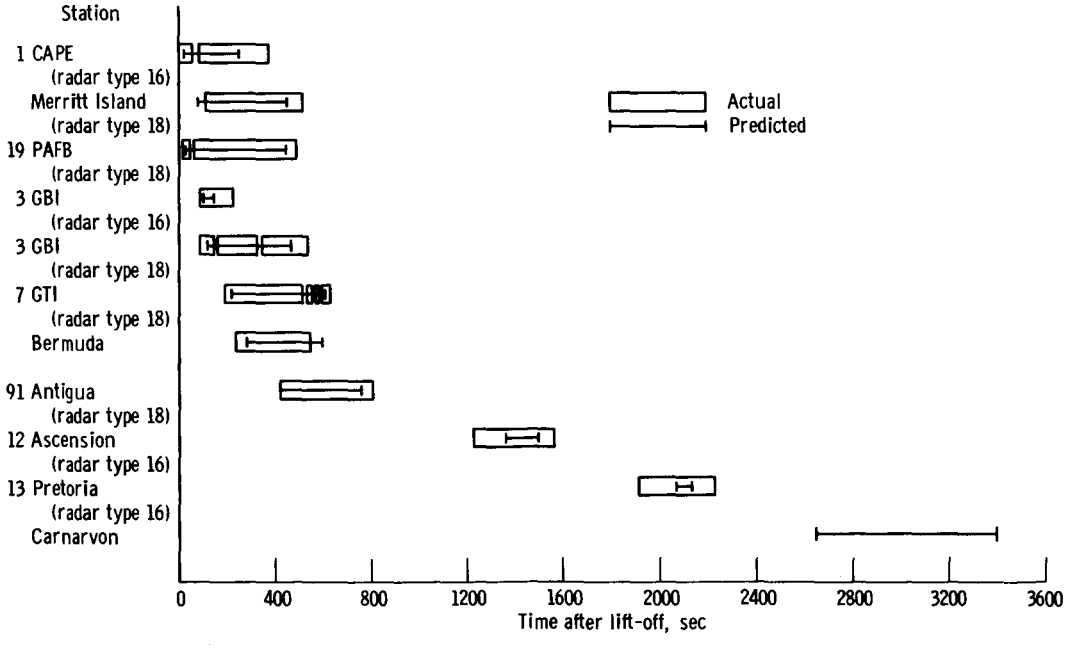

Figure XIII-8. - C-band radar coverage for AC-8. Indicates auto beacon track only. Carnarvon did not track Centaur during first pass.

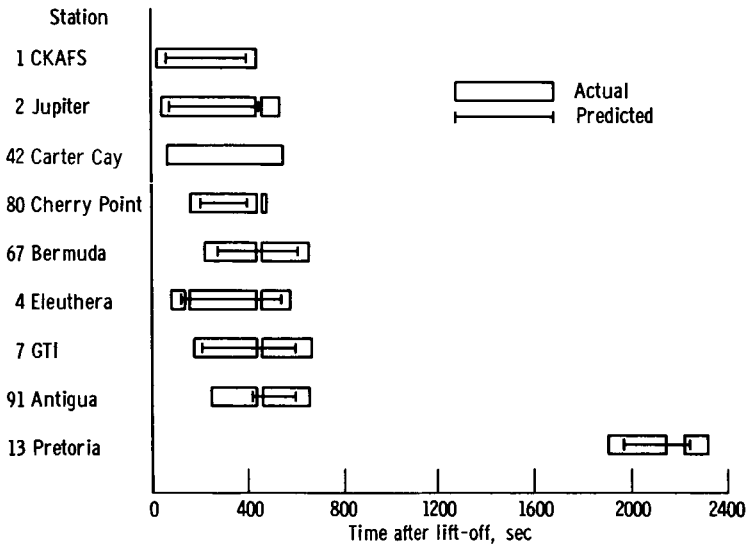

Figure XIII-9. - AC-8 Glotrac coverage.

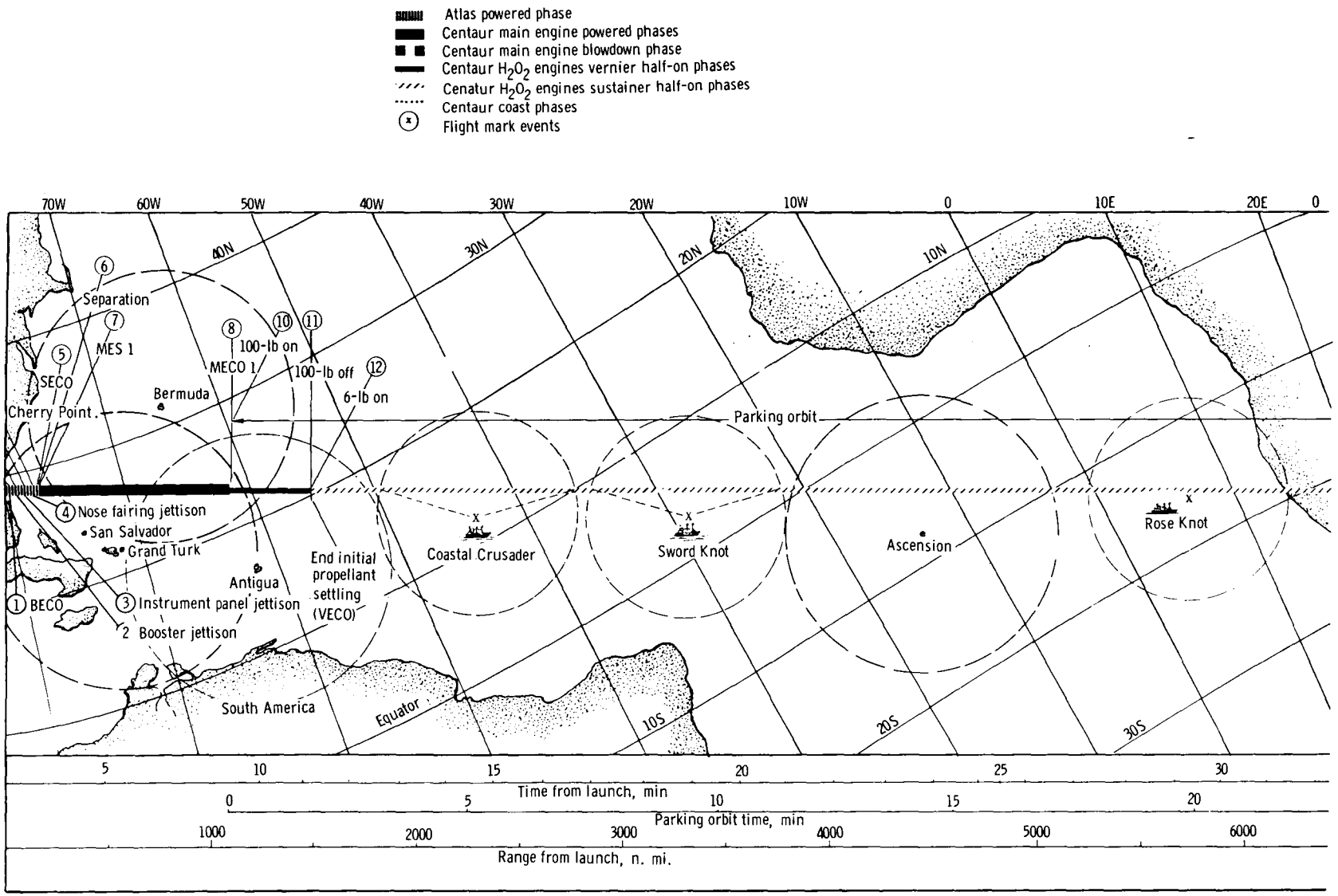

Figure XIII-10. - Predicted AC-8 Earth trace showing instrumentation coverage. Launch azimuth, 103°; parking orbit altitude, 90 nautical miles; radar coverage, available at all land stations except Tananarive. Telemetry coverage shown indicates periods of best reception. Continuous telemetry data from launch to end of mission is possible but not likely.

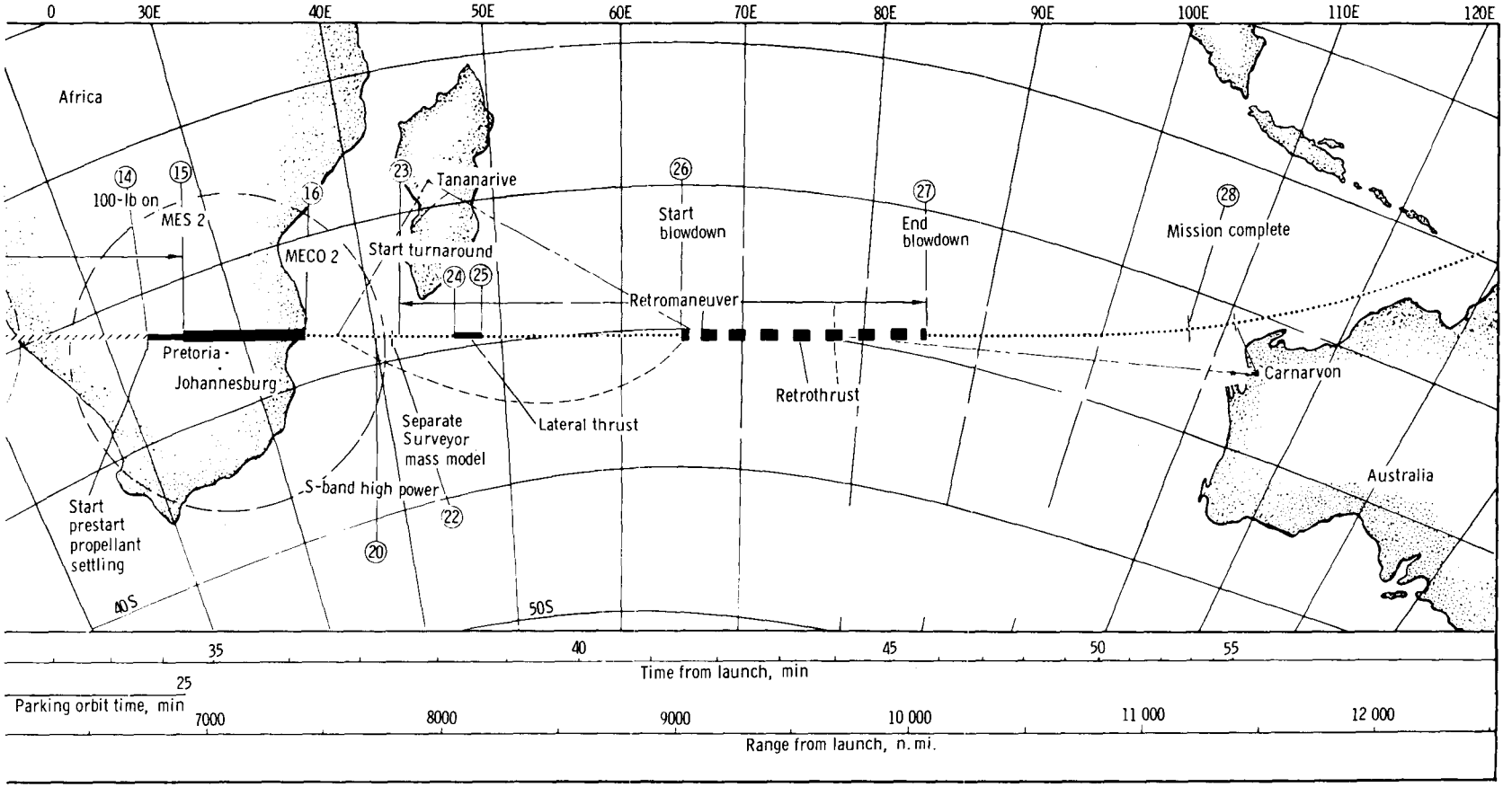

Figure XIII-10. - Concluded.

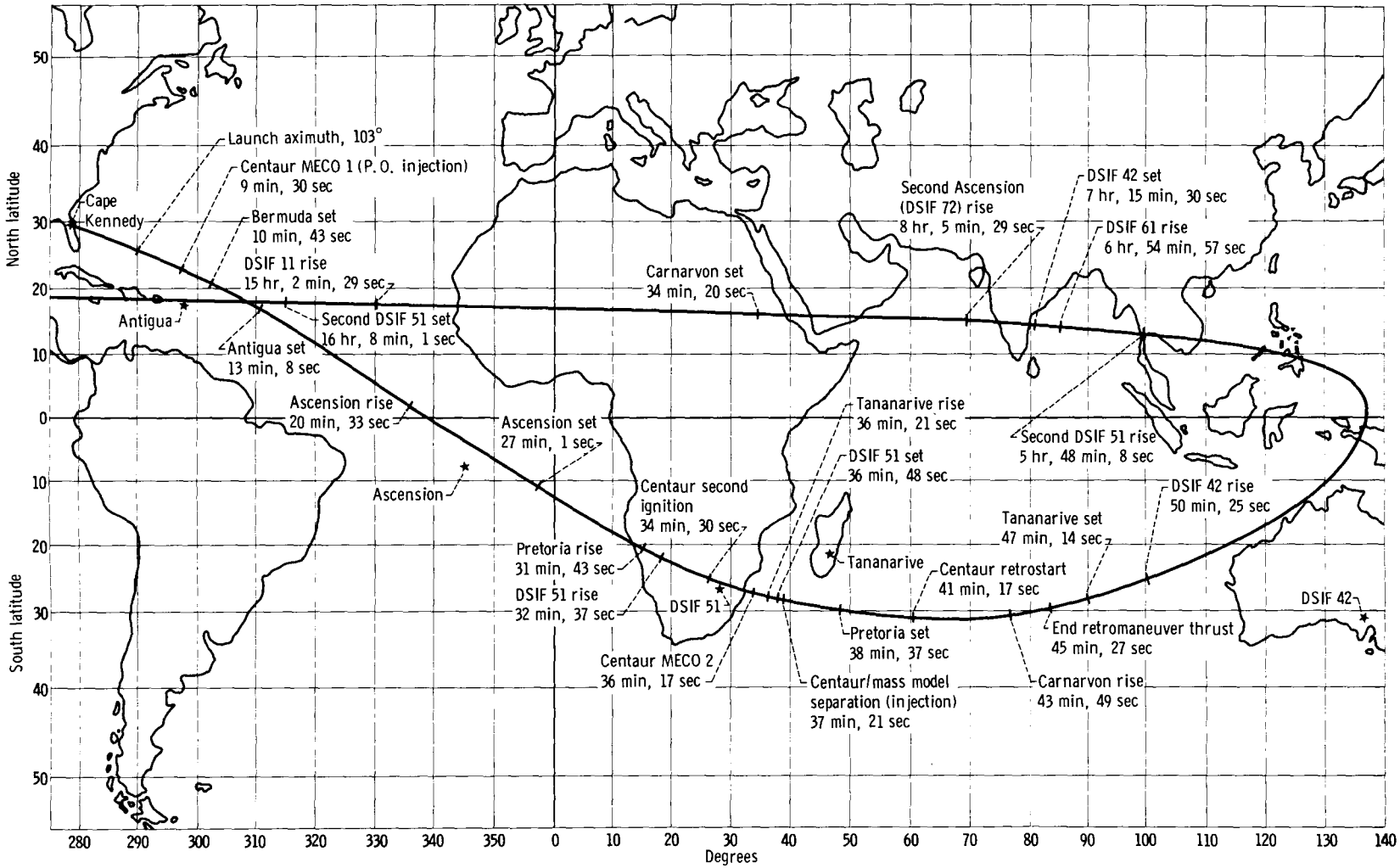

Figure XIII-11. - Predicted AC-8 Earth trace showing DSIF tracking coverage. AFETR and NASA stations rise and set based on elevation angle of 0^{o}. DSIF status rise and set based on physical viewing constraints. DSIF 61 and 72 not committed to AC-8.

APPENDIX - ABBREVIATIONS

A-C	Atlas-Centaur
AFETR	Air Force Eastern Test Range
A. G. C.	automatic gain control
AOS	acquisition of signal
A/P	autopilot
ac	alternating current
BECO	booster engine cutoff
BET	best estimate of trajectory
BPS	boost pump start
CAPE	Cape Kennedy
CKAFS	Cape Kennedy Air Force Station
CRT	Composite Readiness Test
cg	center of gravity
cps	cycles per second
DA	double amplitude
DSIF	deep space instrumentation facility
dBm	decibels above 1 milliwatt
dc	direct current
EDO	error demodulator output
EST	Eastern Standard Time
ETR	Eastern Test Range
FACT	Flight Acceptance Composite Test
F -	days prior to launch day
F +	days after launch day
FLSC	flexible linear shaped charge
GBI	Grand Bahama Island
GD/C	General Dynamics/Convair
GH_2	gaseous hydrogen
Glotrac	global tracking station
GMT	Greenwich mean time
GN_2	gaseous nitrogen
GSE	ground support equipment
GTI	Grand Turk Island
gal	U.S. gallon
He	helium
Hz	hertz
H_2O_2	hydrogen peroxide
IAT	initial acceptance test
IGS	inertial guidance system
I_{sp}	specific impulse
LHe	liquid helium
LH_2	liquid hydrogen
LN_2	liquid nitrogen
LOS	loss of signal
LO_2	liquid oxygen
MBU	MECO backup signal
Mc	megacycles
MDF	mild detonating fuse
MECO	main engine cutoff
MES	main engine start
MUIA	mass unbalance input axis

mA	milliamperes
mW	milliwatts
NPSH	net positive suction head
NPSP	net positive suction pressure
n. mi.	nautical mile
PAFB	Patrick Air Force Base
PLIS	propellant level indicating system
PSD	power spectral density
PU	propellant utilization
psi	pounds per square inch
psia	pounds per square inch absolute
psid	pounds per square inch differential
psig	pounds per square inch gage
Q	quadrant
RF	radiofrequency
RSC	Range Safety Command
rpm	revolutions per minute
SANSAL	San Salvadore
SAO	Smithsonian Astronomical Observatory
S-band	frequency band used in radar (range, 1.55 to 5.20 gigacycles)
SECO	sustainer engine cutoff
SLV	Space Launch Vehicle
S/N	signal to noise ratio
STL	Space Technology Laboratories
T -	time prior to launch (2-in. motion)
T +	time after launch (2-in. motion)
TCA	temperature control amplifiers
TEL	Telemetry station
TRW	Thompson Ramo Woolridge
VECO	vernier engine cutoff

REFERENCES

1. Foushee, B. R.; and Wentink, R. S.: Centaur Monthly Configuration, Performance, and Weight Status Report. Rep. No. GDC 63-0495-34, General Dynamics/Convair, Mar. 21, 1966.

2. Smith, Orvel E.: A Reference Atmosphere for Patrick AFB, Florida. (Annual). NASA TN D-595, 1961.

3. Minzner, R. A.; Champion, K. S. W.; and Pond, H. L.: The ARDC Model Atmosphere, 1959. Air Force Surveys in Geophysics No. 115 (AFCRC TR 59-267), Aug. 1959.

4. Smith, J. W.; and Vaughan, W. W.: Monthly and Annual Wind Distribution as a Function of Altitude For Patrick Air Force Base, Cape Canaveral, Florida. NASA TN D-610, 1961.

5. Staff of Lewis Research Center; Postflight Evaluation of Atlas-Centaur AC-4 (Launched Dec. 11, 1964). NASA TM X-1108, 1965.

6. Environmental Design and Test Requirements for Project Centaur Equipment, Specification for, Rep. No. 55-00200E, Contract NAS 3-3232.